NUREG/CR–4977
EGG–2505
Vol. 2

SHAG Test Series

Seismic Research on an Aged United States Gate Valve and on a Piping System in the Decommissioned Heissdampfreaktor (HDR): Appendices

Prepared by R. Steele, Jr., J. G. Arendts

Idaho National Engineering Laboratory
EG&G Idaho, Inc

Prepared for
U.S. Nuclear Regulatory
Commission

AVAILABILITY NOTICE

Availability of Reference Materials Cited in NRC Publications

Most documents cited in NRC publications will be available from one of the following sources:

1. The NRC Public Document Room, 2120 L Street, NW, Lower Level, Washington, DC 20555

2. The Superintendent of Documents, U.S. Government Printing Office, P.O. Box 37082, Washington, DC 20013-7082

3. The National Technical Information Service, Springfield, VA 22161

Although the listing that follows represents the majority of documents cited in NRC publications, it is not intended to be exhaustive.

Referenced documents available for inspection and copying for a fee from the NRC Public Document Room include NRC correspondence and internal NRC memoranda; NRC Office of Inspection and Enforcement bulletins, circulars, information notices, inspection and investigation notices; Licensee Event Reports; vendor reports and correspondence; Commission papers; and applicant and licensee documents and correspondence.

The following documents in the NUREG series are available for purchase from the GPO Sales Program: formal NRC staff and contractor reports, NRC-sponsored conference proceedings, and NRC booklets and brochures. Also available are Regulatory Guides, NRC regulations in the *Code of Federal Regulations*, and *Nuclear Regulatory Commission Issuances*.

Documents available from the National Technical Information Service include NUREG series reports and technical reports prepared by other federal agencies and reports prepared by the Atomic Energy Commission, forerunner agency to the Nuclear Regulatory Commission.

Documents available from public and special technical libraries include all open literature items, such as books, journal and periodical articles, and transactions. *Federal Register* notices, federal and state legislation, and congressional reports can usually be obtained from these libraries.

Documents such as theses, dissertations, foreign reports and translations, and non-NRC conference proceedings are available for purchase from the organization sponsoring the publication cited.

Single copies of NRC draft reports are available free, to the extent of supply, upon written request to the Office of Information Resources Management, Distribution Section, U.S. Nuclear Regulatory Commission, Washington, DC 20555.

Copies of industry codes and standards used in a substantive manner in the NRC regulatory process are maintained at the NRC Library, 7920 Norfolk Avenue, Bethesda, Maryland, and are available there for reference use by the public. Codes and standards are usually copyrighted and may be purchased from the originating organization or, if they are American National Standards, from the American National Standards Institute, 1430 Broadway, New York, NY 10018.

DISCLAIMER NOTICE

NUREG/CR-4977
EGG-2505
Vol. 2
R1

SHAG Test Series

Seismic Research on an Aged United States Gate Valve and on a Piping System in the Decommissioned Heissdampfreaktor (HDR): Appendices

Manuscript Completed: July 1989
Date Published: August 1989

Prepared by
R. Steele, Jr., J. G. Arendts

Idaho National Engineering Laboratory
Managed by the U.S. Department of Energy

EG&G Idaho, Inc.
P.O. Box 1625
Idaho Falls, ID 83415

Prepared for
Division of Engineering
Office of Nuclear Regulatory Research
U.S. Nuclear Regulatory Commission
Washington, DC 20555
NRC FIN A6322
Under DOE Contract No. DE-AC07-761D01570

SUMMARY

Volume 2 of this report contains Appendices A through E, which present details and specifics of the tests and results reported in Volume 1. Appendix A, the valve anomaly appendix, is a copy of the report that describes the investigation, results, and conclusions of the INEL effort to determine the cause of the reduced performance of a naturally aged Crane gate valve with a Limitorque motor operator. Appendix B describes the VKL instrumentation for the SHAG test series. Appendices C and D provide supplementary information regarding snubbers and transducers used in the HDR tests. Appendix E discusses the analyses of the frequency response functions recorded during the HDR testing.

CONTENTS

APPENDIX A
VALVE ANOMALY

ABSTRACT

This report describes the investigation, results, and conclusions of the INEL effort to determine the cause of the reduced performance of a naturally aged Crane gate valve with a Limitorque motor operator. The motor-operated valve served 25 years in the Shippingport Atomic Power Station as a feedwater isolation valve before being refurbished and installed in a piping system in the Heissdampfreaktor (HDR), where valve operability in typical pressure and temperature environments and during simulated earthquakes was studied. During the test program it was discovered that under some valve hydraulic loadings the motor operator failed to reach torque levels high enough to open the closing torque switch. Failure of the torque switch to open caused the motor to go into a stall. In normal plant service, stalling an operator motor can cause motor burnout and render the valve inoperable for subsequent safety functions. The investigation concluded that the poor performance of the valve was caused by heating of the motor windings and by external circuit resistance, both of which prevented the motor from developing its rated torque. The investigation also identified torque spring aging as a problem.

FIN No. A6322—Environmental and Dynamic Qualification Program
and FIN No. A6861—Equipment Survivability Program

SUMMARY

During the HDR SHAG test program, we found that under certain hydraulic loadings the naturally aged motor-operated gate valve obtained from the Shippingport Atomic Power Station did not operate to design requirements. The valve is a 900 lb class Crane gate valve with a Limitorque model SMA size 2 motor operator.

During most of the ambient temperature tests with two valve cycles, the motor operator failed to open the torque switch on the second closing cycle of the valve. As a result, the motor stalled (while still drawing power). During the elevated temperature tests with higher system pressure, the motor stalled at the end of both closing cycles.

We conducted an extensive investigation to try to isolate the cause of the poor performance at the motor operator. This investigation included follow-on in situ tests at HDR, dynamometer testing of the motor operator at the Limitorque laboratory, testing of the torque spring at INEL, dynamometer testing of the motor alone at the Peerless Motor laboratory, and a mathematical analysis of the HDR power circuit. The investigation identified three causes of the motor-operator's poor performance: torque spring aging, heating of the motor windings, and resistance in the dc power cabling at HDR. The investigation also demonstrated that normal plant testing of valves is not adequate to ensure proper performance under flow and pressure loads in combination.

During the follow-on tests at HDR, we found that when the valve was subjected to flow loads and pressure loads in combination, the valve either torqued out in the partially open position, stalled in the partially open position, or stalled in the fully closed position, depending on the load and the torque switch setting. The valve torqued out in the fully closed position only when pressure and flow loads were very low.

Dynamometer testing in the Limitorque laboratory showed that the operator developed 8000-lb thrust to the stem at a torque switch setting of 3 at full rated motor voltage. The motor operator was originally designed to deliver 12,000 lb of thrust at a torque switch setting of 3. The motor operator would require a torque switch setting of about 3.6 to achieve an output thrust of 12,000 lb. Testing of the operator's torque spring and of other new and aged torque springs at INEL confirmed that the difference is the result of a permanent set in the aged torque spring.

The 125-Vdc motor is a 40-ft-lb-rated motor. At motor stall, the motor should develop 62 ft-lb of torque with a stall current of 115 amps. Analyses of the performance data taken at HDR show the motor developed about 20 ft-lb at 50 amps at stall. Dynamometer testing of the motor operator at the Limitorque laboratory showed that the motor stalled at 38 to 45 ft-lb of torque with a stall current of 66 to 75 amps.

The motor operator's motor was manufactured by Peerless Winsmith. Dynamometer testing of the motor at the Peerless laboratory, with the motor removed from the Limitorque gear box, showed that when the motor was at ambient temperature, the locked rotor performance met the original design requirement. However, the motor windings tend to heat up during motor operation. When the motor was loaded with a 50 ft-lb load, its performance degraded at 1 amp per second over a 20 s period.

Dynamometer testing in the Limitorque laboratory and in the Peerless laboratory provided data that exhibited far better motor operator performance than was obtained at the HDR. At HDR, voltages and currents were measured at the motor and, according to those measurements, voltages did not drop below 107 Vdc at motor stall. Even when voltages were dropped during dynamometer testing at Limitorque to 80 Vdc, the HDR performance could not be duplicated.

Coinciding with our investigation Limitorque also participated in a separate investigation of problems with dc-powered valves at a U.S. utility. This investigation pointed out some of the same problems that were experienced at HDR, along with some additional relay and switch problems. Both investigations point out the special requirements of dc-powered valves. The results of the utility investigation prompted us to perform a mathematical analysis of the power circuit to which the motor-operator was connected at HDR. This analysis showed that the main cause of the valve's poor performance at HDR was undersized power cables.

The cables were originally sized (at HDR and at Shippingport) according to the motor controller ratings and the continuous full-load current value stamped on the motor nameplate. However, we now know that this value is the power level at which the motor can run without becoming overheated in its 5-min duty cycle; five times that current level is required for the motor to reach its potential maximum output.

As the loading slows the motor down, dc motors develop their high torque, allowing more current to flow. At motor stall, only the resistance of the motor windings (approximately 1 ohm) limits the current flow, combined with the resistance of the power cables. Thus, the resistance of the power cables becomes an important variable. Typically, the motor armature and the field windings are connected in series through the motor controller, so four long cables, instead of two,

contribute to the resistance of the power circuit. Our analysis showed that this kind of connection also makes it impossible, using conventional methods and instruments, to get true measurements of voltage drop across the motor.

According to our analysis, the 1-ohm resistance of the power circuit at HDR (combined with the 1-ohm resistance of the motor windings) would reduce the output of the motor by approximately one-half at high motor loadings such as those experienced during valve closure against flows. These analysis results correspond well with the measured output at HDR as compared with the output at the Limitorque laboratory, where the large cabling of the power circuit minimized the influence of power circuit resistance.

Torque spring aging can be a problem in motor operators in the field. If the spring has taken a permanent set, the operator might torque out too soon at recommended torque switch settings and under fluid load conditions, leaving the valve in a partially open position.

Under some conditions, heating of motor windings can be a problem in the field. When a valve subjected to high loads is cycled more than once in a short period of time, heating of the motor windings can be the determining factor that causes reduced performance, especially in a marginally powered valve. This was the case at HDR during the two-cycle ambient temperature tests in which the operator failed to torque out on the second cycle of the test.

Undersized power supply cabling has surfaced as a problem in at least two dc motor operators in the field. Though the other two factors contributed to the anomalous performance of the valve at HDR, undersized cabling was the main cause. The NRC has recently issued an information notice regarding the issue.

None of the three problems discovered during the HDR tests and follow-on investigation would be detected during the normal in-plant testing where the valves are subjected to no load or to pressure loads alone. The problems are detectable only at higher loadings, that is, flow loads in combination with pressure loads, where the load slows the motor down such that momentum cannot carry the unit through complete closure and torque out.

APPENDIX A
VALVE ANOMALY

INTRODUCTION

As part of its equipment qualification research program, the Nuclear Regulatory Commission (NRC) installed a refurbished, naturally aged, 8-in. motor-operated gate valve in an existing piping system, the Versuchskreislauf (VKL), at the decommissioned Heissdampfreaktor (HDR) facility in West Germany. The VKL was modified to simulate the flexibility of a nuclear piping system supported by a typical U.S. stiff piping support system. This 30-year-old, 900-lb-class, Crane gate valve was obtained from the Shippingport Atomic Power Station, where it served 25 years (from 1957 until the plant was decommissioned in 1982) in the secondary system as an isolation valve. Identified as 53-H-2-5, the valve was used to isolate the boiler feedwater pump discharge from the safety injection lines. The valve is powered by a Limitorque SMA-2 motor operator equipped with a Peerless 125 Vdc motor.

The valve was included in the SHAG (Shakergebäude) seismic research program conducted by Kernforschungszentrum Karlsruhe (KfK) at the HDR facility. The SHAG tests consisted of shaking the HDR containment using a large coastdown eccentric mass shaker. The objectives and results of the SHAG program are documented in Volume 1 of this report. The equipment qualification program objectives were to determine the valve's in situ response and operability characteristics and compare these to those determined from bench tests performed to equipment qualification standards. The results of these comparisons and other similar test comparisons will be used to supplement the technical bases for assessing the adequacy of nuclear equipment qualification standards and to propose any needed improvements. The Idaho National Engineering Laboratory (INEL) was commissioned to manage this part of the NRC's involvement in the SHAG program.

During the SHAG test program, we found that the valve's motor operator did not develop sufficient torque to open the closing torque switch when the valve was exposed to flow and static pressure loads in combination. Failure of the torque switch to open resulted in motor stall. The investigation that followed concluded that the poor performance of the valve was caused by heating of the motor windings and by external circuit resistance, both of which prevented the motor from developing its rated torque. The investigation also identified torque spring aging as a problem.

The potential safety implications of this problem are significant. Valves powered by direct current, such as this one, are typically installed in applications where the valve function is of concern in losses of ac power and where the valves are needed for control or mitigation of a given operating scenario. The circumstances when this anomaly could further complicate a transient are, of course, plant specific. A generic scenario would feature a normally open valve that is closed on a logic command, such as containment isolation, and then required to reopen to mitigate a transient. The valve fails to torque out on closing, and the motor heats up, opening the thermal switch. The motor is then not available until the thermal switch resets. Even then, the motor will operate less efficiently until the overheated motor windings have a chance to cool. If the thermal switch fails to open, or if it has been bypassed, the motor could burn out under stall conditions, making the valve inoperable for subsequent safety functions.

This appendix documents the acquisition, refurbishment, bench testing, installation, and in situ testing of the valve and describes the investigation, results, and conclusions of the INEL effort to determine the cause of the motor operator's reduced performance.

DESCRIPTION OF THE VALVE ASSEMBLY

Shippingport provided a data package for the 8-in. valve. This data package included a photograph of the Shippingport valve installation, name plate information from the valve and actuator, a copy of the equipment specification, information from Crane Catalog No. 53, and a Limitorque operation and maintenance manual. The package also contained the maintenance history of the valve. This maintenance history consisted of summary sheets with one-line entry items identifying the maintenance performed. The history indicated

that the valve was overhauled in October 1963 and received various maintenance actions from 1971 through 1984. Details and results of each maintenance item or inspection were not available. INEL performed a search of the Nuclear Power Experience Database for records of the Shippingport facility that may have recorded problems with the valve. No incident reports for the valve were found.

Valve

The valve is an 8-in., 900-pound-class, pressure-seal bonnet, cast steel (ASTM, A217 WC 1), flex-wedge gate valve with butt weld ends (see Figure A-1). The valve seats are hard faced with Stellite and are seal welded to the valve body. The one-piece flexible wedge (disc) is also hard faced with Stellite on the seating faces. The valve was manufactured in 1956 by the Crane Co. The following information was contained on the valve identification plate affixed to the valve:

Catalog No.	783 U4
Pressure	900 psi
Temperature	850°F
Part No.	DA B85713B
Size	8
Body	WC 1 Steel
Stem	CR 13
Disc	HF
Seat	HF

In addition, the following information was either cast or engraved on the valve body:

8 Crane
WC 1 Steel
900
NL 326
62987

Actuator

The actuator is a dc motor-driven geared mechanism that controls the opening and closing travel of the valve and limits the torque loads applied to the valve stem. The single torque switch stops the motor and valve travel when a predetermined motor operator torque load has been reached. A clutch mechanism and handwheel can be used to override the electrical operating mode and allow manual operation.

The open limit switch stops the motor and valve travel in the opening mode only. Both the open and close limit switches provide additional contacts for interfacing with a reversing controller and position indication lamps. The motor is compound wound for high-torque, low-starting-current operation, and operates on 125 Vdc. The actuator is of weatherproof construction using Class B insulation, and is capable of opening the valve in a maximum travel time of 15 seconds under no-load conditions.

The actuator was manufactured in 1956 by Philadelphia Gear Works (now Limitorque Corp.). The following information was contained on the actuator identification plate:

Type	SMA
Size	2
Order No.	67910
Serial No.	57400
Valve	8
An-2917	
468817	

In addition, the motor identification plate contained the following data:

_____ hp
_____ kW
750 rpm
COMP wound
5 min duty
125 volts
23 amp
75°C

Type and Frame D 2026
Serial No. HG 50272
40 ft-lb

Motor Controller

The motor controller is a Westinghouse Life-Linestarter Type N, NEMA V reversing. The controller has components for starting and reversing, and has overload protection of the actuator motor. A 3-position, remote, panel-mounted selector switch is used with the controller to select the operating mode (Open—Auto—Close) of the valve assembly.

The controller was manufactured in 1956 by Westinghouse Electric Corporation. The following information was taken from a tag inside the controller:

Class:	15-831-NW2
Style:	16-E-9874
Volts:	125
Size:	2

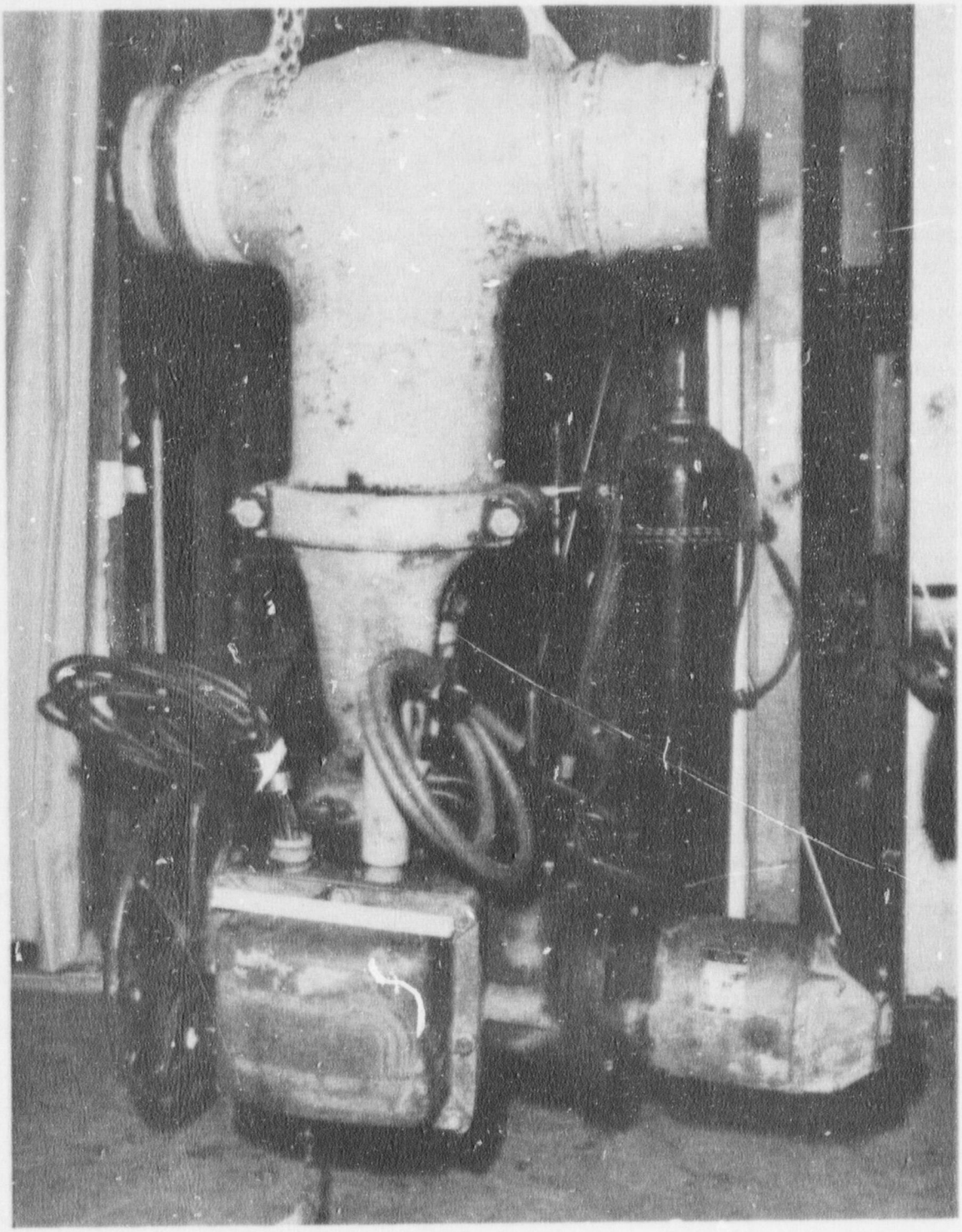

Figure A-1. Eight-inch gate valve and actuator in "as received" condition.

RECEIVING INSPECTION

The valve was supplied from Shippingport with 8-in., Schedule-80 pipe stubs (safe ends) butt-welded to the valve body (see Figure A-1). One pipe stub measured 3.25-in. long; the other measured a minimum length of 1 in. A weld backing ring was found tack-welded to the inside of the 3.25-in.-long pipe-stub-to-body weld. The backing ring was removed by grinding out the tack welds. The 1-in. pipe stub was removed because it was too short to weld a flange to.

The valve was manually opened using the actuator handwheel. The valve was observed to operate smoothly. However, initial inspection of the valve assembly indicated the valve actuator handwheel handle was broken off. No other damage was observed on the outside of the valve.

Initial visual inspection of the valve body internal condition revealed a black-gray oxide coating with some scaling present on the fluid surfaces. Foreign material was also observed on the wedge guide rails when the valve was open and viewed through the end. Inspection of the valve seats revealed a flashing or steam-cut type defect in one of the seat sealing surfaces. The defect appeared as an indentation approximately 0.03 in. deep and 0.25 in. in diameter.

The compartment cover of the valve limit switch was opened and the components shown in Figure A-2 were visually inspected. No sign of moisture, corrosion, wear, or damage was observed. The limit switch and torque switch shaft penetration seals were also inspected. No sign of grease weepage into the limit switch compartment from the actuator housing was observed, indicating the shaft seals were satisfactory. The torque switch setting, "as received," was 2. Initial discussion with the Limitorque Corp., Lynchburg, Virginia, determined that a set point of 2 corresponds to a stem thrust load of approximately 12,000 lb. (After dynamometer testing at Lynchburg, however, old documents were found indicating that a torque switch setting of 3 was required to achieve the 12,000-lb thrust.)

The running torque required for handwheel rotation of the valve was measured using a torque wrench. Both the open and closed valve travel directions required 70-in.-lb of torque on the handwheel. The valve was observed to operate smoothly. The valve stem stroke length was measured at 7-9/16 in.

The actuator was removed from the valve bonnet yoke, and the actuator lubricant was removed for inspection and replacement. Since the actuator uses a grease lubricant, it was necessary to partially disassemble the actuator. The housing cover and motor were removed to allow access for grease removal. Approximately 18 lb of grease was removed, with some residual grease remaining. The lubricant was visually examined for wear products, metal particles, and foreign material. No contamination from foreign material or metal particles was found in the lubricant. The amount of lubricant recommended by the Limitorque operation and maintenance manual ranged from 13 to 25 lb for the type SMA-2 actuator. Approximately 12 lb of Chevron Heavy Duty Grease-1, equivalent to the Limitorque recommended grease Exxon Nebula EP-1, was placed in the actuator housing. A new grease seal was also installed in the housing cover.

While the actuator motor was removed, the motor shaft drive gear was turned by hand and was observed to rotate freely. No lateral or axial play in the motor shaft was observed, indicating that the motor bearings were in satisfactory condition.

The motor controller and 3-position panel switch for the valve were shipped separately from Shippingport. The cover on the motor controller unit was removed, and the internal components shown in Figure A-3 were inspected. No evidence of moisture, corrosion, or damage was found inside the controller. One mounting screw from a terminal block or contact set was found loose in the housing and was replaced. The contact sets were operated by hand and found to operate smoothly. All circuits were resistance-checked and found satisfactory. The insulation resistance was tested at 500 V and found satisfactory. The 3-position switch was also inspected and found to be in good working condition.

At the conclusion of the visual inspection, the valve was subjected to nondestructive examination, including ultrasonic, magnetic particle, and X-ray inspection, as part of the USNRC Nuclear Plant Aging Research (NPAR) Program. NPAR objectives were (a) to identify and characterize aging and service wear effects associated with electrical and mechanical components, interfaces, and systems likely to impair plant safety, (b) to identify and recommend methods of inspection, surveillance, and monitoring of electrical and mechanical components and systems that will be effective in detecting significant aging effects prior to loss of safety function so that timely maintenance and repair or replacement can be implemented, (c) to identify and recommend acceptable maintenance practices that can be undertaken to mitigate the effects of aging and to diminish the rate and extent of degradation caused by aging and service wear. After the nondestructive examination was completed, repairs were made to the valve sealing surface, and a new safe end was welded on to replace the one cut too short during the valve's

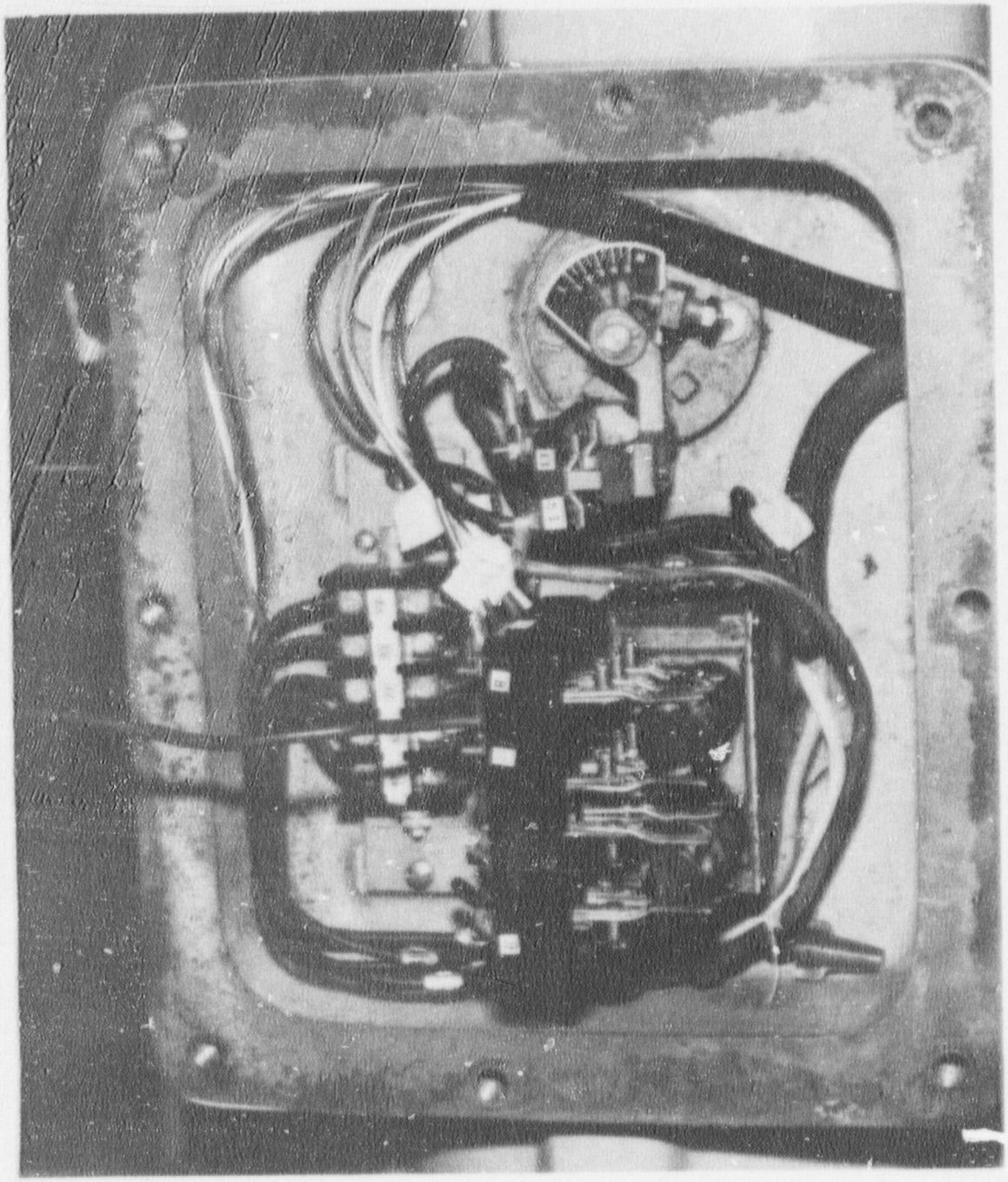

Figure A-2. Limitorque actuator limit switch compartment.

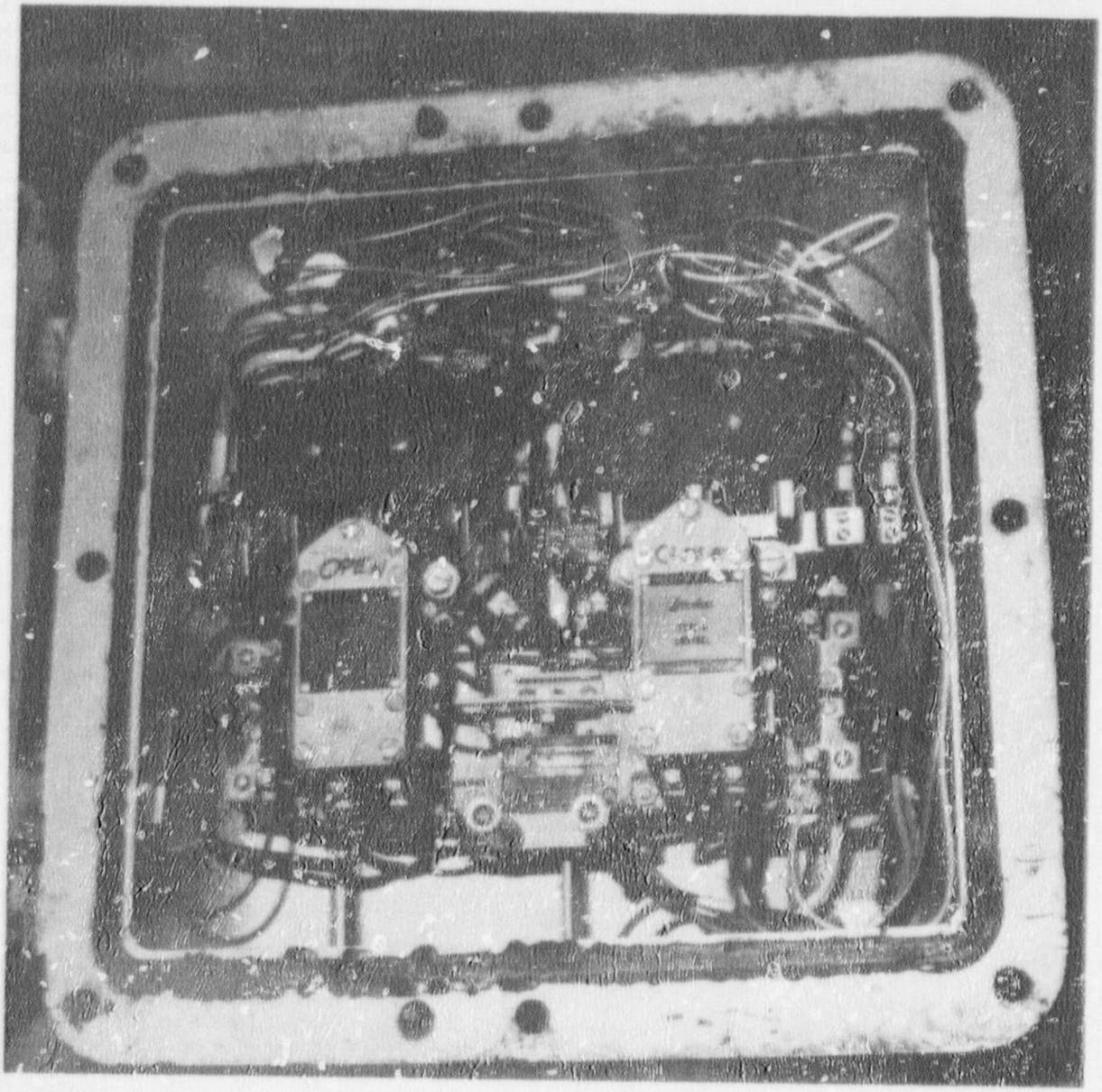

Figure A-3. Limitorque actuator motor controller.

removal from Shippingport. Two new 1500-lb flanges were welded to the safe ends. Selection of materials, welding, and hydrostatic tests were all done to the intent of the current issue of the ASME Boiler and Pressure Vessel Code, Section III, Class 2. The valve was reassembled and remated with the Limitorque actuator.

All electrical connectors, terminals, and fasteners were checked to make sure they were tight. All electrical contact sets were cleaned by nonabrasive means. No other refurbishment was required for the electrical components.

ANSI Standard B16.41, which presents the guidelines for the qualification of nuclear plant valve assemblies, was used in defining test requirements for applicable tests performed at the INEL prior to installation at HDR, and for tests performed at HDR prior to dynamic loading. German DIN (Deutsche Institut für Norming) standards required the valve pressure boundary to be certified prior to installation. The ASME code and ANSI B16.41 tests were substituted acceptably for DIN standard testing. ANSI B16.41 tests that were performed at the INEL before installation at HDR included Annex A, Valve Leakage Test; Annex B, Cold Cyclic Test; and Annex E, Exploratory Vibration Test for determination of fundamental frequencies. Annex G, Flow Interruption Capability Test (the subject of another research program at INEL) was performed at the HDR at both ambient and elevated temperature within the limits of the VKL piping system. A modified version of Annex C, Hot Cyclic Test was performed at the HDR prior to elevated temperature testing. Annex D, Pipe Reaction End Loading Qualification Test, was not performed; this loading is being researched in another program at INEL. Annex F, Seismic Loading, was not performed for two reasons: the test could possibly damage the valve, and the HDR test program was a more realistic simulation of seismic testing. Figure A-4 shows the valve installed in the pressure test fixture at the INEL. The valve successfully completed limited qualification testing and was judged suitable for installation in the VKL at the HDR.

INSTALLATION AT HDR

A section of pipe was cut out of the VKL and replaced with a flanged spool piece consisting of the refurbished valve, safe ends, and flanges. Fifteen-hundred-pound-rated stainless steel flanges were also welded to the pipe ends. The valve spool was installed with spiral-wound Flexitallic gasket. This modification to the piping was completed by changing out an adjacent spring hanger to account for the added weight and by performing a hydrostatic test of the piping system. The HDR facility provided 125 Vdc to which the Limitorque operator and motor controller were connected. The original motor controller from Shippingport was used.

Figure A-5 details the valve instrumentation. Figure A-6 shows the installed valve and a portion of its instrumentation. Important parameters recorded by the instruments include valve stroke time, motor current and voltage, system pressure, valve differential pressure, valve stem position and strain, and system fluid temperature. The valve was installed operator down to avoid structural interference above the pipe run. This type of installation, while not the most preferred, is second choice and typifies many industry applications.

SHAG TESTING AT HDR

Valve tests conducted at the HDR included functional tests (without dynamic loading) at ambient and at elevated temperatures. Dynamic tests also were conducted both at ambient and at elevated temperatures, usually with the valve cycled during the dynamic excitation.

The valve was baseline functional tested with and without internal hydraulic loading (pressure and flow loads) before the SHAG dynamic tests were conducted. The same baseline functional tests were performed at elevated temperatures (200°C) just before the hot dynamic tests.

The first four SHAG dynamic tests were performed to check out instruments, equipment, and data acquisition systems and were conducted at less than maximum dynamic loadings so that building and shaker safety studies could be verified. Many instrument mounting and equipment changes were made during these checkout tests to optimize recording of peak responses; however, the valve instruments and data acquisition systems worked well and produced a complete set of data for the valve during the first four tests. Table A-1 relates the valve operational parameters to the dynamic

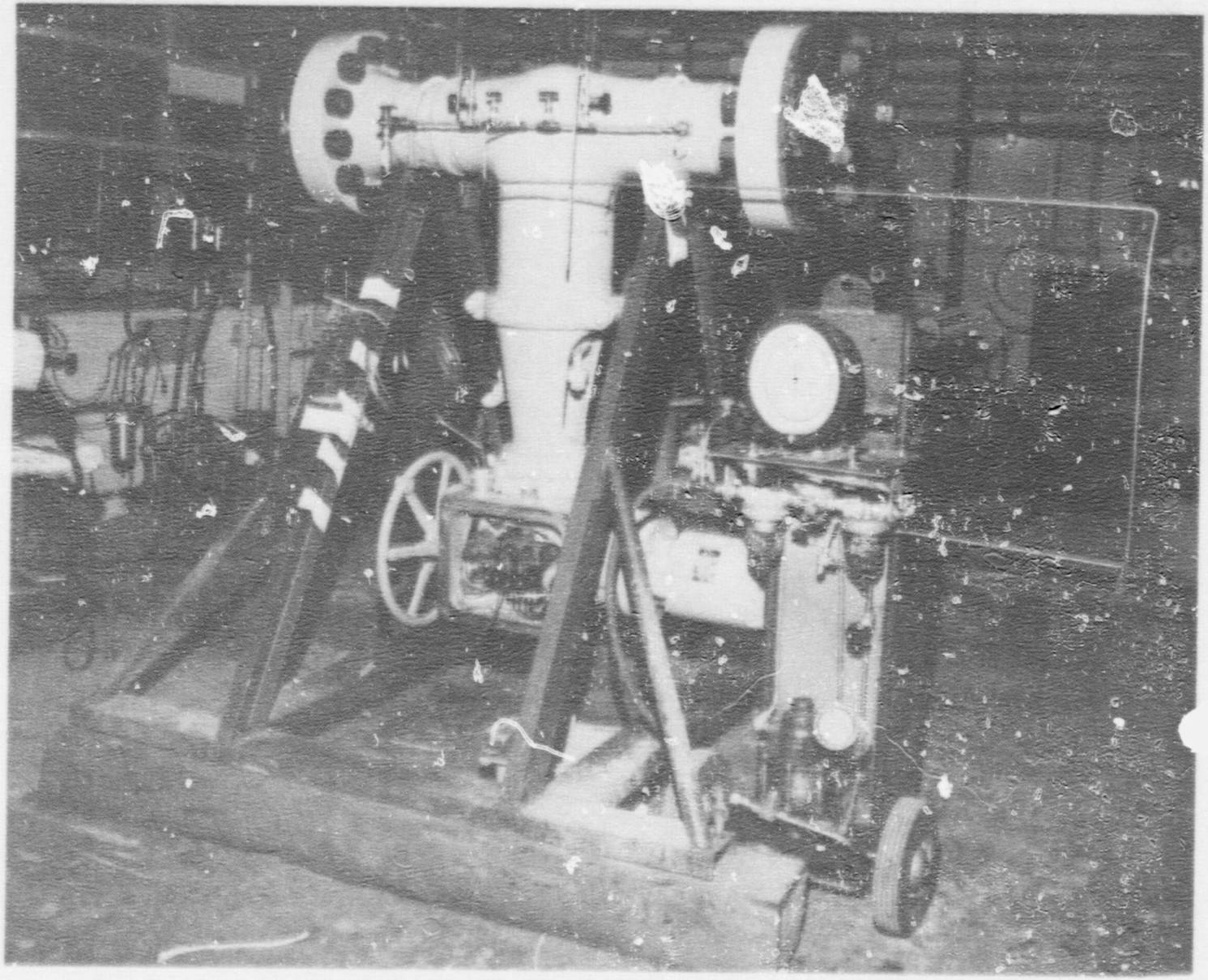

Figure A-4. Valve installed in the pressure test fixture.

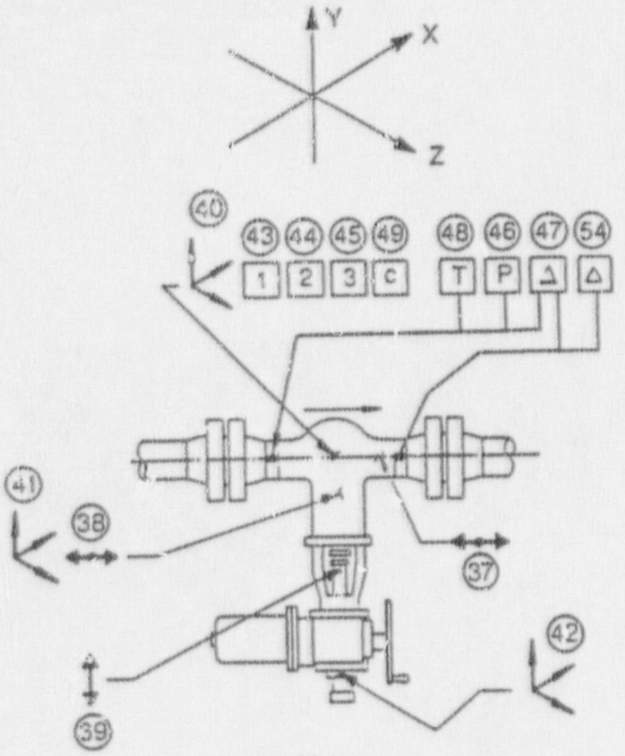

Valve

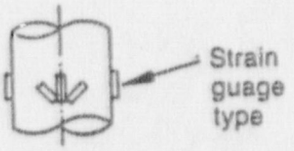

Strain guage

Legend

- Accelerometer and its detection axis
- Single strain guage and its detection axis
- Strain guages (see strain guage detail)
- [D] Displacement guage
- [P] Pressure
- [Δ] ΔP
- [1] Valve position
- [2] Valve current
- [3] Valve voltage
- [T] Temperature

Figure A-5. Valve instrumentation detail.

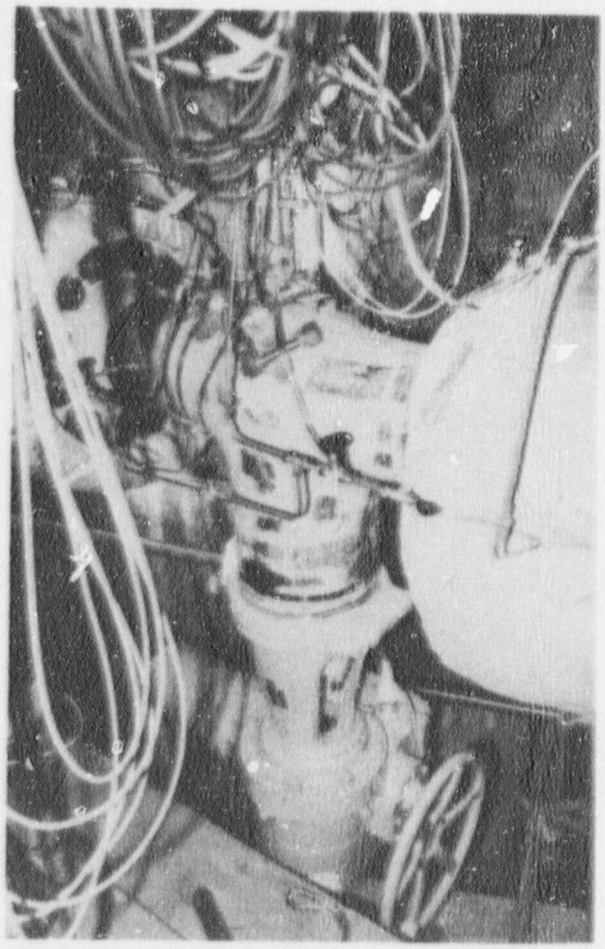

Figure A-6. Installed gate valve and part of the installed instrumentation.

Table A-1. Valve function parameters[a]

Test T40	Temp (°C)	Stroke Time (s)		Current in Amps					Pressure (psi)	
				Closing			Opening			
		Closing	Opening	Run	Peak	Stall	Peak	Run	System	ΔP
AF[b]	20	14.4	14.4	12	12+	—	16.41	10.94	73.95	384
34	20	—	14.7	12	14	—	17.67	10.6	73.95	377
35	20	—	—	12.5	15	—	17	11	15.0	333
36	20	—	15	11	13.5	—	14	9.5	55.5	330
37x	20	—	—	12	13.5	—	17	11	67	333
y	—	—	—	11.5	—	35	13	10	—	—
40x	20	15.5	15.5	12	17	—	17	10	67	259
y	—	—	15.5	12	—	38	20	9	—	371
20x	20	—	15.6	13.5	18	—	24	12	74	344
y	—	17	17	12.5	16	38	25	12.5	—	351
60x	20	—	—	14	19	—	23	11	74	340
y	—	—	16	13.5	—	—	—	—	—	344
50x	20	—	15	12.5	14	—	20	9	67	333
y	—	15.5	16	11	—	38	20	9	—	263
70x	20	—	—	11	13	—	19	7	67	333
y	—	—	16	11.5	—	37	18	7.5	—	263
10x	20	—	—	—	—	—	24	8	70	362
y	—	—	16	12.5	—	38	25	10	—	329
30x	20	—	—	—	—	—	25	10	70	362
y	20	—	16	12.5	—	38	25	10	—	340
31x	20	—	—	—	—	—	25	11	70	348
y		—	16	12.5	—	38	25	11.5	—	333
41	20	—	16	12.5	13.5	—	25	11.5	70	333
21	20	—	16	12	13	—	25	10.5	70	325
11	20	—	14	12.5	13	—	25	11.5	70	329
51x	20	—	—	12.5	—	38	25	11	70	322
y	—	—	17	12.5	—	37	25.5	11	—	333
HF[c]x	210	22	12	17	27	40	12	7	924	313
y	—	22	12	17	27	38	12	7	—	313
52x	210	—	—	12.5	25	37	10	6	924	301
y	—	—	12.5	12.5	25	36	10	7	—	301
32x	210	—	12.5	12.5	25	37	10	5	924	301
y	—	—	12.5	12.5	26	36	11	6	—	301
42x	210	—	12.5	12.5	25	36	10.5	5	924	305
y	—	20	12.5	13.5	25	37	10.5	6	—	305
12	210	19.5	12.5	13	25	38	11	6	924	305
22	50	—	13.5	—	—	—	18	7	70	359
12A	210	20	12.5	13	25	37	10	6.5	924	313
14	40	—	14	10	17	—	17	8	50	350
16	Valve tests were not performed during this dynamic test.									
13	Valves tests were not performed during this dynamic test.									
AF[d]x	40	14.5	14	13	19	—	20	12	74	359
y	—	15	14	13	19	41	22	11		354

a. The first and second cycles of two-cycle tests are indicated by x and y.

b. Functional test performed at ambient temperature at the beginning of the test sequence.

c. Functional test performed at elevated temperature.

d. Functional test performed at ambient temperature after the elevated-temperature tests were completed.

test series nomenclature, and includes the important parameters recorded for the valve during the test program. The valve performed flawlessly in the first three tests (identified as T40.34, T40.35, and T40.36). Figure A-7 shows valve position and operating current histories for the first two dynamic tests and for a baseline functional test (with flow). There are only slight variations in the overlaid current traces; for all practical purposes, the valve functioned during the first two transients as it did in the baseline tests.

Torque Out Failure

Normally, the high torque produced by the motor when the valve reaches the fully closed position causes the closing torque switch in the motor operator to open and interrupt current to the motor. If the closing torque switch fails to open, the motor stalls and overheats. After the overheating has tripped the thermal overloads, the valve is unavailable until the motor has had a chance to cool. If the thermal overloads are rated too high, or if they have been bypassed, the result can be motor burnout and the functional loss of the valve.

Table A-1 shows that the valve performed without problem also during the third dynamic test. However, during the fourth dynamic test (test T40.37), the torque switch failed to open at the end of the second closing cycle, and the motor went into a stall. Figure A-8 shows the valve position history beginning 4 s before initiation of the dynamic transient and during the first 56 s of the transient. At the start of the transient, the valve was set 35% open so the maximum hydraulic loading (valve fully closed) would occur near the peak of the dynamic loading. The stroke time from fully open to fully closed would have been 15 s; the stroke time from 35% open to fully closed was approximately 6 s. The valve was left closed for 10 s, reopened to 68% open, reclosed for 6 s, then reopened.

Figure A-9 shows the valve motor current history for this same open-close sequence. As shown in Figure A-9, the motor current for the valve opening and closing cycles were normal until the second valve closing cycle, where the operator failed to torque out on closing and the motor went into a stall, with the current rising to 43 amps and holding until the motor was manually reset for reopening. VKL system pressure control requirements mandated that the valve not be left closed longer than 10 s, so manual setting of the motor controls for reopening was required for each valve cycle. The resetting of the motor cancelled the closing signal, and this prevented early detection of the failure to torque out on closing and kept the motor from overheating.

This pattern of the valve failing to torque out on the second cycle repeated itself on most of the subsequent ambient temperature tests where the valve was cycled twice, until the last ambient test prior to elevated

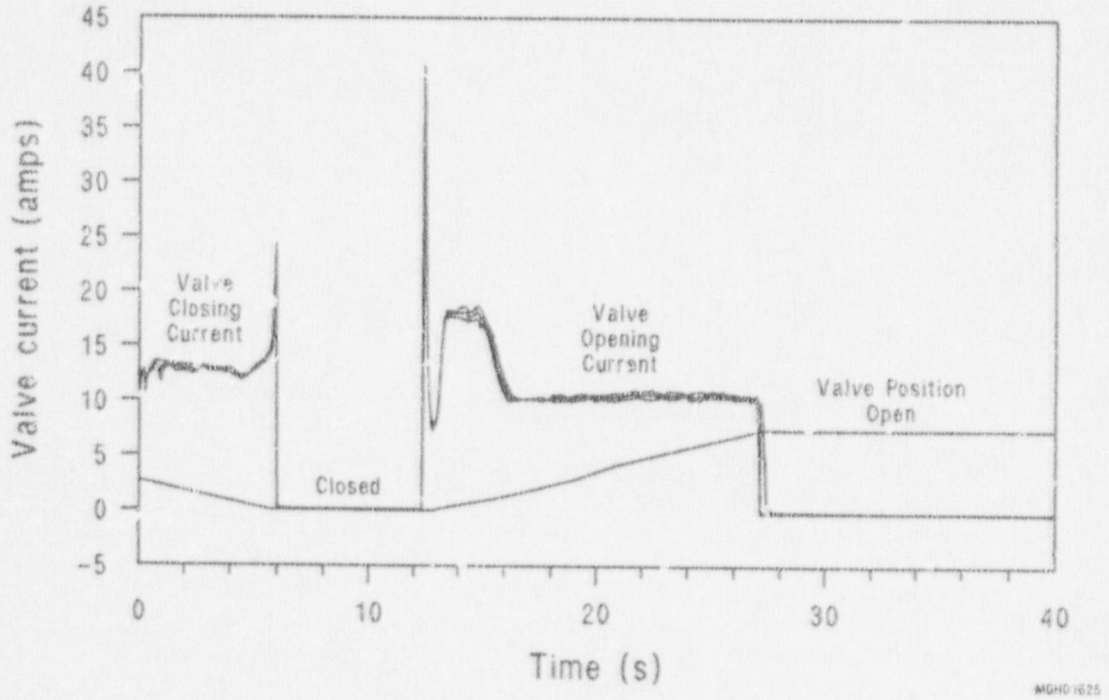

Figure A-7. Composite time histories for valve position and current.

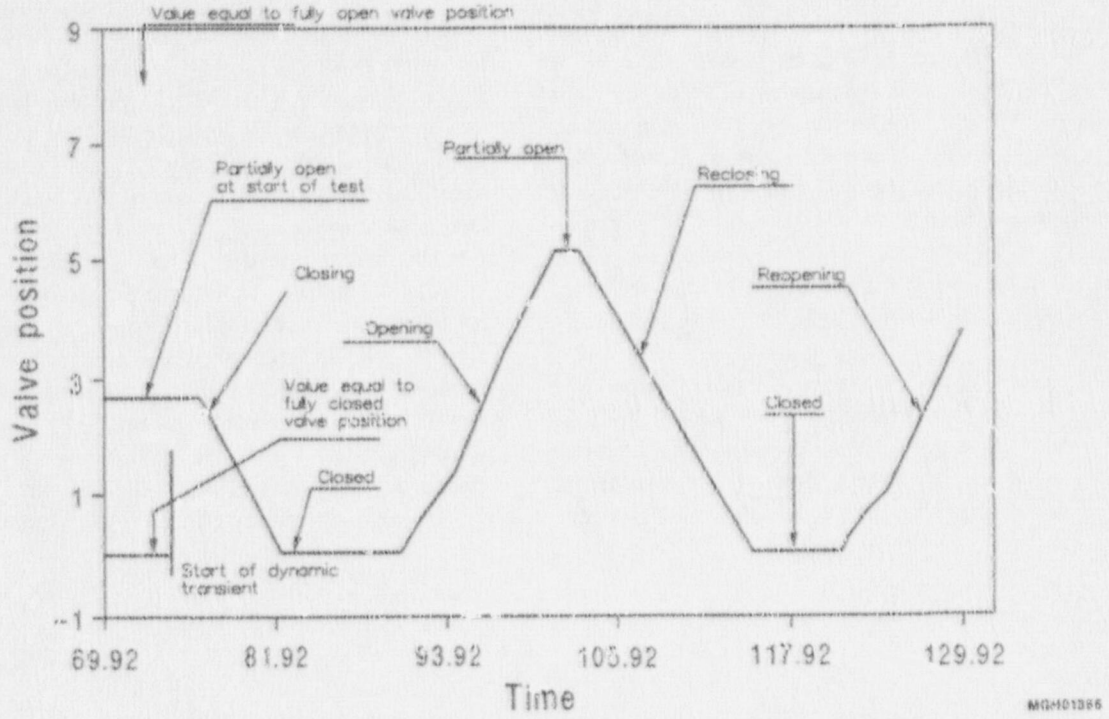

Figure A-8. Valve position versus time during the fourth dynamic test.

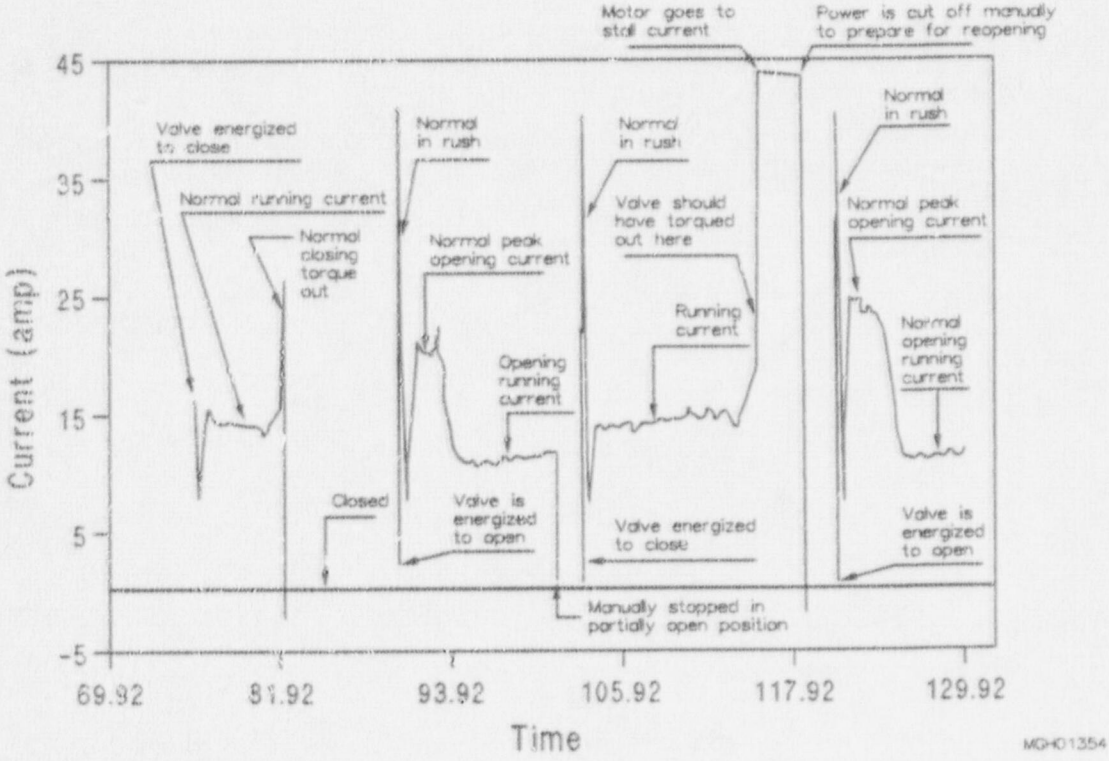

Figure A-9. Valve current versus time during the fourth dynamic test.

temperatures testing, when the valve failed to torque out on both closing cycles in test T 40.51. The valve failed to torque out on closing in all of the elevated temperature tests, including the functional testing without dynamic loading and on both single and multiple cycle tests with dynamic loading. In the subsequent ambient temperature testing, the valve returned to its behavior prior to the elevated temperature testing, failing to torque out on the second cycle of a two-cycle test. This pattern is shown in Table A-1 in the "Stall" column.

Figures A-10 and A-11 show the valve position and valve current histories for two-cycle hot test T40.52; Figures A-12 and A-13 show corresponding histories for a single-cycle hot test. Both sets of figures are typical examples showing the valve's failure to torque out on closing during hot testing.

Basic valve function, i.e., the ability to open and close under normal hydraulic loadings, was affected by the magnitude of the loading. As expected, higher system pressure, imposed during elevated temperature testing, and higher WP across the gate affected stroke times and motor current demands. The range of readings is reasonably small. The measured data indicate that the dynamic loading (from the eccentric mass shaker), in combination with the normal loadings, did not have an adverse impact on valve performance. In fact, the valve closing current was lower during the elevated temperature dynamic testing than during the elevated temperature functional tests (which were run without dynamic input). The vibration during dynamic testing may have helped break friction, thus causing the closing running currents to be lower in the dynamic tests than in the functional tests.

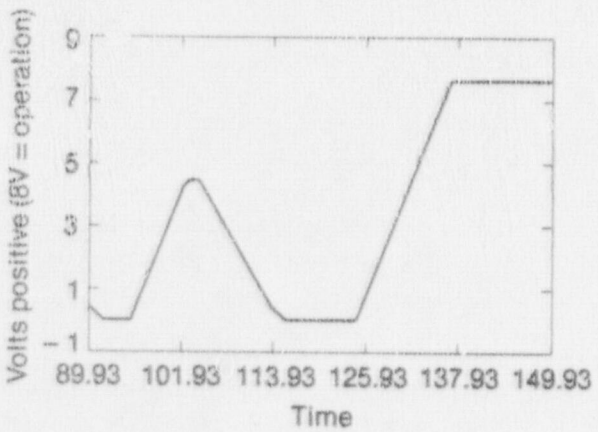

Figure A-10. Valve position versus time during a two-cycle, elevated temperature valve test.

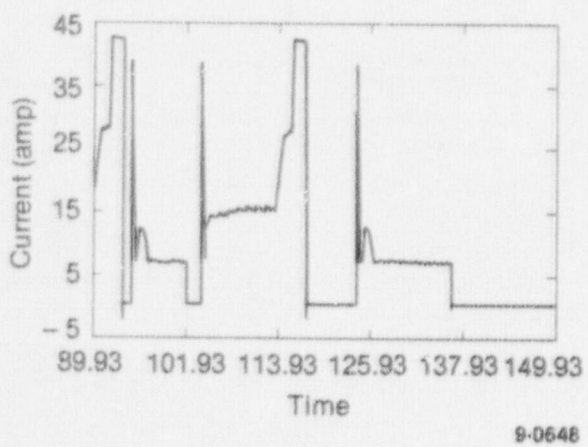

Figure A-11. Valve current versus time during a two-cycle, elevated temperature valve test.

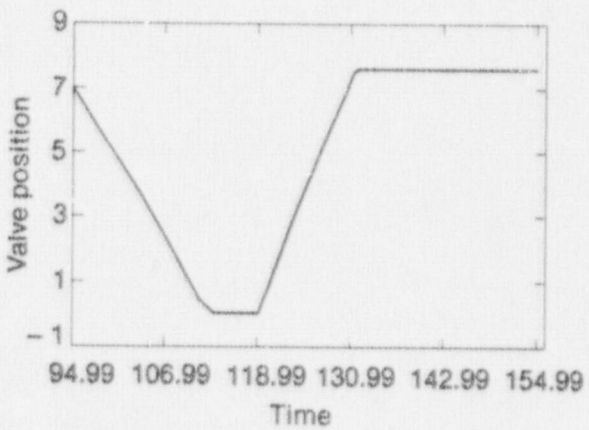

Figure A-12. Valve position versus time during a single-cycle, elevated temperature valve test.

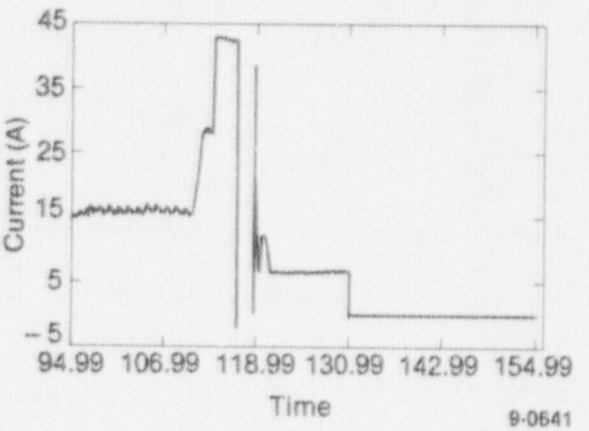

Figure A-13. Valve current versus time during a single-cycle, elevated temperature valve test.

Failure of the valve motor operator to actuate the closing torque switch, which led to subsequent motor stall, appeared to be a motor operator problem rather than a valve problem. This anomaly was not detected during the test portion of the program, because of the format of the quick-look plots and the necessity (mentioned earlier) to manually reset the control to reopen the valve to accommodate system pressure control requirements. The short length of time that the valve was left closed prevented the motor from overheating during stall current, making it impossible to determine if the thermal overloads would have tripped before permanent damage occurred to the motor. Since thermal overload trip was not an objective of this task, no testing was performed to address this capability. Failure of the valve to torque out on closing was detected during posttest data reduction.

Posttest Investigation

A posttest investigation was initiated to determine the probable cause of the valve motor operator anomaly. Limitorque was contacted, and probable causes were discussed. Limitorque suggested at that time that the most likely cause was that the torque switch was set too high. A brief parametric study of the valve's operability was conducted at the HDR facility to determine torque switch setting limits. That study showed that the torque switch was not set too high. In those tests, conducted without flow or pressure loads, a torque switch setting of 4 was found to be too high, but a setting of 3.8 was low enough to allow the motor to trip the switch. A setting of 2.9 had been used throughout the SHAG program. All torque switch locking features were found to be secure.

Further discussions were held with Limitorque and other motor operator experts, and no positive scenarios were developed that could explain the anomalous performance of the valve. According to the voltage readings, the motor voltage even at stall currents did not fall below 107 Vdc. The motor should have performed much better at these voltages. In a subsequent analysis of the power circuit, we demonstrated that those voltage readings were unreliable, and that with conventional methods and instruments, it was impossible to take true measurements of motor voltage on that circuit. In the meantime, our investigation focused on possible causes other than inadequacies in the power supply or the power circuit.

First Review Group Meeting

A review group was established consisting of representatives from the NRC staff, INEL, Oak Ridge National Laboratory (ORNL), and Limitorque, and a meeting was called to assist in identifying the root cause of the valve functional anomoly and to plan a course of action for its timely resolution. The review group was briefed with all the information available at that time, including a motor power curve for a motor similar to the one installed at HDR. As shown in Figure A-14, the curve indicated that the locked rotor current for the motor is approximately 120 amps.

The probable causes of the valve's failure and contributing factors were discussed. The following list contains items that were identified as probable causes either singularly or in combination:

1. Torque switch malfunction
   a. Damaged parts in torque switch assembly
2. Insufficient motor torque to compress the torque spring pack in combination with the valve loads
   a. Internal motor operator friction
   b. Excessive motor power circuit voltage drop
   c. Inadequate electrical power supply
   d. Torque switch set too high
   e. Hydraulic lockup in torque spring package
   f. Internal motor operator damage
   g. Motor operator motor, rotor, stator, or brush degradation.

The meeting provided a panel of knowledgeable and informed people who suggested ideas and provided pro and con arguments for each of the possible causes and contributing causes. The group requested additional information to determine the root cause. This information, subsequently obtained from the HDR, did not substantially change the measured data obtained during the SHAG testing or provide an obvious answer to the motor operator anomaly. Therefore, the group recommendation for further testing in the HDR at SHAG hydraulic conditions was pursued. The intent of this additional testing was to duplicate the motor operator anomaly and then to perform tests and inspections to determine the root cause. Limitorque agreed to support this activity from its European office at no charge to the NRC.

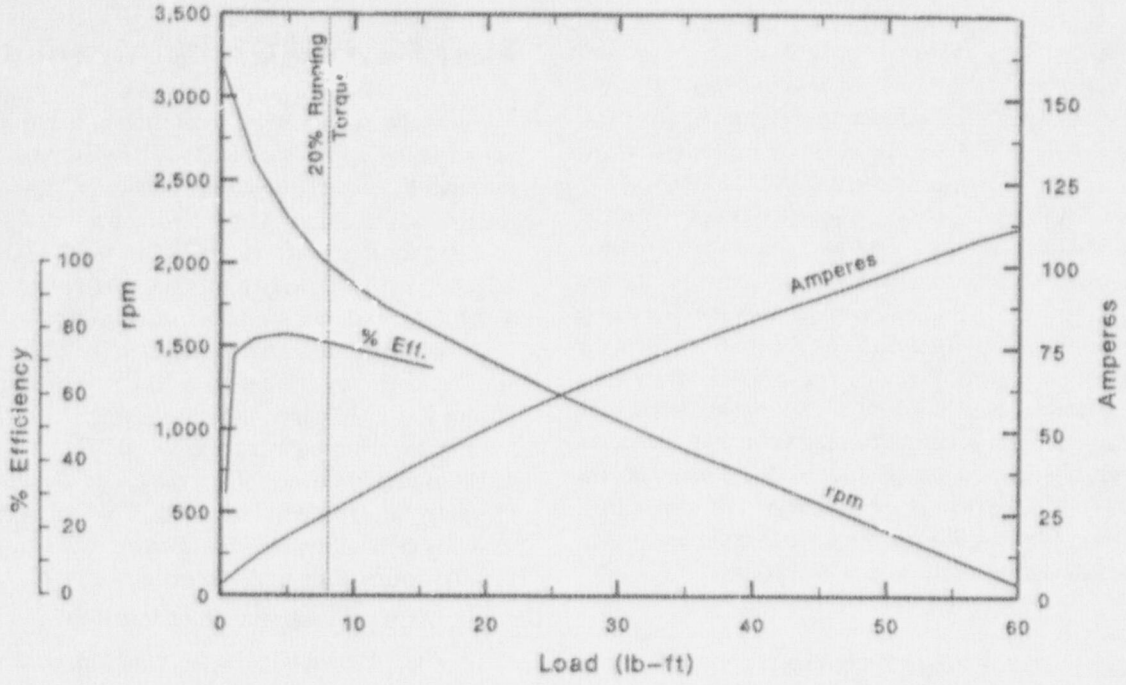

Figure A-14. Motor power curve provided by Limitorque.

ADDITIONAL IN SITU TESTING AT HDR

INEL personnel returned to the HDR test facility to perform the recommended additional testing. The valve was reinstrumented at the motor/limit switch junction strip in the limit/torque switch compartment of the motor operator, and instrument power supplies and recorders were located within a few feet of the valve.

A parametric study was conducted with the objective of obtaining more information on the relationship of the valve's performance to the following parameters:

Torque switch setting	Motor current
Torque spring travel	Motor voltage
Valve disc position	Valve load

This study showed th. he lower torque switch settings, the valve did not . plctely close at higher flows and pressures, while at ..gher torque switch settings the valve operator motor stalled. The valve closed farther with the higher settings, but the motor stalled before the valve closed completely.

The Limitorque representative reviewed the results of the parametric study and inspected the motor operator. It was recommended that additional lubricant be added. This recommendation was followed, but subsequent testing showed no improvement in valve performance.

The motor was removed for disassembly and inspection. The visual appearance of the motor internals was good, but the front motor bearing was rough. One field coil showed a high resistance. After discussions with Limitorque USA, it was decided to rewind the field coils. The field coils were rewound and both motor bearings replaced. The repaired motor was reinstalled on the operator. (Later discussions with the motor manufacturer identified the coil with the high resistance as a shunt field coil, which is a speed control coil that would not affect the performance of the motor under a load.)

In the tests that followed, the valve still showed no noticeable improvement in performance, and after discussion with Limitorque USA and the NRC technical monitor, it was decided that further in situ testing at HDR would be unproductive and that the motor operator should be removed from the valve and returned to the USA. Table A-2 is a summary of the in situ HDR valve testing.

Results and Analysis of In Situ Tests at HDR

The results of these tests indicated that the valve functional problem is hydraulic load sensitive; however, the valve appears to be more sensitive to flow loading in combination with static loading than to

Table A-2. HDR in situ valve testing summary

Test	Torque Switch Setting	Stroke Time Closing (S)	Stroke Time Closing Stall (S)	Stroke Time Opening (S)	Pressure (bar)	Flow (tons/hr)	Torque Switch Deflection Total (Degree)	Torque Switch Deflection Run (Degree)	Current Closing Run (amp)	Current Closing Peak (amp)	Current Closing Stall (amp)	Current Opening Peak (amp)	Current Opening Unseat (amp)	Current Opening Run (amp)	Voltage Closing Run (Vdc)	Voltage Closing Peak (Vdc)	Voltage Closing Stall (Vdc)	Voltage Opening Peak (Vdc)	Voltage Opening Unseat (Vdc)	Voltage Opening Run (Vdc)	Incomplete Closing (in.)	Comments
01	2.9	19.0		16.4	0	0	30.0	12.0	18.5	17.5		26.5		15.0	120.0	120.0		116.0		121.0	0.00	As found
02	2.9	19.2		15.3	10	0	31.0	13.5	19.0	18.2		26.5	13.0	13.5	119.0	120.0		116.0	122.0	122.0	0.00	As found
03	2.9	21.3		14.2	20	0	28.8	14.0	21.0	20.3		26.0	12.1	11.0	118.0	118.2		116.0	121.8	121.8	0.00	As found
04	2.9	19.6		15.0	21	45	26.5	13.5	18.0	25.5		26.0	23.5	10.5	118.0	115.0		116.0	116.0	121.0	0.00	As found
05	2.9	19.0		13.7	25	45	27.0	14.0	17.0	26.5		25.0	22.5	9.0	118.0	115.0		116.0	116.0	121.0	0.00	As found
06	2.9	21.7		14.5	30	80	25.0	17.0	20.5	36.0		26.0	26.0	9.5	118.0	112.5		116.0	116.0	122.0	0.16	As found
07	2.9	21.7		13.5	35	80	25.0	16.0	20.5	35.0		26.0	24.0	7.5	118.0	112.5		116.0	117.0	123.5	0.28	As found
08	2.9	21.5		12.2	40	85	25.3	15.0	19.0	33.7		26.0	21.7	6.5	119.0	113.0		116.0	118.0	123.7	0.32	As found
09	3.1		23.3	12.7	40	85	28.0	13.0	17.0		43.5	25.5	24.3	6.0	119.0		108.7	116.0	116.0	123.7	0.16	As found
11	3.1	16.6		15.6	0	0	34.8	12.5	15.0	15.5		26.8		13.0	119.0	119.0		114.7		120.0	0.00	As found
11A	2.9	17.4		15.4	0	0	34.5	12.0	16.0	15.0		26.5		13.0	119.0	119.0		116.2		120.0	0.00	As found
12	2.0	16.4		15.4	0	0	24.0	8.0	15.5	13.0		26.5		14.0	121.8	122.0		117.2		121.9	0.00	As found
13	2.5	16.7		15.6	0	0	28.3	9.0	15.5	14.0		26.5		14.0	120.0	120.5		116.3		121.0	0.00	As found
14	3.0	16.6		15.6	0	0	29.0	7.5	15.5	15.0		26.5		14.0	121.0	121.0		116.2		121.0	0.00	As found
15	3.5	16.6		15.6	0	0	32.5	7.4	15.0	19.7		27.0		14.0	121.0	117.9		117.2		121.0	0.00	As found
16	4.0		16.8	15.6	0	0	36.0	9.0	15.5		45.5	26.5		14.0	120.0		108.6	116.2		121.0	0.00	As found
17	2.5	16.3		15.4	0	0	30.0	9.0	15.5	13.0		27.0		14.0	121.8	125.0		118.0		122.8	0.00	As found
18	2.5	18.4		15.4	10	0	30.5	14.0	17.5	15.0		27.0		13.5	120.0	120.0		116.2		121.0	0.00	As found
19	2.5	19.0		14.0	20	0	25.3	9.5	18.0	16.4		27.0		11.0	120.0	121.0		117.2		122.7	0.00	As found
20	2.5	20.8		13.7	30	0	23.7	9.5	19.0	17.7		27.0	10.2	9.0	120.0	120.0		116.6		124.0	0.00	As found
21	2.5	22.2		12.2	40	0	24.5	11.0	22.0	18.5		27.0	9.0	7.0	118.0	119.0		116.3		123.7	0.00	As found
22	2.5	20.4		12.0	40	80	16.5	9.5	19.0	27.5		26.0	19.5	6.5	118.0	114.5		116.2	118.0	122.0	0.40	As found
23	2.5	19.1		13.5	30	80	16.5	8.0	17.0	28.0		26.0	22.5	7.5	119.0	114.4		116.2	118.0	122.0	0.32	As found
24	2.5	17.5		13.8	20	80	15.5	6.0	15.0	28.0		25.5	26.5	8.5	120.0	114.4		116.3	115.0	122.0	0.24	As found
25	2.5	17.0		15.5	10	80	18.3	5.8	14.5	24.0		25.5	28.0	10.0	120.0	116.3		116.3	114.4	121.5	0.00	As found
26	3.0	17.0		15.5	10	72	24.0	6.3	14.5	28.8		26.0	27.5	10.5	120.0	114.0		116.0	114.0	121.0	0.00	As found
27	3.0		19.0	14.6	20	80	22.0	7.0	16.0		44.0	25.5	27.5	8.0	119.0		108.2	116.0	114.0	121.8	0.00	As found
28	3.0		20.3	13.7	30	80	21.8	7.8	16.0		42.5	25.0	26.0	7.0	119.0		108.7	116.0	115.0	122.0	0.12	As found
29	3.0		22.2	12.7	40	80	23.0	10.0	18.0		43.5	25.0	22.7	6.5	118.0		108.5	116.0	116.0	123.0	0.16	As found
30	3.0	19.7		11.9	40	0	30.0	11.5	17.0	19.8		26.0	9.0	6.5	120.0	119.0		116.0	122.0	123.6	0.00	As found
31	3.0	18.3		12.7	30	0	27.4	7.4	16.0	18.0		26.0	9.4	7.4	120.0	119.0		116.0	122.0	123.7	0.00	As found
32	3.0	16.7		12.8	20	0	27.0	8.0	14.0	17.0		26.0	10.4	8.0	121.0	120.0		116.0	122.0	122.5	0.00	As found
33	3.0	15.5		13.4	10	0	27.4	5.7	13.0	16.5		26.0	11.4	9.5	121.5	120.0		116.5	122.1	122.5	0.00	As found
34	3.0						27.0															Hand operated
34A	3.5						34.0															Hand operated
35	3.5	15.7		13.7	10	0	34.0	6.5	14.0	19.2		26.4	12.3	11.0	122.5	120.5		118.0	123.7	123.7	0.00	As found
36	3.5		22.2	12.6	40	80	23.5	10.2	19.0		44.0	26.5	24.0	7.0	118.0		108.7	116.0	116.0	123.5	0.24	As found
40	3.1		21.1	14.0	40	85	24.0	12.0	19.7		45.3	26.0	23.0	10.5	119.0		108.7	116.0	117.0	121.8	0.27	After grease
40A	3.1		20.2	13.7	40	85	21.0	9.0	18.0		44.7	26.0	22.5	10.0	119.0		108.7	116.0	117.0	121.8	0.30	After grease
40C	3.1	18.5		15.5	20	80	27.3	10.5	16.0	29.7		25.7	26.0	11.0	120.0	114.4		116.0	115.0	121.8	0.00	After grease
40D	3.1		18.2		20	80	24.8	8.3	15.5		44.5				120.0		108.7				0.00	After grease
40E	3.1	17.5		14.4	20	30	28.5	8.5	16.0	19.7		25.7	19.0	10.7	120.0	118.0		116.0	119.0	121.8	0.00	After grease
41	3.1	17.7		16.3	0	0	23.2	3.2	16.0	17.9		26.0		14.5	120.0	120.0		116.0		120.0	0.00	After rewind
41A	3.1		15.8	0	0							26.0		13.5				116.0		120.0	0.00	After rewind
42	3.0	21.8		14.2	40	80	20.7	9.2	20.0	42.5		26.0	26.2	9.0	119.0	110.6		116.0	116.0	123.0	0.21	After rewind
42A	3.0	19.5		13.8	40	80	16.0	9.5	19.0	29.0		27.5	25.0	8.0	120.0	116.0		116.0	117.0	123.0	0.30	After rewind
42B	3.1		21.7	14.7	40	80	21.6	9.4	18.0		45.5	26.0	30.5	8.5	119.0		108.7	116.0	116.0	122.0	0.16	After rewind
42C	3.1		23.8	14.5	40	80	22.0	8.5	18.5		47.0	26.5	26.5	8.0	118.0		107.8	116.0	116.0	122.0	0.16	After rewind
45	2.8	20.5		13.5	40	80	23.8	13.3	18.0	37.5		26.0	25.0	8.0	118.0	110.6		116.0	116.0	122.0	0.18	After rewind
45A	2.8	20.5		13.7	40	80	19.5	9.5	18.5	38.2		26.0	25.0	8.0	118.0	110.6		116.0	116.0	122.0	0.18	After rewind
46	2.8	19.3		16.3	0	0	24.9	6.0	18.0	18.0		26.5	16.5	9.0	120.0	120.0		116.0	121.0	122.0	0.00	After rewind
46A	2.8	18.2			0	0	25.5	6.7	17.0	18.5					120.0	120.0					0.00	After rewind

increased static pressure load alone. During qualification testing, the valve closed successfully with a full design pressure static load of 2300 psig, which is significantly higher than any static pressure load at HDR. With a static pressure load alone, the load on the valve is constant throughout the closing cycle, and motor speed is not affected. When a flow load is applied along with the static load (as was sometimes the case during subsequent testing), motor speed is affected as the gate closes and as WP across the valve increases. The slowing of the motor speed affects the total momentum of the motor operator and its ability to open the torque switch. This, of course, is true only in a marginally powered valve and is dependent on the torque switch setting.

Figures A-15 and A-16 show this valve disc velocity relationship for the valve closing stroke at three pressures with and without flow. With pressure alone (no flow), the stroke time increases with pressure (Figure A-15). Note in Figure A-16 the decrease in the disc velocity, indicated by the slope of the trace, for all three pressure cases (with flow) as the disc approaches the closed position. In the cases with flow, the torque switch failed to open. The extent to which the valve remains open is increasingly greater with each increase in pressure combined with the flow load. Figure A-17 shows a 147 psig static pressure case with flow, along with the three pressure cases shown in Figure A-16. The disc velocity near closing for the 147 psig pressure case does not decrease as much as it does for the higher pressure cases. I[illegible] the valve torque switch opened. The valve stem area is 2.77 square inches. The difference between the torque switch opening and failing to open is the 407 lbf reduction in the stem rejection load.

Review of the data obtained from the in situ HDR tests (see Table A-2) shows that when the valve was subjected to the higher flow and pressure loads in combination (≥80 t/hr flow and ≥30 bar), the motor operator consistently failed to completely close the valve, and at torque switch settings greater than 2.9 or 3.0, the operator also failed to open the torque switch (3.0 was the setting recommended by Limitorque). Normal in-plant valve testing would not detect this type of marginal valve performance. Typically, testing is performed with no load or with a static load alone, and assessment of performance is based on changes in valve current and stroke time. This type of marginal performance would not even be detected by MOVATS or similar motor operator performance equipment that monitors operation of a valve with a static load alone.

Second Review Group Meeting

Another review group meeting was held to discuss the results of the in situ tests and to plan a course of

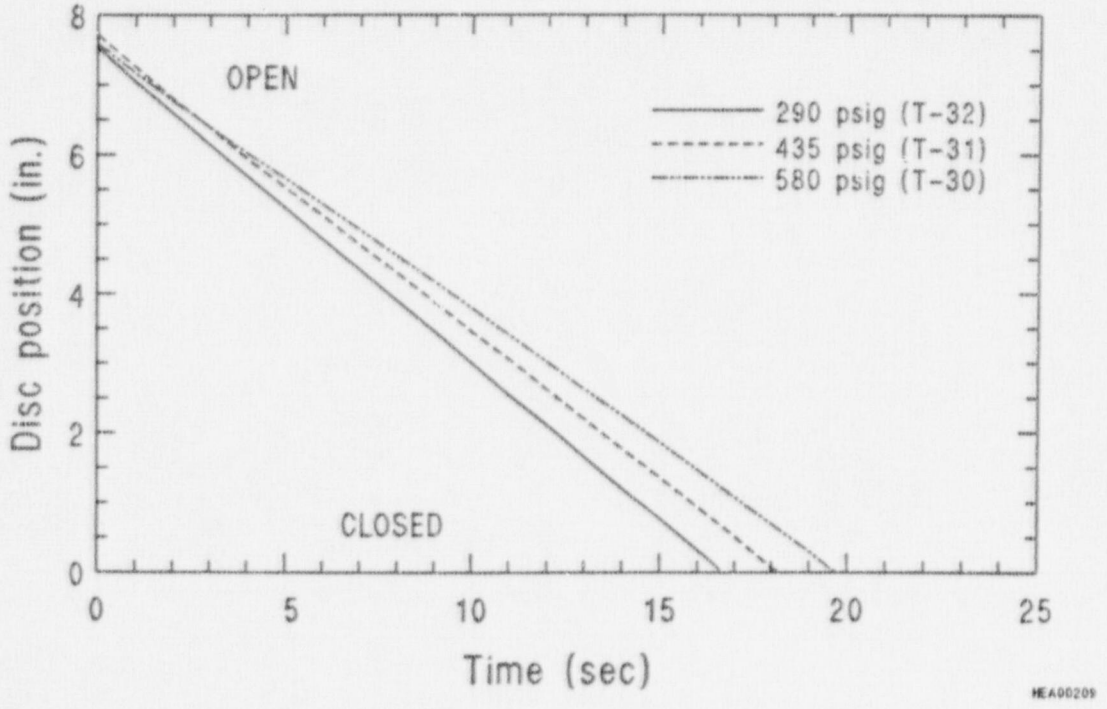

Figure A-15. Valve position during closing stroke under three different static pressure loads with no flow.

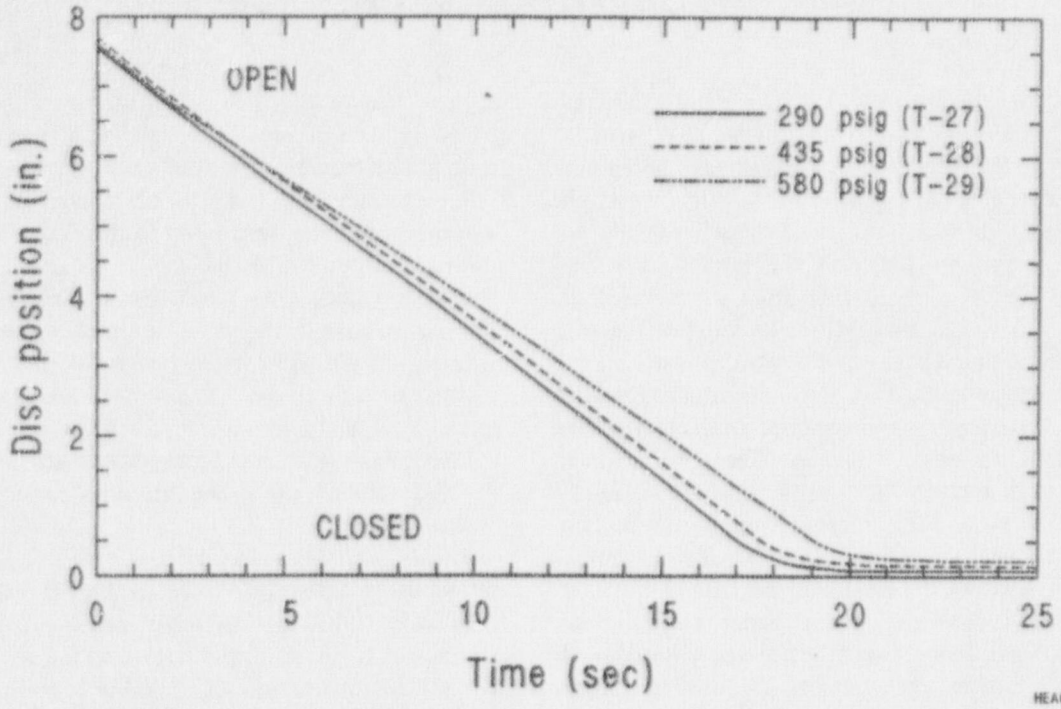

Figure A-16. Valve position during closing stroke with flow (360 gpm) under three different static pressure loads.

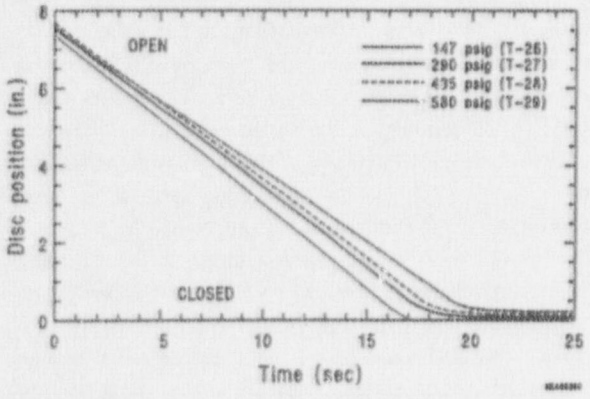

Figure A-17. Valve position during closing stroke with flow (360 gpm) and with a fourth static pressure load.

action for the timely resolution of the anomaly. All of the necessary background information was reviewed, and new information from the in situ tests was discussed with the review group. Additional questions and comments concerning particular items were discussed; the highlights of that discussion are given in the following list.

1. Concern was expressed over the increase in closing times at higher loads. This change may be significant for plant safety concerns since demonstrations of stroke times are typically performed at ambient conditions. The stroke times under higher loads may not fall within the technical specification limits.
2. For many valve assemblies in safety systems, the thermal overload protective devices are either set too high or bypassed to prevent motor cut out while performing its safety function. If the operator stalls, motor burnout is likely to occur, making the valve unavailable for subsequent operation.
3. Testing of valve assemblies at less than design loads may not be adequate.

The general consensus of the meeting was that the motor operator anomaly was probably the result of a marginally sized motor; the motor achieves successful operation only when allowed to seat the valve at full speed, with momentum compressing the torque spring to the switch set point.

The review group recommended the following:

1. Perform a dynamometer check of the motor operator to determine its torque/speed and torque/current characteristics. Compare the results to the HDR test data.
2. If motor is undersized, determine if it is the result of a manufacturing problem or some type of aging effect. Determine what in the motor has degraded.
3. If the motor operator is not the problem, re-evaluate the HDR power supply.

Limitorque agreed to dynamometer test the motor operator assembly on its arrival from Germany.

LIMITORQUE DYNAMOMETER TESTS

Dynamometer testing was performed at the Limitorque facility with representatives from INEL present to witness the results. The Limitorque Laboratory motor controller and amp meter were different enough in performance from those used in earlier testing to make comparison difficult. The motor controller dropout time was longer, and the amp meter lock-in feature did not consistently give an accurate reading of the highest current drawn during torque out. On request from the INEL, the control circuit was rewired to include the Shippingport motor controller and a standard shunt to measure current. The dynamometer loading was applied slowly to the operator in an attempt to simulate the increasing hydraulic loading on an in-service gate valve during the closing stroke. Table A-3 shows the results of that testing.

During the first seven tests, chatter was observed in the operator torque switch, and arcing was observed across the torque switch contacts. There are redundant contacts on this model torque switch, and the circuit was reinstalled on the rear contacts for the remainder of the testing.

Results and Analysis

The original design specification stem thrust requirement for the valve and operator at Shippingport was 12,000 lb. The Limitorque manual for this operator specifies a maximum torque switch setting of 2. The operator was set at 2 when originally received from Shippingport. At the time of the dynamometer testing, Limitorque had not found any records on this unit to show that a torque switch setting over 2 was required to meet the original design requirements. During functional testing at the INEL after valve refurbishment, it was necessary to change the torque switch setting to slightly less than 3 to obtain tight shutoff. For 25-year-old sealing surfaces this was not considered unusual, and the opening and closing currents were well within motor ratings. After the dynamometer testing at the Limitorque facility was completed, old records were found at Limitorque that show that a setting of 3 was necessary to obtain an output thrust of 12,000 lb. Figure A-18 shows the original design torque spring compression versus torque output. The 1-3/4 in. dimension is the radius of the torque switch arm, and the numbers 1 through 5 around that radius indicate the torque switch settings. Figure A-19 shows the type of torque switch used in this application. Item number five in this drawing shows the torque switch tripper arm, which has the 1-3/4-in. radius shown in Figure A-18. Item 4 is the torque switch dial showing the settings from 1 to 5. The torque switch is adjusted by moving Item 14 in and out. Figure A-20 is a simplified diagram of part of a motor operator. The splined output shaft drives the worm, which turns the worm gear and the stem nut. The stem nut drives the threaded valve stem. As the valve seats and the worm gear resists motion, the worm climbs the worm gear, floating on the splined shaft and compressing the torque spring until the shoulder of the worm contacts and rotates the arm of the torque switch and opens the torque switch. The higher the torque switch setting, the further the worm must compress the spring before the torque switch opens and interrupts current to the motor.

Review of the dynamometer tests results (Table A-3) shows that a setting of 3 increased the stem thrust to only about 8,000 lb. The table also shows that the operator required a torque switch setting of 3.75 to develop an output thrust of 12,000 lb. The most likely reason for the higher torque switch setting required to produce the rated torque is a change in the torque spring constant or length. The spring must be compressed further to produce the same force. This type of aging in coil springs is not unusual, but it does create a problem. The problem would not be discovered in normal in-plant valve testing where a change in stroke time is the primary go or no go criterion and where valves are typically tested without hydraulic loading. Gate valves such as this one are typically never used in normal service to control flow or to close against flow and could go for years without such a problem being discovered. If the valve were needed to mitigate an accident, a flow load might make the motor operator torque out early and leave the gate partially open.

Dynamometer testing results also show a marked improvement in motor operator motor performance over the results obtained at the HDR. Stall currents as shown in Table A-3 are between 66 and 75 amps, producing 30 to 32 ft-lb motor torque. This is below the performance specified by the motor manufacturer in Figure A-14. The stall current should be 115 amps with 62 ft-lb torque. The stall currents at HDR were near 50 amps with a maximum of 21 ft-lb torque.

Third Review Group Meeting

The results of the dynamometer testing at Limitorque were presented to the review group and are summarized as follows:

1. It was determined that under ideal laboratory conditions the motor operator performance was better than at HDR.

Table A-3. Results of motor operator testing at Limitorque Laboratory

Test No.	Torque Switch Setting	Set Voltage (Vdc)	Minimum Voltage[a] (Vdc)	Plotter Peak Current (amp)	Peak Torque (ft-lb)	Peak Thrust (lb)	Comments
1	—	—	—	9.0	—	—	No load/baseline
2	2.00	110	108	15.0	99	4480	
3	2.00	125	110	15.0	88	3982	
4	2.50	125	121	21.0	125	5656	
5	2.50	110	107	21.0	132	5973	
6	2.90	110	105	25.0	154	6969	
6.1	2.90	110	105	25.7	185	8371	
7	2.90	125	120	26.0	169	7647	
8	2.90	125	120	29.5	176	7964	
9	3.10	125	119	34.0	220	9955	
10	3.10	110	104	35.0	229	10362	
11	3.10	100	95	34.0	231	10453	
12	3.50	100	94	41.0	242	10951	
13	3.50	100	94	39.0	275	12444	
14	3.50	110	104	40.0	242	10951	
15	3.50	125	119	38.0	264	11946	
16	3.75	125	118	39.0	277	12534	
17	3.75	110	103	42.0	264	11946	
18	3.75	100	94	42.0	245	11086	
19	4.00	100	93	46.0	286	12942	
20	4.00	110	103	46.0	286	12942	
21	4.00	125	118	46.0	264	11946	
22	4.20	100	93	50.0	308	13937	
23	4.50	100	92	58.0	352	15928	
24	4.50	100	91	56.0	363	16426	
25	4.50	110	102	54.0	330	14933	
26	4.50	125	116	51.0	308	13937	
27	4.75	125	112	75.0	484	21901	Stall
28	4.75	110	99	66.0	407	18417	Stall
29	3.50	90	85	39.0	231	10453	
30	3.50	80	75	40.0	255	11539	
31	3.50	80	73	41.0	220	9955	
32	3.50	80	79	5.5	—	—	No-load
33	3.50	90	89	5.3	—	—	No-load
34	3.50	100	99	6.0	—	—	No-load
35	3.50	110	109	6.0	—	—	No-load
36	3.50	125	124	6.0	—	—	No-load

a. Derived from visual readings.

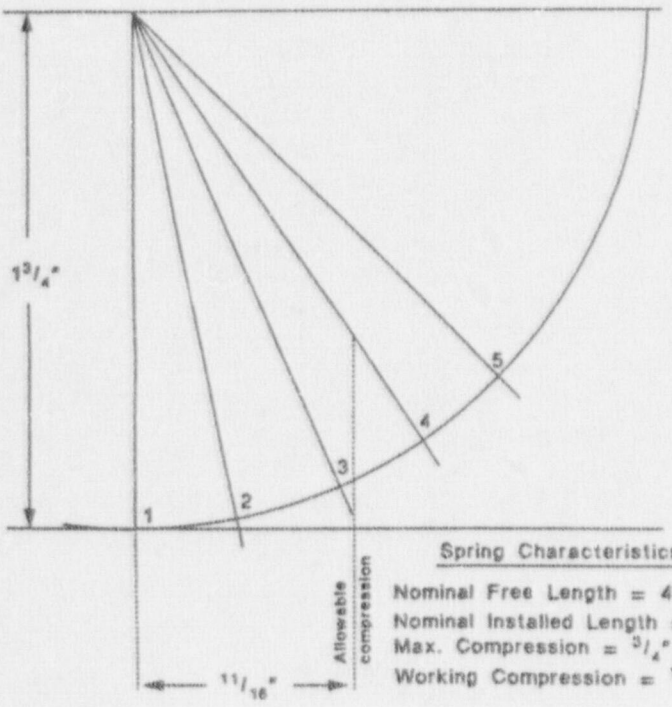

Motor Operator Torque Output		
Torque Switch Position	Spring comp. in inches from preload position	Output Torque ft–lbs
1	(Preload: equals .25)	67.75
1.5	.16	111
2	.32	155
2.5	.484	199
3	.648	244
Wire dia.		3/8"

BMG00044

Figure A-18. Torque switch setting versus spring compression and torque output (HDR valve).

Single torque switch

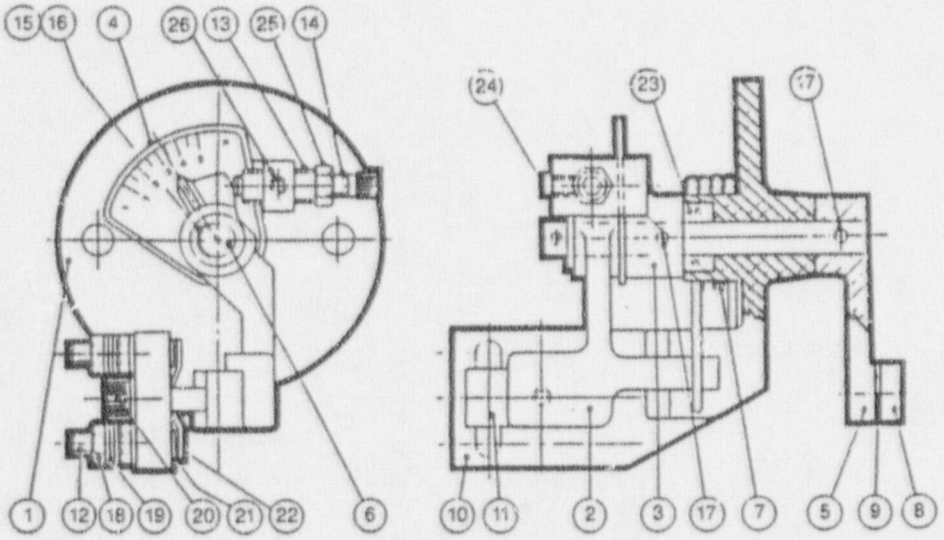

Parts list		PC No.	Name	PC No.	Name	PC No.	Name
PC No.	Name	7	Spring	15	Cotter pin	23	Oil seal
		8	Roller	16	Washer	24	set screw
1	T.S. Bracket	9	Roller pin	17	Taper pin	25	jam nut
2	Actuating arms	10	Sta. terminal block	18	Hex nuts	26	Bushing lock screw
3	Dial holder	11	Movable term block	19	Lockwashers		
4	Dial	12	Term. studs	20	Capscrew		
5	Tripper arm	13	Threaded bushing	21	Contacts		
6	Actuating arm shaft	14	Sock HD.C'SCR (knurled)	22	Contactor		

7-8903

Figure A-19. Limitorque torque switch cross section from the LMI-157 operation and maintenance manual.

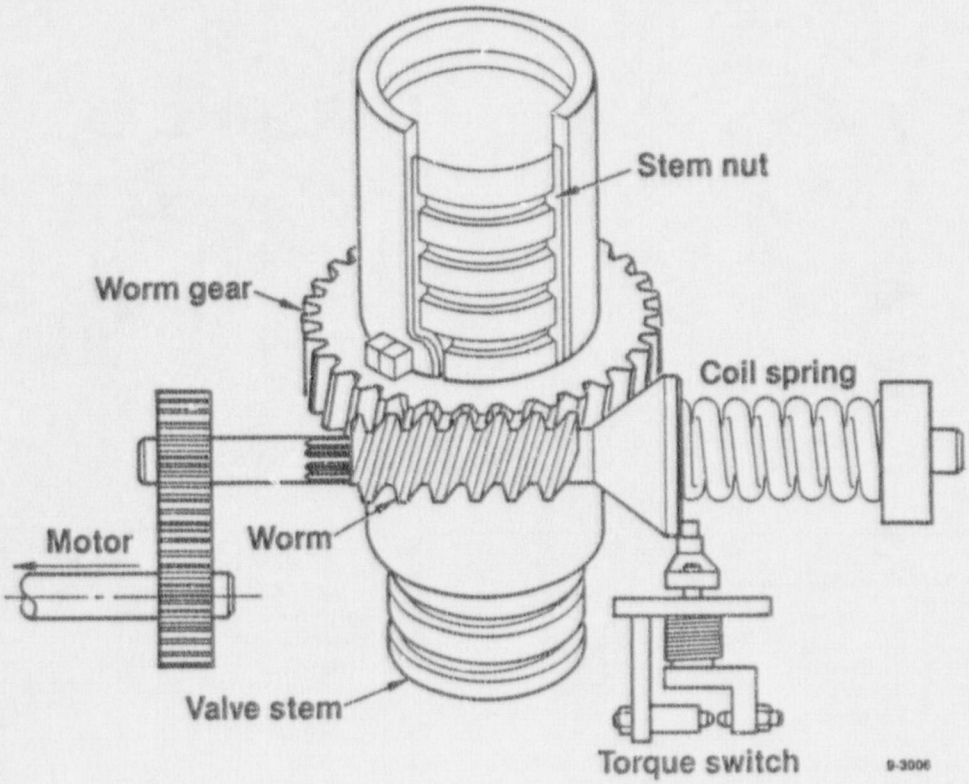

Figure A-20. Limitorque SMA-2 motor operator cross section from the LMI-157 operation and maintenance manual.

2. It was determined that the dc motor performance was less than originally specified.

3. It was determined that the torque output versus torque switch setting was lower than originally specified.

The review group recommended removing the torque spring and dc motor for further testing to complete the investigation and to have a final meeting when the results become available.

At the completion of the investigative dynamometer testing at Limitorque, the dc motor was removed and a new ac motor was installed. The motor operator was returned to the dynamometer and its performance characterized. The results of these dynamometer tests will be compared to in situ performance when the motor operator is remated with the valve at the HDR. The dc motor was sent to the motor manufacturer, Peerless Winsmith, for dynamometer testing, and the motor operator returned to the INEL for installation of a new torque spring and torque switch. The recommended spring testing would be completed at the INEL during torque spring change out.

SPRING TESTING

After its removal from the operator, the old torque spring was measured for length and compared with a new spring purchased from Limitorque as a replacement. Both springs had the same wire size and number of coils. The new spring measured 4.461 in., and the old spring measured 3.981 to 4.006 in. in length. The old spring was shorter on one side than the other. The average length of the old spring (3.994 in.) was .468 in. less than the length of the new spring. According to information obtained from Limitorque, the nominal free length of a spring should be 4.312 in. The shorter free length of the old spring explains the torque switch position versus torque output obtained during the Limitorque dynamometer testing, where a higher torque switch setting was necessary to obtain the design output.

Both torque springs were then load tested. Figure A-21 shows the results of those tests. The old spring was approximately 1/2 in. shorter, so the curve for the old spring does not start showing a loading for the first 1/2 in. displacement. Because of a misunderstanding between Limitorque and the INEL about allowable spring travel, the springs were taken to coil touch during load testing. As can be seen in Figure A-21, at about one inch travel on the first loading of the new spring, yielding took place and the spring developed a permanent set of .22 inches. On the second loading cycle no significant yielding took place. The old spring was also load cycled twice to coil touch. Figure A-21 shows no yielding took place on either cycle. Note that in Figure A-21 the second cycle for each spring was moved slightly to the right of the first cycle for clarity. It can also be seen from the figure the spring constant for both springs (K-factor) was the same (within the accuracy of the equipment) for all loadings. The final length of the new spring after testing was .1 in. shorter than the nominal length (4.312 in.) of a new spring.

During the disassembly of the actuator to remove the old spring, it was noted that there was no preload on the old spring. The preload should have been .25 in., as can be seen in Figure A-18. The information contained in this figure was not obtained from Limitorque until after the spring testing had been completed. As shown in Figure A-18, the maximum allowed compression was 0.75 in. plus 0.25 in. preload. This explains why the new spring showed significant yielding after one inch of travel during the first test. It also shows why there was no preload on the old spring. The correct installed length for the spring is 4 1/16 in., and the old spring was slightly less than 4 in. long. This confirms the hypothesis developed during the dynamometer testing at Limitorque that the torque spring was too short, requiring a higher torque switch setting to achieve the torque output versus torque switch setting shown on Figure A-18.

Another spring, similar to the spring in the HDR Shippingport valve assembly, was obtained from Oak Ridge National Laboratory (ORNL). This spring was removed from Shippingport valve Number 54475D with a Limitorque motor operator type SMA-1 S/N 08531A. The free length of this spring was 3.745 in. Figure A-22 shows the relationship of torque switch setting versus spring compression for the ORNL valve, as Figure A-18 does for the INEL/HDR Shippingport valve. The information obtained from Limitorque used to draw Figure A-22 specified two springs with different free lengths: 3-7/8 in. and 3-13/16 in., as shown. Limitorque did not know from the old records which of the two springs was installed in this valve. This spring is short by either slightly more than 3/16 in. or slightly more than 1/16 in., depending on which

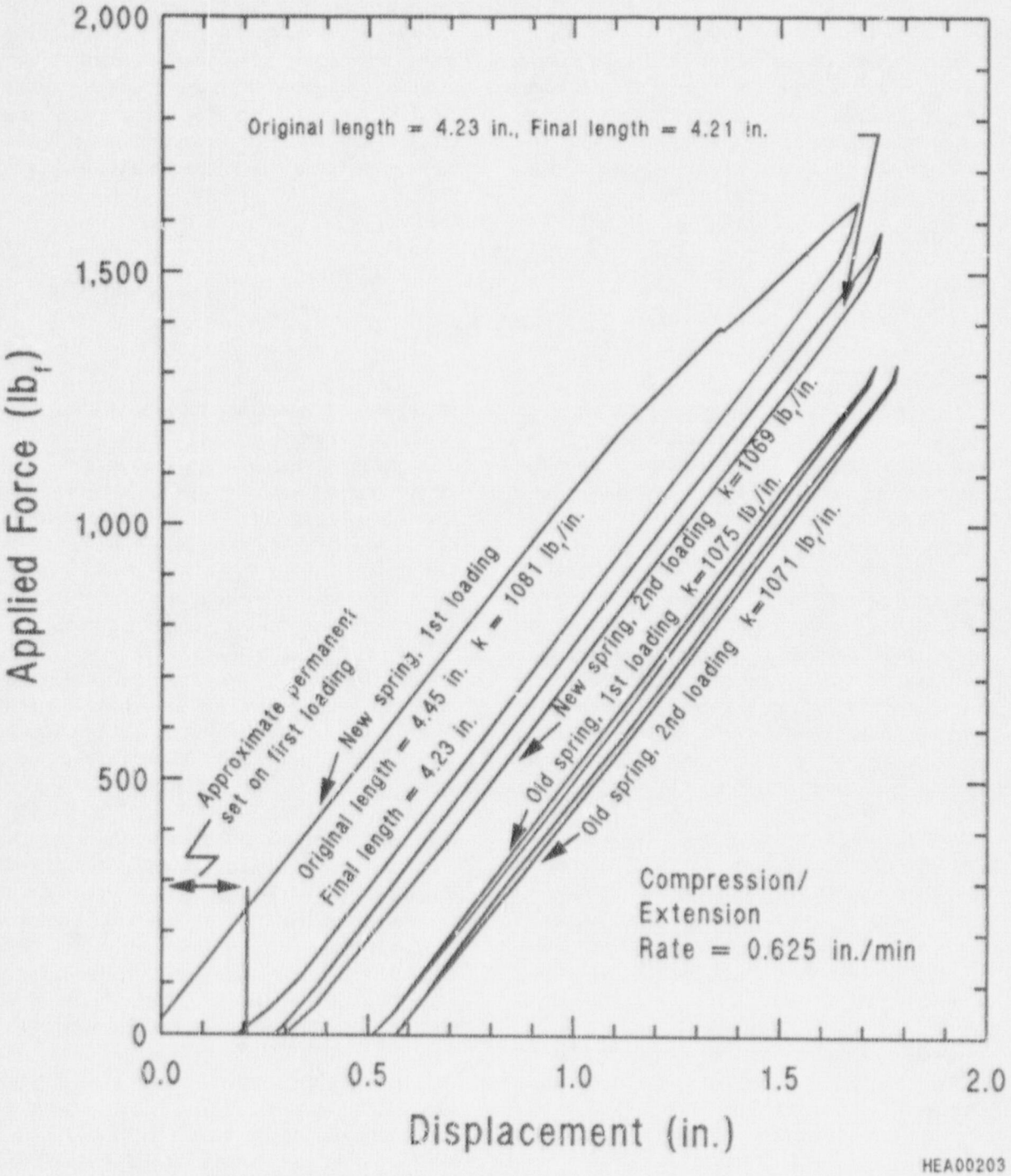

Figure A-21. Load testing of old and new torque springs.

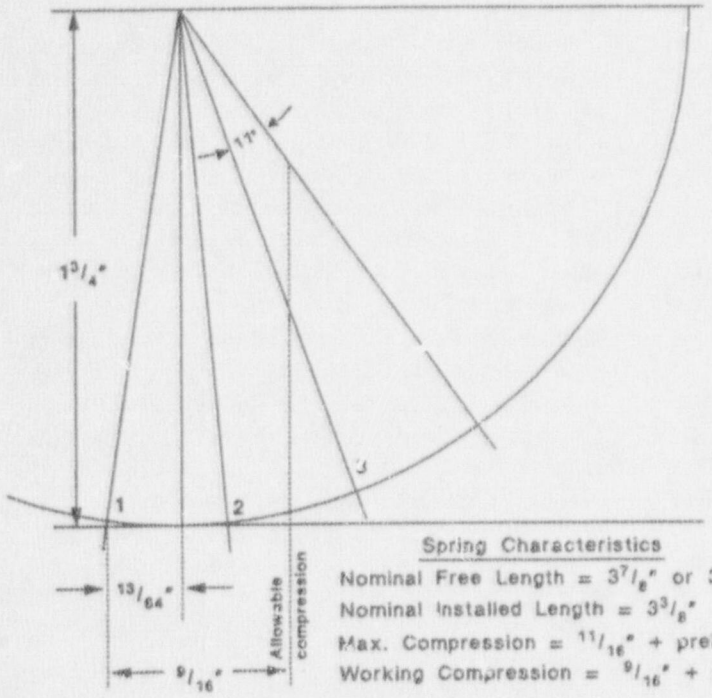

Motor Operator		
Torque Output		
Torque Switch Position	Spring comp. in inches from preload position	Output Torque ft–lbs
1	(Preload: equals .50)	415
1 1/2	.167	555
1 5/8	.207	587
2	.335	
2 1/2	.502	
2 3/4	.563	
Wire dia.		1/2"

* depending on date of manufacture

BMG00073

Figure A-22. Torque switch setting versus spring compression and torque output (ORNL valve).

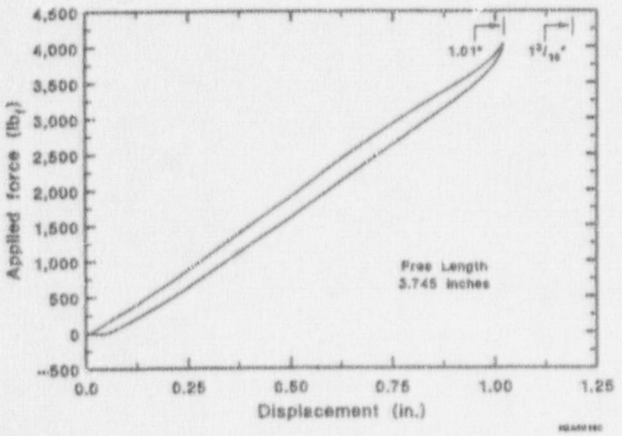

Figure A-23. Load testing of ORNL torque spring.

spring was used. Figure A-23 shows the load test for this spring. The total allowable elastic travel for this spring should be 1.188 or 1-3/16 in. plus or minus a small margin for tolerances. As can be seen from the load test, the spring went nonlinear at 1.01 in. The difference between the allowable installed travel (1.188 in.) and the load test travel (1.01 in.) provides a good indication the spring was originally 3-7/8 in. long and has nearly 3/16-in. permanent set. The ORNL valve, like the Shippingport valve, was a normally closed valve, which means the spring was normally in the compressed position for the life of service (>25 years). It is believed this near full time compression may accelerated spring aging.

MOTOR TESTING AT PEERLESS

The Limitorque dynamometer testing showed a marked improvement in motor performance over that obtained at HDR; however, it still did not meet the motor performance curve (Figure A-14) provided earlier by Limitorque for a motor similar to the one on the SMA actuator. The motor manufacturer, Peerless Winsmith, agreed to perform dynamometer testing on the motor alone to determine if the apparent reduced performance of the motor actuator was in the motor. Figure A-24 shows the results of the dynamometer testing of the motor. At motor loads of less than 30 ft-lb, the actual performance follows the predicted performance very well for both rpm versus load and current versus load. Above 30 ft-lb, the measurements of rpm versus load are fairly close to predicted values, but the current falls off, indicating that the motor is not meeting predicted load requirements. The higher torque loadings resulted in significant motor heating, with smoke coming from inside the motor. The motor was not permanently damaged by overheating during these high loadings, and time was allowed between each test for the motor to cool. At the request of the INEL, the dynamometer loadings were applied slowly to simulate the closing of a valve with a 15 second stroke time.

Another test was conducted to evaluate the effects of motor heating. Before the test, the motor load was adjusted to 45 ft-lb, and then the motor was cooled to ambient temperature. The motor was brought to speed without a load, and the preset load was then applied. The motor speed slowed immediately and stabilized within 2 seconds. Figure A-25 shows the results of this test. The load was applied for 20 seconds. Internal motor heating caused the motor to drop in current demand at 1 amp per second for 20 seconds. In round numbers, for each 2-amp reduction in demand, motor output is reduced by one ft-lb of torque. The motor output performance was reduced by 10 ft-lb in 20 seconds.

The engineers at Peerless supplied a motor performance curve for the subject motor (Figure A-26). Performance characteristics shown on this plot are similar to those shown on the one Limitorque had supplied earlier in the program (Figure A-14). Figure A-26 also shows the peak torque obtained in each of the parametric test programs.

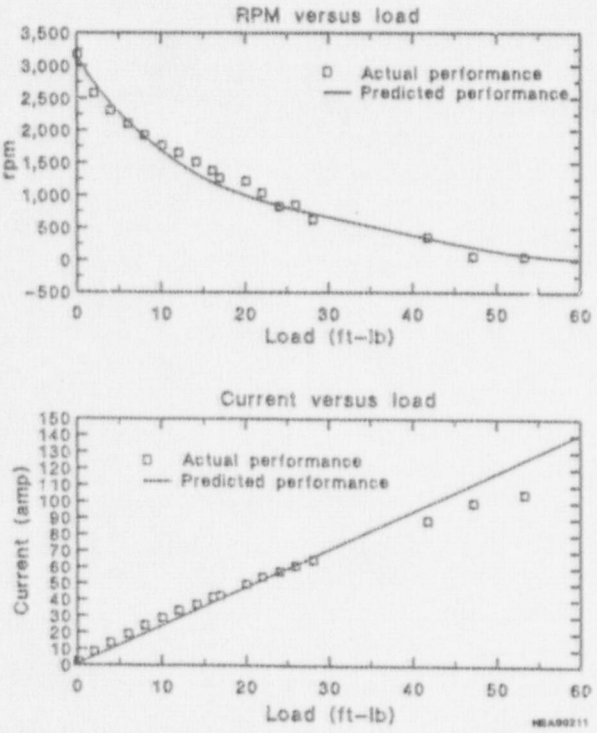

Figure A-24. Motor dynamometer testing at Peerless.

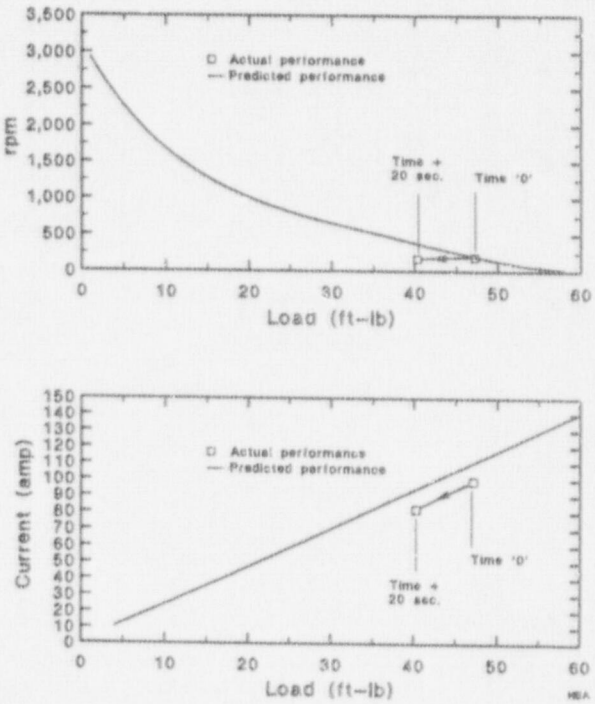

Figure A-25. Effects of motor heating on motor output.

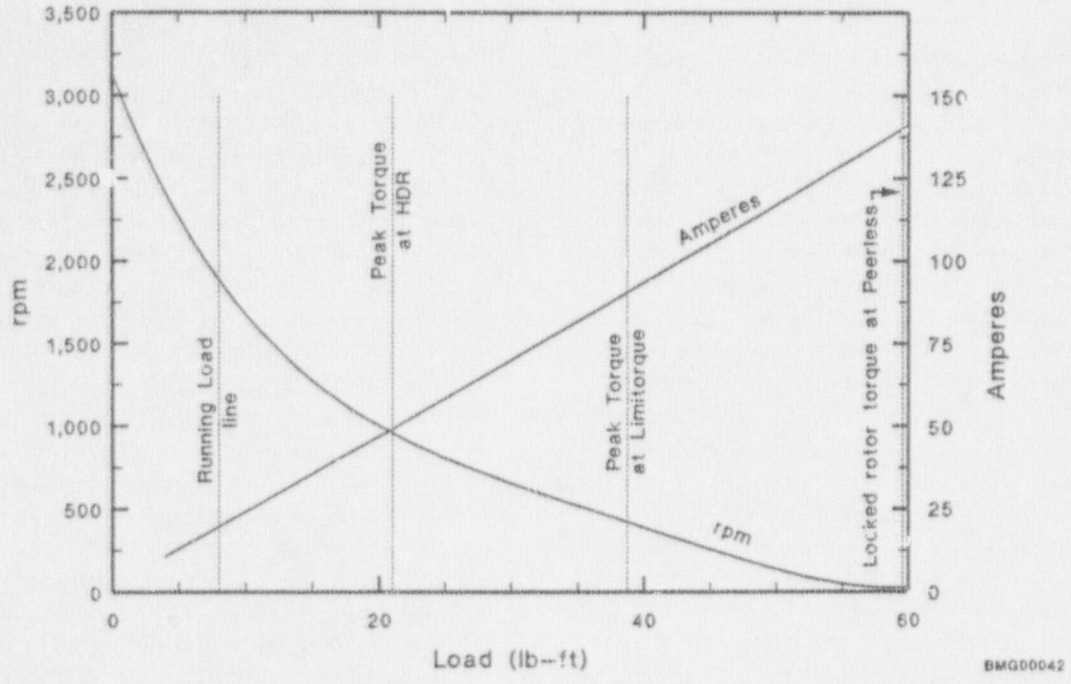

Figure A-26. Motor performance curve obtained from Peerless Motors and peak torque values obtained during testing.

ANALYSIS OF THE HDR POWER CIRCUIT

Concurrent with Limitorques assistance to the INEL, with the HDR investigation, a utility called upon Limitorque to assist with similar dc motor-actuated valve problems. The utility was a two unit station, and all of the dc powered valve problems were associated with one unit. Several control circuit problems were found during the investigation, and the root cause of the dc motor failures had been attributed to those problems. Interestingly, the power cables in the unit having problems were smaller than those in the other unit. However, this difference was not highlighted in the investigation.

Shortly afterwards, Limitorque published a maintenance letter that contained an electrical circuit calculation basis for dc motor operated valves. This calculation was developed from Limitorque's investigations of dc motor problems at HDR and at the utility mentioned above. In most dc motor operated valve control circuits, the armature coil and the series fields are interconnected through the motor controller, and four power cables must be considered in the calculation, not two as one might assume. Limitorque recommended using this calculation to determine voltage drop instead of trying to measure the voltage drop in the circuit; in attempts to measure the ltage drop, it is very difficult to load the circuit and m the various voltage drops.

From this new methodology we developed an analytical model for the HDR valve power circuit to determine the influence of external circuit resistance on the HDR valve anomaly. The HDR in situ tests and the Limitorque tests were chosen for comparison, as the motor operator was operated a comparable number of times over a short period of time at both locations and the size of the large external circuit cabling at Limitorque should eliminate the influence of any external circuit resistance. Two different calculations of the HDR power conductor resistance were made: one was based on the size and approximate length of the cables, and the other on measurements of the current through the circuit and the voltage drop across the portion of the circuit that was measured. The calculations were comparable. Four times the calculated resistance for a single cable was inserted in the analytic model to account for the armature and the field being connected in series through the motor controller. The measured parameters from the HDR in situ testing and the Limitorque dynamometer testing were then analyzed and actual motor resistances calculated. Very good comparisons were found. The results demonstrate that the differences between the motor operator performance at HDR and the performance at Limitorque were caused by external circuit resistances.

These results point out the significance of the external circuit resistance and motor heatup in reducing the safety margins of motor operator torque output. The motor operator operated successfully with no pressure, static pressure alone, and with static pressure and very low differential pressure. When the differential pressure from the flow load was increased, the valve either failed to close all the way or the operator motor stalled, depending on the torque switch setting.

To understand this phenomenon, one must understand dc motors. These motors generate a back electromotive force (EMF) when turning. This back EMF acts like a bucking voltage in the circuit. Stated in very simple terms, this back EMF limits the current in the circuit much the way a resistance would. The back EMF is proportional to the motor speed and current. These high-torque compound-wound motors have a weak shunt field and act very much like a series wound motor in application. As the load is increased the motor slows down, reducing the back EMF. This allows more current to flow, thus producing higher torque. This behavior continues down to motor stall, where the dc resistance of the motor is the only internal resistance to current flow. These motor resistances at or near locked rotor are in the 1.0 to 1.5 ohm range for a 40 to 60 ft-lb output torque motor operating on 125 Vdc. Because the field and armature cabling are connected in series through the motor controller, four long cable runs, not two, contribute to the resistance of the external circuit. External circuit resistance of just 0.5 to 1.0 ohm can reduce the motor output torque by 1/3 to 1/2.

During normal valve testing or operation, the resulting motor loadings are in the 20 to 30% running torque range. The back EMF or effective motor resistance would be approximately 5 ohms, and a 0.5 to 1.0 ohm external resistance would not significantly degrade motor performance. This conclusion was supported by the results of the HDR static pressure testing. However, during a transient or a line break where isolation is required, the high differential pressure across the valve disc would require a higher motor output, and the external circuit resistance in series with the motor resistance could reduce the output torque of the motor significantly, as it did at the HDR during tests with flow loads.

At the end of our investigation of the valve's anomalous performance at HDR, we had identified three separate problems. The potential safety implications of these problems are significant. Spring aging can result in a valve that torques out early and, depending on the extent of the degradation, can leave the valve partially open. Aged coil springs in the older SMA motor operators may go undetected, as there are fewer diagnostic test systems adaptable to these units. Motor heating can reduce motor operator output if valve is cycled more than once without time for the windings to cool. If a marginally powered valve is subjected to high loads on closing, this reduced output can result in motor stall, probably with the valve partially open. External circuit resistance also can cause the motor to stall before the valve fully closes. Motor stall can cause the thermal overload switches to open and render the motor operator temporarily unavailable for use. If the thermal overload switches have been bypassed or set too high, or if they malfunction, the motor will burn out. Both the SMA and the newer SMB operators with dc motors and high external circuit resistance can go undetected in normal in situ valve testing.

The HDR anomaly would not have been discovered in normal plant testing, where valves are tested without hydraulic loading and usually stroke time change is the go or no go criterion. The problems are detectable only at higher loadings when the motor is slowed down and momentum cannot carry the unit through torque out. Flow loads in combination with static pressure stem rejection loads present a more demanding load on motor operators than do stem rejection loads alone. The data and the design of a Limitorque operator tend to cast some doubt on the validity of using opening loads to predict closing loads. When the valve opens, the dog that creates the hammer blow allows the motor to come to speed prior to engaging the stem drive gear; the hammer blow then assists in breaking friction, and the stem rejection load then assists in opening the valve. Adding two times the stem rejection load to this load in calculations will not account for the motor slowdown and the decreased efficiency of the unit. Motor speed and total actuator momentum appear to be important factors in predicting valve closure. The concerns expressed here for dc motors are not limited to the SMA design. The newer SMB have the same motor design as the SMA.

SUMMARY OF RESULTS AND ANALYSIS

The initial failure of the valve at the HDR to close completely, even at stall currents, when exposed to the higher hydraulic loadings was caused by the combined influences of undersized power cables, motor heating, loss of motor momentum due to motor slowdown, and loss of gear efficiency due to actuator slowdown near the fully closed position.

A good example of undersized power cables and motor heating can be seen from tests 42 and 42A (see Table A-2). Test 42 was the first test run with pressure and flow loads after motor field rewind, and the motor was at ambient temperature. The torque out current was 42.5 amps, and the valve closed to within 0.2 inches of being fully closed. The 42.5 amps is less than it should have been and is a result of the voltage drop in the undersized cables. During the very next cycle, test 42A, the torque out current was 29 amps, and the valve closed to within 0.3 inches of being fully closed. The 25 amp closing shows the combined affect of undersized cables and motor heating. Test 42 was the only test where an ambient-temperature motor was known to be subjected to a maximum flow and pressure load. The degradation shown in test 42A is significant. Two full cycles on the valve are equivalent to one minute of motor operating time with a 15 second average stroke time.

The motor test at Peerless shows the motor performs very close to design, except at the higher loads, where heating starts to reduce performance. The peak performance differences between the Limitorque dynamometer tests and the Peerless motor dynamometer tests are due to motor heating, and they are fairly significant: 75 amps versus 105 amps at motor stall.

Because of motor slow down under load, there was no momentum to assist in compressing the torque spring. This total unit loss of efficiency could be very significant in marginally powered units in the field. The HDR static pressure loadings during the elevated temperature test were equal to the original valve design pressures, but static pressure loadings during all other tests were much lower than design. The maximum VKL flow of 360 gpm is a very small flow for an 8-in. valve. The valve performed poorly even when pressure and flow loads were well below design loads (see Figures A-15, A-16, and A-17).

The degraded torque output versus torque switch position was caused by a short torque spring. Maximum torque switch settings during the HDR tests were not high enough to cause the permanent set in the torque spring. The initial dynamometer test at Limitorque isolated the problem. The highest torque switch settings in subsequent dynamometer tests did enter into the permanent set travel range; however, tests following the high torque switch tests do not show further degradation.

It is unknown how many SMA operators there are installed in nuclear plants. The SMA operator was manufactured from the mid-1950s to the mid-1960s, when it was replaced by the SMB design. Four plants are known to have SMA operators in 33 applications: Haddam Neck (16), Oyster Creek (9), Nine Mile Point (2), and San Onofre (6).

Discussions at the review group meetings indicated that in the 20 plus years since the SMA design has been manufactured, considerable experience and information acquired in the field and at Limitorque on this design has been lost. A large part of the work in trying to determine the root cause of the valve functional anomaly was spent by the INEL and Limitorque learning the design characteristics of these operators. Additionally, the dc motor is not as common as the ac motor, and less is understood about its performance characteristics under extreme loadings.

Other work is underway that will address some of the issues of this report. The current work and research being performed for IE Bulletin 85-03 and Generic Issue 87 are programs designed to determine valve closure requirements under extreme loads. In the follow-on HDR testing, the dc motor on the HDR SMA motor operator was changed out to an ac motor of the same horsepower rating. Those tests will allow us to compare the performance of ac- and dc-powered motor operators.

CONCLUSIONS AND RECOMMENDATIONS

Failure of the HDR valve to close under certain hydraulic and pressure loadings was due to a combination of problems, including a) undersized power cables, b) motor heating, c) torque spring aging, and d) loss of motor operator momentum at load.

One can analyze power cables for possible undersizing using a procedure recommended by Limitorque that considers the length of the four cables and the peak power of the motor. The effects of motor heating can be estimated. Those effects should be included in the motor operator motor sizing calculation.

Torque spring aging can be detected on some SMA and SMB type motor operators by a simple torque wrench handwheel test. Others will require that the springs be removed, measured, and compared to the length specified in the original drawings.

Motor operator momentum should not be a problem in a correctly sized and adequately powered motor operator. However, it is something that must be considered in testing and analysis of dc-powered motor operators.

The HDR anomaly would not have been discovered in normal plant testing, where valves are tested without hydraulic loading and usually a stroke time change is the go or no go criterion. Flow loads in combination with static pressure stem rejection loads appear to present a more demanding load on motor operators than do stem rejection loads alone. The data and the design of a Limitorque operator tend to cast some doubt on the validity of using opening loads to predict closing loads. When the valve opens, the dog that creates the hammer blow allows the motor to come to speed prior to engaging the stem drive gear; the hammer blow then assists in breaking friction, and the stem rejection load then assists in opening the valve. Adding two times the stem rejection load to this load in calculations will not account for the motor slowdown and the decreased efficiency of the unit. Motor speed and total actuator momentum appear to be important factors in predicting valve closure. The concerns expressed here for dc motors are not limited to the SMA design. The newer SMB have the same motor design as the SMA.

APPENDIX B
INSTRUMENTATION OF THE VKL FOR THE SHAG TEST SERIES

APPENDIX B
INSTRUMENTATION OF THE VKL FOR THE SHAG TEST SERIES

Appendix B provides details with respect to the VKL instrumentation for the SHAG test series. Figure B-1 indicates instrument locations for the U.S. stiff configuration; Table B-1 identifies the type and number of instruments at each location. INEL and KfK divided instrument responsibilities on the VKL. Staatliche Materialprüfungsanstalt (MPA) of the Universitat Stuttgart assisted INEL in installing strain gages and instrumentation cables and recording test data from a portion of the instruments. INEL installed the U.S. instruments and recorded test data for a portion of the instrumentation. HDR installed all KfK instrument cables and recorded all of their data. KfK was responsible for providing a single set of data tapes with a unified time base for all participants.

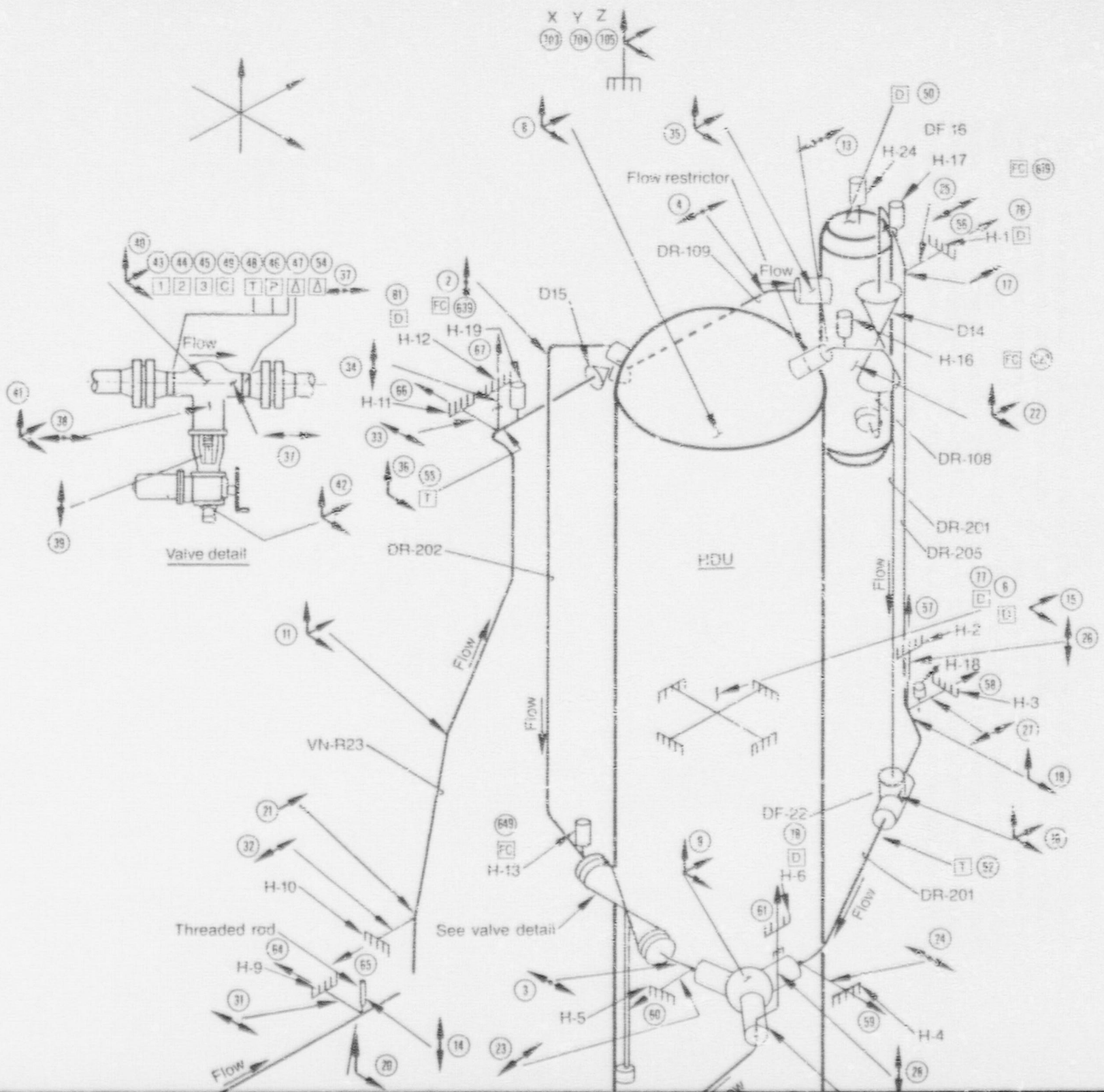
X Y Z
Flow restrictor
DF-15
H-24
H-17
H-1
DR-109
Flow
D15
D14
H-16
DR-108
DR-201
DR-205
DR-202
HDU
Valve detail
H-19
H-12
H-11
H-2
H-18
H-3
VN-R23
DF-22
H-6
DR-201
H-13
See valve detail
Threaded rod
H-10
H-9
H-5
H-4
Flow

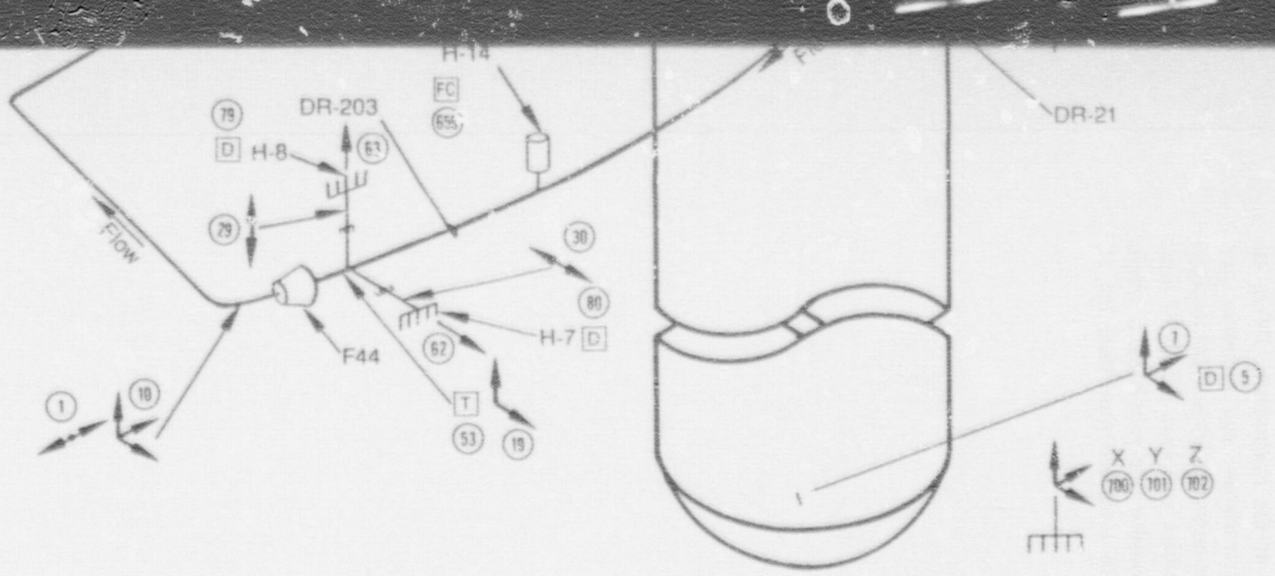

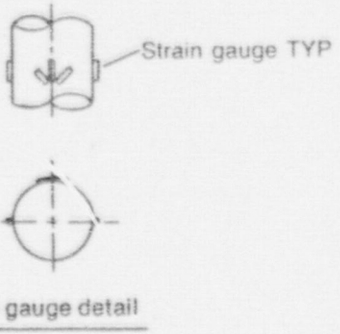

Strain gauge detail

Legend

- Accelerometer and its detection axis
- Single strain gauge and its detection axis
- Strain gauges (see strain gauge detail)
- D Displacement gauge
- P Pressure
- Δ ΔP
- 1 Valve position
- 2 Valve current
- 3 Valve voltage
- T Temperature
- F Flowrate
- C Video camera
- FC Force

7-8578

Figure B-1. HDR Instrumentation.

Table B-1. Detailed U.S. and German Instrumentation

Location Number	Instrument Type	German	U.S.	Remarks
1	Strain	6	—	Bending elbow
2	Strain	6	—	Bending nozzle DR202
3	Strain		—	Bending transition between valve and spherical tee
4	Strain	6	—	Bending nozzle DR109
5	Displacement	2(XZ)	—	—HDU rocking
6	Displacement	2(XZ)	—	—HDU rocking
7	Acceleration	3(XYZ)	—	HDU response bottom
8	Acceleration	3(XYZ)	—	HDU response top
9	Acceleration	3(XYZ)	—	—Spherical tee response
10	Acceleration	3(XYZ)	—	—Elbow response
11	Acceleration	3(XYZ)	—	—Piping response
12	Was not installed owing to discontinuities in piping and nozzle.			
13	Strain	—	6	Nozzle loads DR201
14	Strain	—	1	Threaded rod
15	Acceleration	—	2(XZ)	Impact/load input HDU
16	Acceleration	—	3(XYZ)	Mass response normal tee
17	Acceleration	—	1(X)	Support location U.S. H-1
18	Acceleration	—	2(YZ)	Support location U.S. H-2, H-3
19	Acceleration	—	2(YZ)	Support location U.S. H-7, H-8
20	Acceleration	—	2(YZ)	Support location U.S. H-9 and threaded rod
21	Acceleration	—	1(X)	Support location U.S. H-10
22	Acceleration	—	3(XYZ)	Manifold input mass and other piping (DF16)
23	Strain	—	1(X)	Support H-5
24	Strain	—	1(Z)	Support H-4
25	Strain	—	1(X)	Support H-1
26	Strain	—	1(Y)	Support H-2
27	Strain	—	1(X)	Support H-3
28	Strain	—	1(Y)	Support H-6
29	Strain	—	1(Y)	Support H-8
30	Strain	—	1(Z)	Support H-7
31	Strain	—	1(Z)	Support H-9
32	Strain	—	1(X)	Support H-10
33	Strain	—	1(Z)	Support H-11
34	Strain	—	1(Y)	Support H-12
35	Acceleration	3(XYZ)	—	DF16 nozzle
36	Acceleration	—	2(YZ)	Support location U.S. H-11, H-12
37	Strain	—	6	Valve nozzle loads
38	Strain	—	6	Valve body loads
39	Strain	—	2	Valve shaft axial forces
40	Acceleration	—	3(XYZ)	Valve body centerline
41	Acceleration	—	3(XYZ)	Valve/actuator center of gravity
42	Acceleration	—	3(XYZ)	Valve Actuator
43	Valve position	—	3	Variable/limit stops
44	Valve current	—	1	Motor current
45	Valve voltage	—	1	Motor voltage
46	Pressure	—	1	Valve inlet pressure
47	Differential	—	1	Pressure across valve pressure
48	Temperature	—	1	Fluid temperature at valve
49	Video camera	—	1	Visual valve monitor
50	Displacement	—	1(Y)	Thermal growth at DF16

Table B-1. (continued)

Location Number	Instrument Type	German	U.S.	Remarks
51	Accelerometer	—	1	Valve noise
52	Temperature	—	1	System thermal response normal tee
53	Temperature	—	1	System thermal response H-7
54	Pressure	—	1	Valve internal measurement
55	Temperature	—	1	System thermal response H-11
56	Acceleration	—	1(X)	HDR structure (H-1)
57	Acceleration	—	1(Y)	HDR structure (H-2)
58	Acceleration	—	1(X)	HDR structure (H-3)
59	Acceleration	—	1(Z)	HDR structure (H-4)
60	Acceleration	—	1(X)	HDR structure (H-5)
61	Acceleration	—	1(Y)	HDR structure (H-6)
62	Acceleration	—	1(Z)	HDR structure (H-7)
63	Acceleration	—	1(Y)	HDR structure (H-8)
64	Acceleration	—	1(Z)	HDR structure (H-9)
65	Acceleration	—	1(X)	HDR structure (H-10)
66	Acceleration	—	1(Z)	HDR structure (H-11)
67	Acceleration	—	1(Y)	HDR structure (H-12)
68	Force	—	1(−X)	Cloud impact (H-1)
69	Force	—	1(−Y)	Cloud impact (H-2)
70	Force	—	1(−Y)	Cloud impact (H-6)
71	Force	—	1(+Z)	Cloud impact (H-7)
72	Force	—	1(−Z)	Cloud impact (H-7)
73	Force	—	1(+Y)	Cloud impact (H-7)
74	Force	—	1(−Y)	Cloud impact (H-7)
75	Force	—	1(−Y)	Cloud impact (H-12)
76	Displacement	—	1(X)	Pipe displacement at snubber location (H-1)
77	Displacement	—	1(Y)	Pipe displacement at snubber location (H-2)
78	Displacement	—	1(Y)	Pipe displacement at snubber location (H-6)
79	Displacement	—	1(Y)	Pipe displacement at snubber location (H-8)
80	Displacement	—	1(Z)	Pipe displacement at snubber location (H-7)
81	Displacement	—	1(Y)	Pipe displacement at snubber location (H-12)
87	Force	—	1(+Y)	Cloud impact (H-12)
88	Force	—	1(+Y)	Cloud impact (H-6)
700-1-2	Acceleration	3(XYZ)	—	HDR structure near HDU bottom
703-4-5	Acceleration	3(XYZ)	—	HDR structure near HDU top
619	Force	1(Y)	—	Spring hanger UD 20-1-6
629	Force	1(Y)	—	Spring hanger UD 20-5-8
639	Force	1(Y)	—	Spring hanger UD 50-1-1
649	Force	1(Y)	—	Spring hanger (H-13)
659	Force	1(Y)	—	Spring hanger UD 20-3-2

APPENDIX C

INVESTIGATION OF SNUBBER MALFUNCTIONS

APPENDIX C
INVESTIGATION OF SNUBBER MALFUNCTIONS

INTRODUCTION

The HDR experiments provided a very good place to test snubbers in an in situ environment. The results address some of the functional problems encountered by snubbers in response to seismic loading. The information produced by the HDR tests can provide additional technical input to the NRC effort to finalize snubber test requirements. This appendix describes the snubbers used in the HDR tests and reports the poor performance of the INC snubbers.

SNUBBER DESCRIPTIONS

Snubbers have two proper functions: (a) they should move freely at low accelerations and (b) they should resist motion (a state commonly referred to as "lock up") at higher accelerations. They are frequently used in areas where piping must be allowed to undergo free thermal expansion movement, but where clearance is limited or where inertial movements caused by seismic or hydrodynamic events must be restrained because of stress considerations. Mechanical snubbers can malfunction either by failing to lock up when they should, such as during a dynamic event, or by locking up when they should allow movement to accommodate thermal expansion of the piping. Hydraulic snubbers can develope leaks, lose their fluid and fail to lock up when they should.

Snubbers are of two basic types: hydraulic and mechanical. The hydraulic type includes a double-acting cylinder, a flow control device, and a hydraulic fluid reservoir (Figure C-1). During slow movements, such as when piping experiences free thermal expansion, hydraulic fluid passes from one side of the piston to the other. However, at higher load rates the flow of fluid is restricted and motion is limited. Hydraulic snubbers are velocity controlled. Release rate velocities are controlled by bypass flow circuits or through leakage inherent in the flow control device. An external reservoir accommodates the thermal expansion of the fluid and volumetric changes during snubber motion. It also provides reserve fluid.

Figure C-2 illustrates a Pacific Scientific mechanical snubber, which is the most popular mechanical snubbers. Any movement of the pipe to which the snubber is connected causes a compressive or tensile load into the left end of the snubber. This force is converted from linear motion to rotary motion by means of a ball screw. The ball screw is keyed to a torque transfer drum that surrounds a capstan spring and causes it to rotate also. The two ends of the capstan spring protrude through a slot in the torque transfer drum and contact shoulders located on the inside of the inertia mass. When the torque transfer drum turns, it bears against one end of the capstan spring and moves it. The opposite end of the capstan spring bears against the inertia mass, which turns on a bearing. If an acceleration greater than approximately 0.02 g is imposed, the torque carrier (the ball screw and the torque transfer drum) attempts to accelerate also. Because of its inertial resistance, the inertial mass will resist acceleration. This causes a relative angular displacement between the torque carrier and the inertial mass, which tightens the capstan spring around a mandrel that is an integral part of the main housing; thus, the constricting action creates a braking force. When the acceleration drops below 0.02 g, the inertia mass no longer exerts sufficient force to limit motion, and the capstan spring relaxes.

Figure C-3 illustrates a second mechanical snubber design, an International NuclearSafeguards Company (INC) snubber. The function of this snubber is similar to the Pacific Snubber; however, the lockup is not as soft. The INC snubber incorporates a nonrotating screw that moves through a rotating nut, integral adapter, and friction plate. The friction plate is maintained between fixed flanges, at a minimal clearance, by a centering spring. For normal operation, the thermal growth of the piping or attached equipment is accommodated by the linear translation of the screws, which rotates the nut-adapter assembly and causes a change in the effective strut length. For this operating mode, the frictional areas are in a maintained

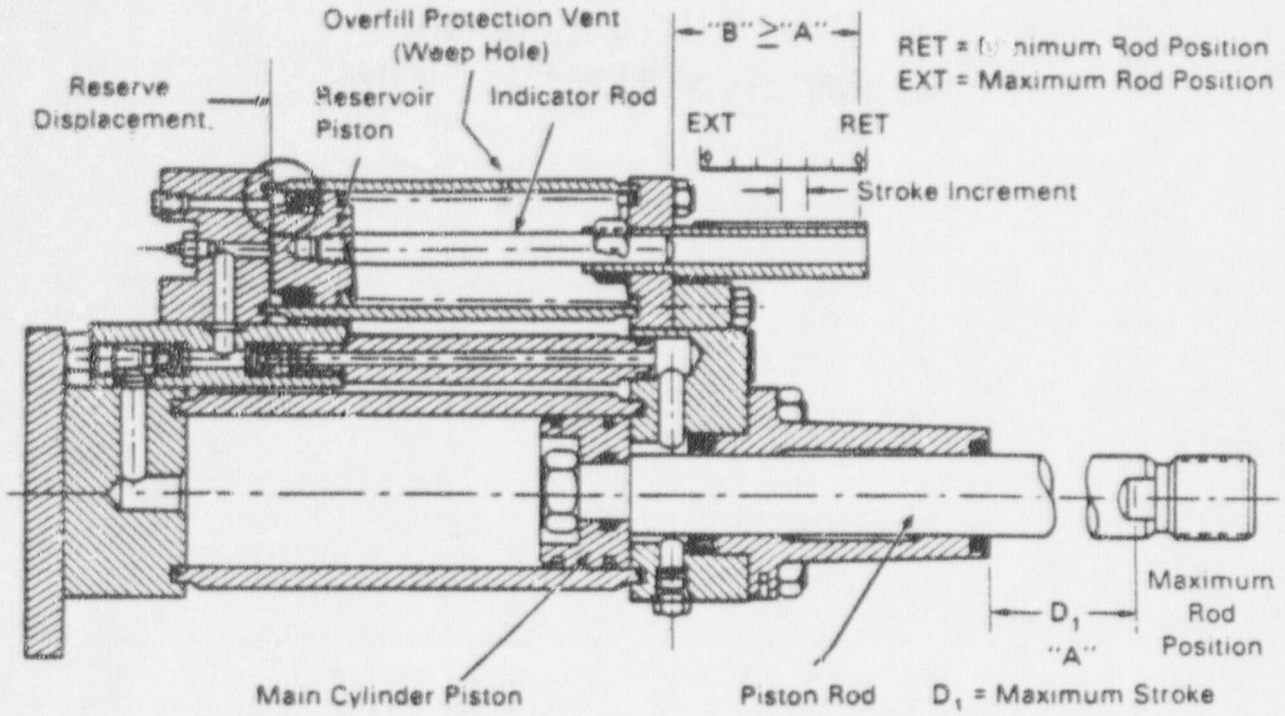

Figure C-1. Schematic of hydraulic snubber.

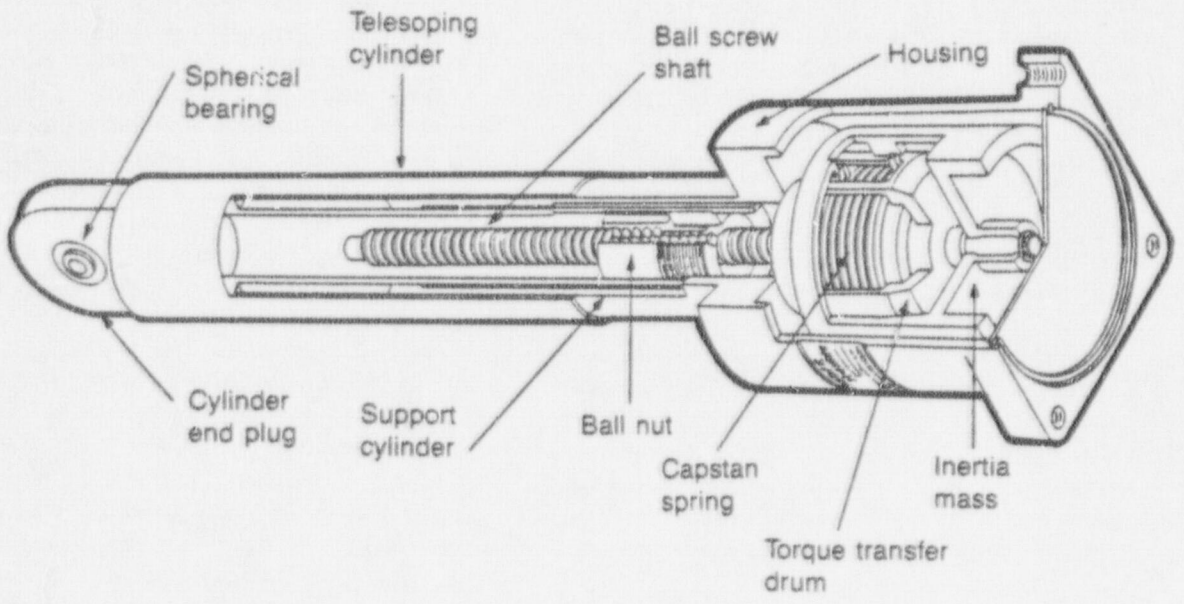

Figure C-2. Schematic of Pacific Scientific mechanical snubber.

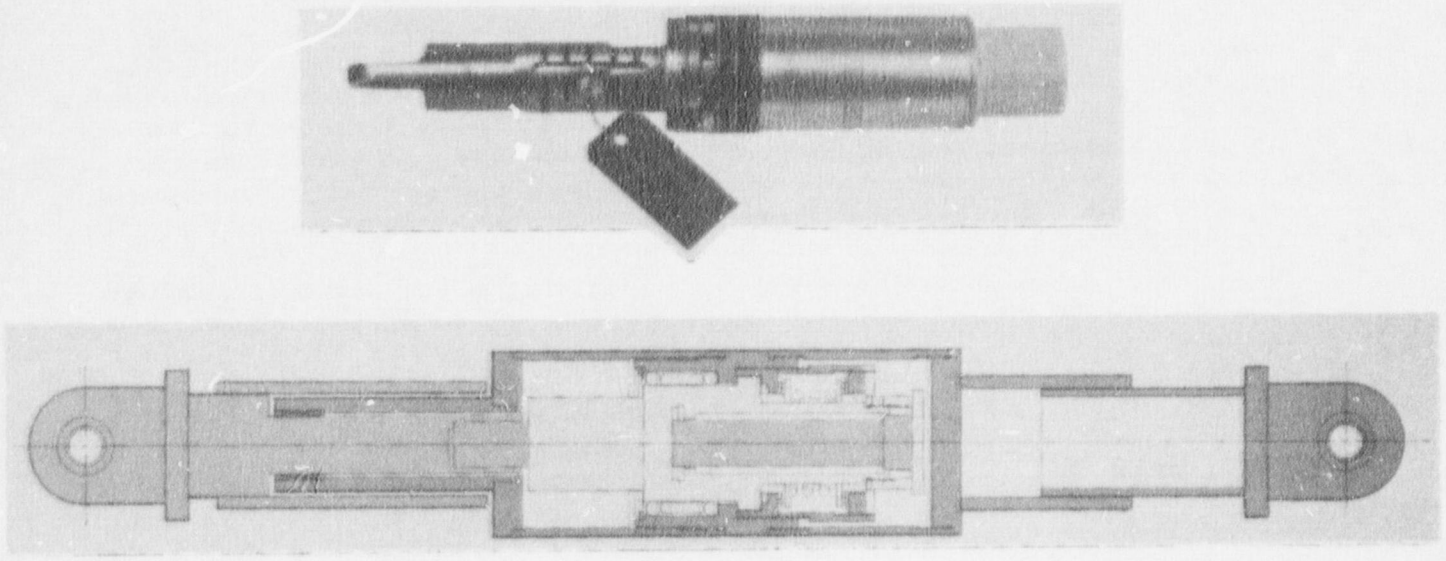

Figure C-3. Schematic of International NuclearSafeguards Company (INC) mechanical snubber.

position owing to the reactive force of the centering spring. When subjected to a shock loading, the inertia of the nut-adapter causes the centering spring to compress, resulting in a mating of the friction surfaces and a consequent resistance to the externally applied force.

Both types of snubbers were used in the U.S. stiff pipe support system—five mechanical snubbers and one hydraulic snubber. Originally, four of the mechanical snubbers were of INC design, and the fifth was manufactured by Pacific Scientific. Because of their erratic performance during the preliminary tests, the INC snubbers were replaced by Pacific Scientific snubbers for the remaining tests. The hydraulic snubber was produced by Bergen-Patterson. Table C-1 defines the snubbers used in the tests. The INC snubbers were located in positions H-6, H-7, H-8, and H-12 during the preliminary tests.

Table C-1. Snubber descriptions

Support Location	Direction	Snubber Model	Snubber Type
H-1	Horizontal and perpendicular to horizontal run	Pacific Scientific PSA-1	Mechanical
H-2	Vertical	Bergen-Patterson 2525-10	Hydraulic
H-6	Vertical	Pacific Scientific PSA-1	Mechanical
H-7	Horizontal and perpendicular	Pacific Scientific PSA-3	Mechanical
H-8	Vertical	Pacific Scientific PSA-1	Mechanical
H-12	Vertical	Pacific Scientific PSA-1	Mechanical

EVALUATION OF INC SNUBBER PERFORMANCE

Because the INC snubbers were installed only during the preliminary shakedown tests, acceleration measurements are not generally available; thus, only measured displacement and force are reported and analyzed here.

The four snubbers manufactured by INC, an affiliate of Bergen Pipe Support Corporation, U.S.A., were originally NRC-owned spares for the Loss of Fluid Test (LOFT) Facility at the INEL. The four snubbers were all model MSVA AS, one a size 1, and three a size 2. The four units were all N-stamped and met all requirements for installation in a nuclear plant.

The snubber locations suspected of reduced performance were H-6, H-7, H-8, and H-12. Snubbers at H6, H-7, and H-8 were MSVA-SA-size 2; the snubber at H-12 location was size 1.

Figures C-4 through C-7 compare force and displacement at the four snubber locations for test T40.34. The displacement time histories indicate that in each case there was sufficient motion at each snubber location to activate the snubber. The histories also indicate that the displacements got larger when snubbers quit operating. The force histories show when a snubber was resisting motion and when it was not. They also provide evidence of the maximum force at which each snubber reacted. These forces are all less than normal and upset design loads specified by the manufacturer.

Figure C-8 compares the force time history recorded at the Pacific Scientific snubber located at H-1 with the force history recorded at the INC snubber located at H-6 during test T40.34. The snubber at H-1 resisted motion, as shown in the force history, whereas the snubber at H-6 performed erratically.

The displacement histories provide evidence there was sufficient motion of the piping to cause the snubbers to operate beyond the time at which they failed. The displacement histories associated with the erratic snubber performance show that displacement increases during the time that snubber performance decreases. Acceleration time histories from later tests, recorded at the same locations and shaker starting frequencies, verify that sufficient motion was available to actuate the snubbers.

The posttest visual examination and manual actuation of the snubbers provided no insight into the malfunctions of the snubbers. The snubbers that performed erratically when installed in the VKL system performed erratically also when tested manually after removal from the system.

During our investigation, we discussed the snubber problem with snubber vendors and staff from the NRC Office for Analysis and Evaluation of Operational Data (AEOD). The discussions verified our conclusions. The company is now out of business, and apparently most, if not all, of the INC snubbers in nuclear plants have been replaced. AEOD also said that IE had issued several reports and bulletins concerning snubbers in general, but none specifically warning of problems with INC devices. Further notice may be needed to ensure all INC snubbers have been replaced.

Comparison of the responses of the hydraulic snubber at H-2 and the Pacific Scientific mechanical snubber at H-1 with the responses of the INC snubbers provided evidence that the INC snubbers were not performing to design requirements. The snubbers were removed and manually checked for operation. Each performed erratically when exercised by hand. The snubbers were replaced by mechanical snubbers provided by Pacific Scientific Company.

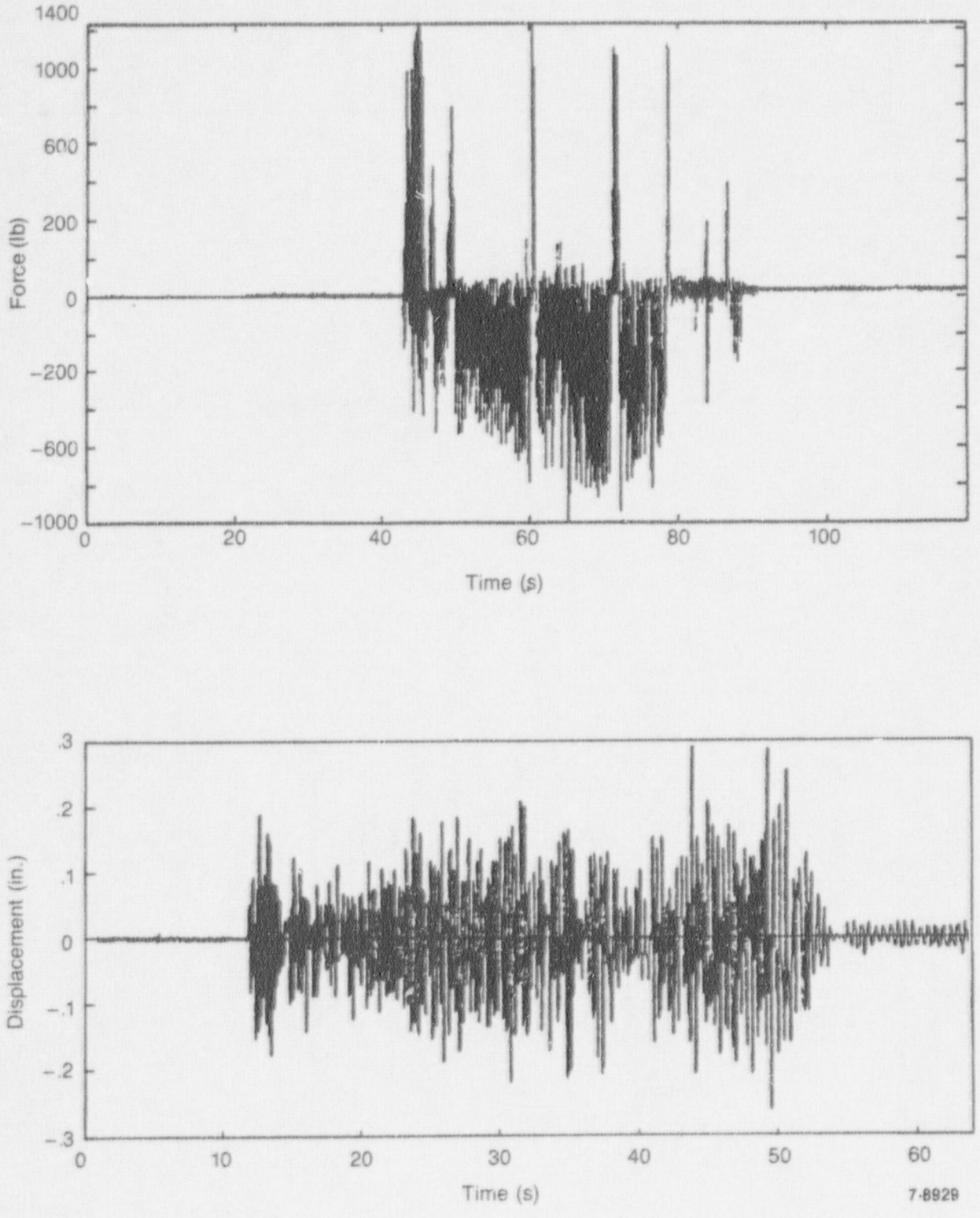

Figure C-4. Comparison of force and displacement at support location H-6. Note the erratic behavior of the snubber from 45 to 80 s. The snubber is locking up only in the negative direction throughout most of this period.

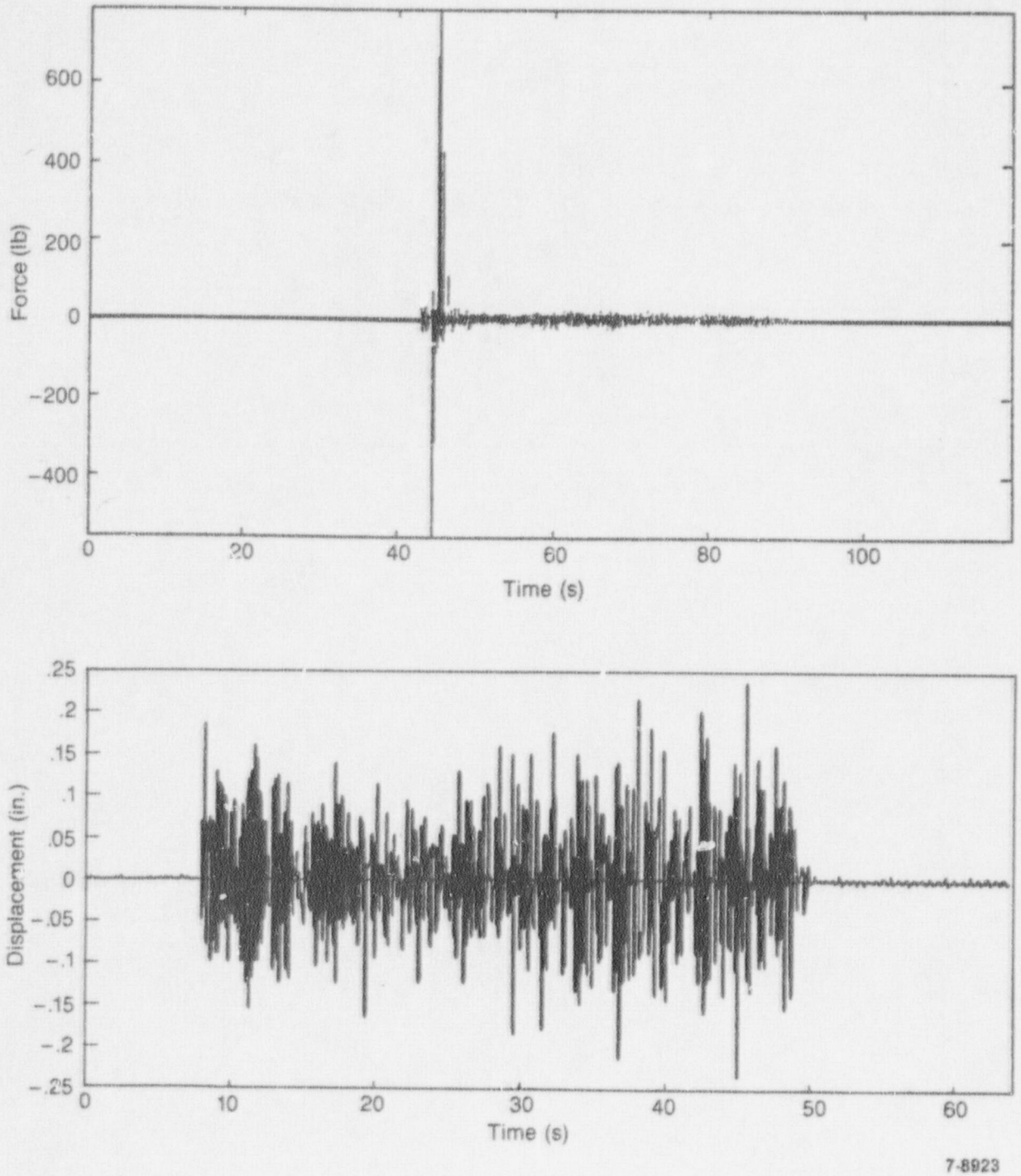

Figure C-5. Comparison of force and displacement at support location H-8. This snubber resisted motion for only 2 or 3 s.

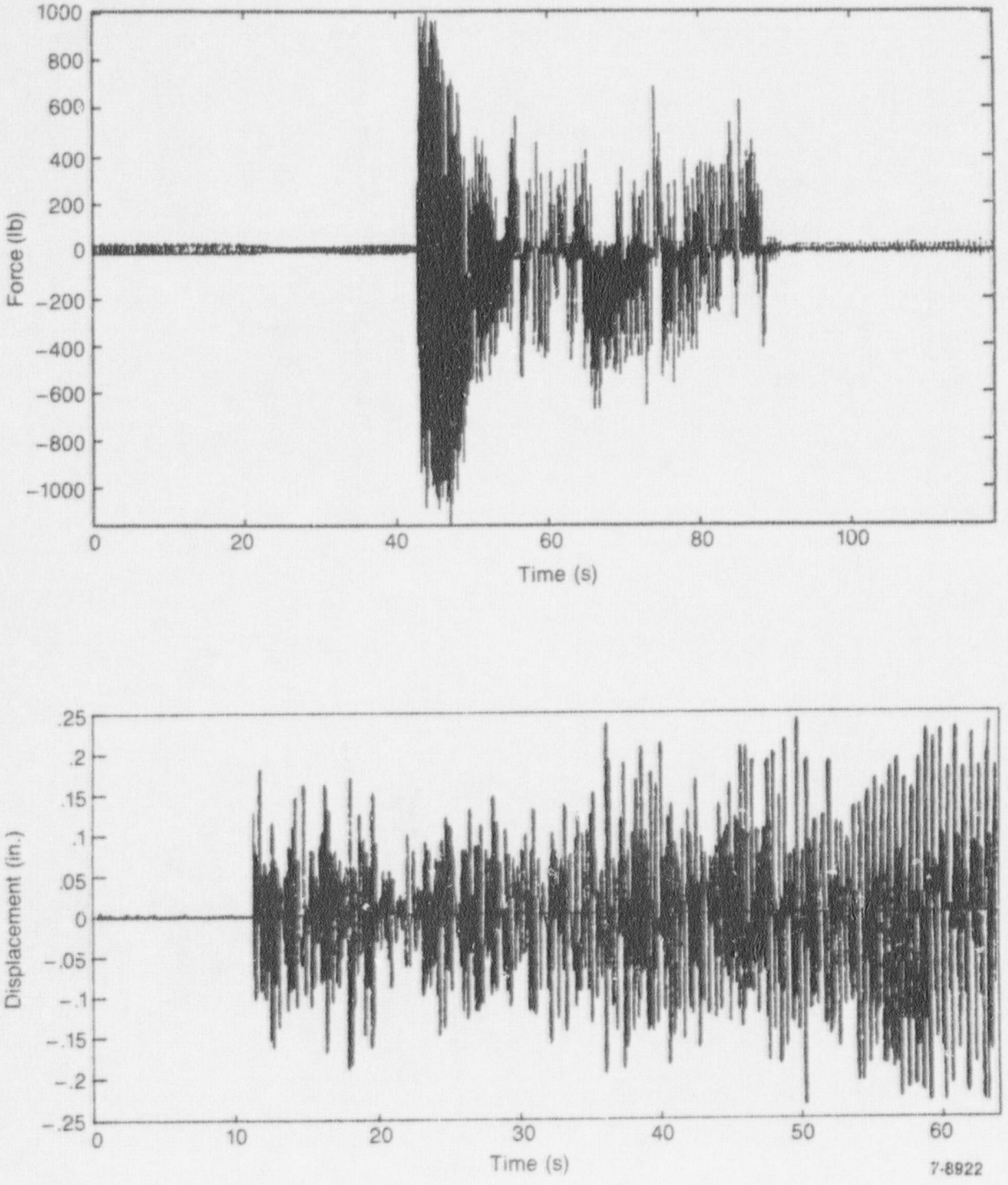

Figure C-6. Comparison of force and displacement at snubber location H-7. This snubber performed reasonably well from 40 to 80 s. Note that as the snubber performance becomes more erratic, the displacement increases.

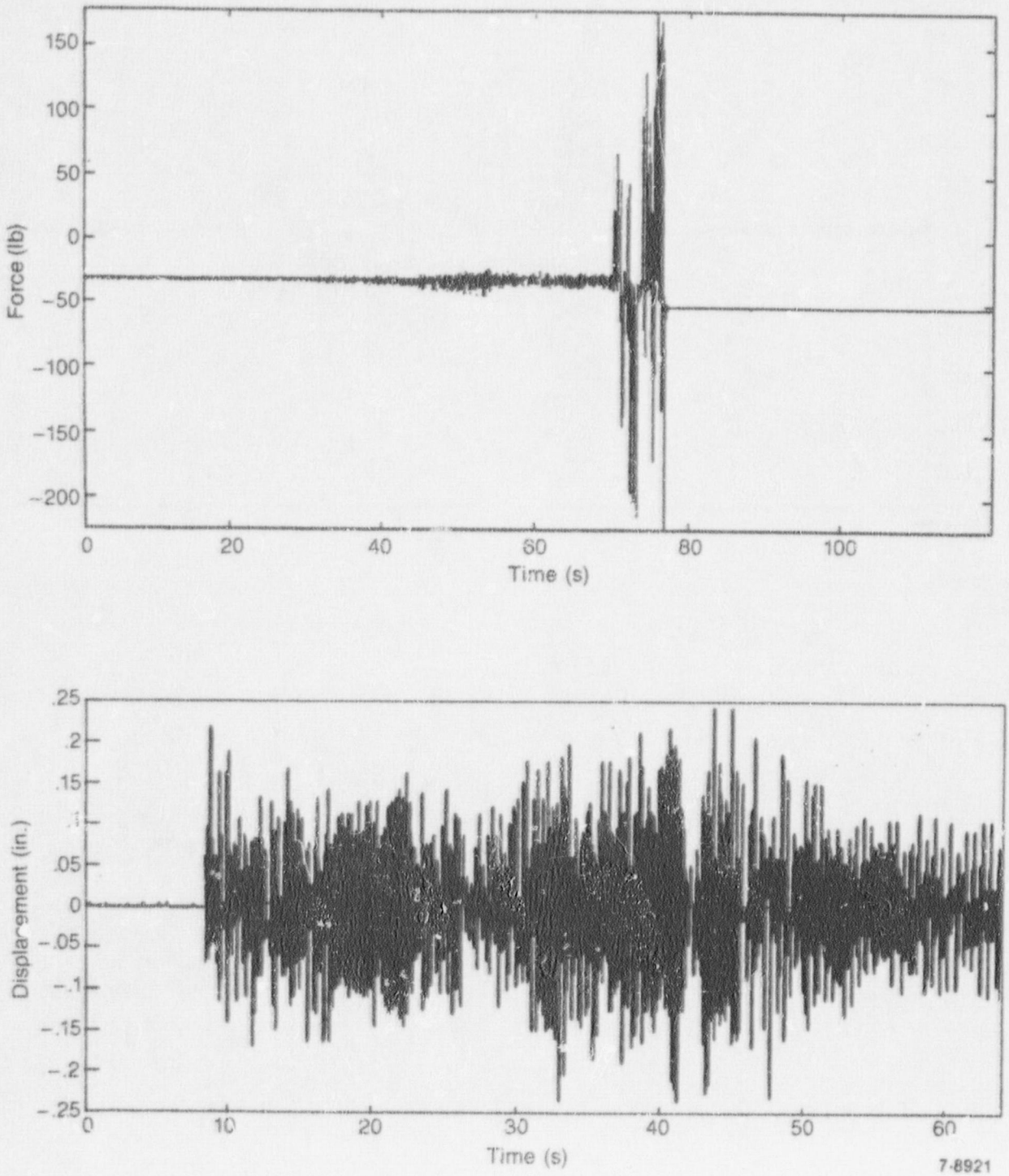

Figure C-7. Comparison of force and displacement at snubber location H-12. This snubber operated erratically for a few seconds then failed to resist motion for the remainder of the transient.

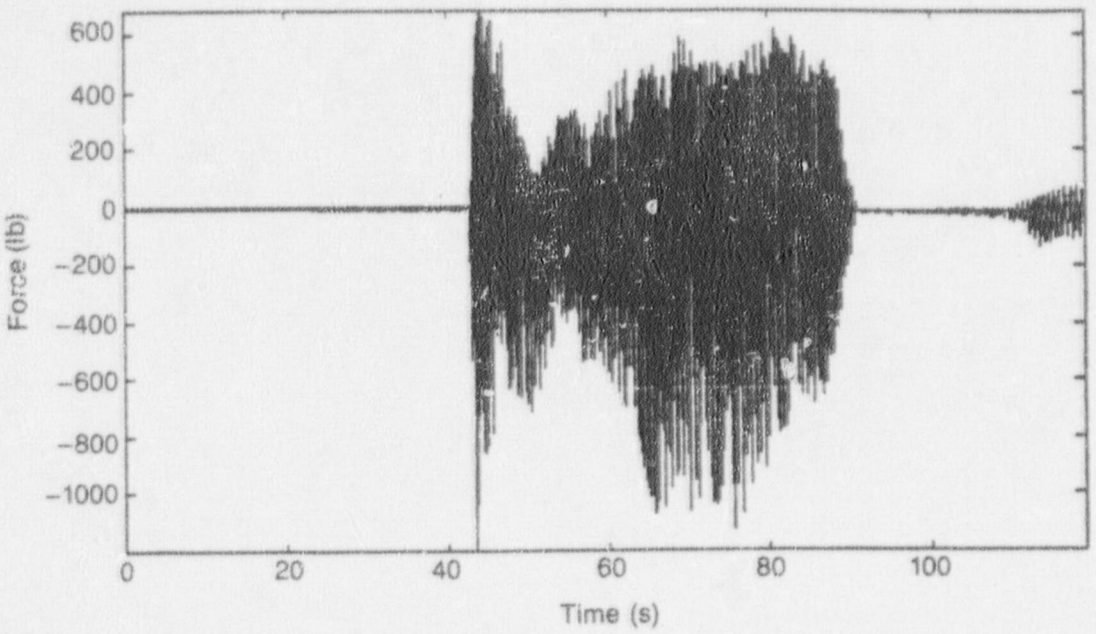

a. Location H-1

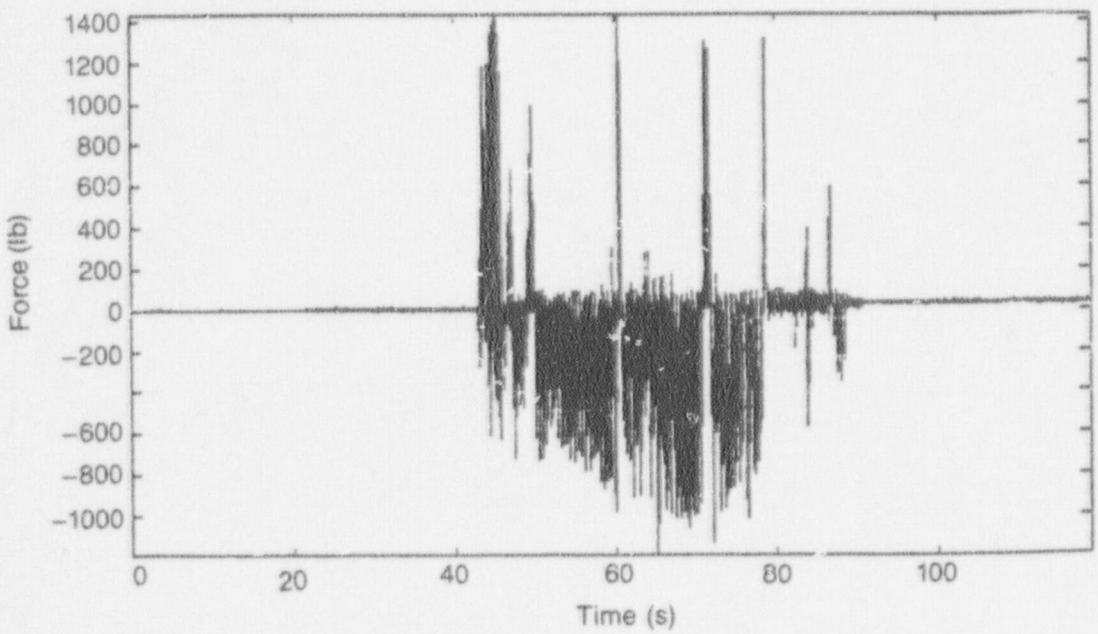

7-8901

b. Location H-2

Figure C-8. Comparison of force time histories for the snubber located at H-1 with the snubber at H-6.

APPENDIX D
INVESTIGATION OF SPURIOUS DISPLACEMENT READINGS AT HDR

APPENDIX D
INVESTIGATION OF SPURIOUS DISPLACEMENT READINGS AT HDR

Displacements recorded during SHAG testing at HDR indicated that the five Pacific Scientific mechanical snubbers and the Bergen-Patterson hydraulic snubber allowed displacements greater than 0.1 in. peak to peak, the maximum specified by Pacific Scientific for the mechanical snubbers. Figure D-1 shows the four responses recorded at snubber location H-12 during one of the tests. These responses are typical of those measured at all snubber locations.

Although the displacement readings were greater than they should have been, forces measured at the snubber pins indicated that the snubbers resisted motion. Measurements of piping acceleration also indicated that the snubbers functioned properly, though the acceleration responses were large enough that if the major frequency content was at low enough frequencies, the large displacements were theoretically possible.

The apparent excessive motion allowed by the snubbers, as indicated by the displacement measurement, is of concern. Piping systems in nuclear plants are designed and analyzed for small dynamic displacements, and larger displacements allowed by snubbers could cause higher stress, or even impacting, where piping systems are installed close together. Pipe impacting with valve operators is of even greater concern, where structural damage could prevent valve operation.

The displacements were measured by Celesco PT101-20A position transducers. The transducers were

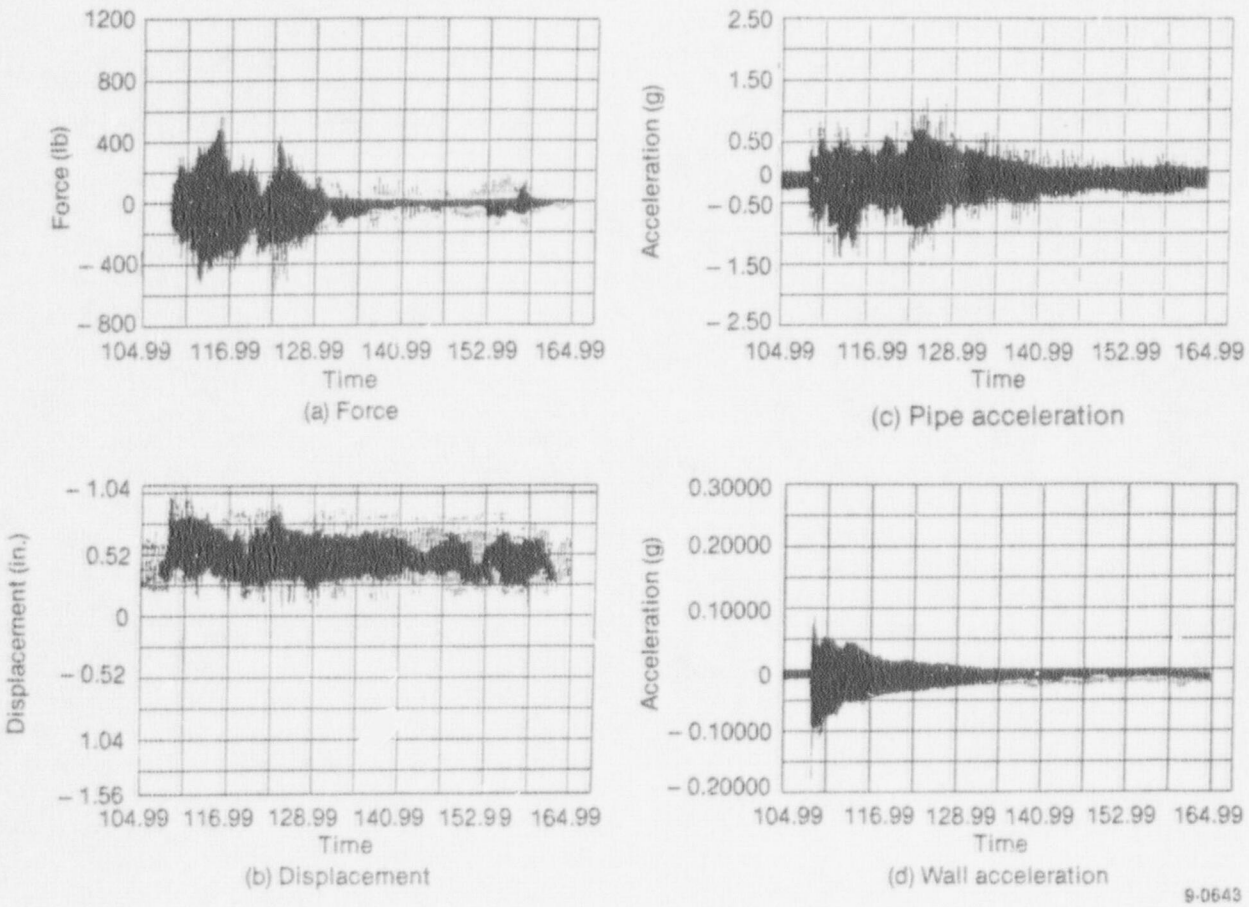

Figure D-1. Responses recorded at Pacific Scientific snubber location H-12 during Test T40.30, 8-Hz starting frequency.

mounted solidly to the HDR structure perpendicular to the run of pipe at each snubber location. The cable from the transducer was then fastened to the pipe. The transducer function, simply described, is a potentiometer, turned by displacement of the cable, that is continually preloaded by an internal spring. The potentiometer output wiper voltage is calibrated to read cable travel in inches. Where extra long distances between the structure and pipe existed, an additional length of cable was added to the transducer cable. Transducer calibrations performed at HDR prior to testing and during the test program indicated that static deflection of the transducer cables provided accurate measurements.

We conducted a posttest investigation at the INEL dynamics laboratory to determine whether the Pacific Scientific snubbers, the most widely used mechanical snubber used in U.S. nuclear plants, were in fact allowing displacements larger than the 0.1-in. peak-to-peak dead band specified by the manufacturer. The investigation indicated that the large displacement readings were a product of the Celesco transducers rather than the actual movement of the piping. The results of that investigation are reported in the following paragraphs.

One way to check measured displacements is to calculate displacements from the measured accelerations. For each of the snubber locations, we double integrated the acceleration histories to determine how well the calculated displacements would correlate with the recorded displacements. The results of this work confirmed that the displacements allowed by the snubbers, as determined from integrated acceleration, were within the tolerance specified by the manufacturer. As can be seen from the examples shown in Table D-1, displacements recorded by the Celesco transducers were generally an order of magnitude greater than those calculated from the double-integrated accelerations.

The displacement transducers, excitation power supplies, accelerometers, recording equipment, and other associated equipment used in the HDR work were set up in the INEL dynamics laboratory. Using a small electromechanical shaker, we simultaneously subjected the accelerometers and displacement transducers to various vibration histories, including random and sine. The accelerometer histories were double-integrated and compared to displacement histories recorded by the transducers. Figure D-2 is an example of this work with a random signal comparison. The comparison shows that the recorded displacement and acceleration-derived displacement correlate very well.

Four of the snubbers were returned to Pacific Scientific for testing. The snubbers met all performance requirements.

The Pacific Scientific snubber from location H-1 at HDR was installed on a test machine at INEL. The snubber was subjected to random, sine, and sine with random noise superimposed. The random and random sine signals were used to more closely duplicate natural earthquakes and the SHAG spectra. Pacific Scientific is not equipped to subject snubbers to these types of signals. The snubber met or exceeded the manufacturer's dead band tolerances for all signals imposed with loadings up to ASME code Level C rating.

Table D-1. Comparison of recorded displacements and double-integrated accelerations

	Zero-to-peak Displacement (in.)	
Location	Celesco	Double Integration
H-1	0.7	0.064
H-8	0.45	0.013
H-12	0.42	0.035

A seventh Celesco displacement transducer was used at HDR to measure thermal growth at the DF 16 manifold, instrument location 50 (see Figure 5, Vol. 1). This transducer also measured the manifold's vertical displacement during dynamic excitation. Adjacent to this displacement location was an accelerometer, instrument 35. We double integrated the acceleration history for test T40.30 (U.S. stiff piping configuration) at 8-Hz starting frequency and compared it to the displacement history. Figure 61, Vol. 1, shows this comparison. The correlation is very good. Both plots show approximately 0.2-in. double amplitudes.

All seven of the transducers were excited and recorded at HDR with the same equipment. The data inconsistencies cannot be attributed to difference in measurement technology. The following theory is offered as a possible explanation. The manifold was restrained in both horizontal axes by large circumferential restraints, allowing only vertical motion. The piping at the snubber locations responded in all three axes, including axial motion parallel to the pipe. This axial motion is offered as the primary difference in the specimen response between the six transducers at snubber locations and the one at the manifold.

The logic for the transducers' anomalous response is as follows. The transducer system consisted of a cable wound up on a preloaded drum attached to a multiturn potentiometer. We believe the spurious transducer readings are a result of cable whip. The mass of the cable and the rotational inertia of the

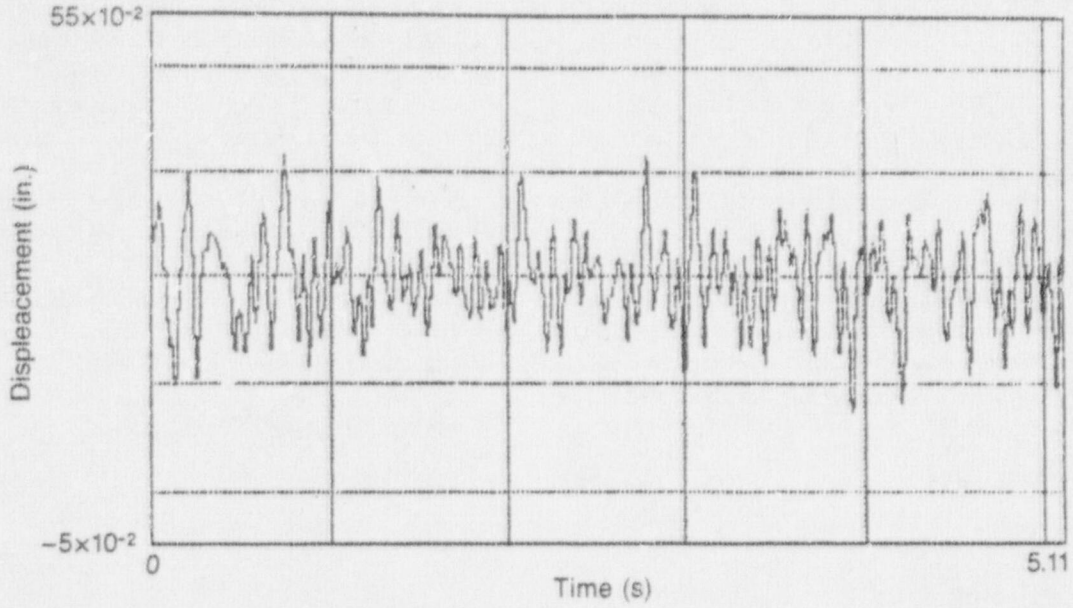

(a) Displacement transducer time history.

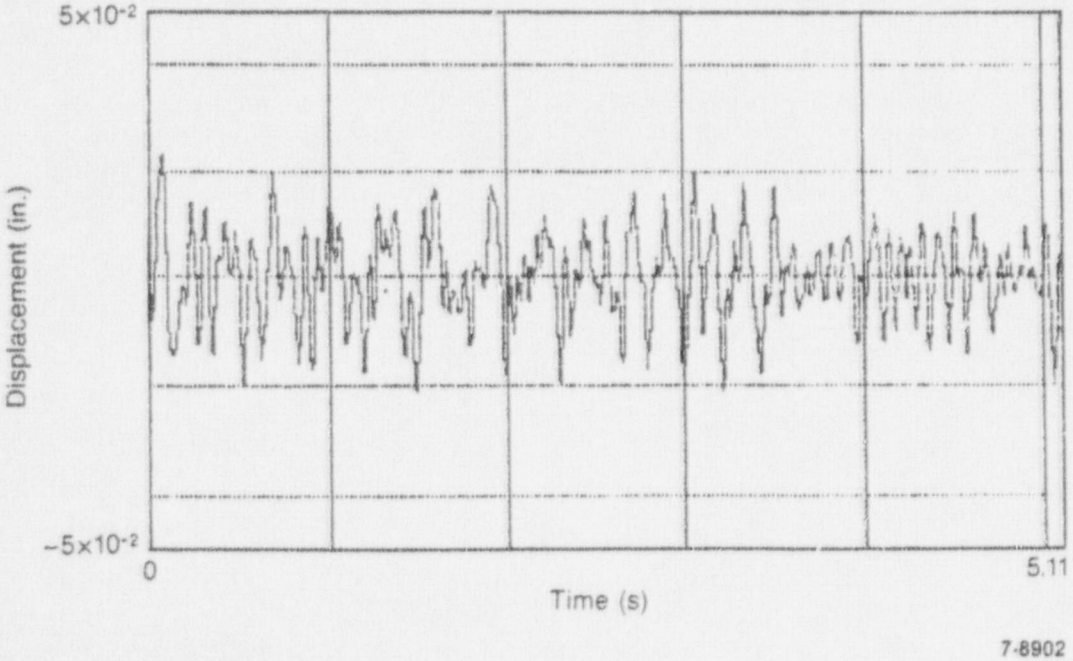

(b) Accelerometer double-integrated acceleration history.

Figure D-2. Laboratory test comparison of a displacement time history and an accelerometer double-integrated acceleration history.

preloaded drum were excited by transverse and parallel vibration simultaneously. This resulted in a resonance situation that caused the potentiometer to read one or more cable drum system harmonic vibrations and add them to the actual displacement of the piping.

The Celesco Transducer Company worked very closely with INEL Engineers to resolve the displacement measurement anomaly. This work included considerable work at their expense. In the end, agreement could not be reached and the following is a quote from Celesco:

"Celesco transducers were operated in a condition exceeding their published specifications, i.e., g forces. Operating under these conditions, as well as with the use of external attachments, i.e., extension cables, could provide an adverse effect on the performance of the transducers."

INEL research does not support this conclusion offered by Celesco, for the following reasons. The transducers installed without cable extension, i.e., where extended to midstroke (H-1 and H-7), yielded some of the most inconsistent data. Pipe accelerations of 1 to 3 g are not outside the published envelope for this model of Celesco transducer. The actual response of the transducer is outside its published operating envelope, and, as previously stated, we believe to be a result of cable-drum resonance.

In later tests conducted at the HDR, the same type of snubbers were subjected to dynamic loads created by servohydraulic shakers attached to the VKL. Those tests used Linear Variable Displacement Transducers (LVDTs) instead of Celesco transducers to measure displacements allowed by the snubbers. The results of those tests confirmed that the snubbers performed within manufacturer's specifications.

APPENDIX E
VALVE RESPONSE FREQUENCY ANALYSIS METHODOLOGY

APPENDIX E
VALVE RESPONSE FREQUENCY ANALYSIS METHODOLOGY

INTRODUCTION

Frequency analysis of time-history transducer records sometimes yields additional information that is not apparent in the original time records. Perhaps the most useful frequency domain method of data analysis is the computation and examination of frequency response functions (FRFs). However, this procedure requires one or more time-synchronized reference signal(s) that may be interpreted as input(s) to the system. In the present study, there exist a number of inputs to the system such that use of FRFs would become a difficult and costly task. An alternate, but less powerful, method of frequency domain analysis is the study of individual response signals. The primary disadvantage of this method is that phase information is lost; relative behavior of response signals is unattainable. The most useful form of frequency domain function, when individual time responses are transformed into the frequency domain, is termed autospectrum, mean-square spectral density, or power spectral density (PSD). Owing to the complexity and number of force inputs to the VKL system, the PSD was the method of choice for frequency domain analyses.

This appendix presents discussions of structure, PSD computation techniques, and theory used in the frequency analysis.

All of the data reduction reported herein was performed on a GenRad 2508 minicomputer system using the MODAL PLUS software package from Structural Dynamics Research Corporation (SDRC). Standard MODAL PLUS time data files consist of sequential frames of data, each of which contain 1024 discrete values of digitized data with constant time-step. Data acquired by MPA was digitized with time-step equal to 4.6 ms, whereas data acquired by KfK was digitized with time-step equal to 8 ms. Thus, each data frame, in the time domain, represented 4.71 s and 8.18 s for MPA and KfK acquired data, respectively.

Data Analysis

Standard procedures were used to calculate PSDs of the acceleration time records. Briefly, for each time record studied, this consisted of (a) multiplying the time frame by a window function (Hann function) to reduce distortion or leakage of the resultant PSD, (b) Fourier transforming the windowed time frame, (c) multiplying the transform by its complex conjugate, and, finally (d), multiplying the result by a scale factor to account for loss of power during the windowing process and to scale the squared transform by its bandwidth. This operation is symbolically described as follows:

Let $S(\omega)$ = Power Spectral Density (PSD)

$$= B_w \, \mathcal{F} \, [w(t)g(t)]^2$$

where

B_w	=	effective bandwidth
$\mathcal{F}$ [ ]	=	Fourier transform of time function
$w(t)$	=	window function
$g(t)$	=	time domain acceleration.

Owing to the differing time-steps employed in data acquisition, net (upper bound) frequency band widths were 108.7 Hz and 62.5 Hz for MPA and KfK-acquired data, respectively. The effective band width was taken to be 0.8 times the net band widths, or 87 Hz and 50 Hz, respectively, to account for finite roll-off of antialiasing filters. Thus, for subsequent calculations and comparisons, a common effective band width of 50 Hz was used. Since 1024 point time frames were used in the Fourier transforms, frequency resolution was net band width divided by 512, or 0.212 Hz and 0.122 Hz for MPA- and KfK-acquired data, respectively.

A standard technique used in frequency analysis is to average the PSDs obtained from several sequential time frames in order to minimize the effect of noise in the measurements. However, for the measurements studied herein, several of the resonant peaks in the PSDs were changing in frequencyas a function of the time frame studied due to shaker coastdown. Thus, averaging several sequential frames had the effect of smearing these variable PSD peaks. In order to reduce this smearing effect, it was decided to study and compare the data on a frame-by-frame basis. However, owing to the differing time frame lengths between MPA- and KfK-acquired data, and since the MPA-acquired frames were approximately one half the length of the KfK frames, two adjacent PSDs resulting from

MPA data were averaged together for comparison with an individual frame PSD resulting from KfK data. Thus, each PSD frame from KfK acquired data (spherical tee and top of the HDU) represents 8.18 s and each resultant averaged PSD frame from MPA acquired data (valve body, valve actuator, and standard tee) represents 9.41 s of acquired time data. The start time of the first frame of time data chosen for transformation was taken to be approximately 1 s before transient initiation. It was found that the major response, for each location studied, was contained in either of the first two frames, or before approximately 16 s after initiation of the transient. Thus, subsequent discussion of analysis and results deals with the first two frames of KfK data, or the first two composite frames of MPA data.

In order to refine and allow more quantitative evaluation of the PSDs, integration of the raw PSDs was performed. Three integration procedures were used: first, integration and subsequent square root of the entire PSD; second, integration and square root of selected frequency bands through significant peaks in the PSDs; and, third, cumulative sums (as a function of frequency) of the band integrated PSDs were found. A symbolic description of each of these reductions may be given as follows:

The average power of the measurement (mean square) between frequencies ω_1 and ω_2 is,

$$G^2 = \int_{\omega_1}^{\omega_2} S(\xi)\,d\xi$$

or

$$G_{rms} = \left\{ \int_{\omega_1}^{\omega_2} S(\xi)\,d\xi \right\}^{1/2}.$$

Average acceleration from 0 to f Hz is

$$G_{rms}(f) = \left\{ \int_{0}^{f} S(\xi)\,d\xi \right\}^{1/2}.$$

If $S(\omega)$ is concentrated in discrete bands, $[\omega_{i1}, \omega_{i2}]$, let:

$$S_i(\omega) = S(\omega),\ \omega_{i1} \leq \omega \leq \omega_{i2}$$

$$= 0,\ \omega < \omega_{i1},\ \omega > \omega_{i2}$$

and

$$S(\omega) = S(\omega) - \sum_{i=1}^{n} S_i(\omega),$$

then cumulative acceleration from 0 to f Hz is

$$G_{rms}(f) = \left\{ \int_{0}^{f} S(\xi)\,d\xi \right\}^{1/2} + \sum_{i=1}^{n} \left\{ \int_{0}^{f} S_i(\xi)\,d\xi \right\}^{1/2}$$

The first reduction technique may be interpreted as the root mean square (rms) average acceleration, from zero to a given frequency, of each frame of data. The second technique may be interpreted as the rms acceleration contribution of each significant resonance peak contained in the PSD. The third technique represents the sum, as a function of frequency, of all of the resonance peaks contained in the PSD.

Analysis Results

Figures E-1 through E-60 reproduce PSDs found from frequency analysis of the 30 acceleration time records (X, Y, and Z directions for each of the five locations and for each of the two tests). The first two frame PSDs are shown in all cases. The most significant aspect of the PSDs is the relatively large magnitude high-frequency content of valve operator PSDs, especially for excitation in the Z direction. Examination of PSDs for the other four locations studied does not indicate nearly the degree of high frequency content. Due to the relative difficulty of quantitative examination of the PSDs, the band integrated representation of the data results is discussed.

Tables E-1 through E-3 present rms values of the resultant band integrations performed for all significant peaks in the data studied (PSD frames 1 and 2 of the 30 acceleration time records). Each table represents a direction, and each horizontal group of values represents a location. The first two columns represent frames one and two of test T40.10, and the last two columns represent corresponding frames of test T40.30. The data are given as a number (the integrated rms acceleration in G) followed by a bracketed range (the band over which the integration was performed in Hz). In general, each row of data represents common frequency bands for significant peaks found in the PSDs. Thus, where blanks occur in the data tables, there are no corresponding significant peaks in the PSD. For each frame of data, the sum of all of the major contributing bands is given. This sum may be interpreted as the rms acceleration of the corresponding time frame in the case where frequency components are additive. In general, comparison of the summed rms accelerations with the

corresponding time records does indicate that the frequency components are additive.

The tabulated data are graphically represented in Figures E-61 through E-96. These figures are three-dimensional bar chart representations of the band integrated data where the height of each bar indicates rms acceleration, and the width indicates the band over which each integration was performed. The first set of bar chart figures, E-61 through E-90, graphically reproduce the numerical values given in Tables E-1 through E-3, where results of both data frames are shown on a figure. These figures illustrate variability of some of the component frequency bands as a function of time, where the shift to lower frequencies of some of the bands is evident. The bands that exhibit this shift are, generally, in the lower frequency region, from 5 to 15 Hz. If all of the bands contained in a PSD are classified in two categories—those that are associated with natural modes of vibration of the VKL system, and those that are associated with the input driving force—then the bands that do not vary in frequency are natural modes and those that do vary reflect the driving force. The second set of bar chart figures, E-91 through E-96, graphically illustrates the degree of acceleration amplification from the valve body to the valve actuator (first frame). Note that this amplification is especially significant for higher frequencies in the horizontal directions. Unfortunately, data that were acquired by KfK was low-pass filtered at 30 Hz during the acquisition process. Thus, potential high frequency (35 Hz to 50 Hz) information present at the top of the HDU vessel and at the spherical tee has been removed from the acceleration histories recorded for these locations.

Figures E-97 through E-102 illustrate the average rms acceleration, as a function of frequency, for all five location first frame PSDs. Figures E-103 through E-108 illustrate corresponding cumulative accelerations for the five locations as continuous functions of frequency. Note that the cumulative functions are similar to a running sum of the band integrated data, except that PSD information not included in the individually integrated bands is shown in the continuous cumulative functions. The average and cumulative functions represent, respectively, lower and upper bounds of time domain rms acceleration. The average data would more accurately represent the time data in the case where there is little direct superposition of frequency components, whereas the cumulative functions would more accurately reflect the case where there is significant superposition. If the rms values are multiplied by a factor of 1.414 to approximate the change from rms to peak, comparison of these frequency distributions with corresponding time records indicates that the cumulative distributions more accurately represent the peak measured accelerations.

CPS VALVE RESPONSE

To further verify the significant high-frequency valve operator acceleration response observed during the HDR SHAG tests, we performed a limited examination of the results of a similar but related study, the Containment Penetration System (CPS) dynamic test (reported in NUREG/CR-4734).

The CPS test program was designed to examine the response of typical containment penetration piping systems and associated components for a variety of loads. Of the systems tested in the CPS program, two contained large valves: one was an 8-in. system with gate valves, representing a containment spray system, and one was an 8-in. system with butterfly valves, representing a containment purge and vent system. One of the loadings imposed on the system was a simulated SSE three-dimensional dynamic shake. The CPS dynamic tests were designed so that the piping systems studied were supported from a large stiff integral framework (see Figures E-109 and E-110). For the SSE tests, this framework was excited through a number of hydraulic actuators so that a full three-dimensional base-motion SSE excitation was accurately simulated.

A striking similarity is evident when CPS gate and butterfly valve acceleration responses are compared with the corresponding HDR SHAG test gate valve acceleration response. This observation is even more significant when the complete dissimilarity between CPS and HDR VKL system geometries and excitation methods are taken into account. We conclude that the observed frequency-dependent behavior of the three valves studied is primarily a function of the valves' dynamic characteristics rather than the piping system geometry or method of input loading excitation. However, the observed behavior may depend on the valve being installed in a prototypical piping system, versus bench or analytic frequency determination.

The CPS dynamic testing provides two additional references for valve in situ response. Both valves are modern nuclear N-stamped valves from cancelled nuclear facilities, Hope Creek and WPPSS 4. The valve manufacturers have determined the valve fundamental frequencies are greater than 33 Hz, but, like the HDR valve, both show amplification under 33 Hz, as well as the high-frequency response. HDR and CPS are two of the largest full-scale simulated seismic test programs performed. There are some distinct similarities in response, that point out possible shortcomings in current valve qualification standards for seismic qualification and for single effects testing. The results of the test programs will be presented to the ASME valve qualification subcommittee for review.

Data and Test Description

ANCO engineers supplied CPS system dynamic tests, instrumentation, and data acquisition. For both of the valves in the simulated SSE tests, ANCO digitized and recorded full triaxial acceleration of the valve body and actuator. The duration of each SSE excitation was approximately 30 s, during which all data were acquired and simultaneously digitized with sample rate and antialiasing filter frequency set at 200 sps and 45 Hz, respectively. Thus, the useful bandwidth of the data was 50 Hz, as was the case with HDR SHAG data. All data were available via magnetic tape in standard ANCO ASCII format.

Data Analysis

Data analysis of CPS valve acceleration data was performed on the GenRad 2508 minicomputer-based systems in a manner similar to HDR SHAG data analysis. In the present case, strong motion valve acceleration data was of 30-s duration. Thus, for the CPS test sample rate (200 sps or time step equal to 5 ms), five data frames were available, each consisting of 1024 data points with 5.1 s duration. Each data frame was transformed, as previously discussed, to a PSD. In the case of CPS data, no frequency shifts of major PSD peak values appeared when individual frame PSDs were compared. Thus, to minimize noise inherent in the recorded acceleration data, all five PSD frames were averaged together. Figures E-111 and E-112 give the resultant average PSDs (X, Y, and Z directions for each of the two valve bodies and actuators). Figure E-111 represents response of the gate valve; Figure E-112 represents response of the butterfly valve. As opposed to the HDR SHAG PSDs, there are few distinct major peaks in the CPS valve PSDs. Thus, band-integrated rms accelerations were obtained with fixed integration frequency bands, each with a 5-Hz bandwidth, resulting in 10 integration bands per PSD. Tables E-4 and E-5 give the results of these band integrations. For each band, valve body and operator rms accelerations are compared through use of an amplification factor (operator acceleration divided by valve body acceleration). Finally, frequency-dependent average rms accelerations were found through integration of each PSD across the entire 50 Hz band. Figures E-113 through E-116 show the results of these integrations, where each figure represents triaxial acceleration for a given location and valve, with all three average rms acceleration functions superimposed.

Analysis Results

Both CPS valve acceleration responses exhibited significant high-frequency response and amplification, as was observed for response of the valve installed in the HDR VKL system. This is most significant in the horizontal response directions (X and Z directions), which are normal to the axes of the valve operators.

In the case of the gate valve, the greatest response and amplification occur for response in the X direction and in the higher-frequency range (35 to 45 Hz). However, for gate valve response in the Z direction, the greatest response and amplification occur in the intermediate-frequency range (20 to 30 Hz). In addition, a small degree of intermediate-frequency acceleration amplification may be observed for response parallel to the valve actuator stem axis (Y direction).

Butterfly valve results are similar to results found from the gate valve response. However, for the butterfly valve, greater response and amplification in the higher frequency range are found in the Z direction than the X direction. We note that for response in the X direction, amplification occurs across a wide-frequency range (8 to 45 Hz).

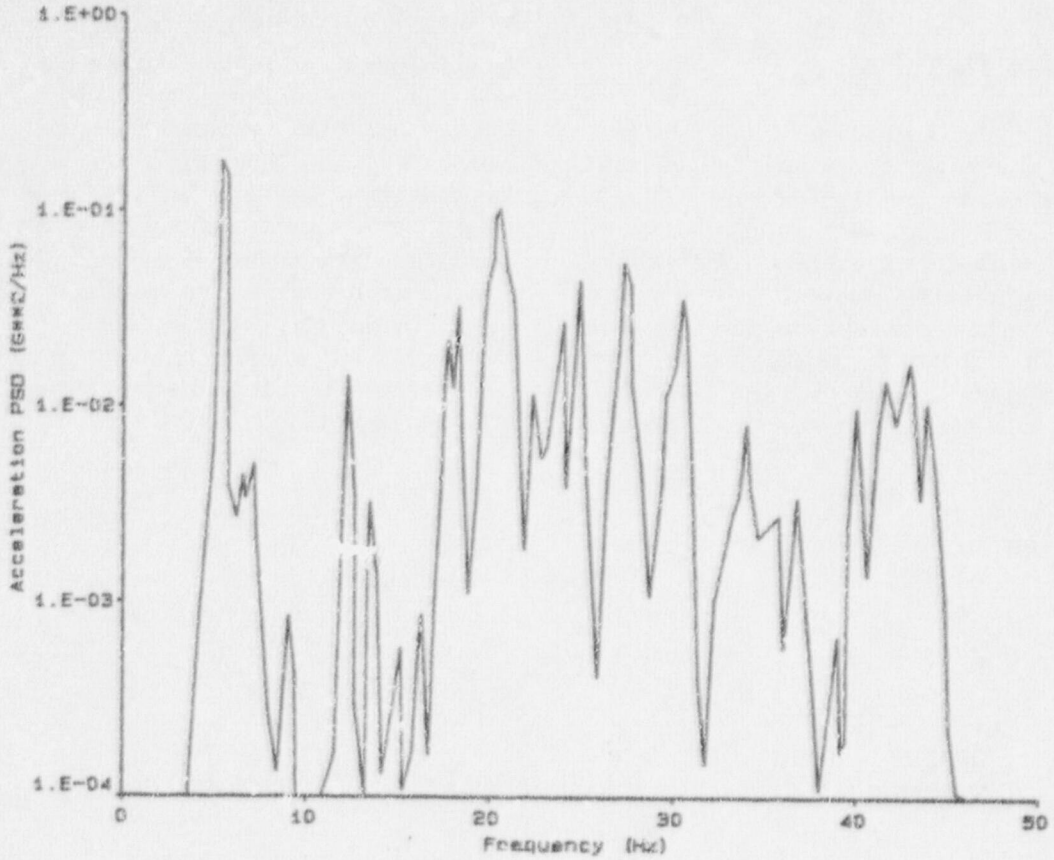

Figure E-1. Power Spectral Density: Test T40.10, valve operator, frame #1-X.

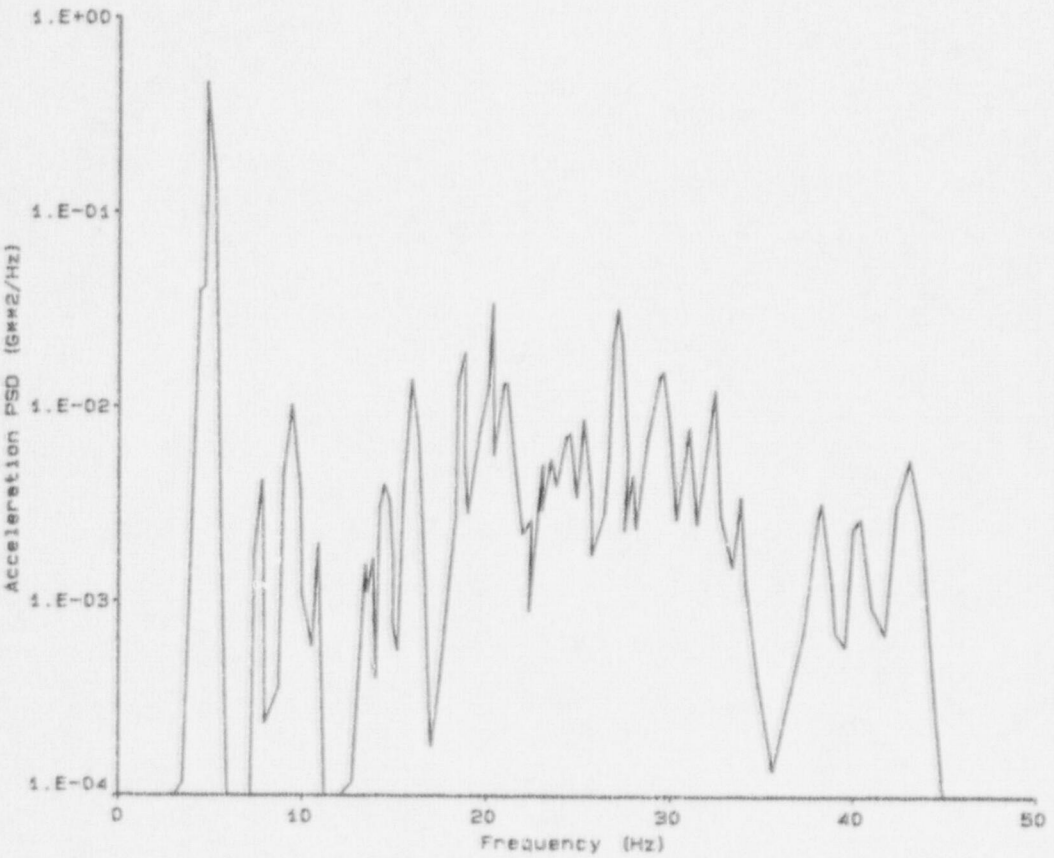

Figure E-2. Power Spectral Density: Test T40.10, valve operator, frame #2-X.

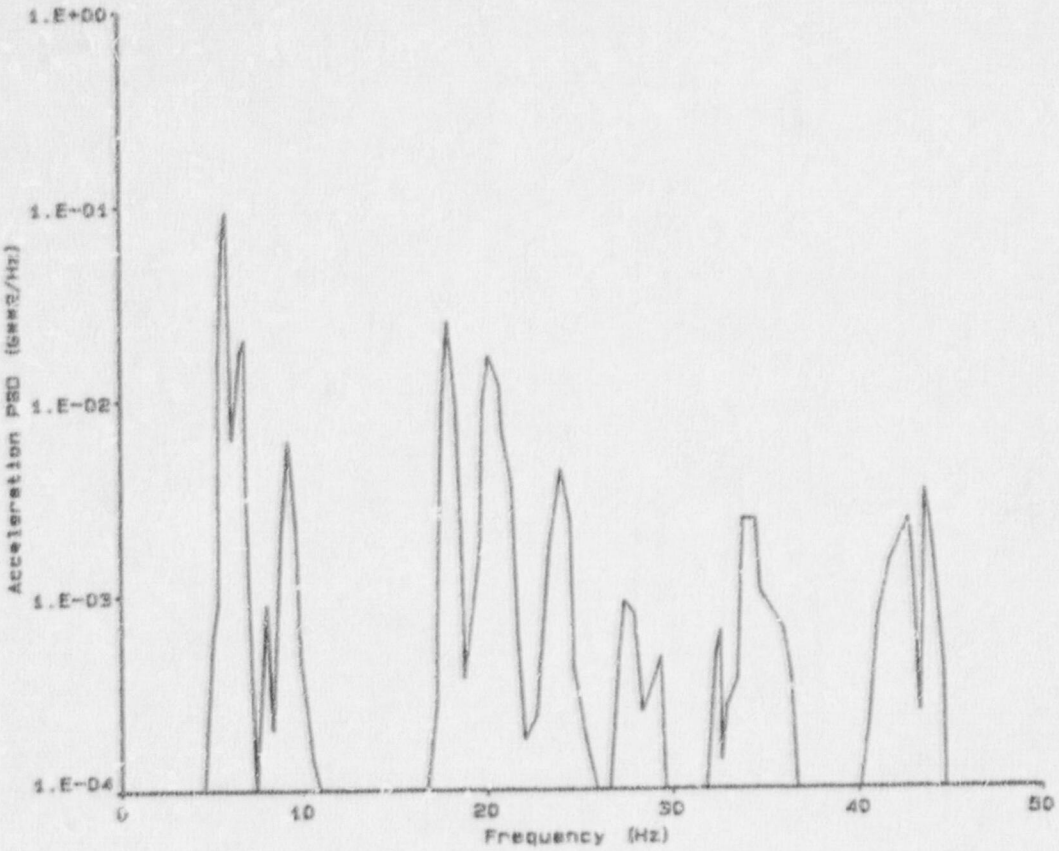

Figure E-3. Power Spectral Density: Test T40.10, valve operator, frame #1-Y.

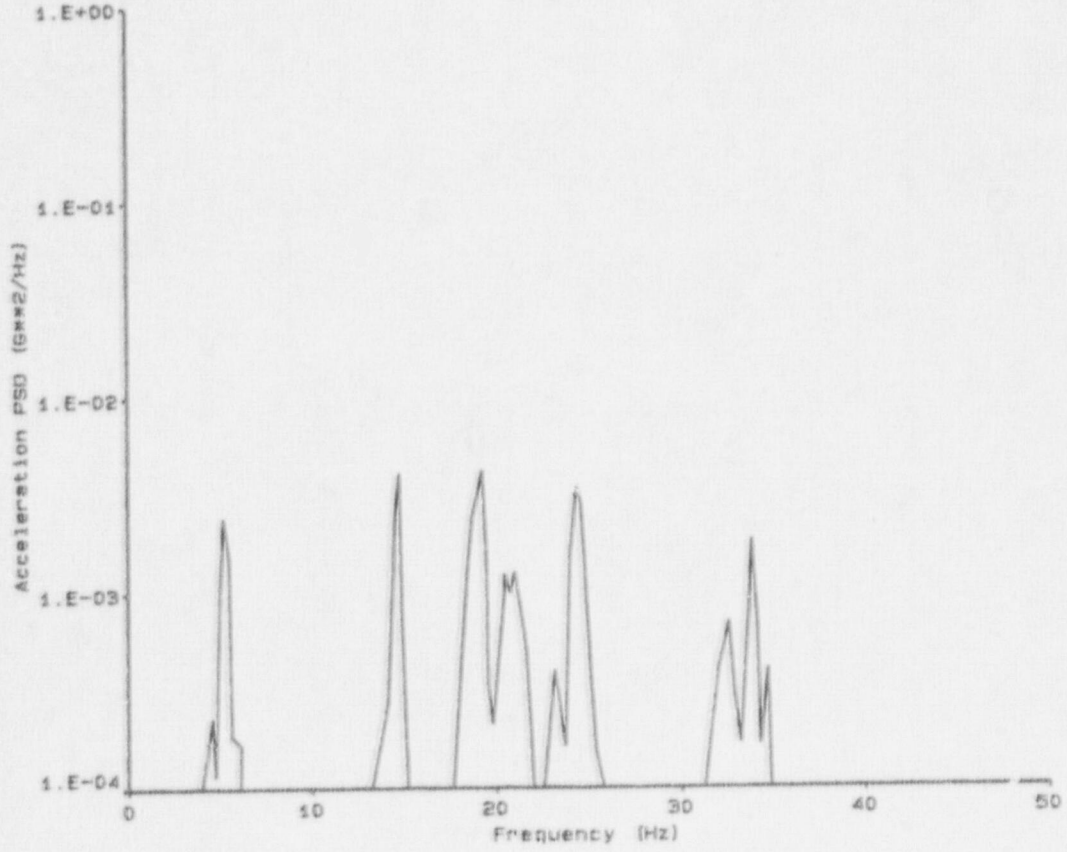

Figure E-4. Power Spectral Density: Test T40.10, valve operator, frame #2-Y.

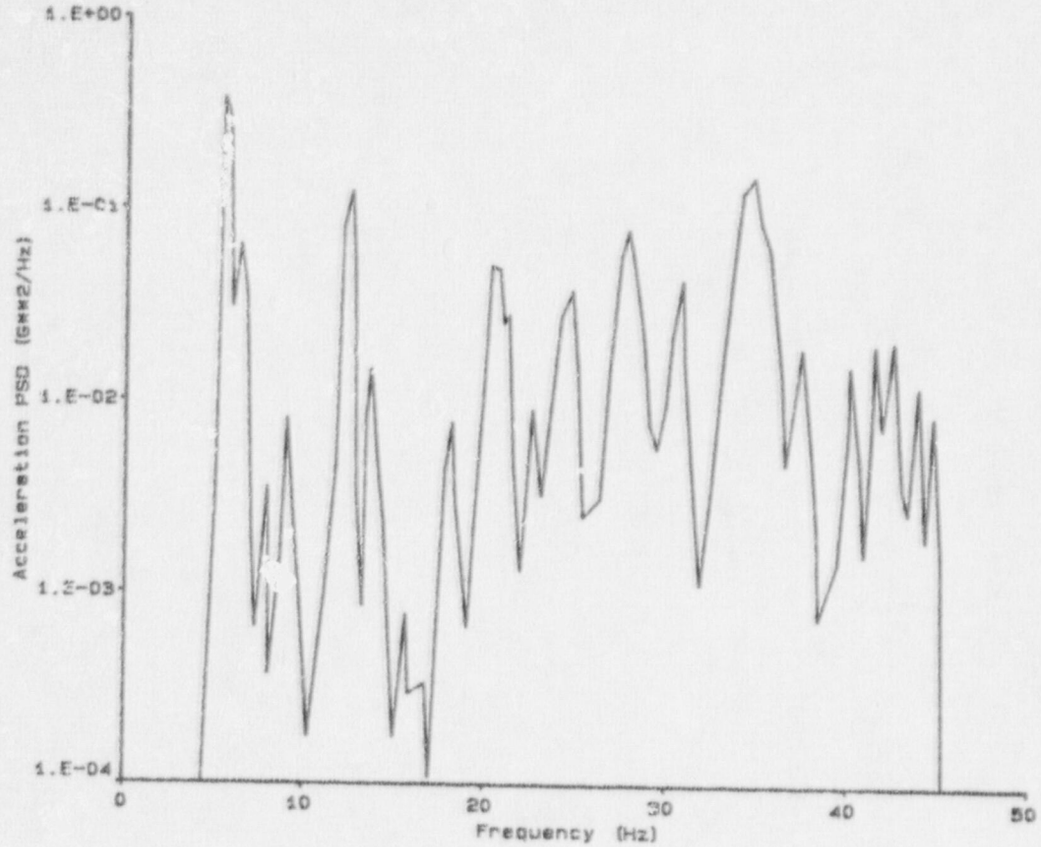

Figure E-5. Power Spectral Density: Test T40.10, valve operator, frame #1-Z.

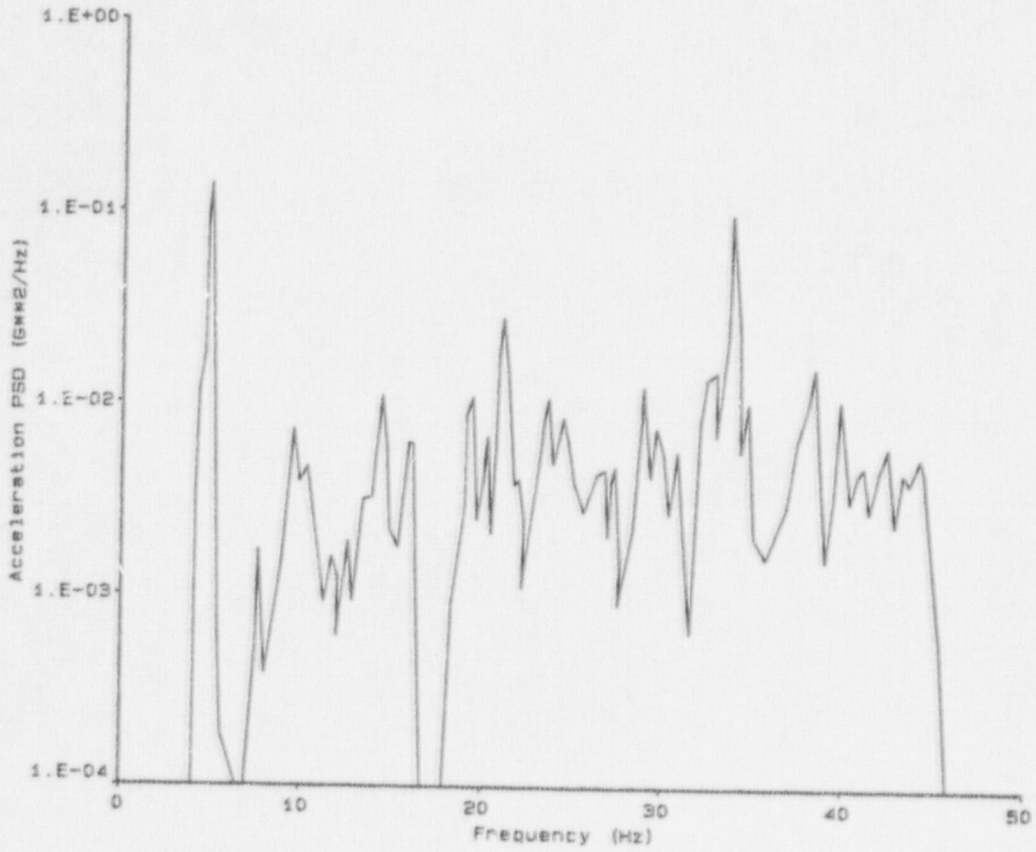

Figure E-6. Power Spectral Density: Test T40.10, valve operator, frame #2-Z.

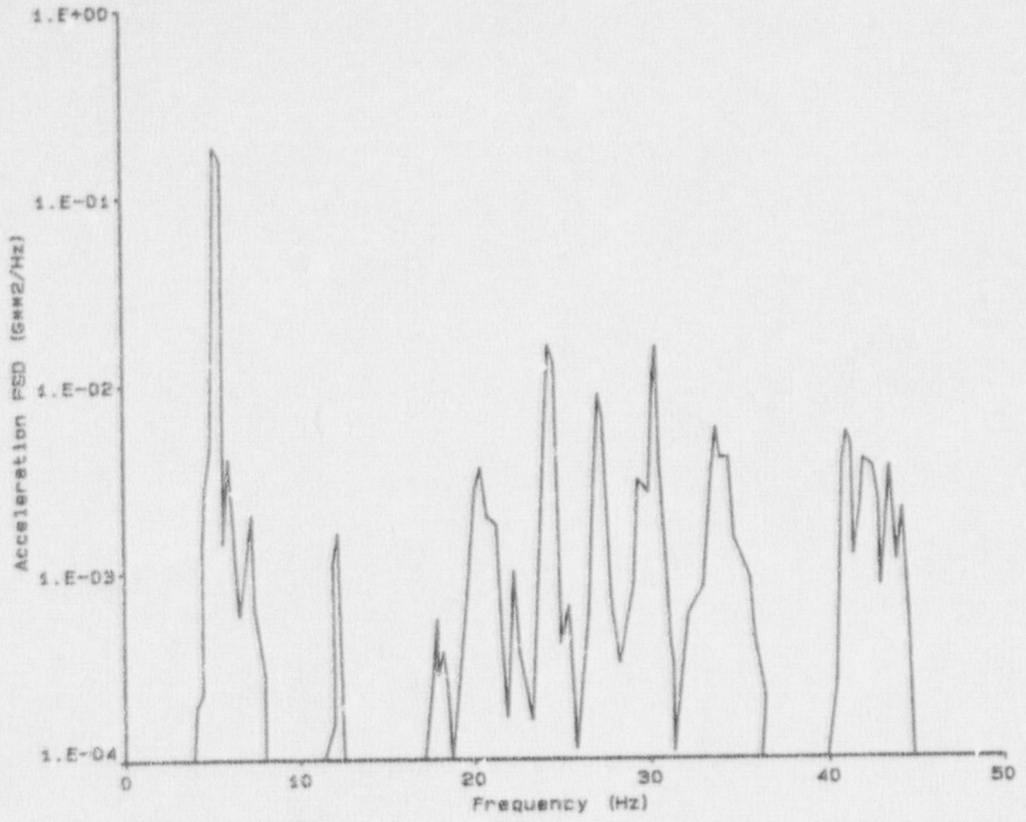

Figure E-7. Power Spectral Density: Test T40.10, valve body, frame #1-X.

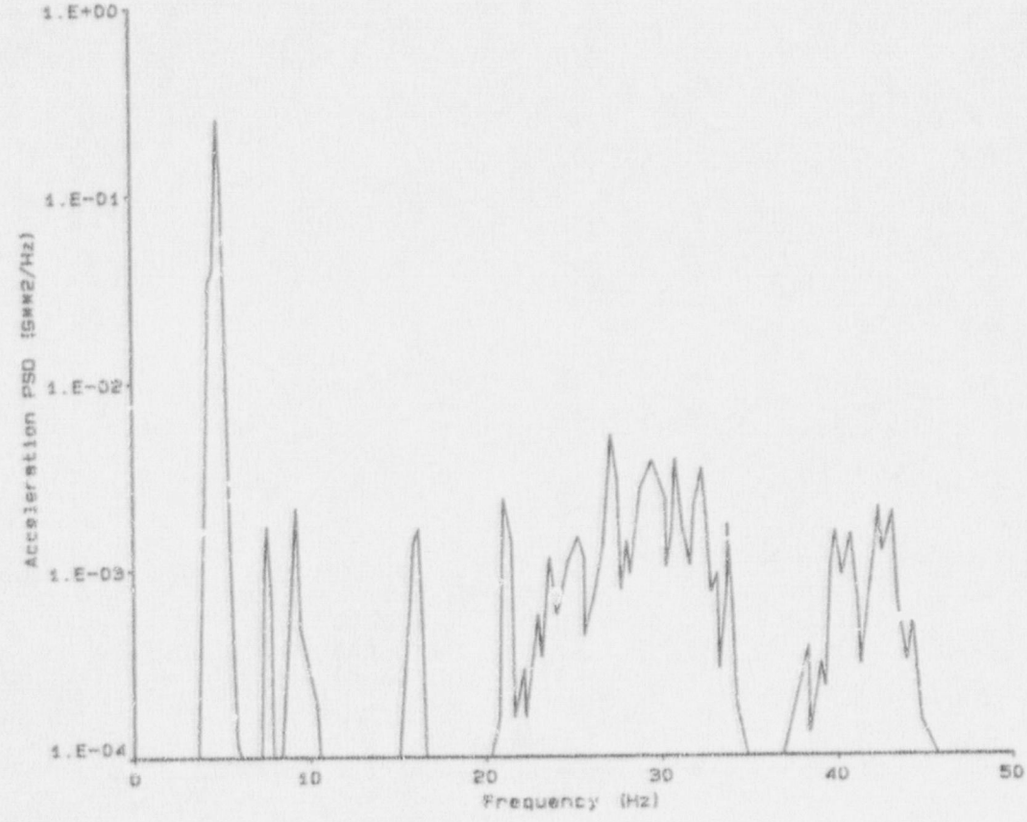

Figure E-8. Power Spectral Density: Test T40.10, valve body, frame #2-X.

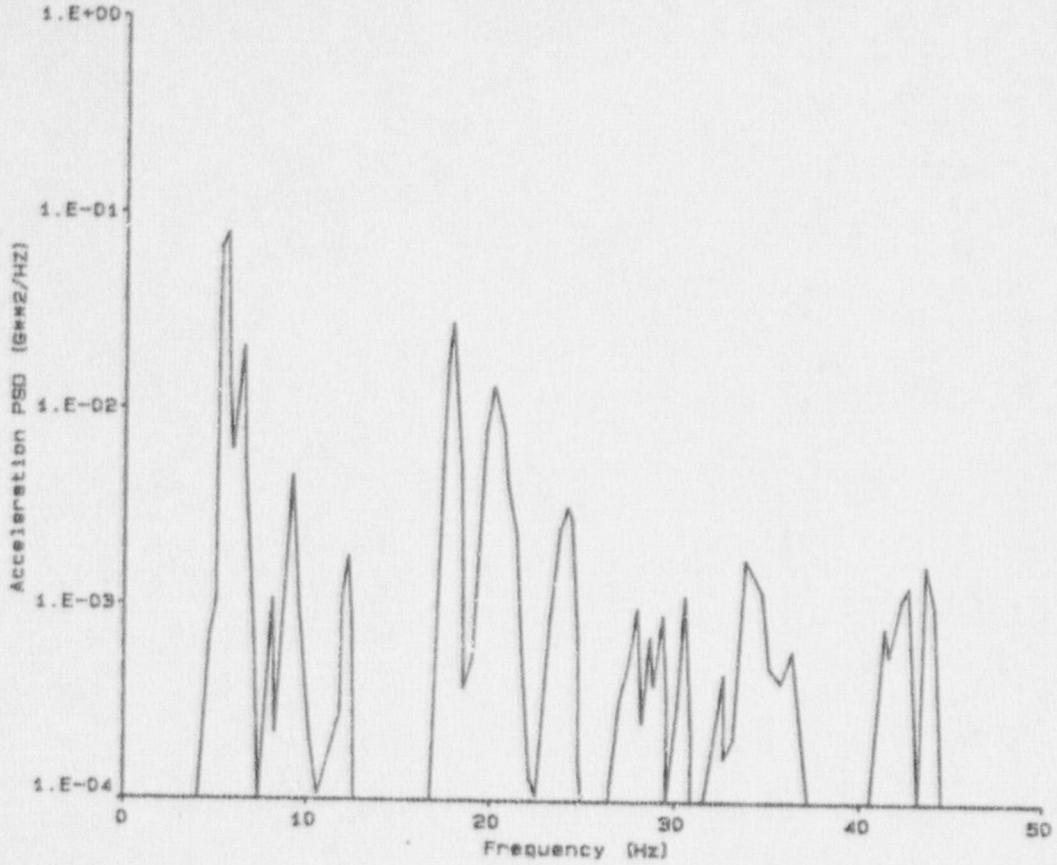

Figure E-9. Power Spectral Density: Test T40.10, valve body, frame #1-Y.

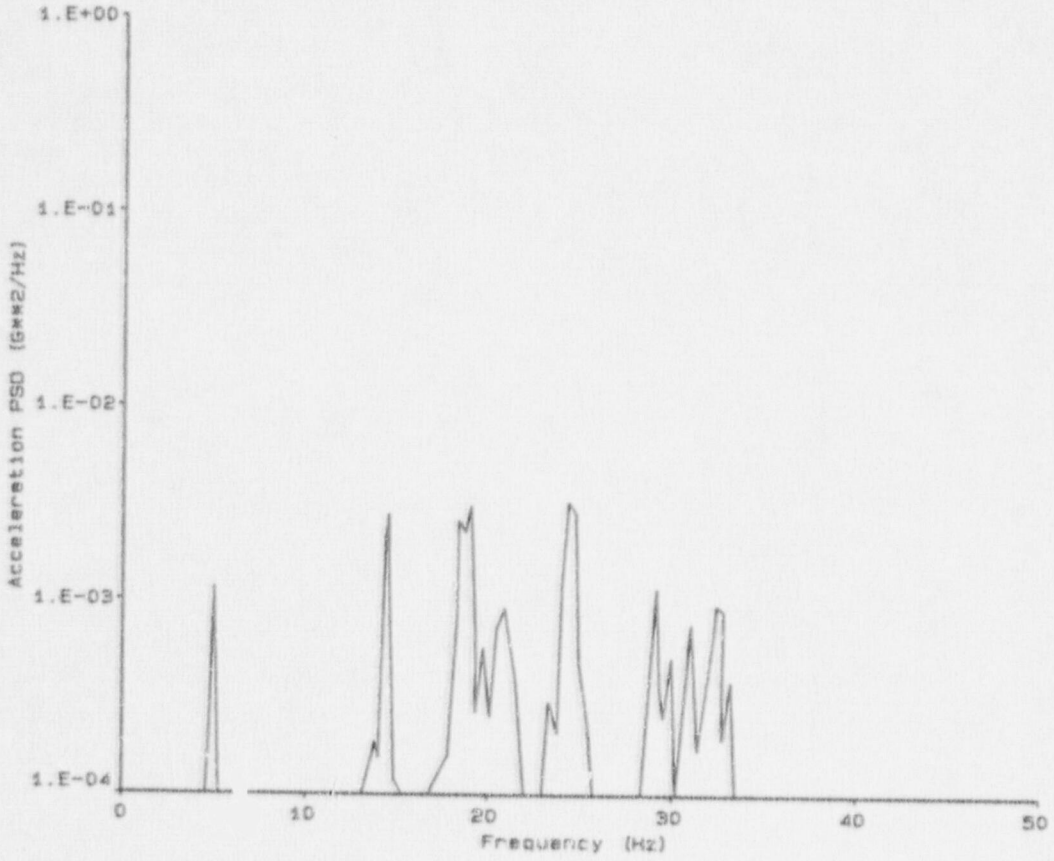

Figure E-10. Power Spectral Density: Test T40.10, valve body, frame #2-Y.

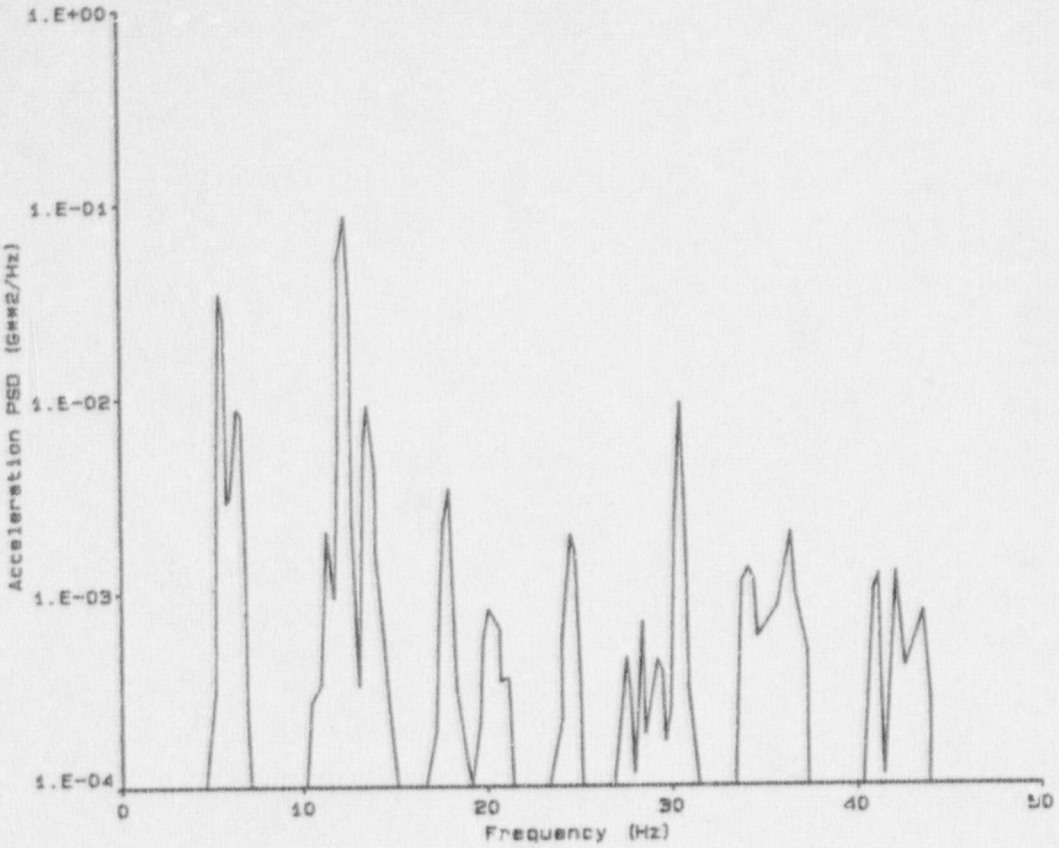

Figure E-11. Power Spectral Density: Test T40.10, valve body, frame #1-Z.

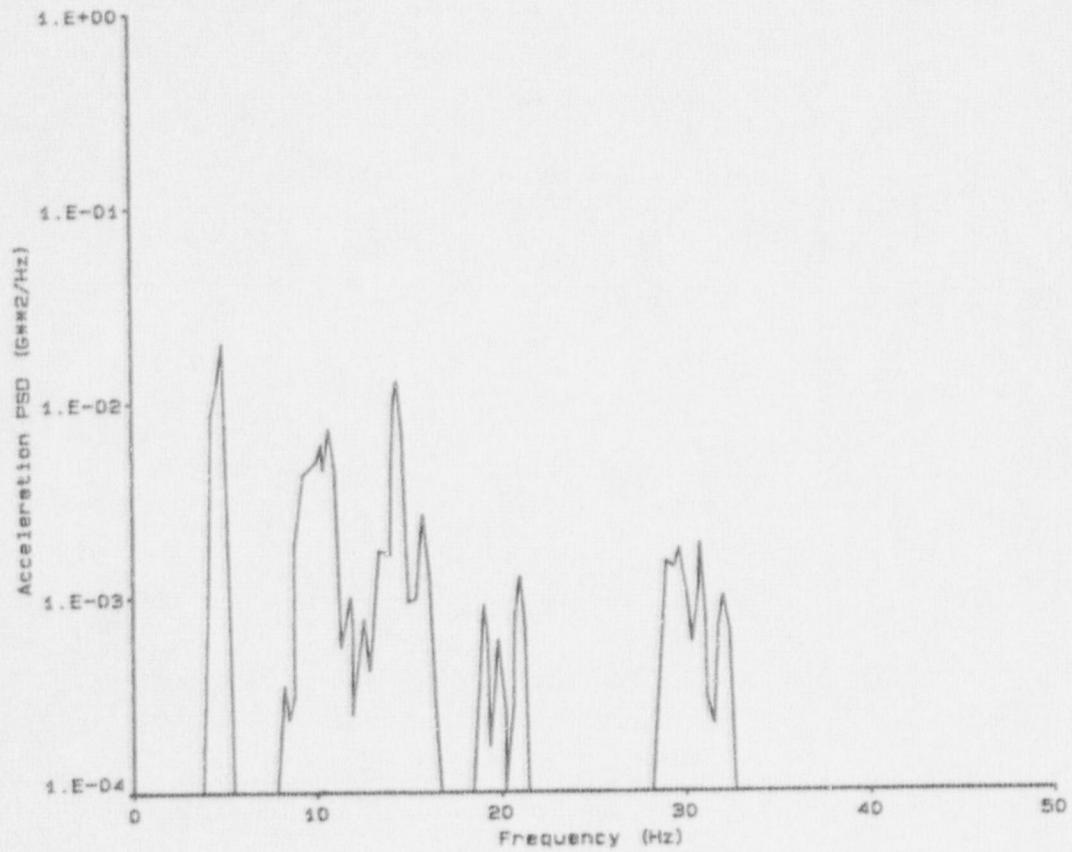

Figure E-12. Power Spectral Density: Test T40.10, valve body, frame #2-Z.

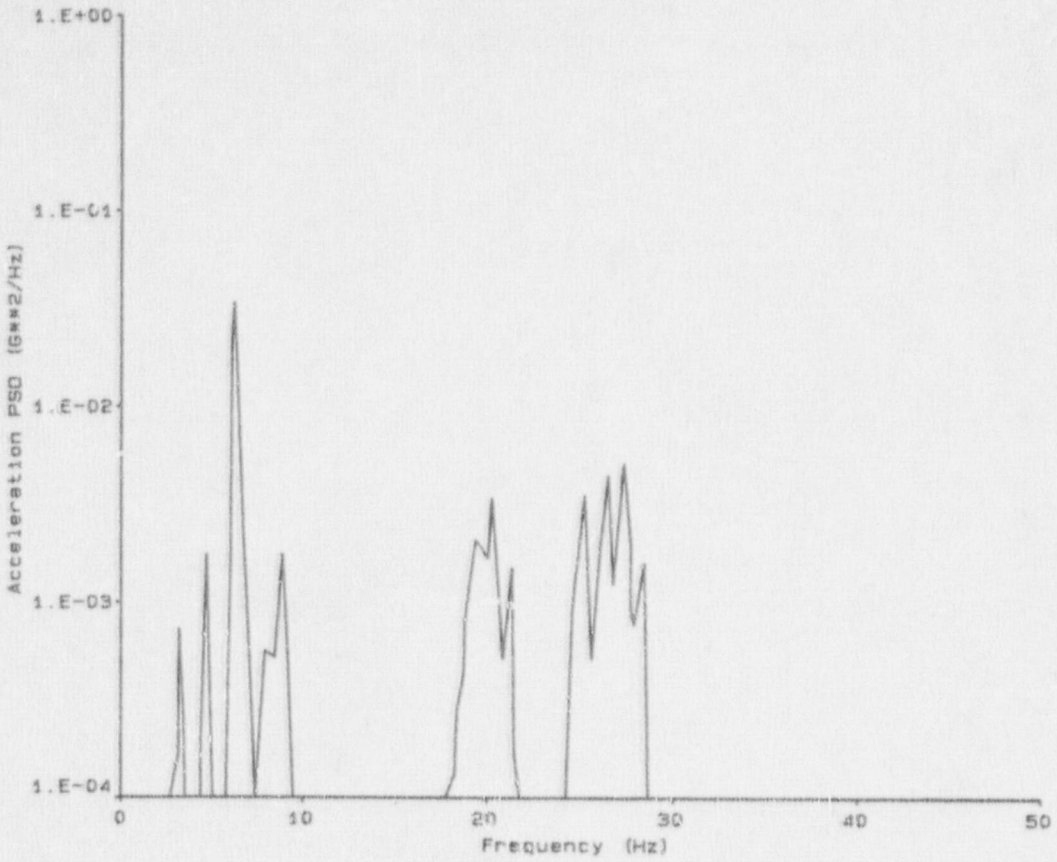

Figure E-13. Power Spectral Density: Test T40.10, spherical "T", frame #1-X.

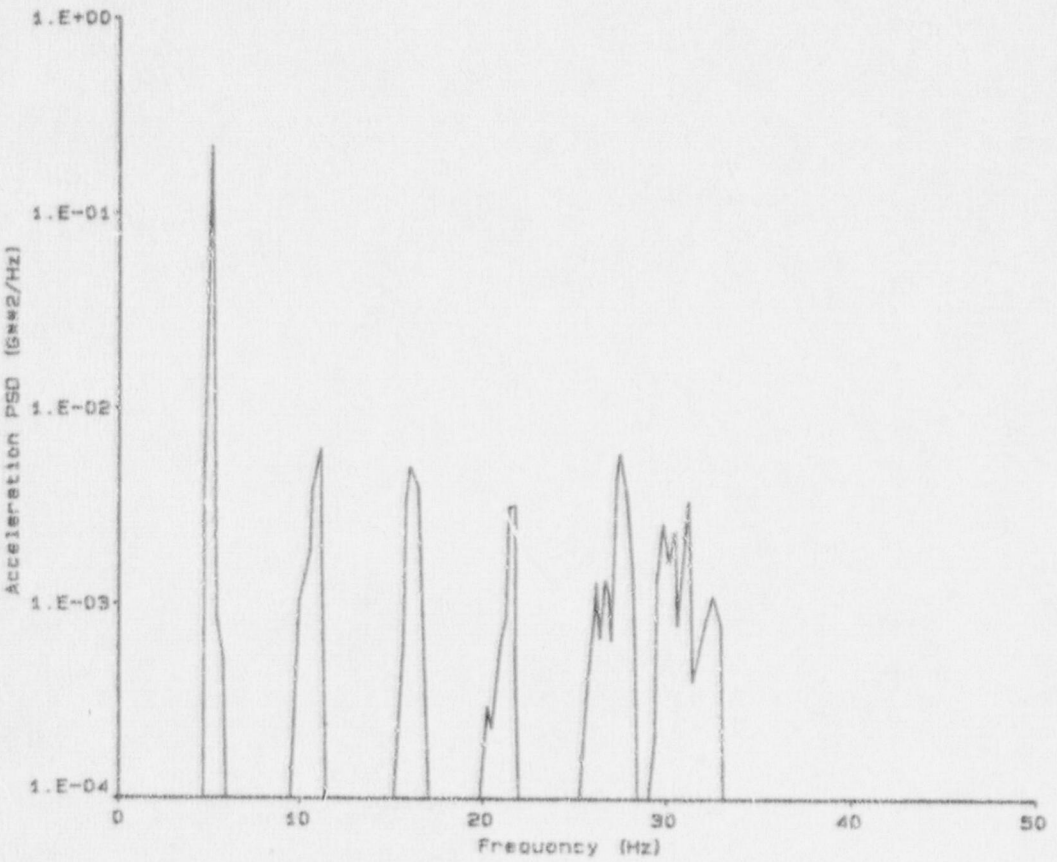

Figure E-14. Power Spectral Density: Test T40.10, spherical "T", frame #2-X.

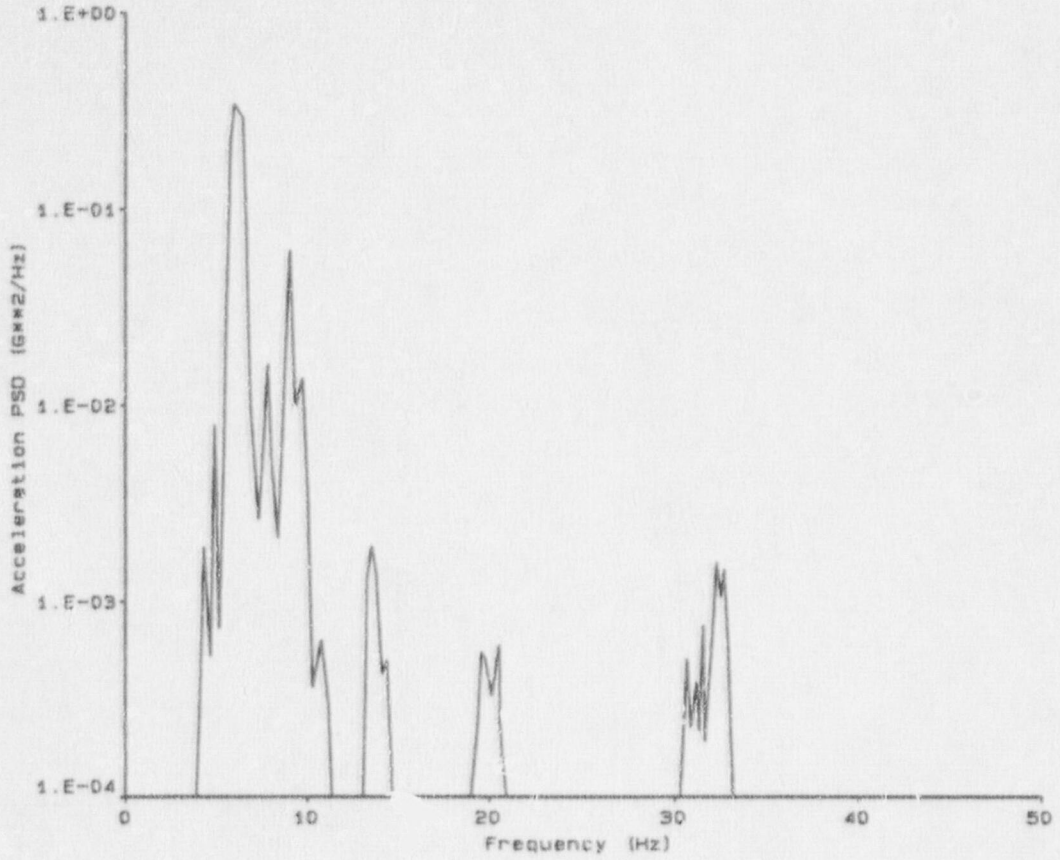

Figure E-15. Power Spectral Density: Test T40.10, spherical "T", frame #1-Y.

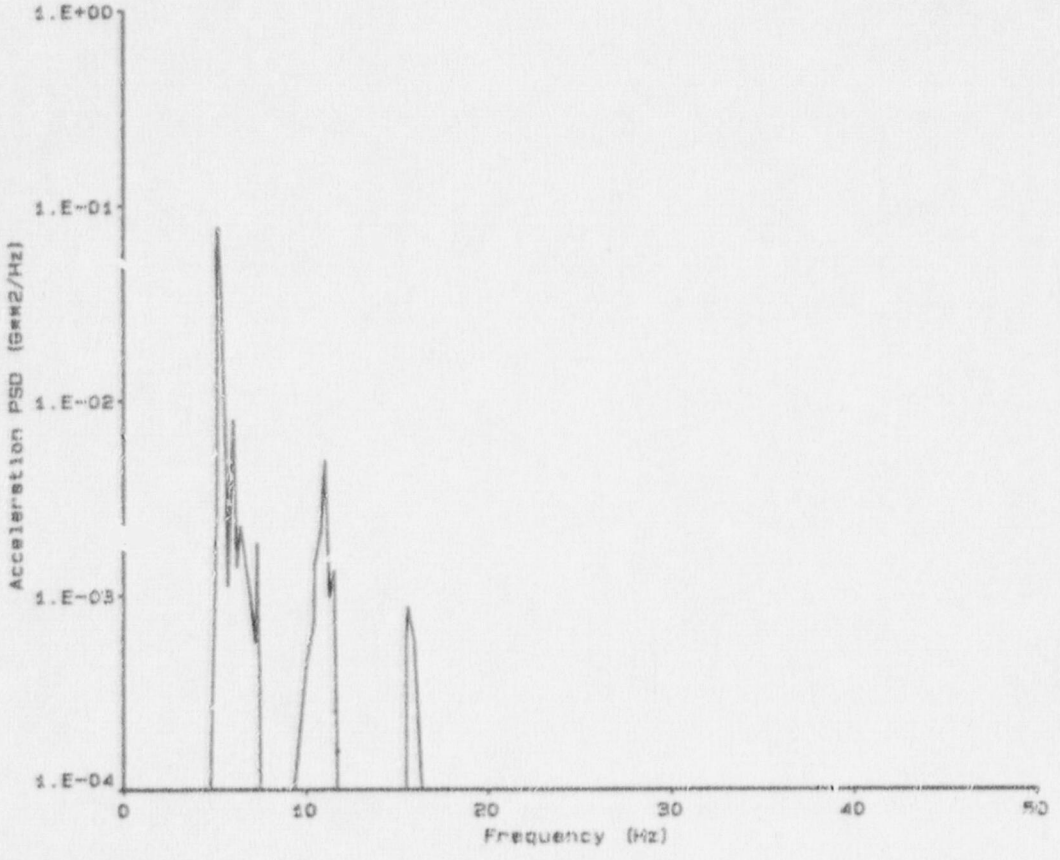

Figure E-16. Power Spectral Density: Test T40.10, spherical "T", frame #2-Y.

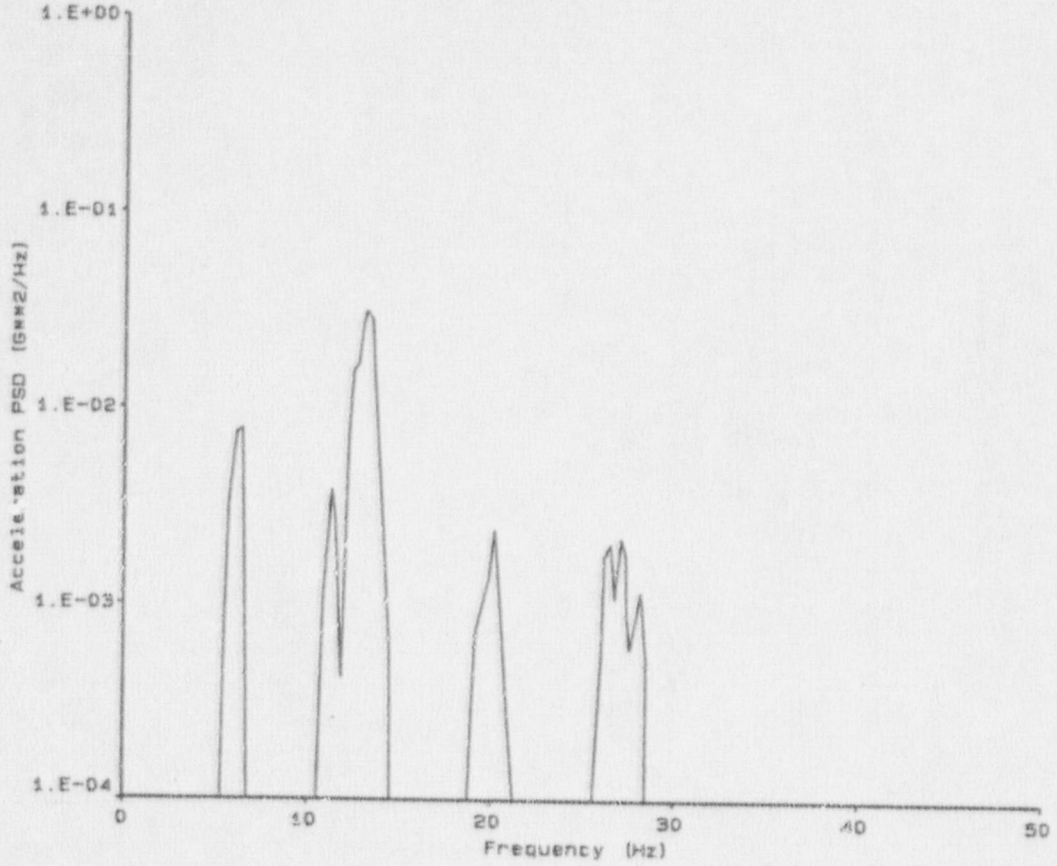

Figure E-17. Power Spectral Density: Test T40.10, spherical "T", frame #1-Z.

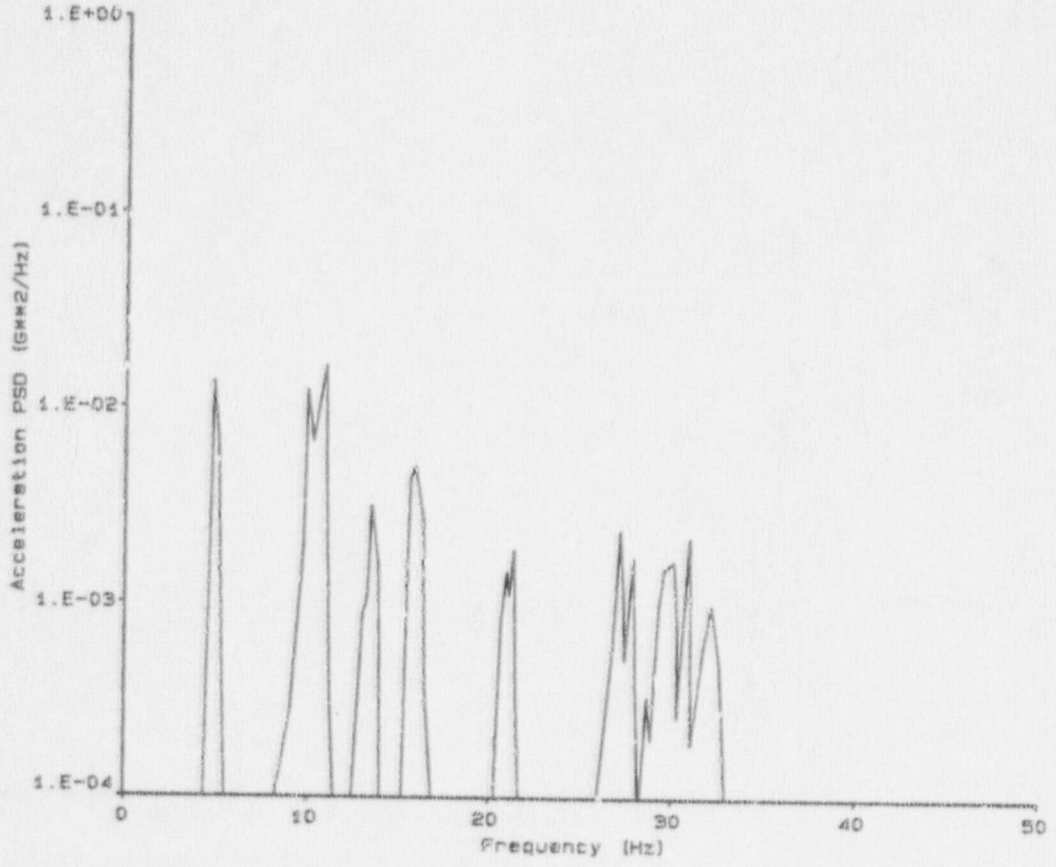

Figure E-18. Power Spectral Density: Test T40.10, spherical "T", frame #2-Z.

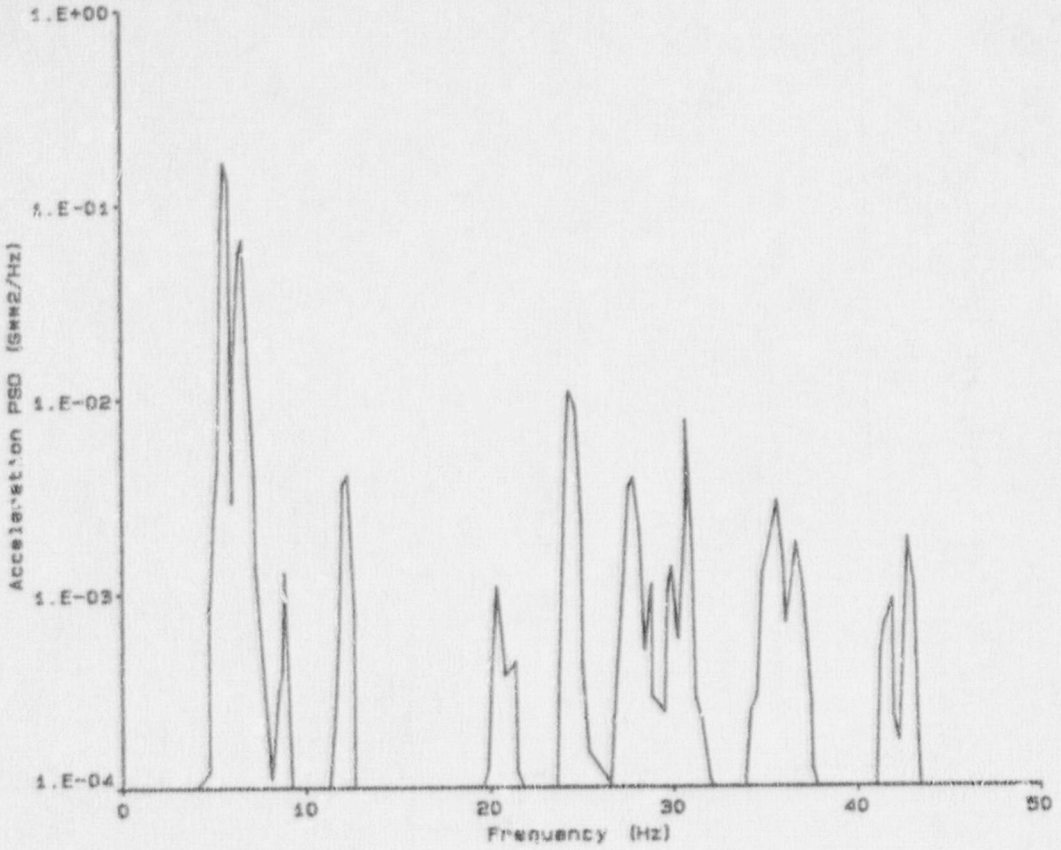

Figure E-19. Power Spectral Density: Test T40.10, standard "T", frame #1-X.

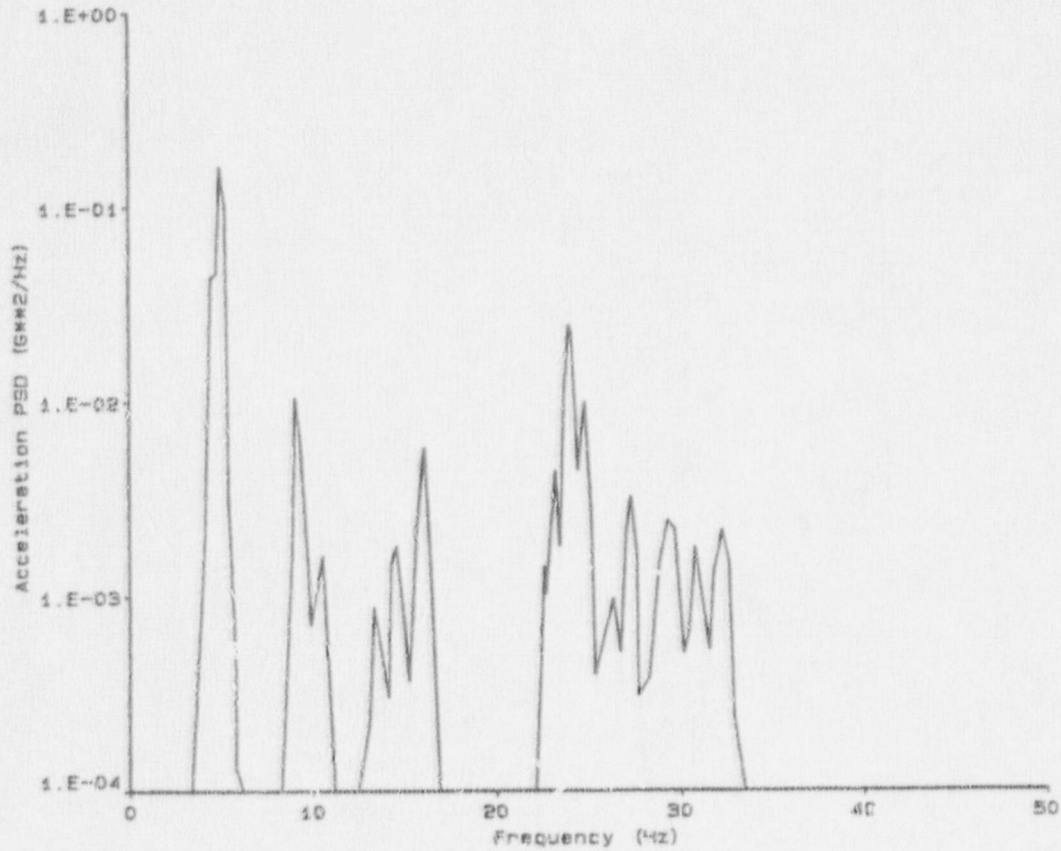

Figure E-20. Power Spectral Density: Test T40.10, standard "T", frame #2-X.

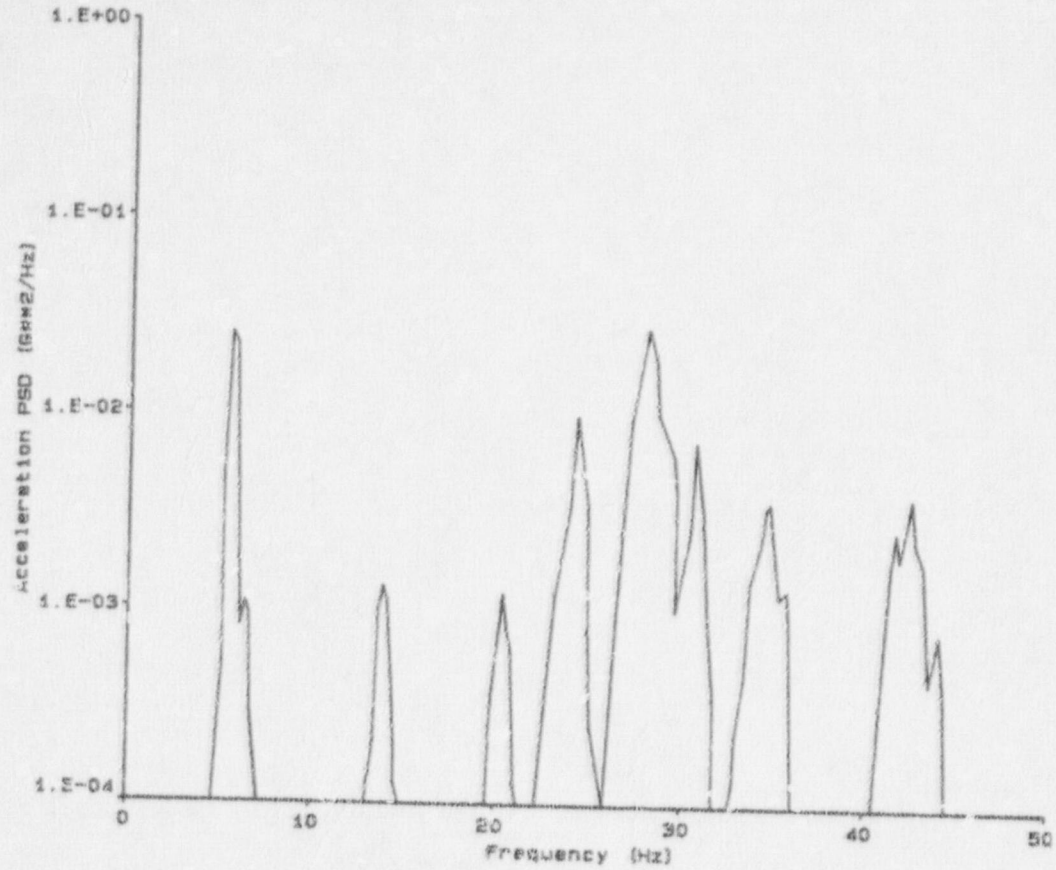

Figure E-21. Power Spectral Density: Test T40.10, standard "T", frame #1-Y.

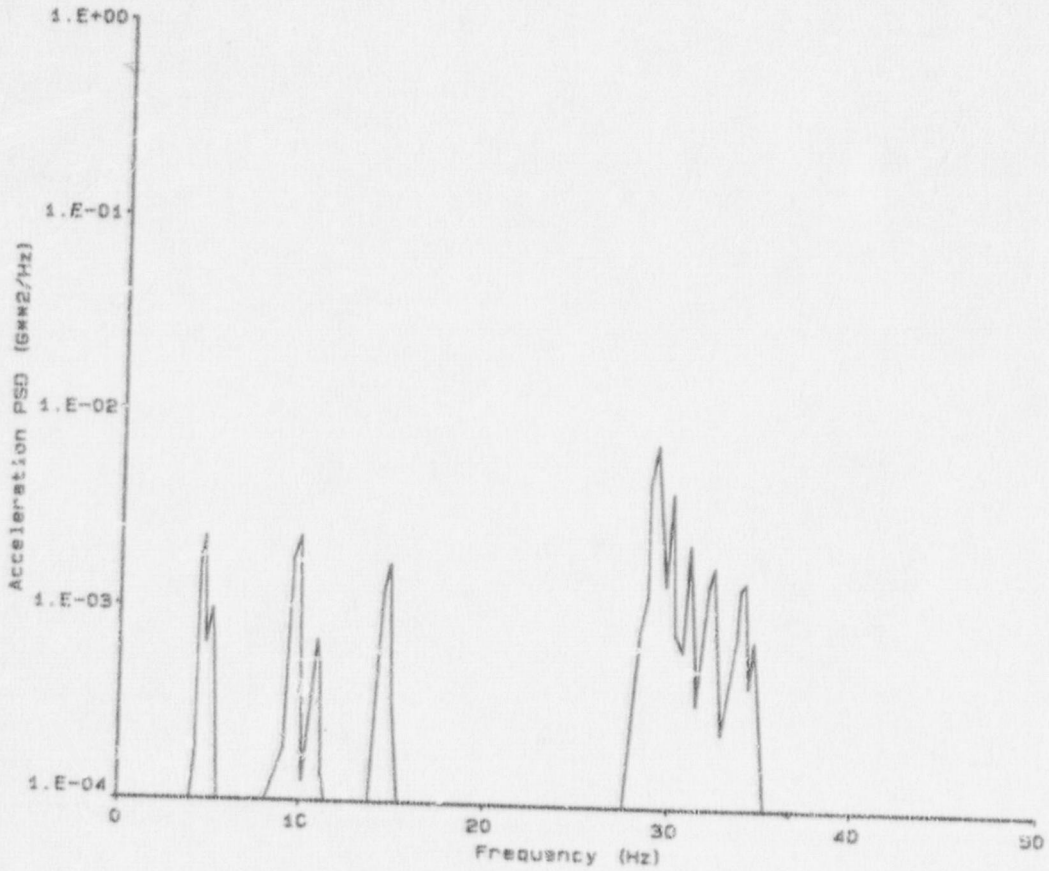

Figure E-22. Power Spectral Density: Test T40.10, standard "T", frame #2-Y.

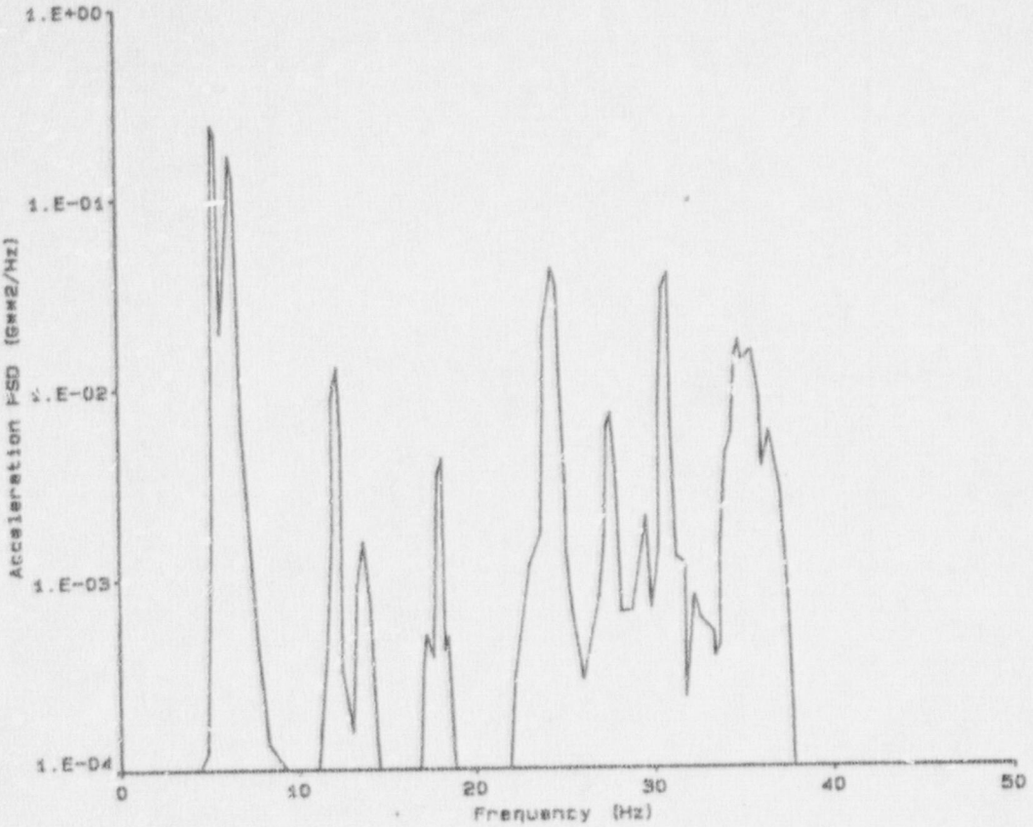

Figure E-23. Power Spectral Density: Test T40.10, standard "T", frame #1-Z.

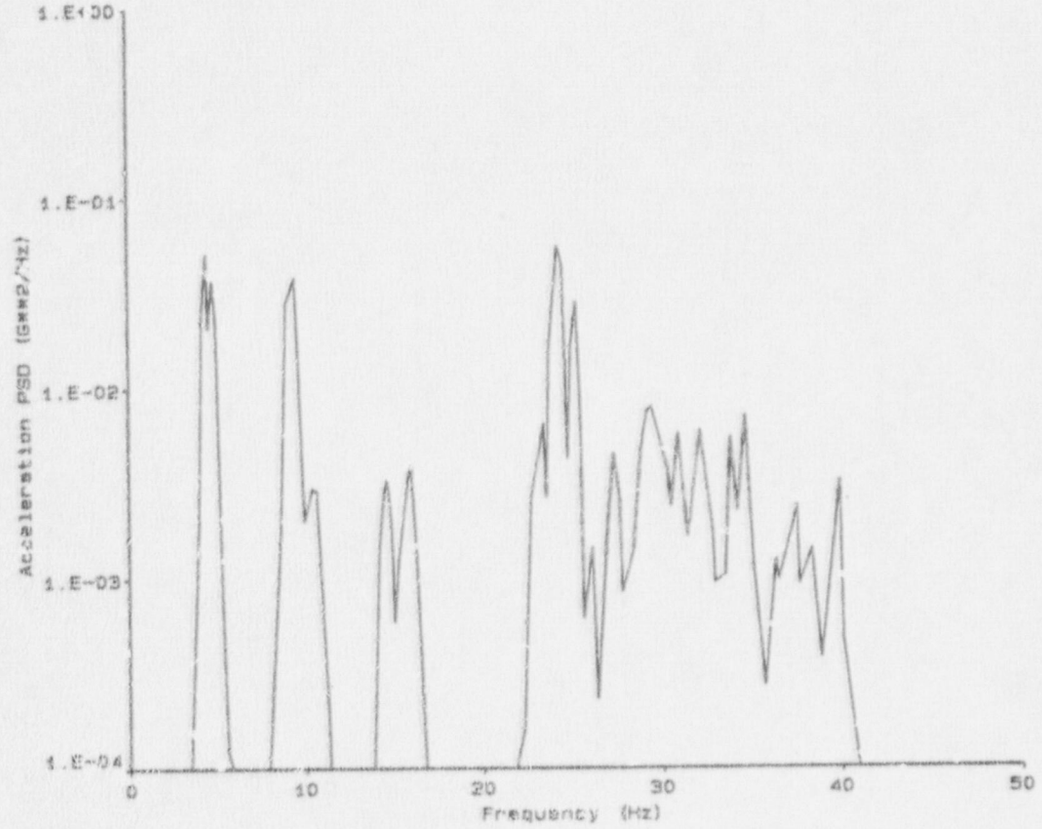

Figure E-24. Power Spectral Density: Test T40.10, standard "T", frame #2-Z.

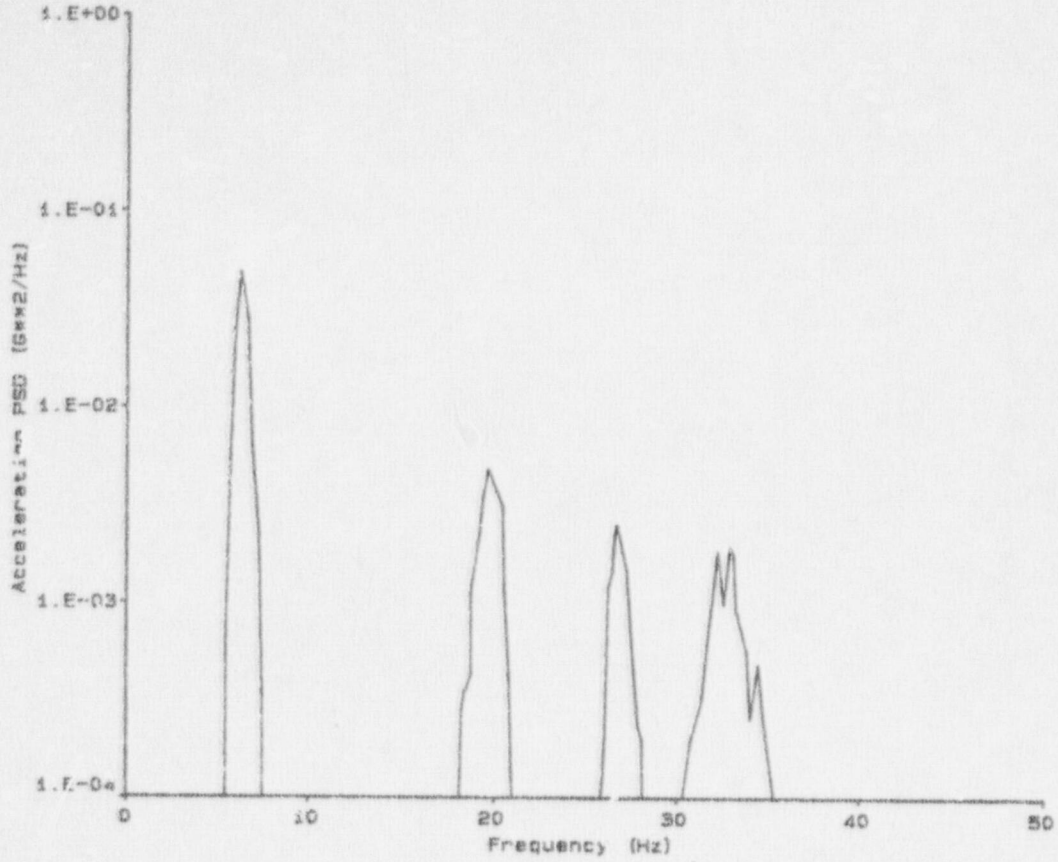

Figure E-25. Power Spectral Density: Test T40.10, top HDU, frame #1-X.

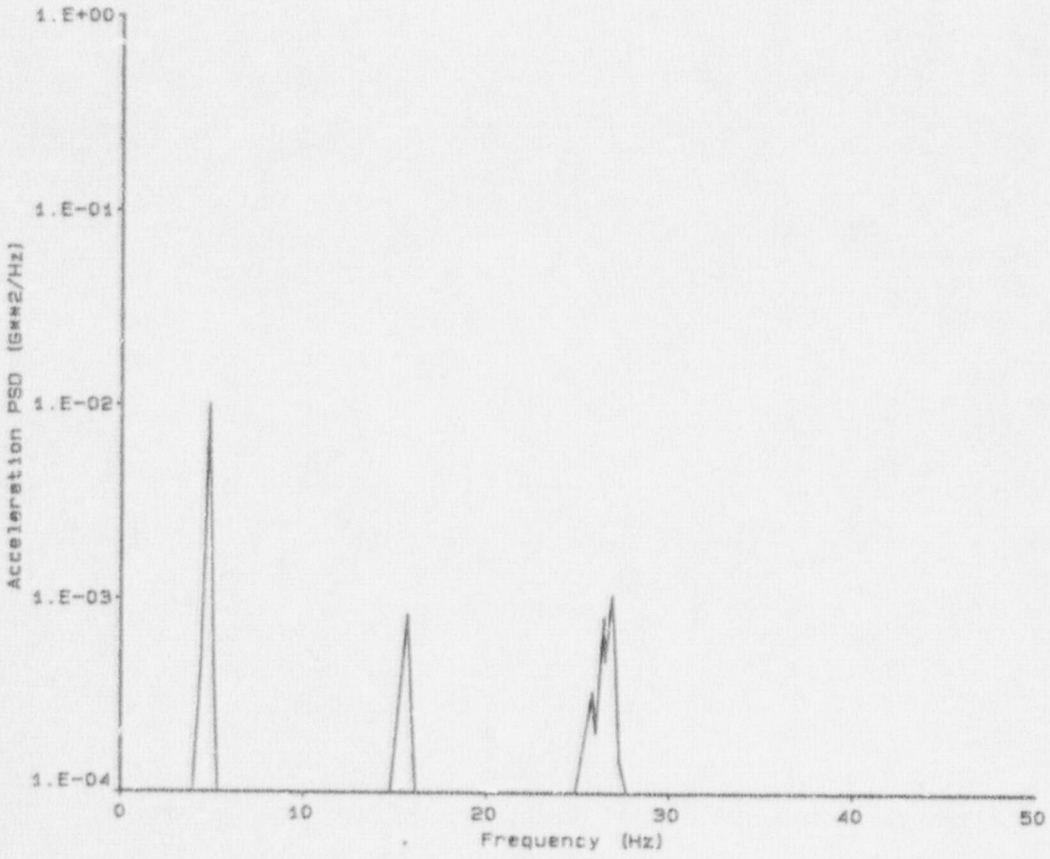

Figure E-26. Power Spectral Density: Test T40.10, top HDU, frame #2-X.

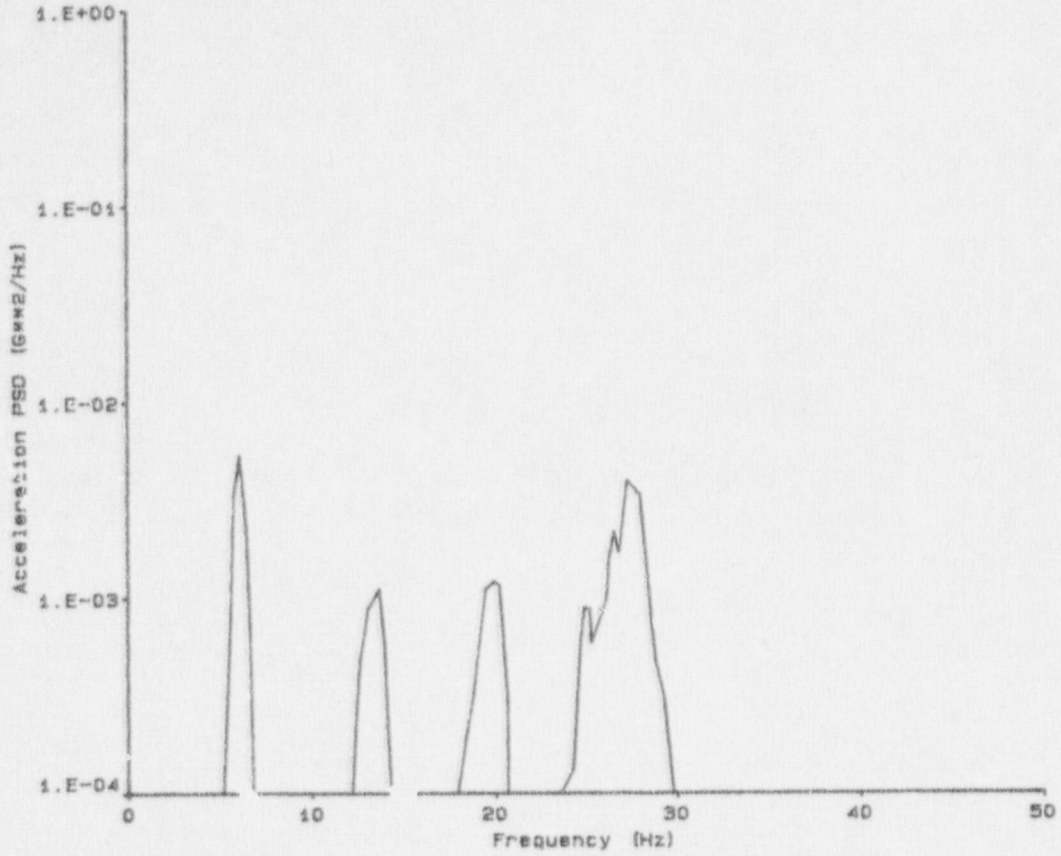

Figure E-27. Power Spectral Density: Test T40.10, top HDU, frame #1-Y.

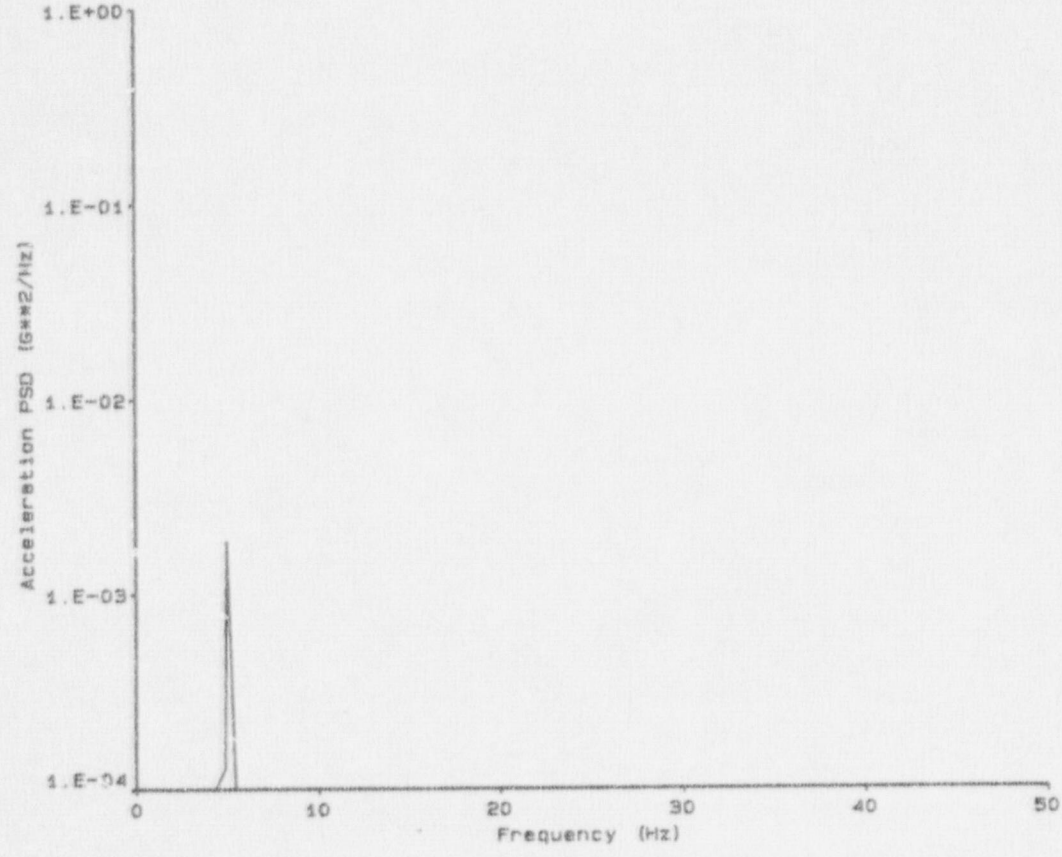

Figure E-28. Power Spectral Density: Test T40.10, top HDU, frame #2-Y.

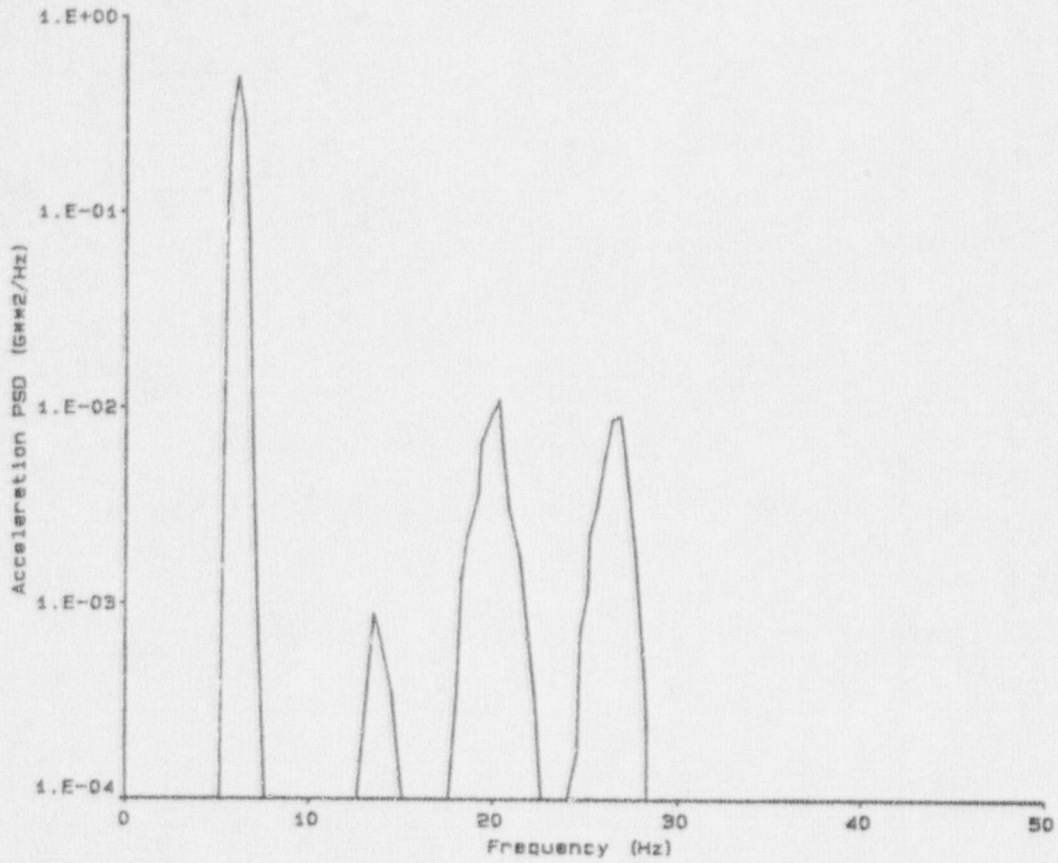

Figure E-29. Power Spectral Density: Test T40.10, top HDU, frame #1-Z.

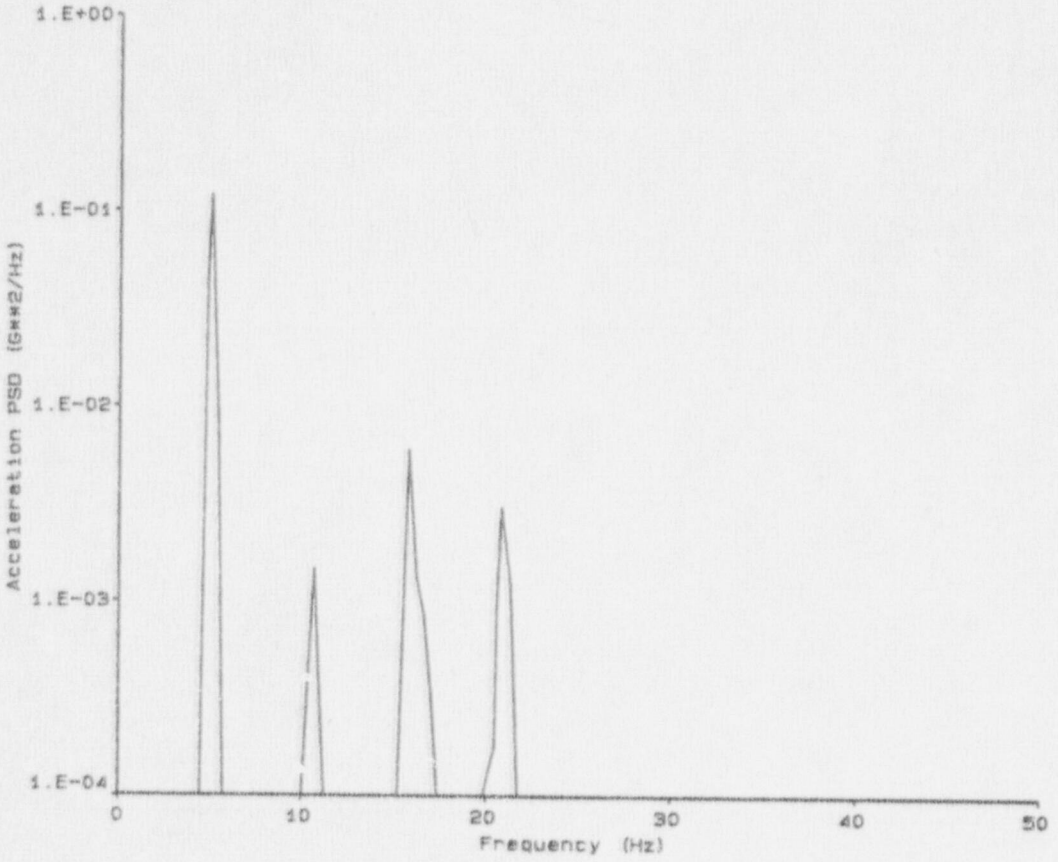

Figure E-30. Power Spectral Density: Test T40.10, top HDU, frame #2-Z.

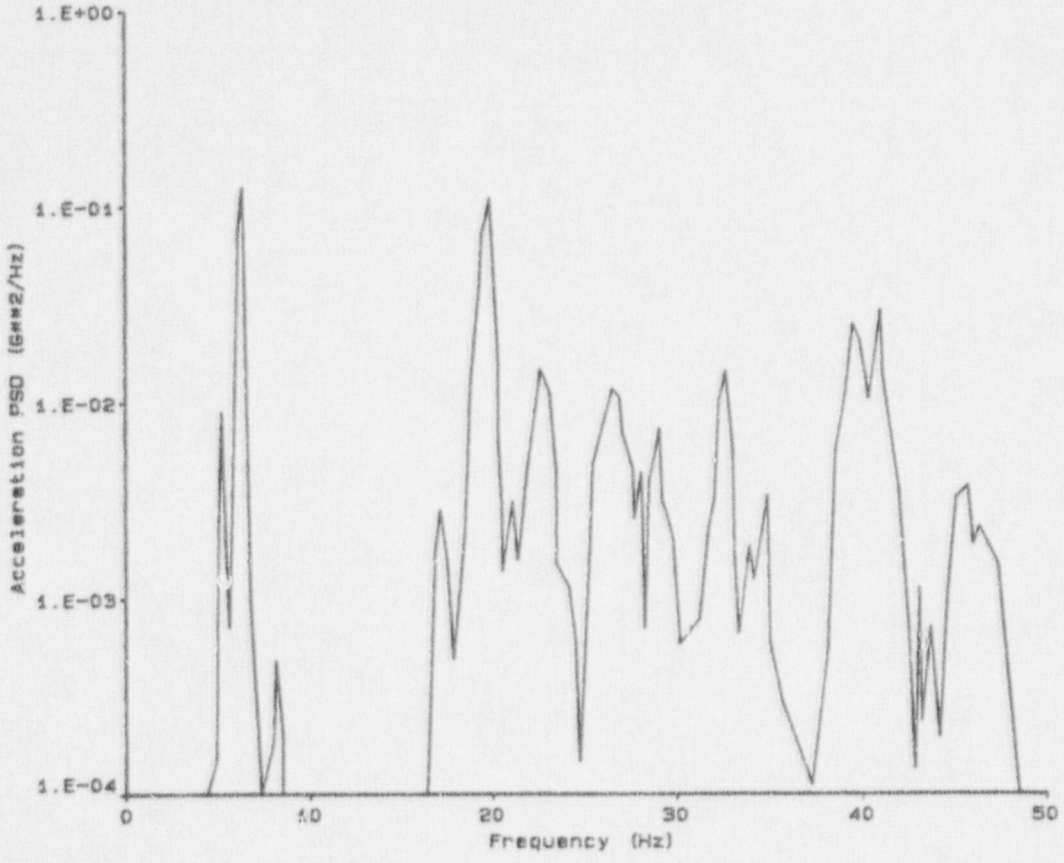

Figure E-31. Power Spectral Density: Test T40.30, valve operator, frame #1-X.

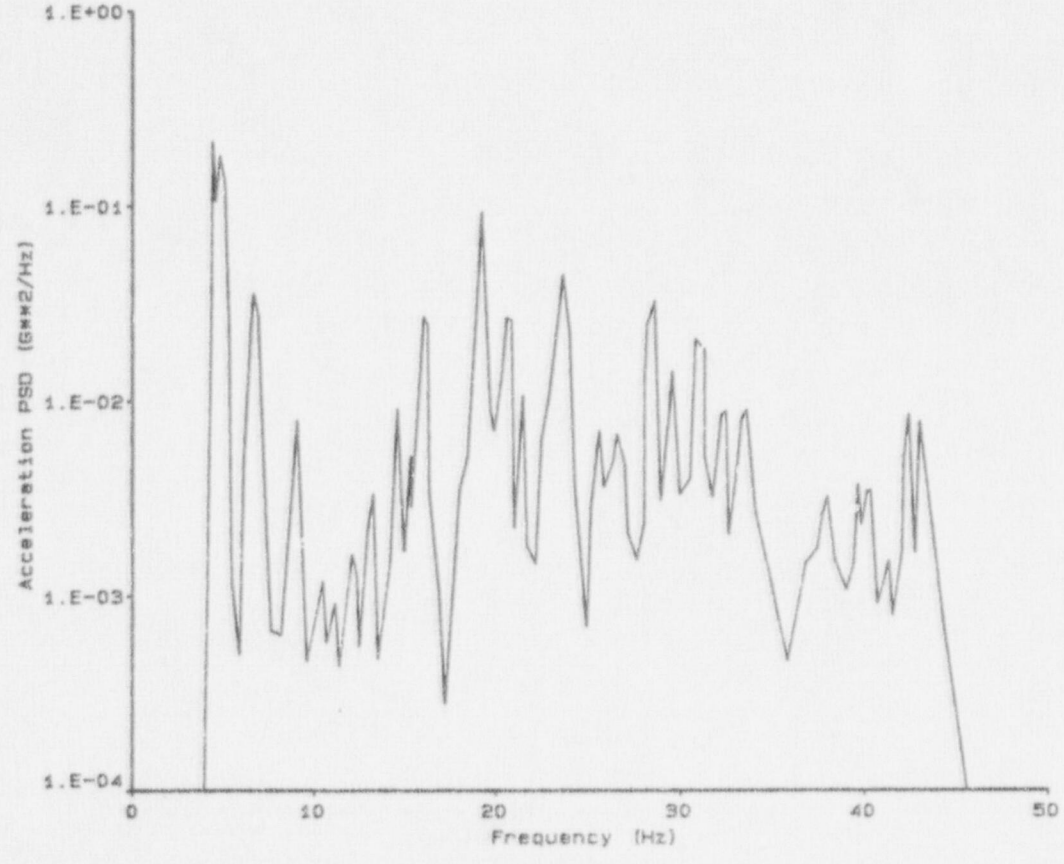

Figure E-32. Power Spectral Density: Test T40.30, valve operator, frame #2-X.

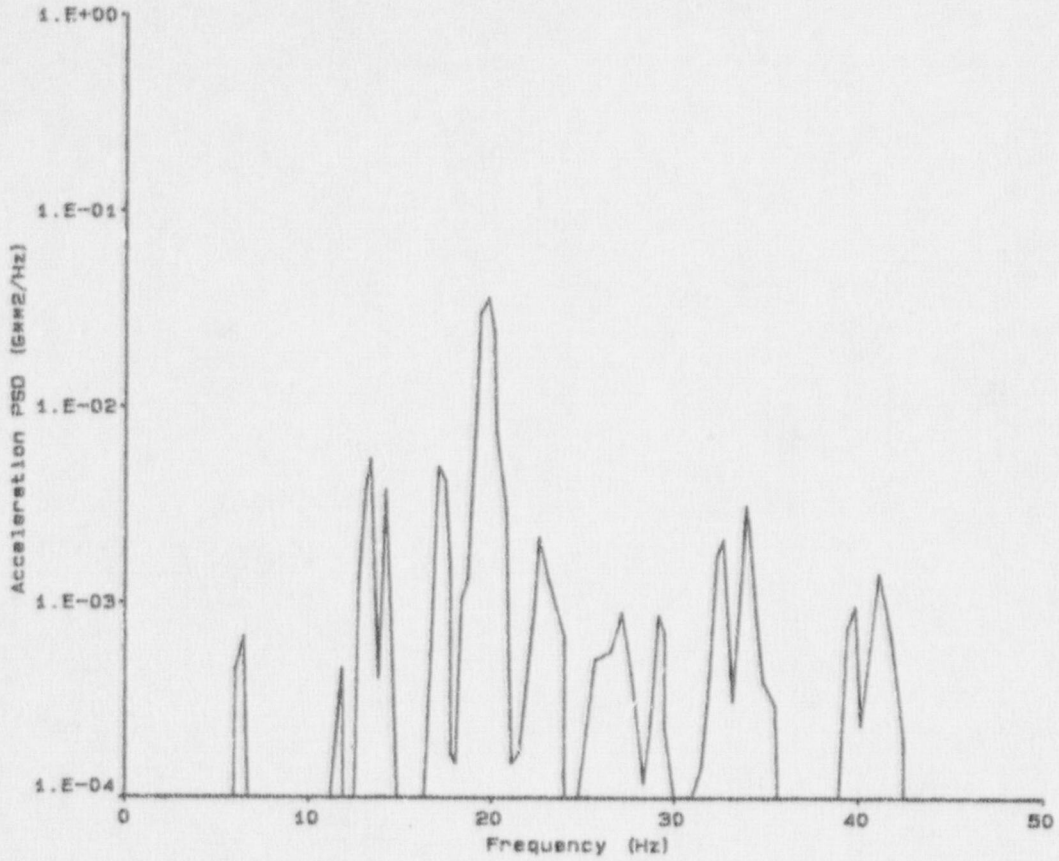

Figure E-33. Power Spectral Density: Test T40.30, valve operator, frame #1-Y.

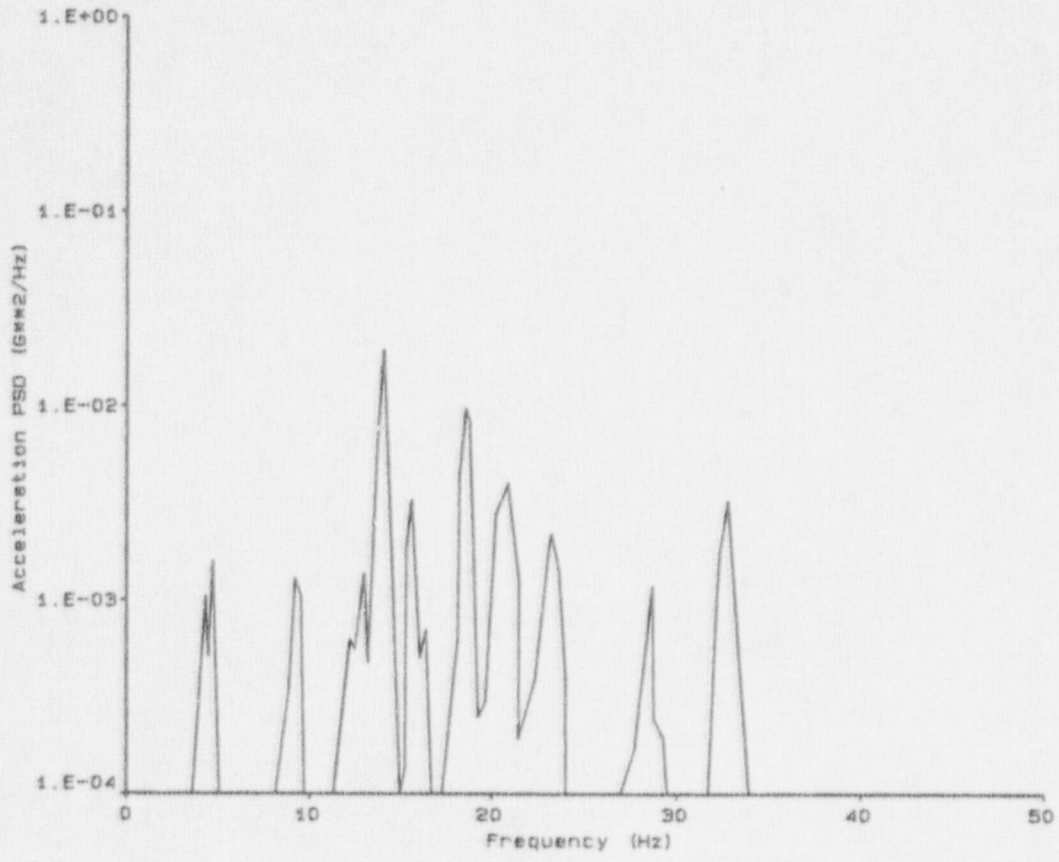

Figure E-34. Power Spectral Density: Test T40.30, valve operator, frame #2-Y.

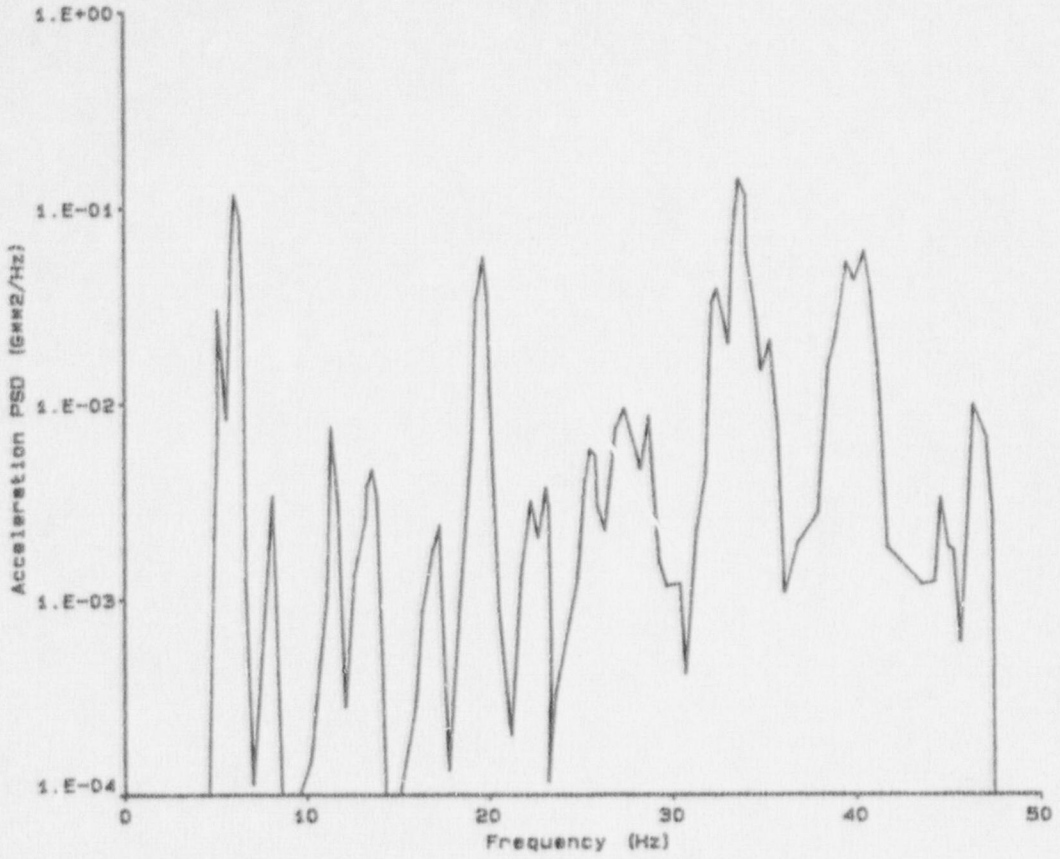

Figure E-35. Power Spectral Density: Test T40.30, valve operator, frame #1-Z.

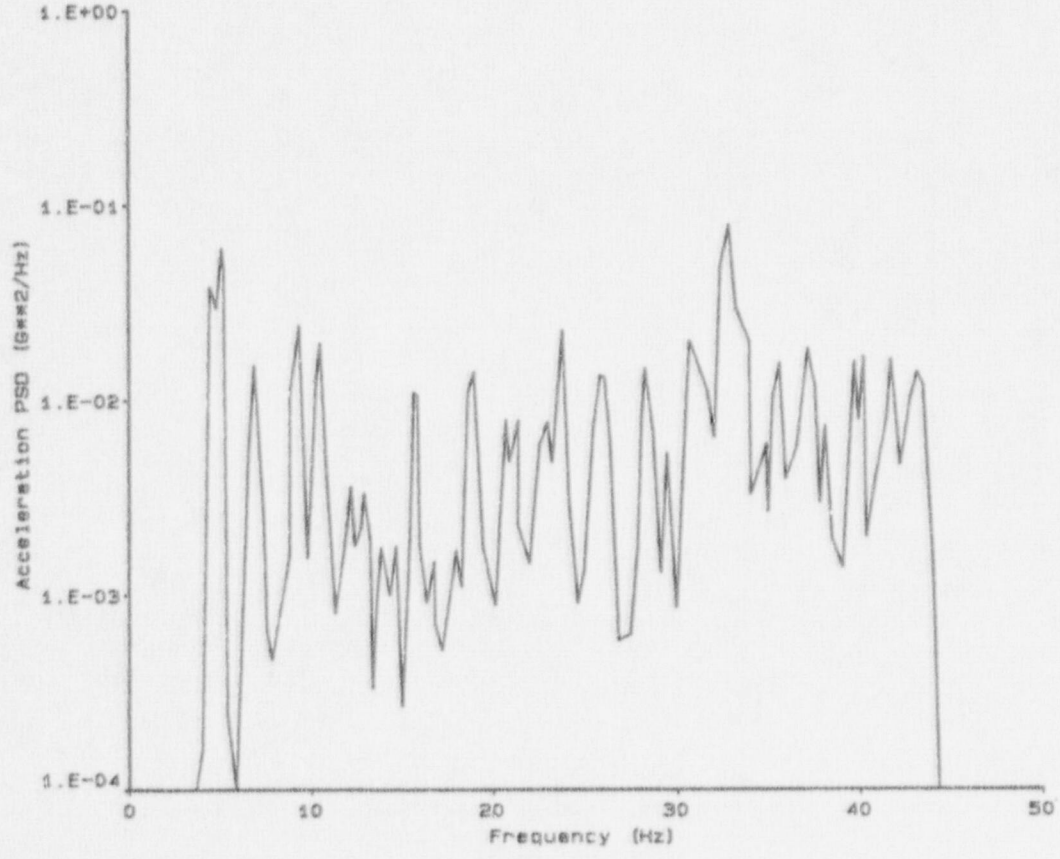

Figure E-36. Power Spectral Density: Test T40.30, valve operator, frame #2-Z.

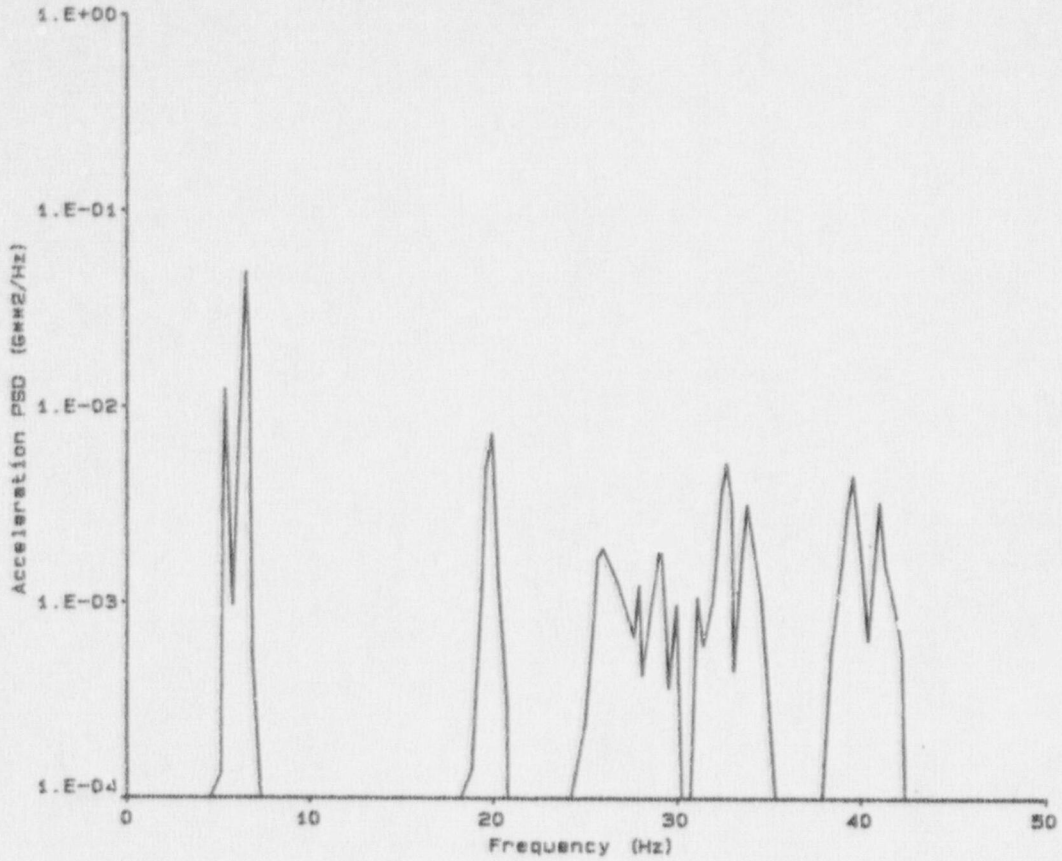

Figure E-37. Power Spectral Density: Test T40.30, valve body, frame #1-X.

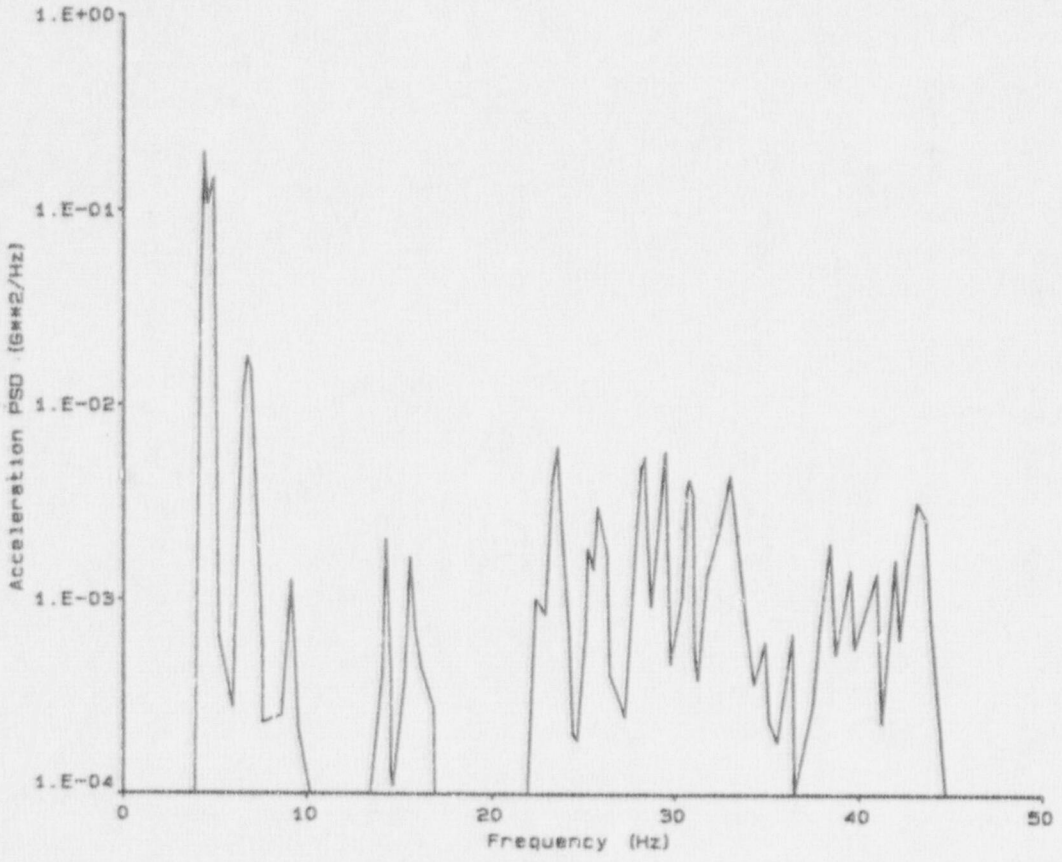

Figure E-38. Power Spectral Density: Test T40.30, valve body, frame #2-X.

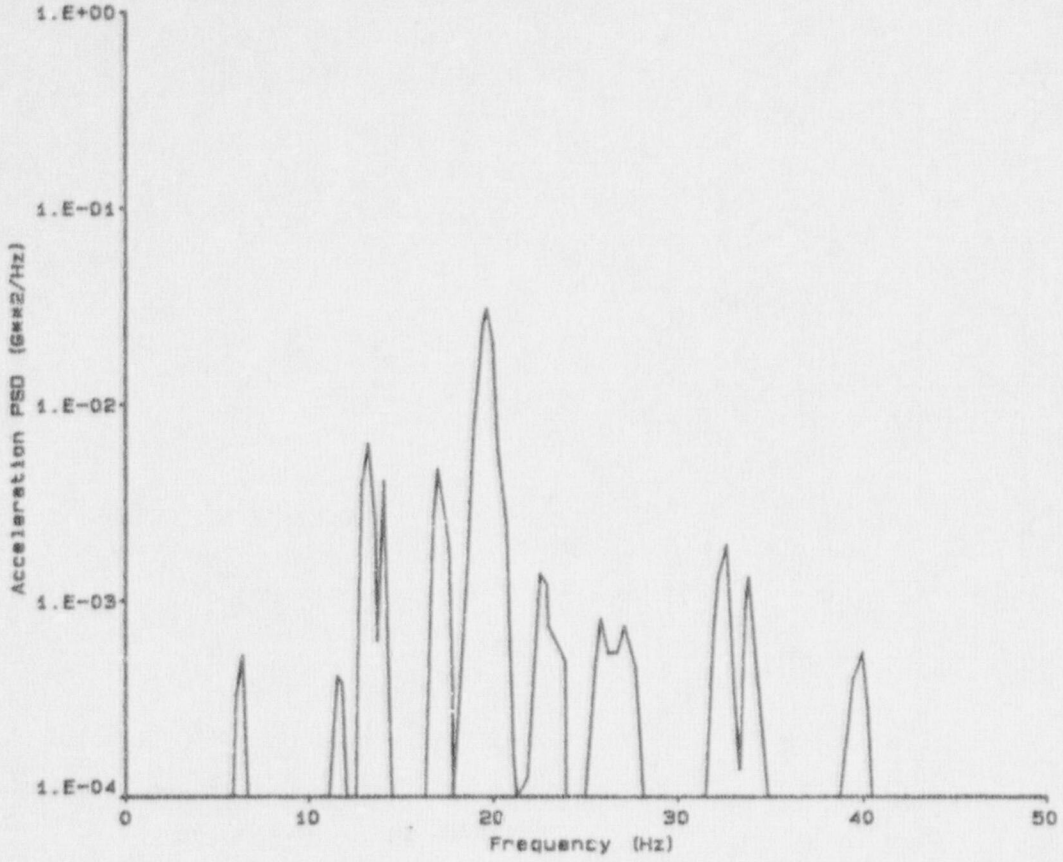

Figure E-39. Power Spectral Density: Test T40.30, valve body, frame #1-Y.

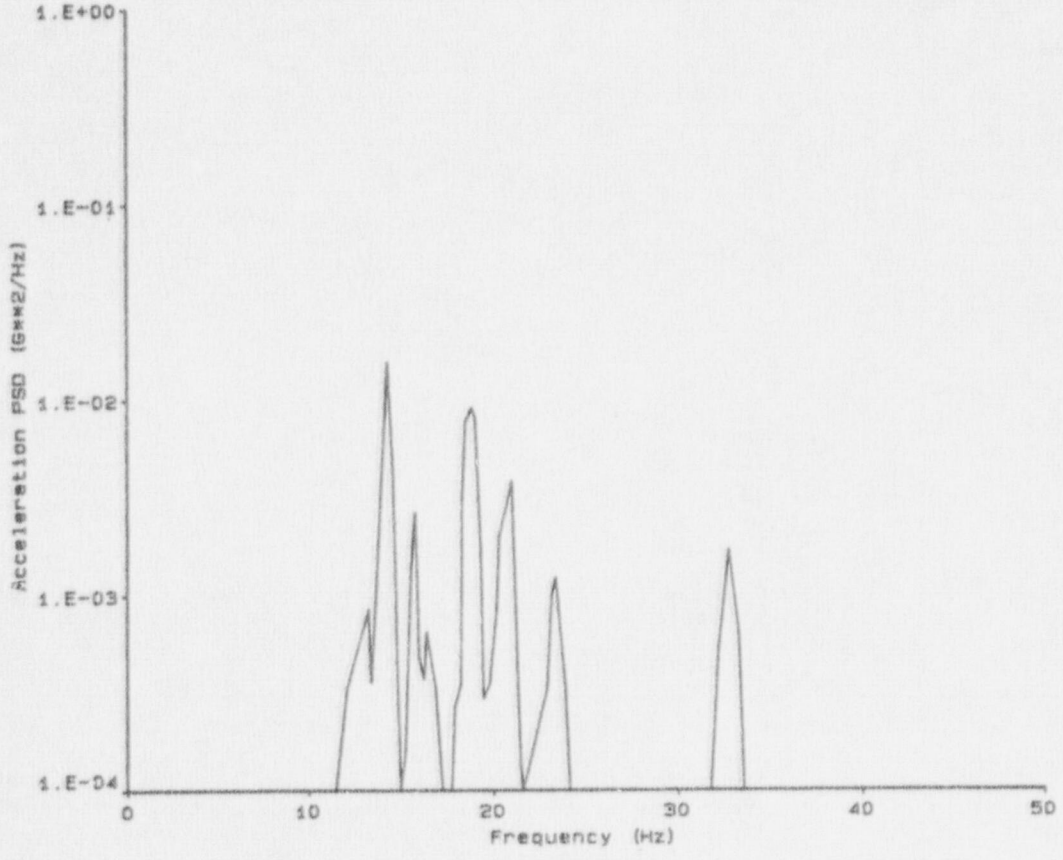

Figure E-40. Power Spectral Density: Test T40.30, valve body, frame #2-Y.

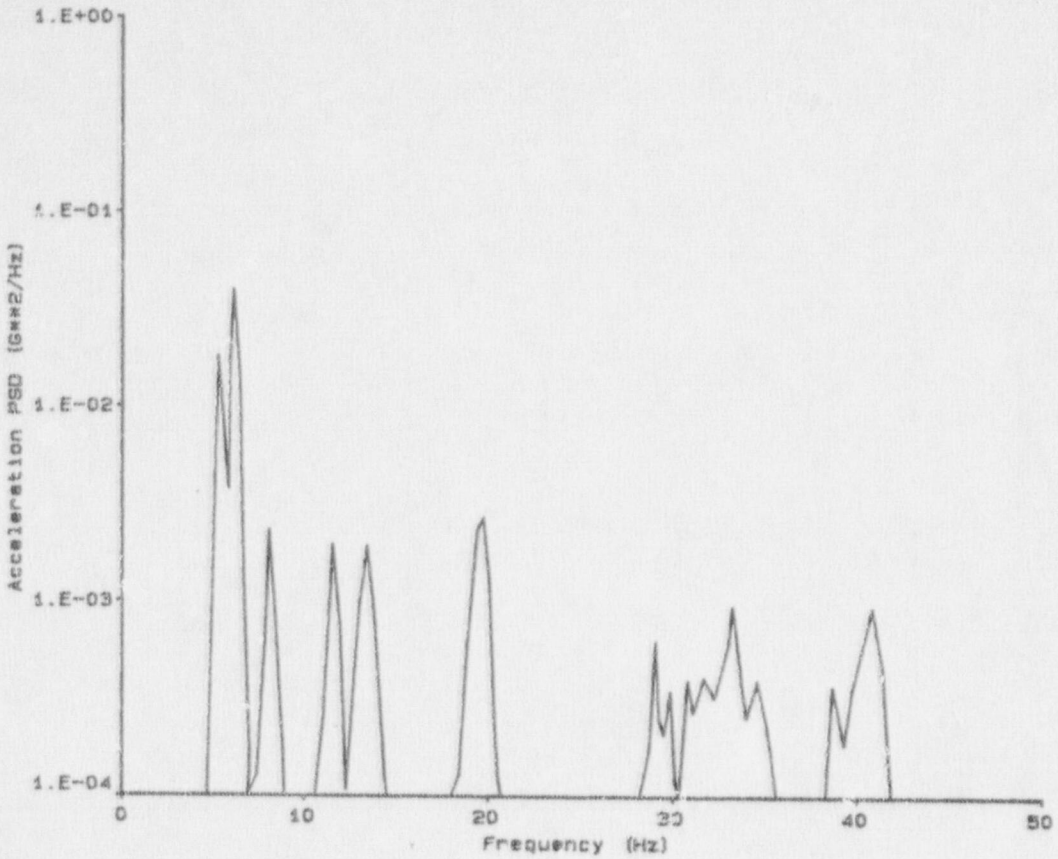

Figure E-41. Power Spectral Density: Test T40.30, valve body, frame #1-Z.

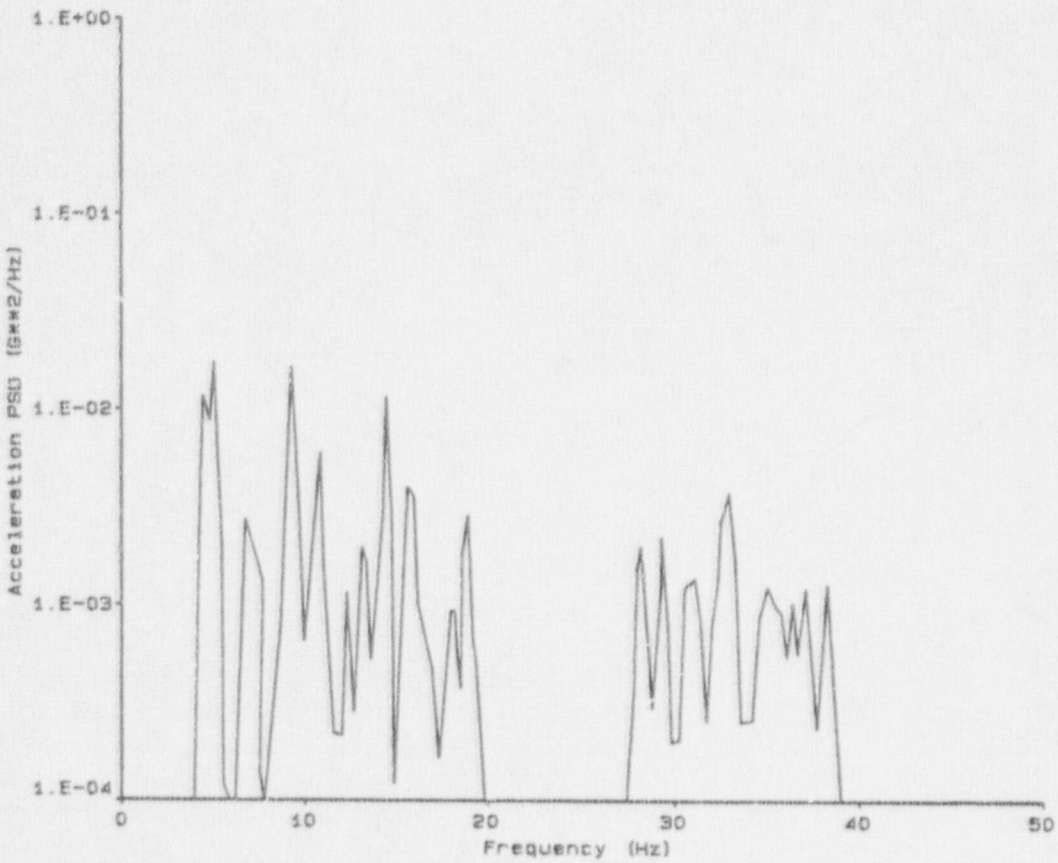

Figure E-42. Power Spectral Density: Test T40.30, valve body, frame #2-Z.

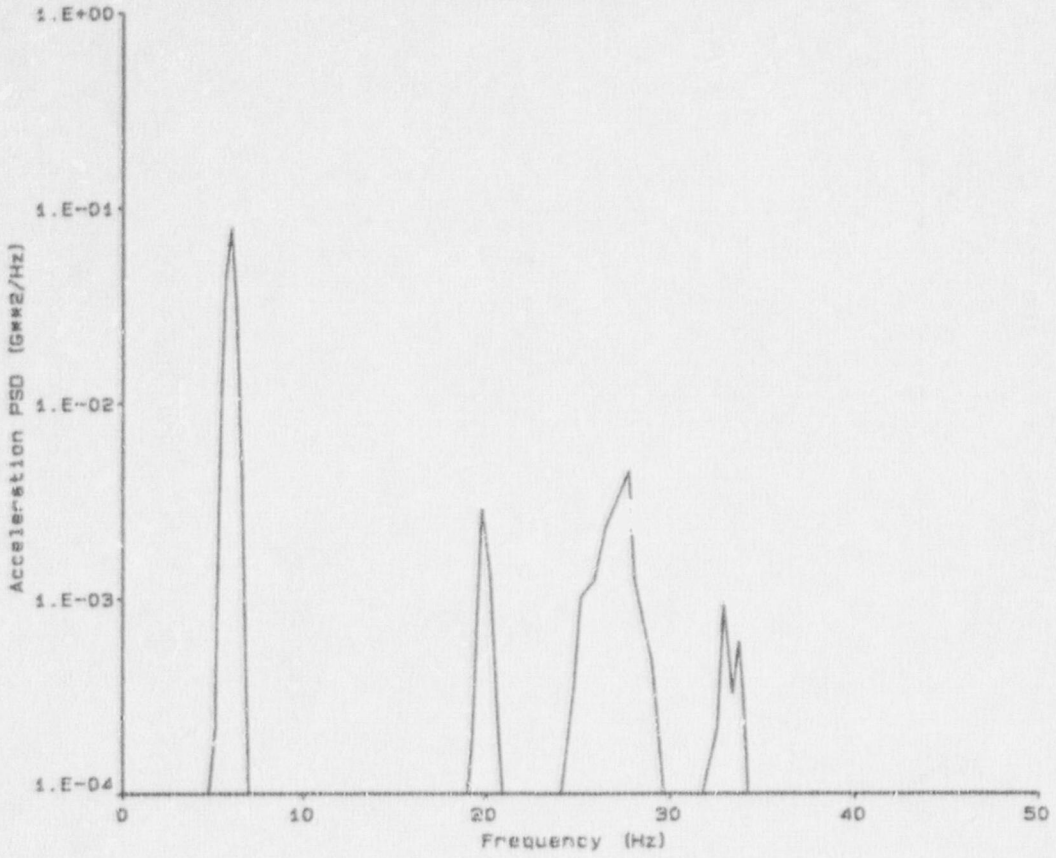

Figure E-43. Power Spectral Density: Test T40.30, spherical "T", frame #1-X.

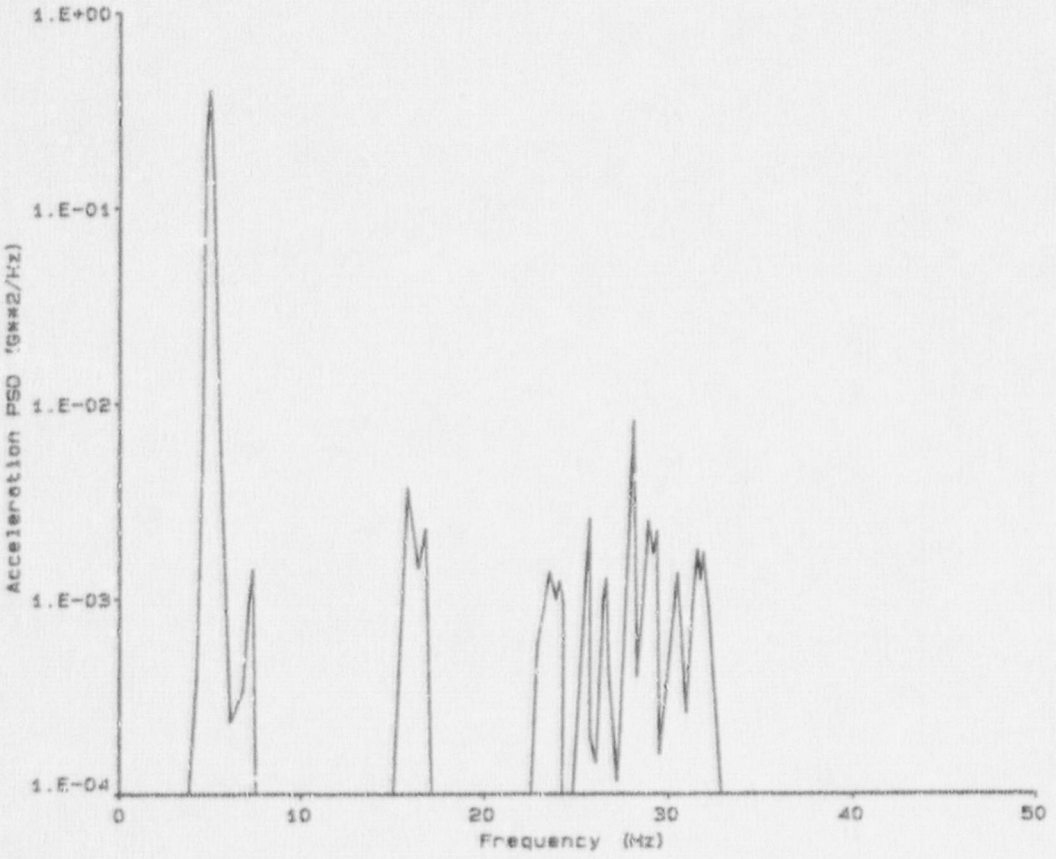

Figure E-44. Power Spectral Density: Test T40.30, spherical "T", frame #2-X.

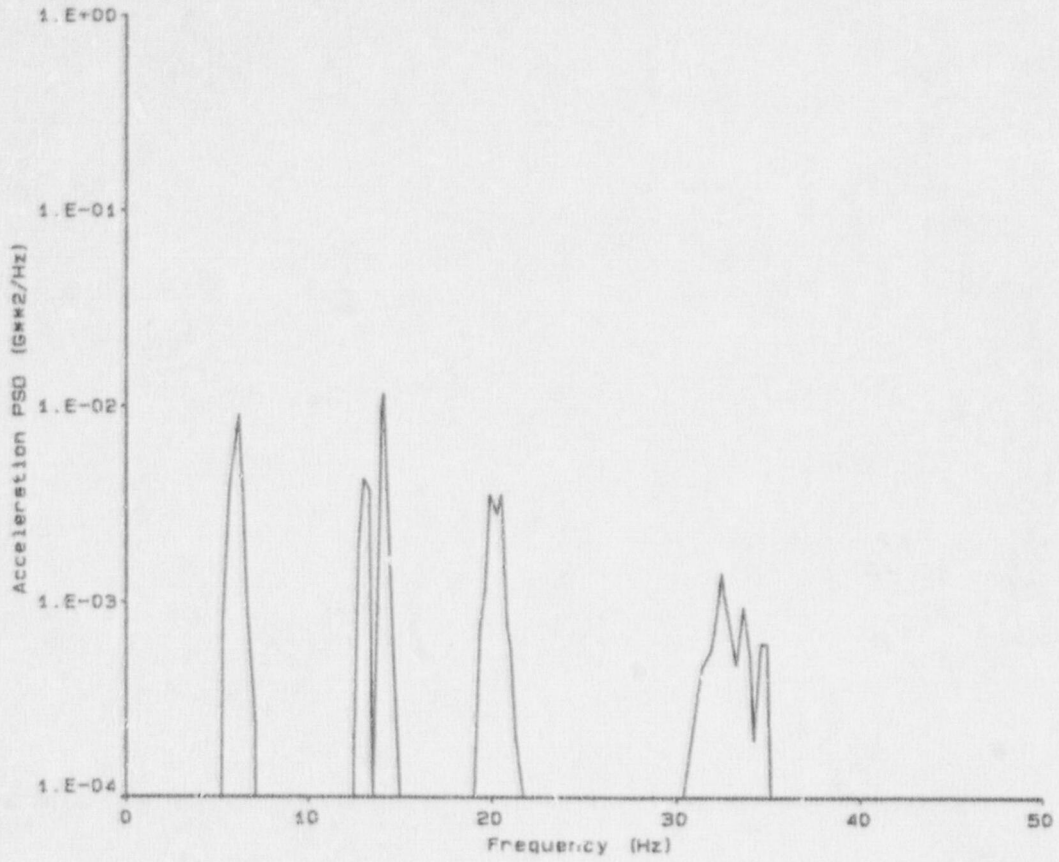

Figure E-45. Power Spectral Density: Test T40.30, spherical "T", frame #1-Y.

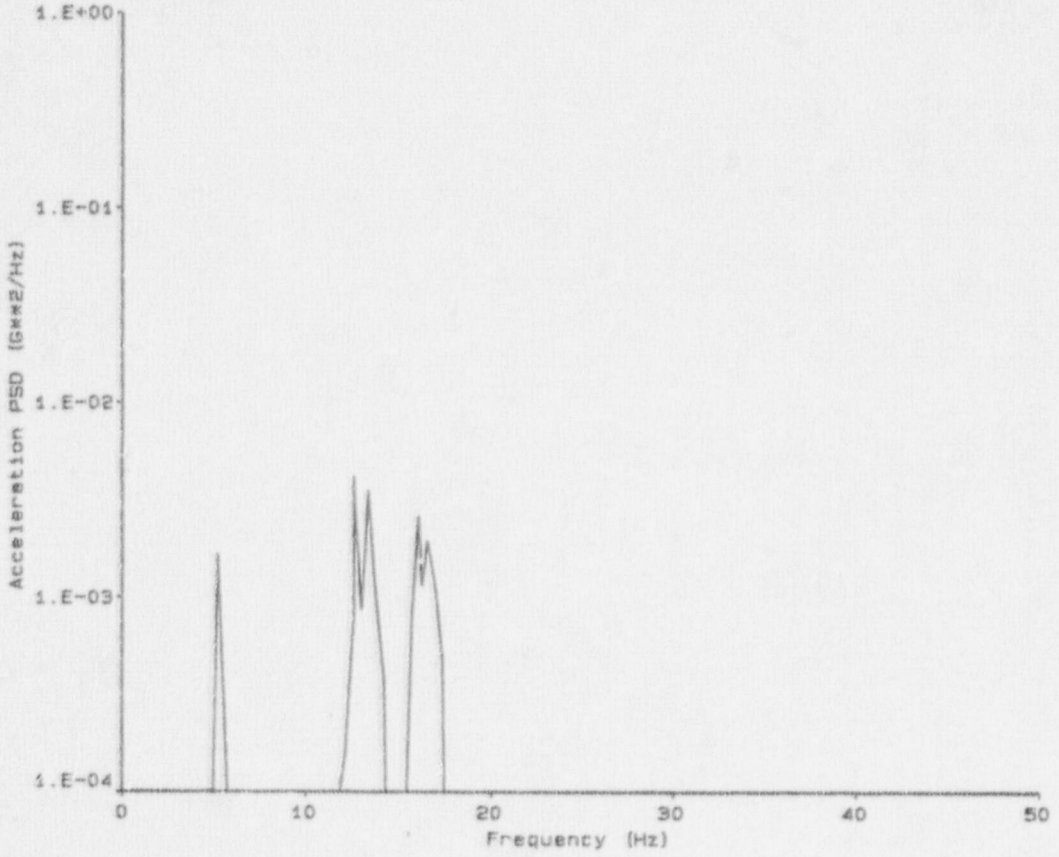

Figure E-46. Power Spectral Density: Test T40.30, spherical "T", frame #2-Y.

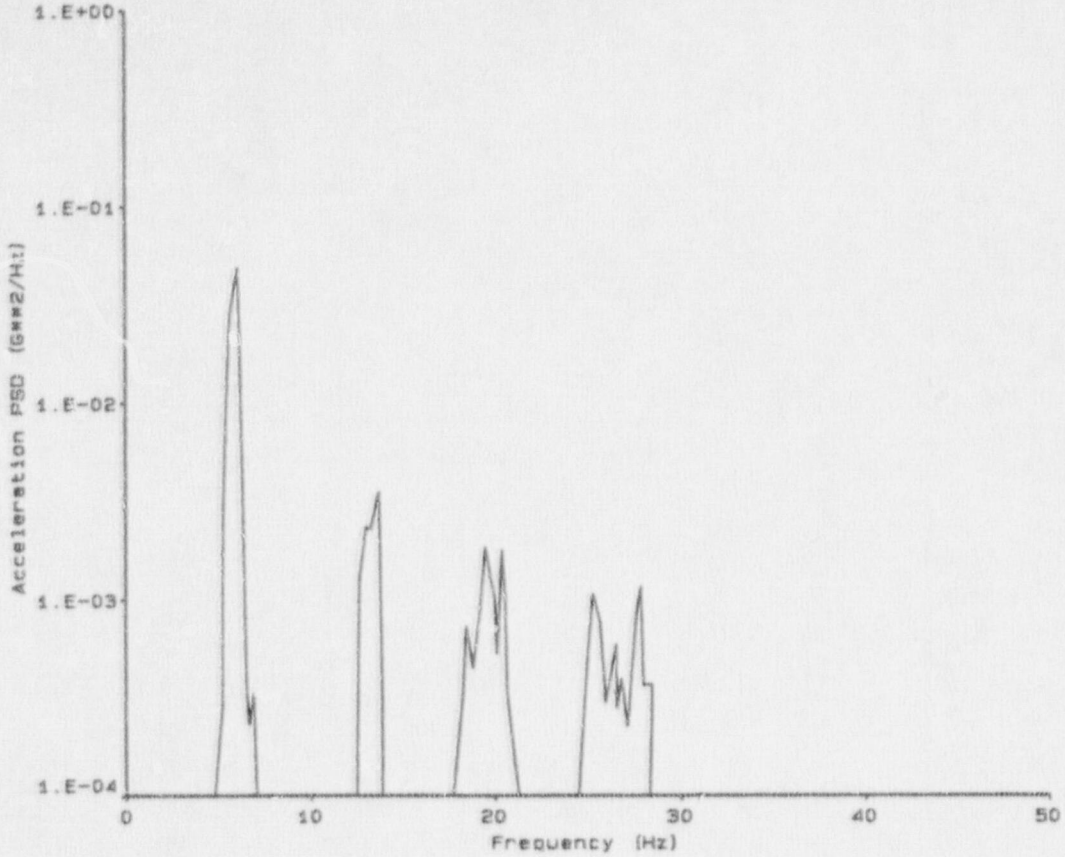

Figure E-47. Power Spectral Density: Test T40.30, spherical "T", frame #1-Z.

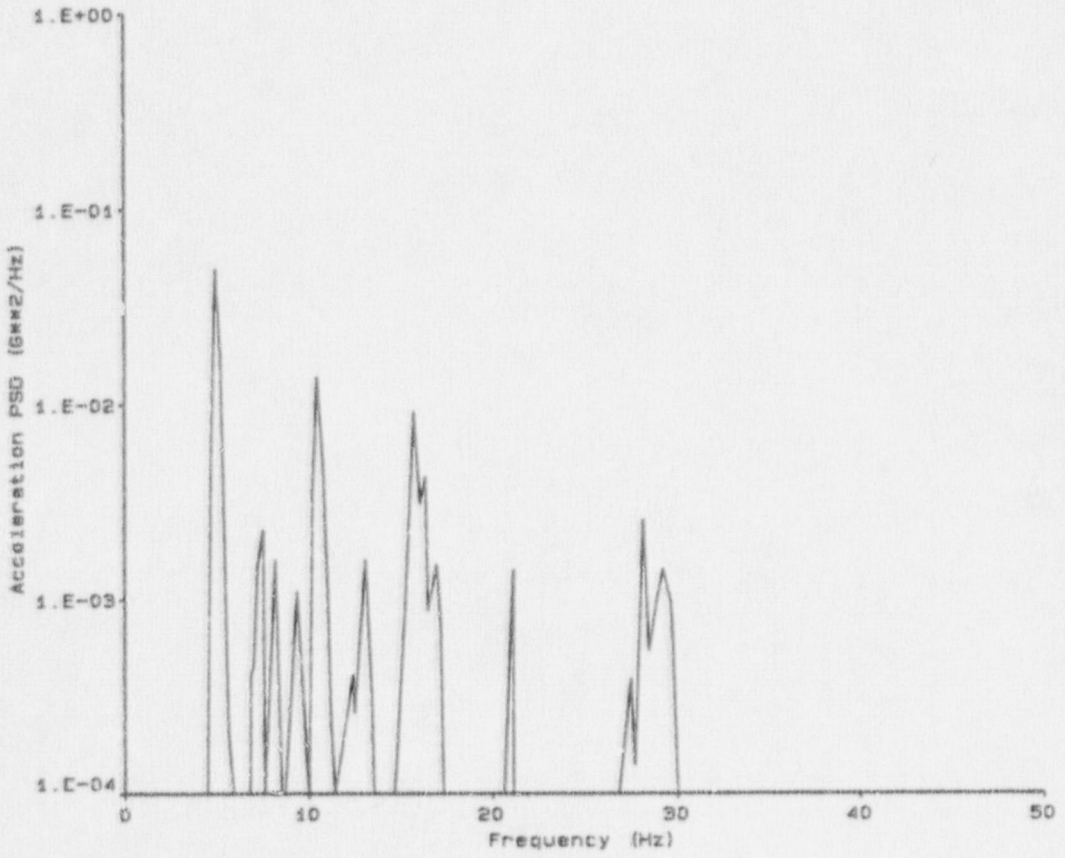

Figure E-48. Power Spectral Density: Test T40.30, spherical "T", frame #2-Z.

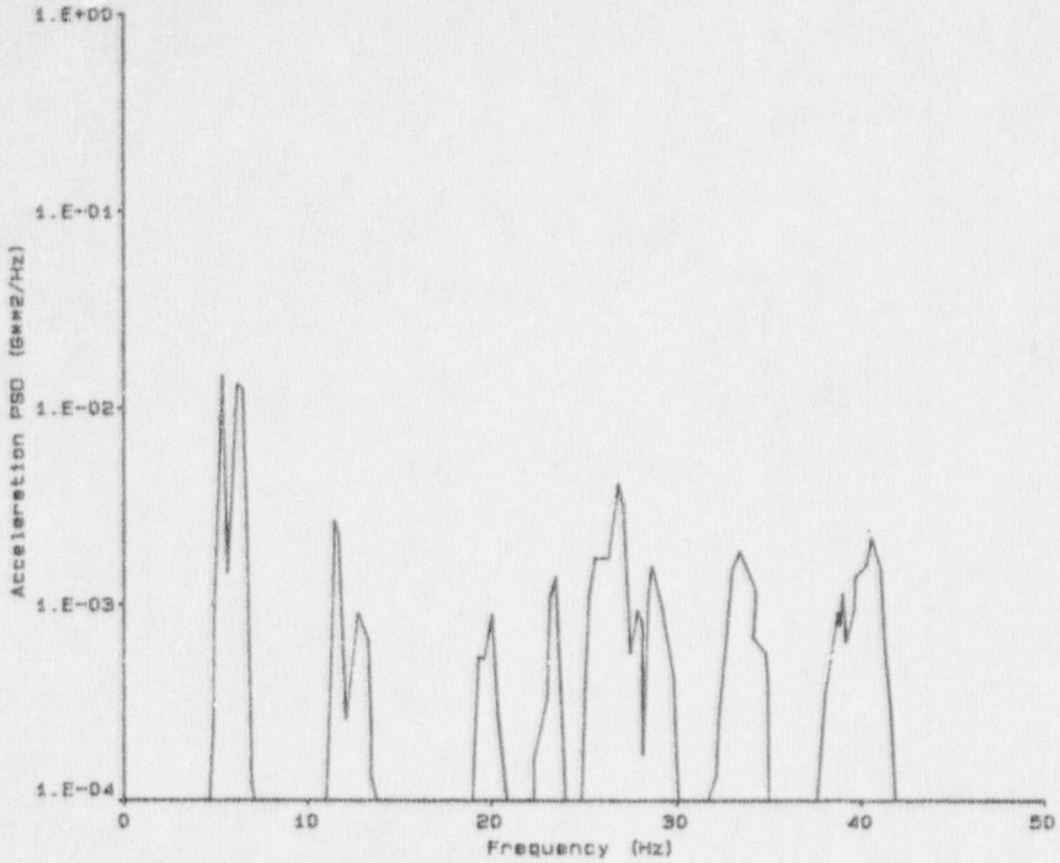

Figure E-49. Power Spectral Density: Test T40.30, standard "T", frame #1-X.

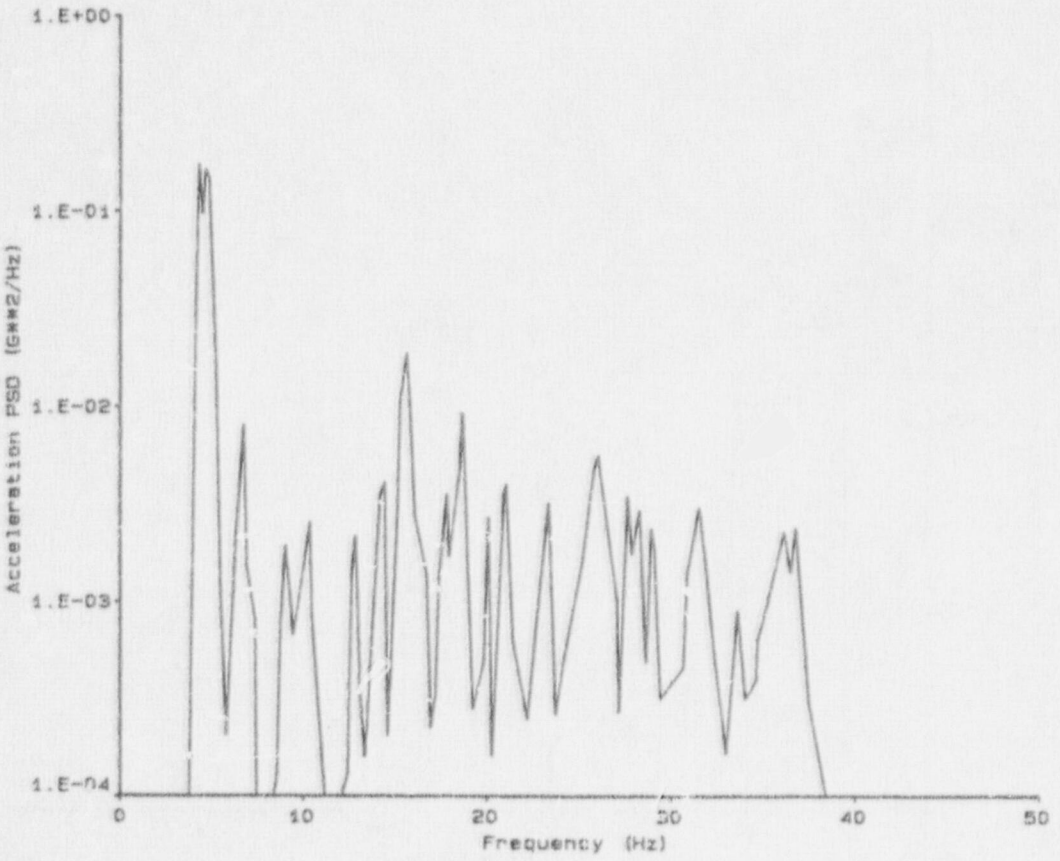

Figure E-50. Power Spectral Density: Test T40.30, standard "T", frame #2-X.

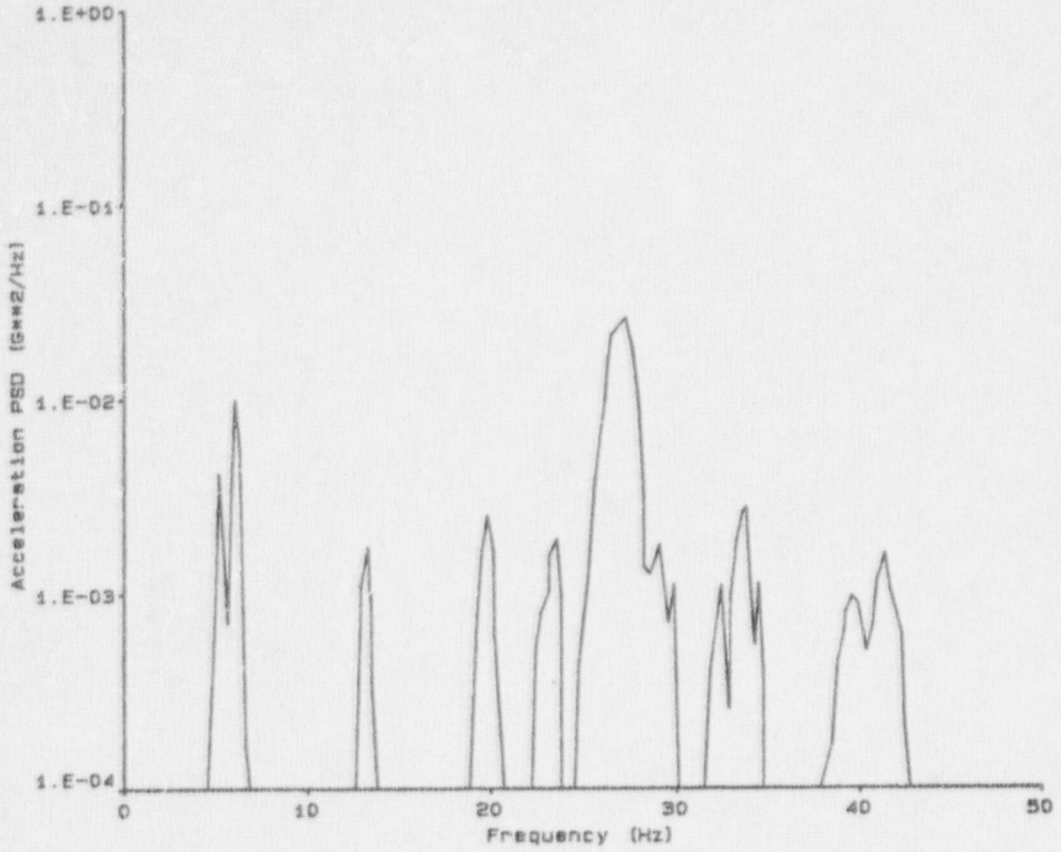

Figure E-51. Power Spectral Density: Test T40.30, standard "T", frame #1-Y.

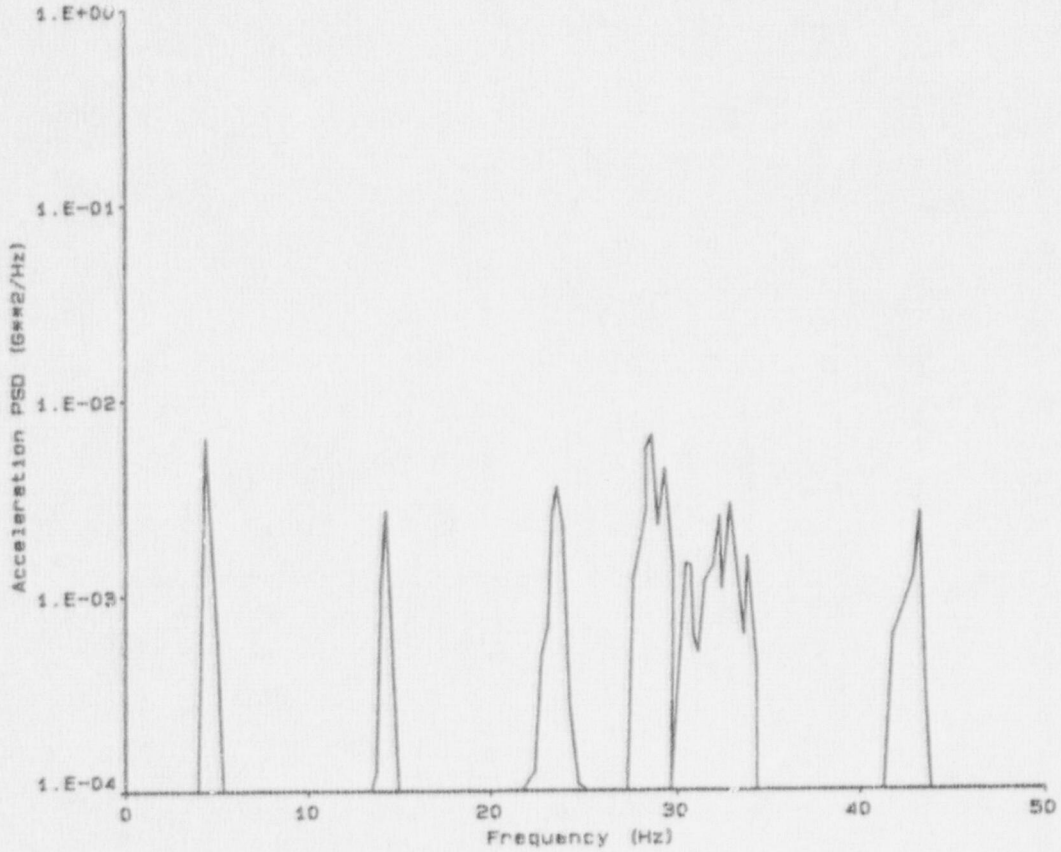

Figure E-52. Power Spectral Density: Test T40.30, standard "T", frame #2-Y.

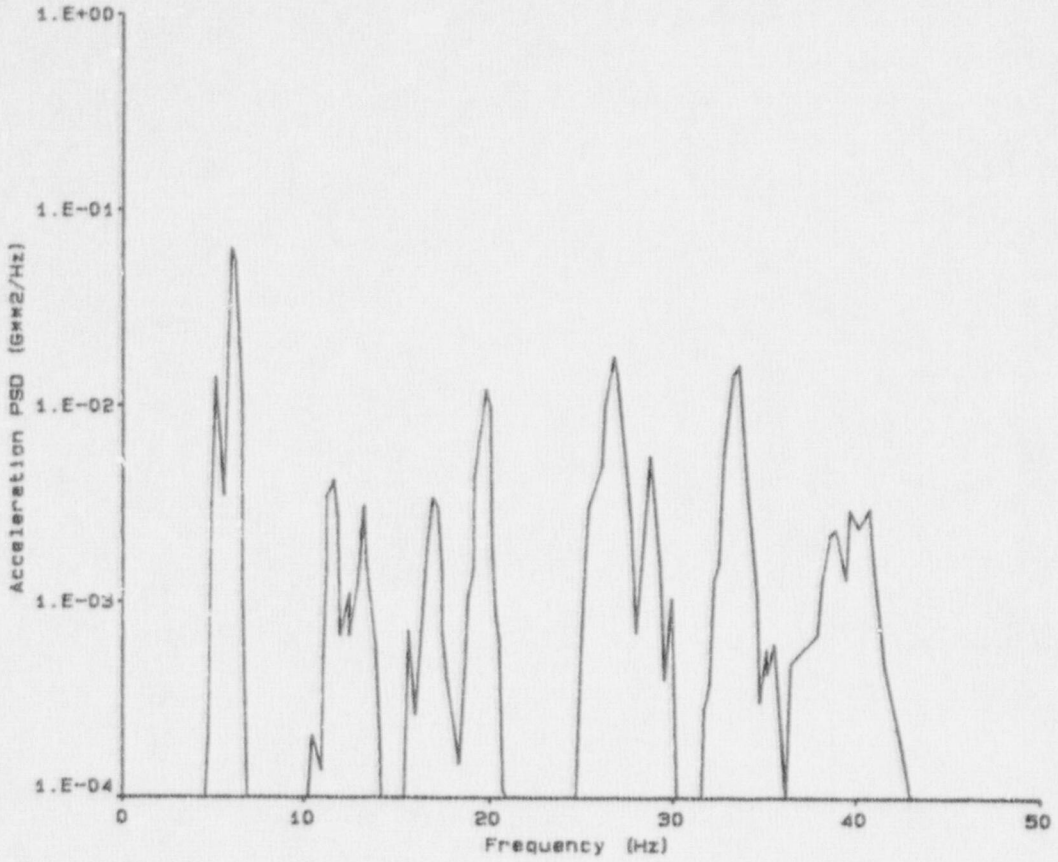

Figure E-53. Power Spectral Density: Test T40.30, standard "T", frame #1-Z.

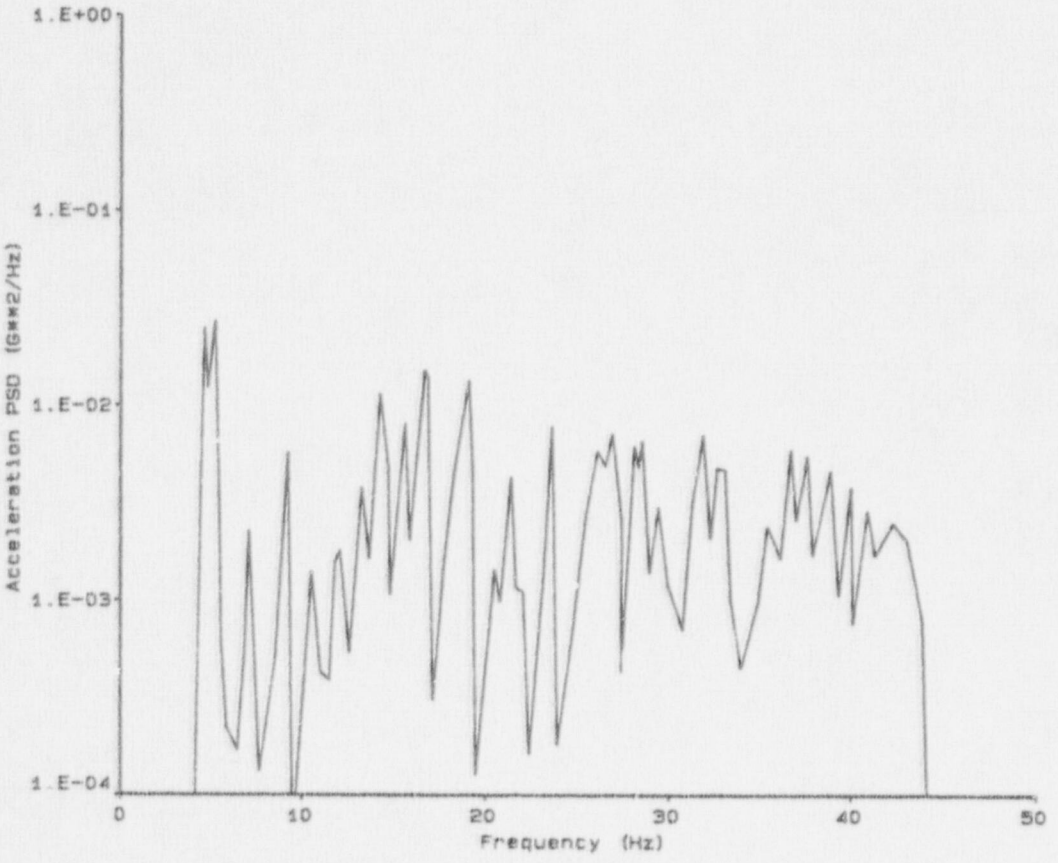

Figure E-54. Power Spectral Density: Test T40.30, standard "T", frame #2-Z.

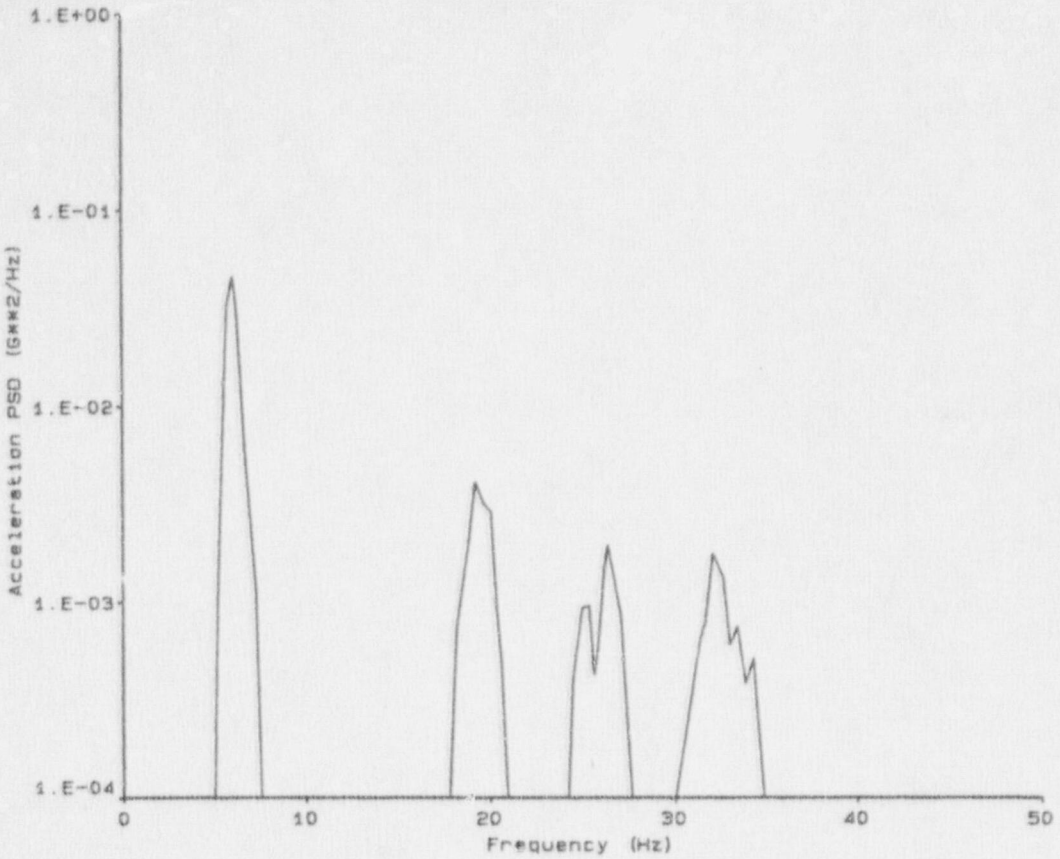

Figure E-55. Power Spectral Density: Test T40.30, top HDU, frame #1-X.

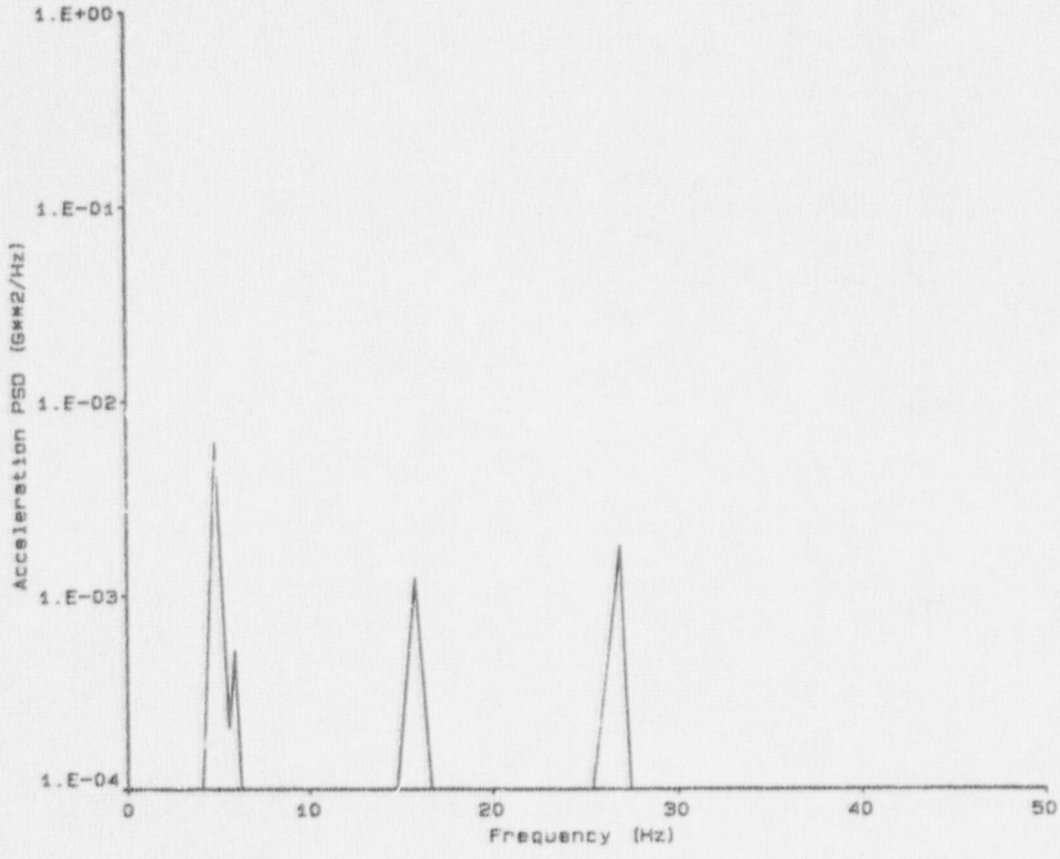

Figure E-56. Power Spectral Density: Test T40.30, top HDU, frame #2-X.

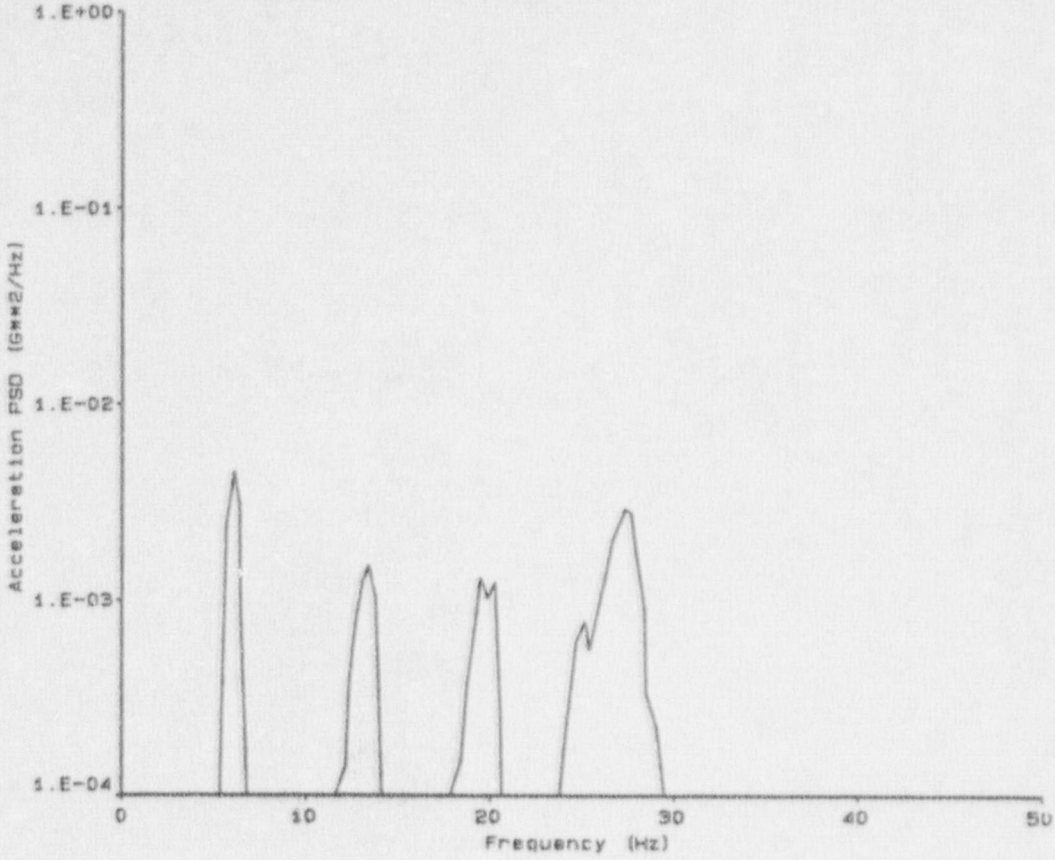

Figure E-57. Power Spectral Density: Test T40.30, top HDU, frame #1-Y.

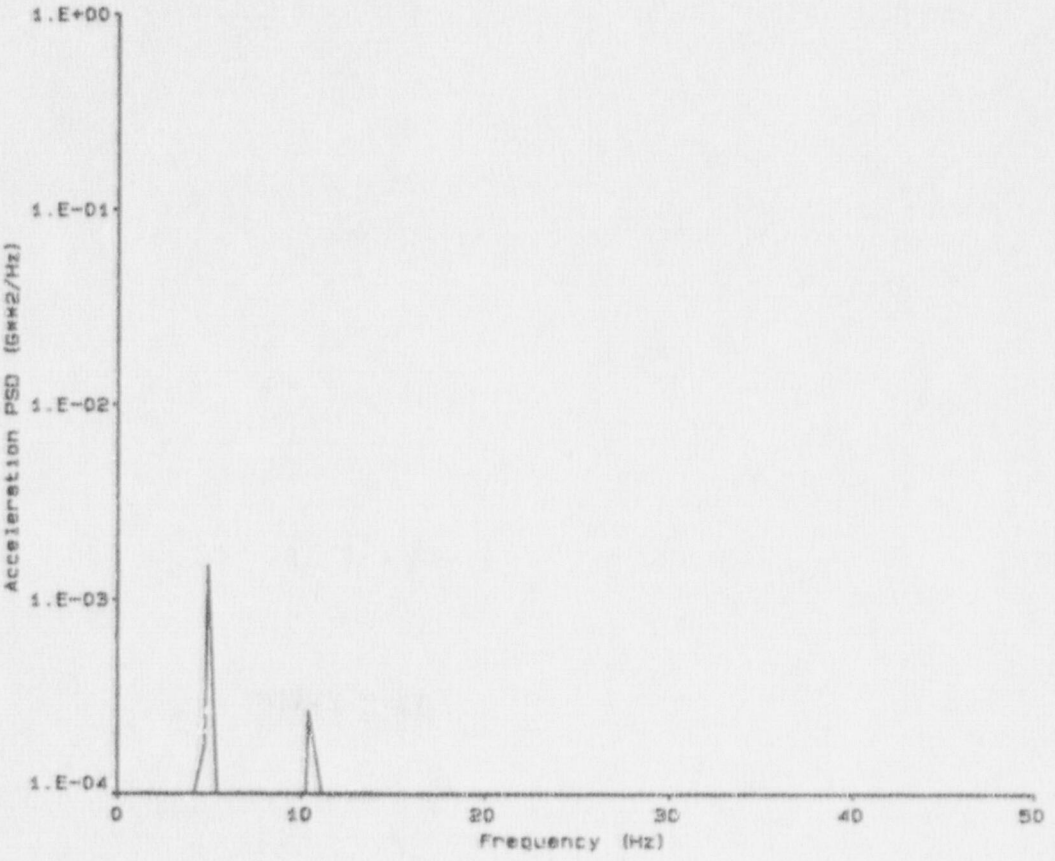

Figure E-58. Power Spectral Density: Test T40.30, top HDU, frame #2-Y.

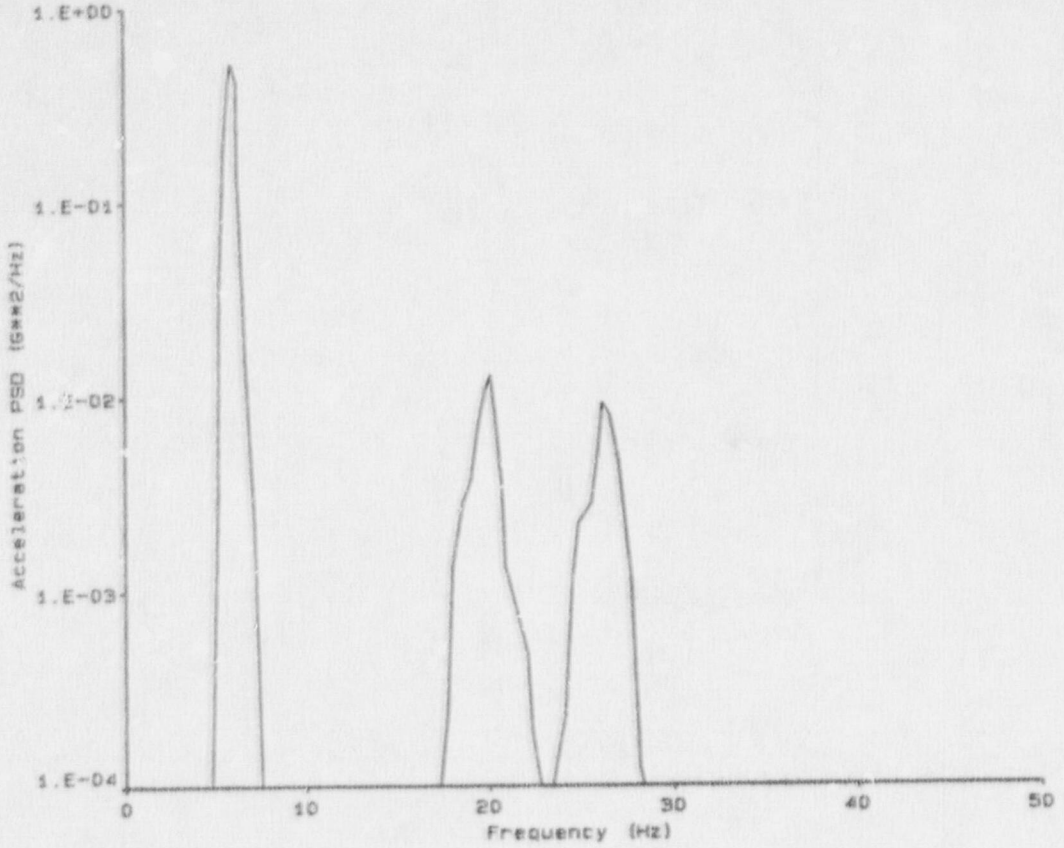

Figure E-59. Power Spectral Density: Test T40.30, top HDU, frame #1-Z.

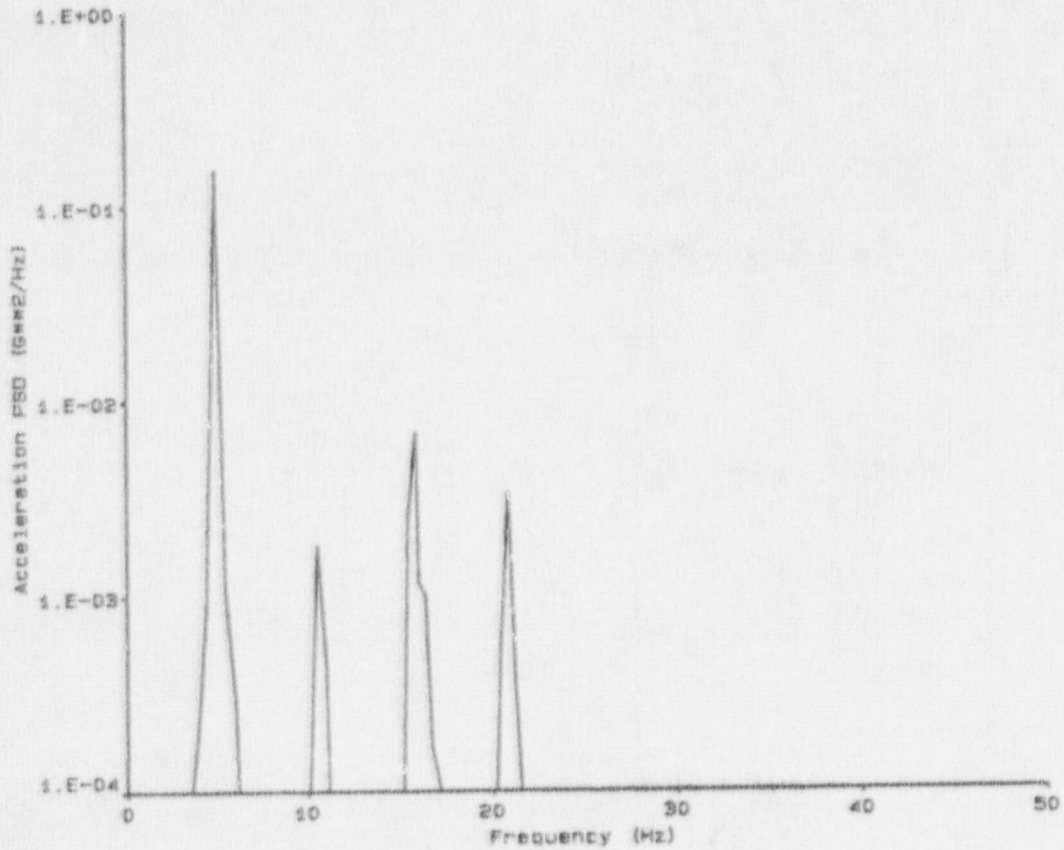

Figure E-60. Power Spectral Density: Test T40.30, top HDU, frame #2-Z.

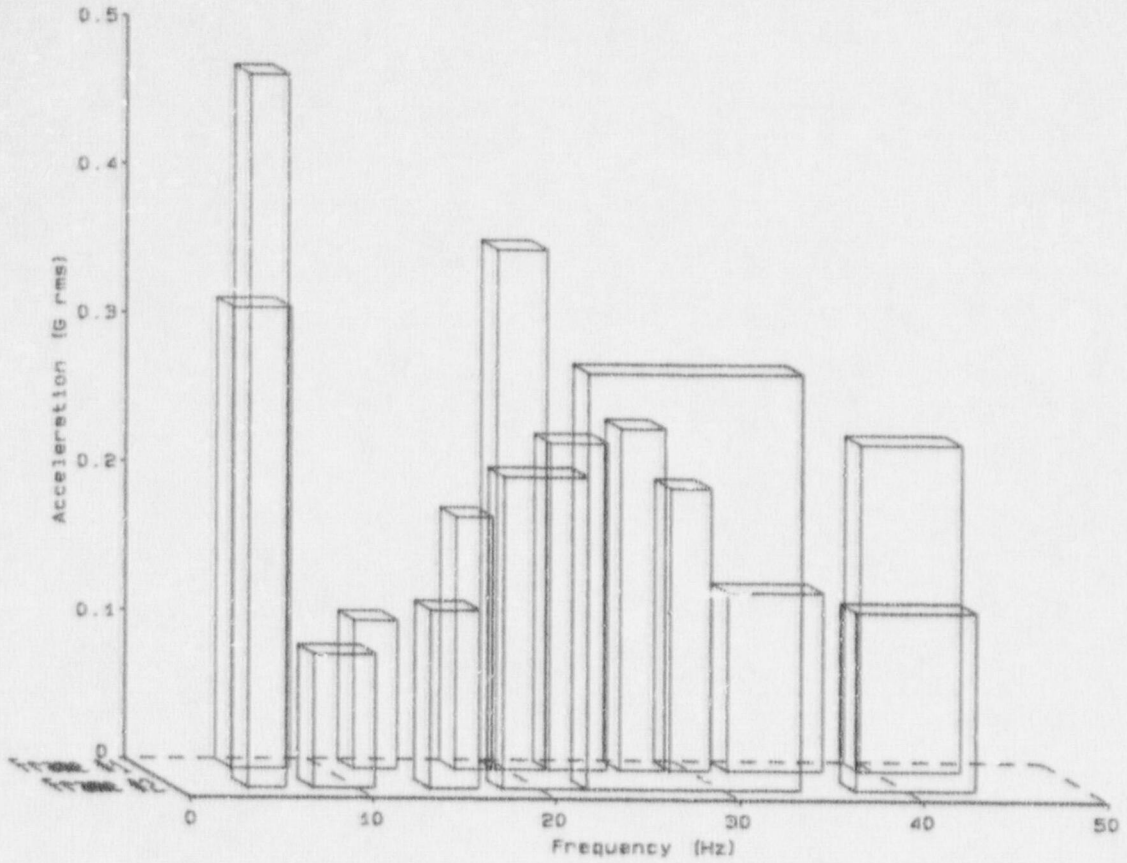

Figure E-61. Band Integrated Acceleration: X direction, valve operator, Test T40.10.

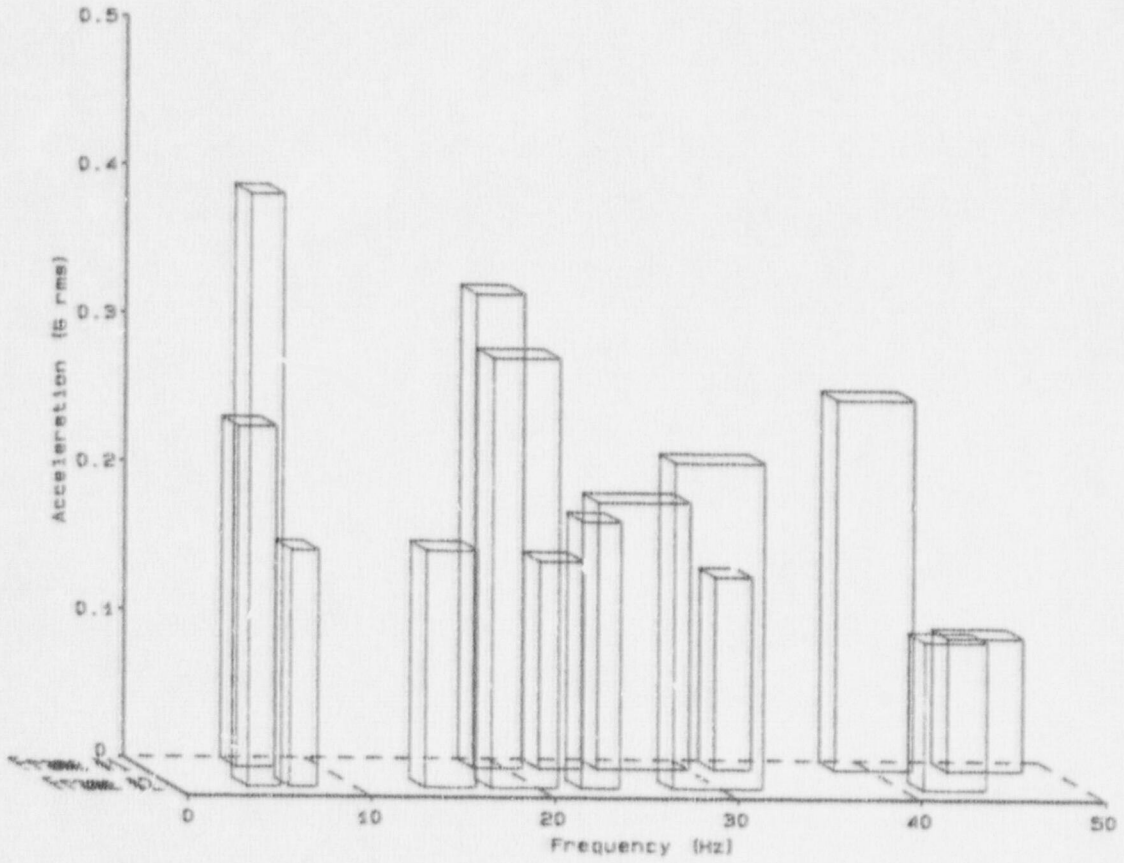

Figure E-62. Band Integrated Acceleration: X direction, valve operator, Test T40.30.

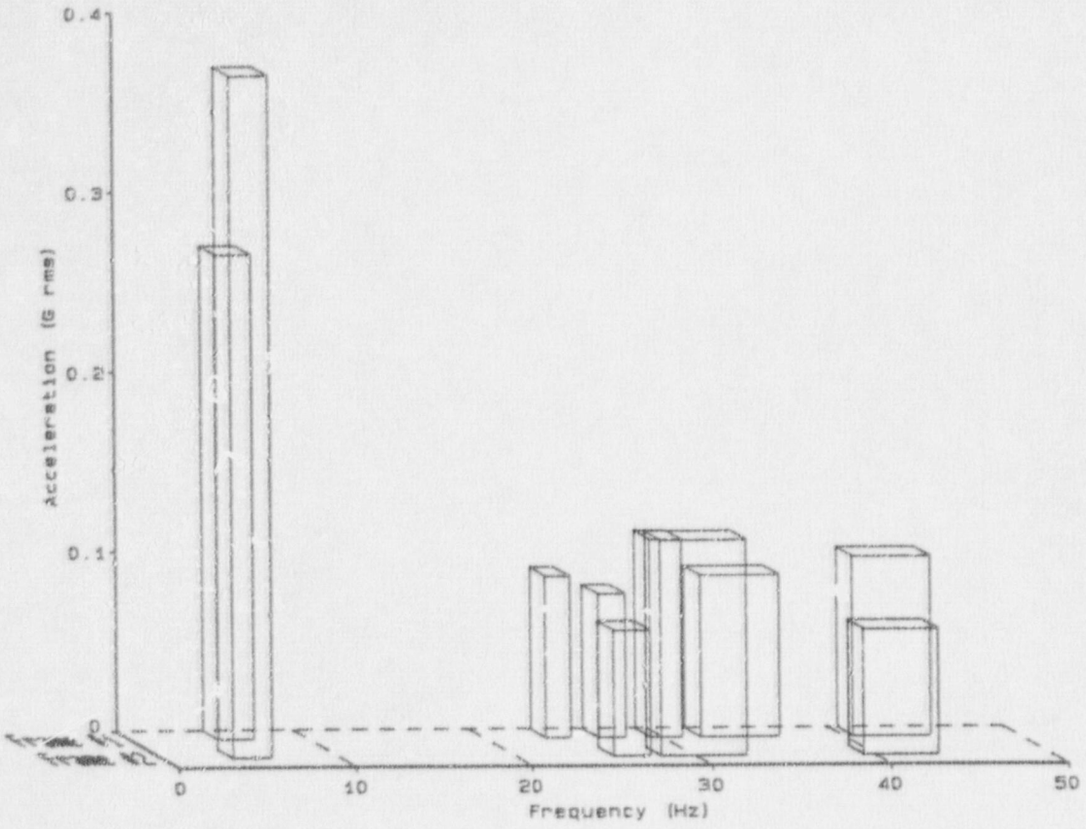

Figure E-63. Band Integrated Acceleration: X direction, valve body, Test T40.10.

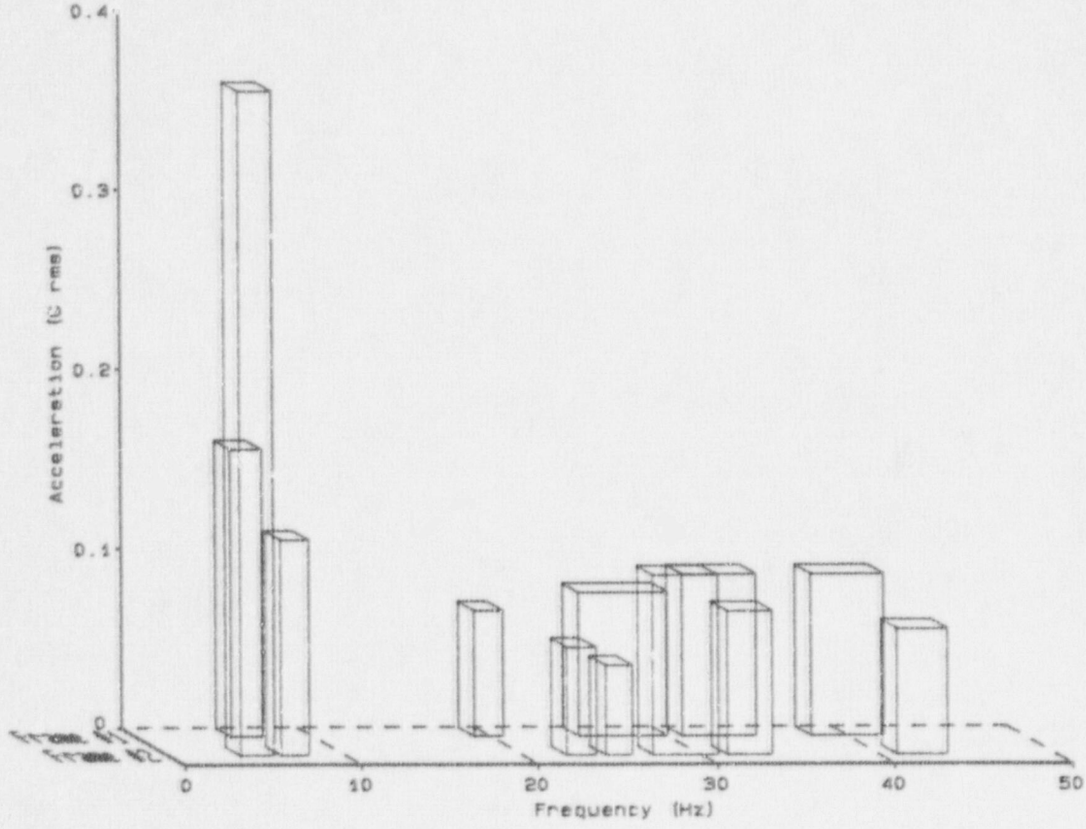

Figure E-64. Band Integrated Acceleration: X direction, valve body, Test T40.30.

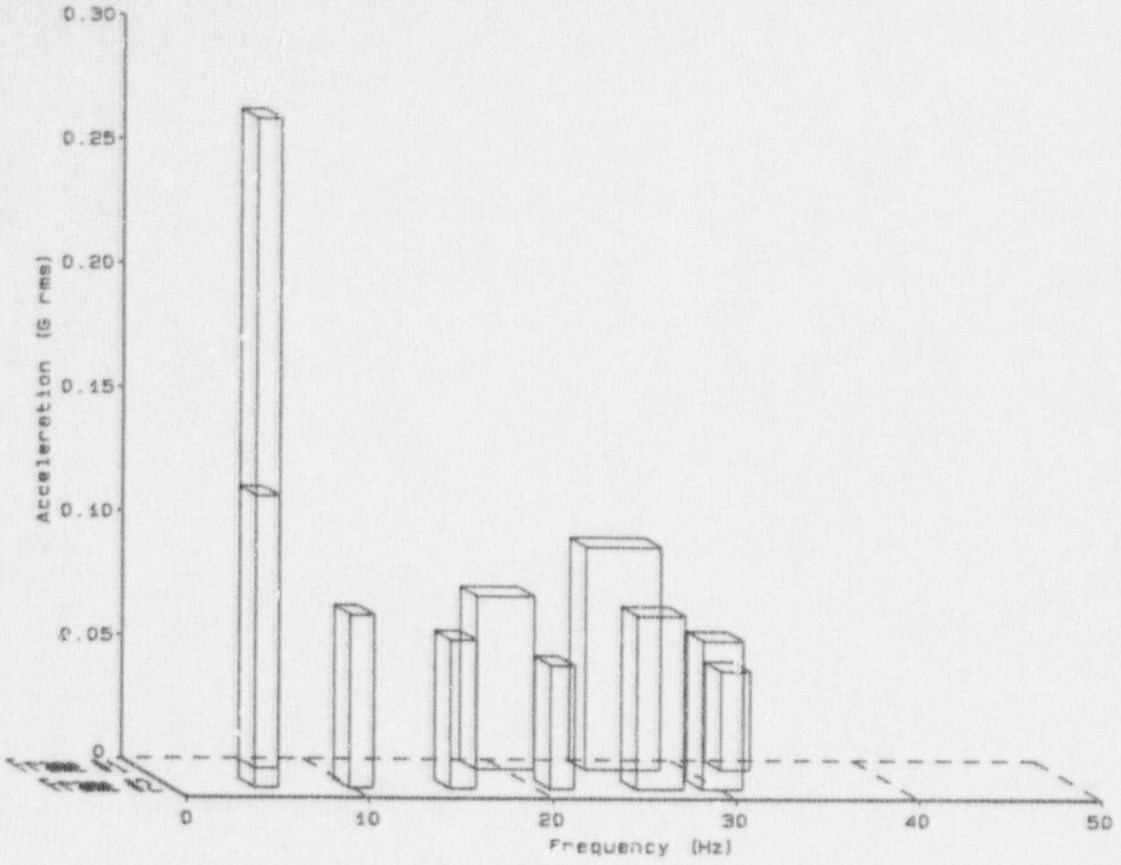

Figure E-65. Band Integrated Acceleration: X direction, spherical "T", Test T40.10.

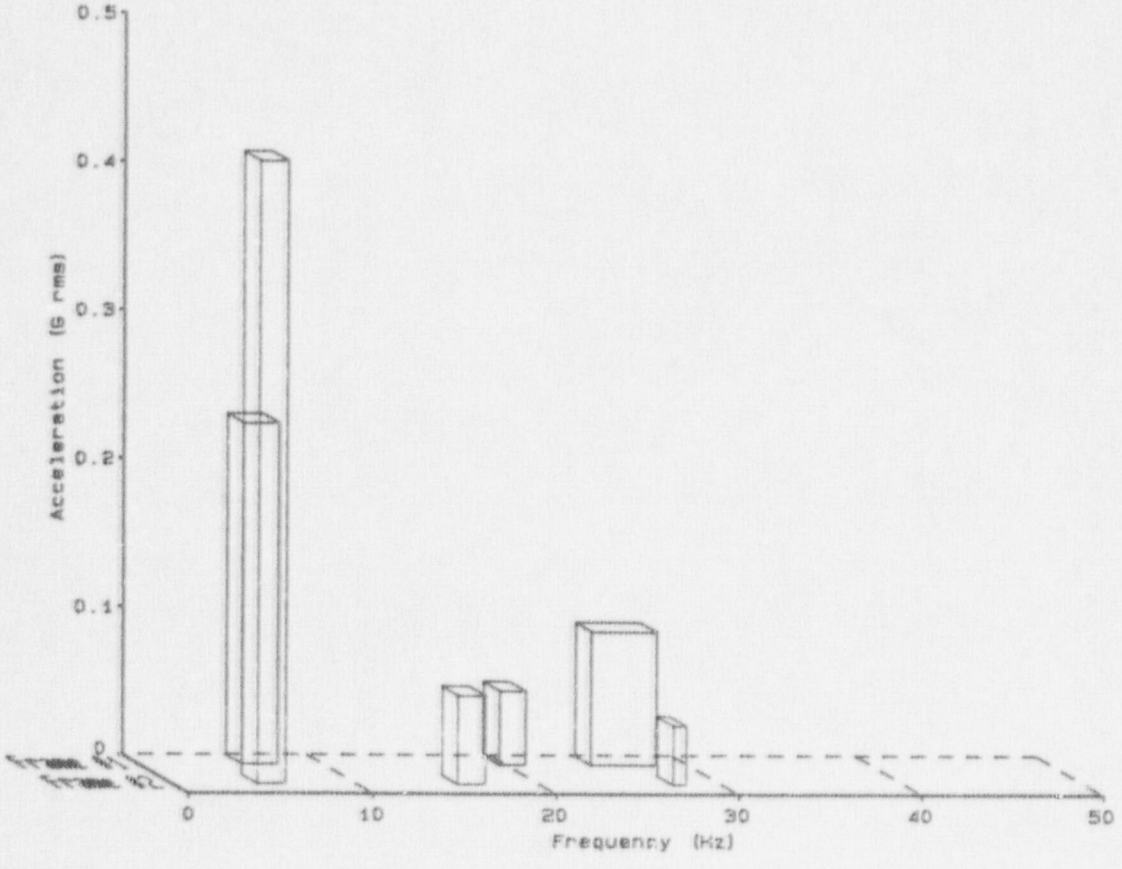

Figure E-66. Band Integrated Acceleration: X direction, spherical "T", Test T40.30.

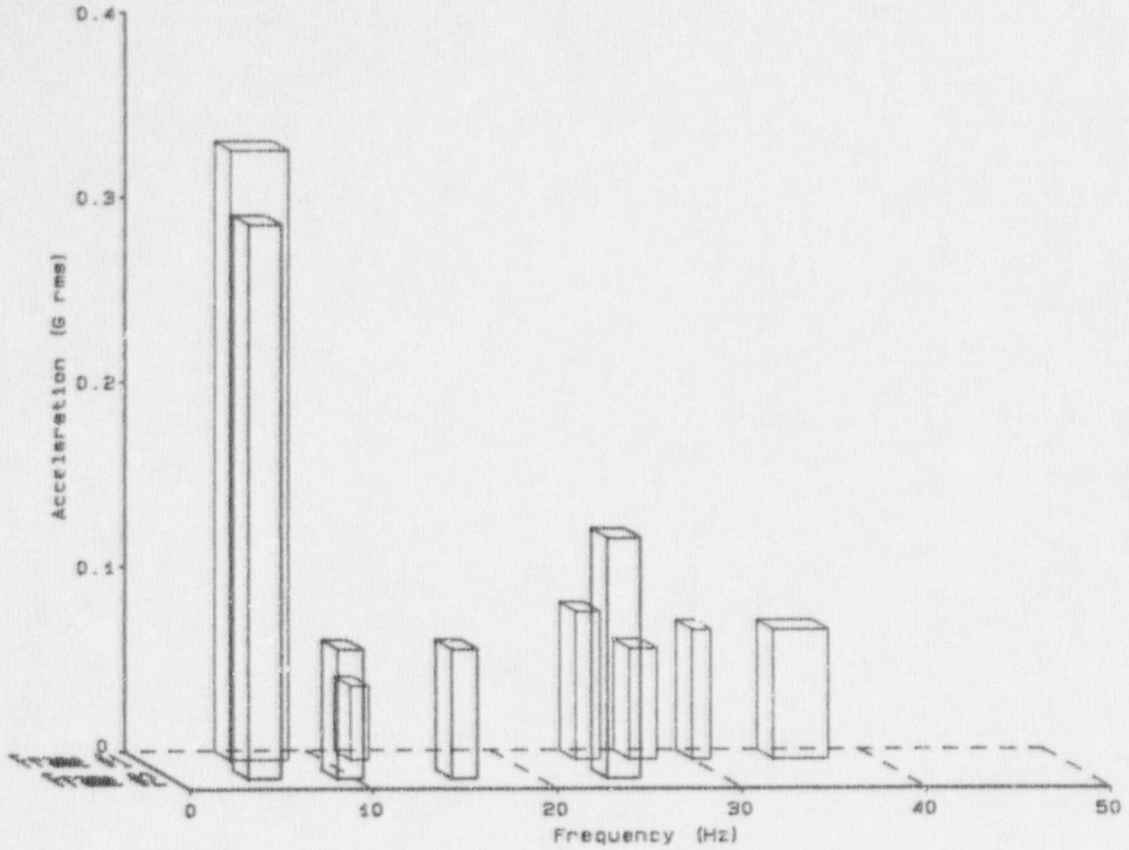

Figure E-67. Band Integrated Acceleration: X direction, standard "T", Test T40.10.

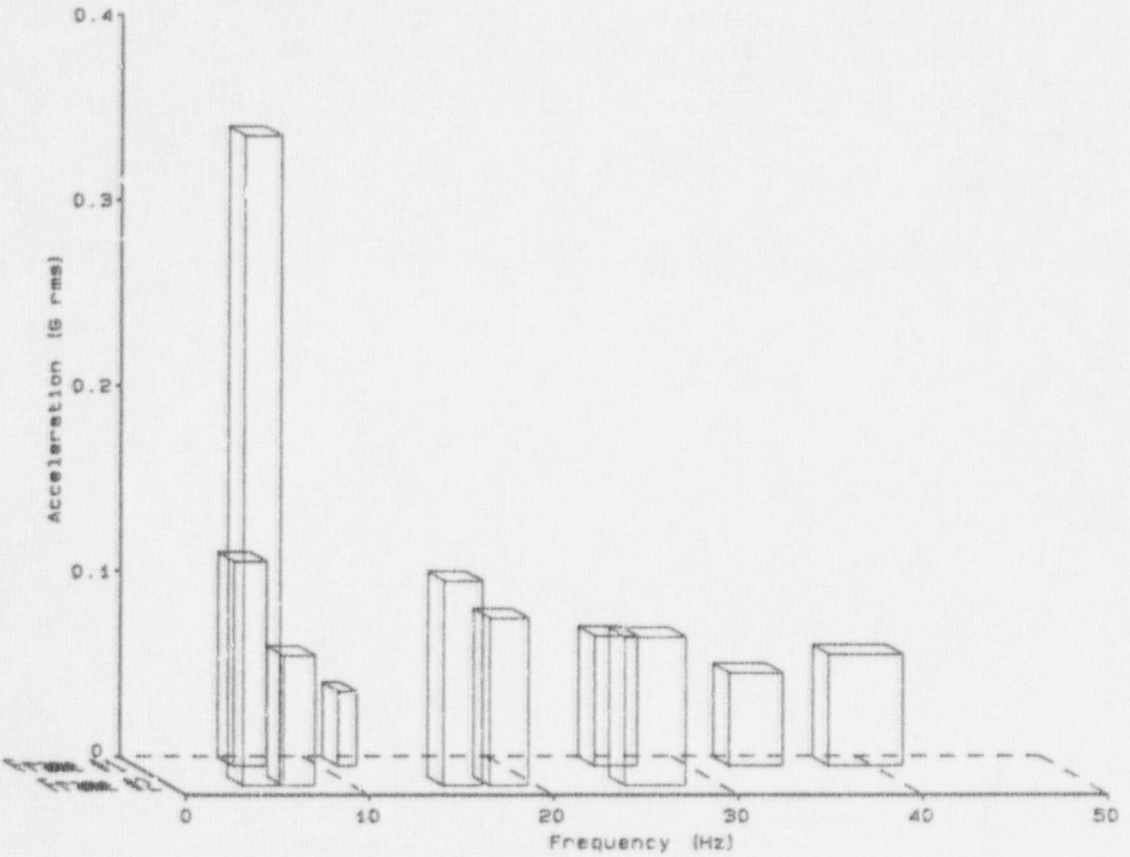

Figure E-68. Band Integrated Acceleration: X direction, standard "T", Test T40.30.

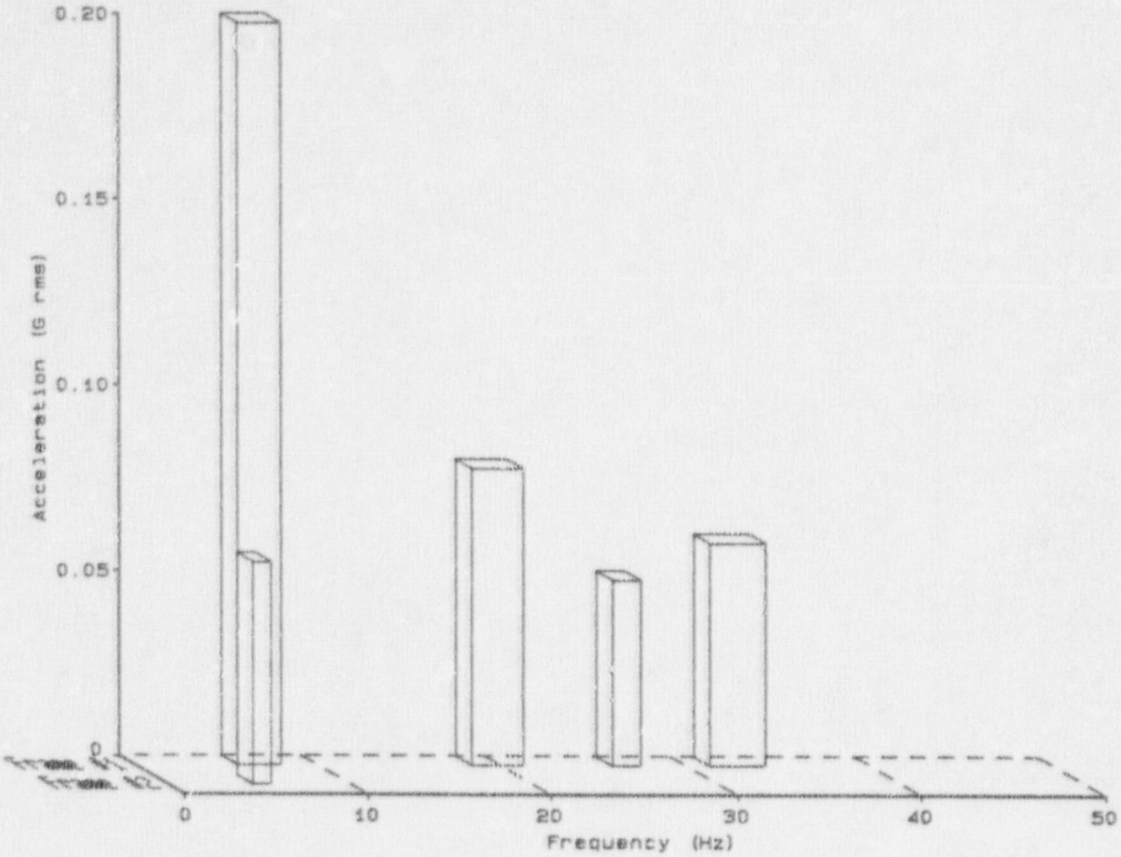

Figure E-69. Band Integrated Acceleration: X direction, top HDU, Test T40.10.

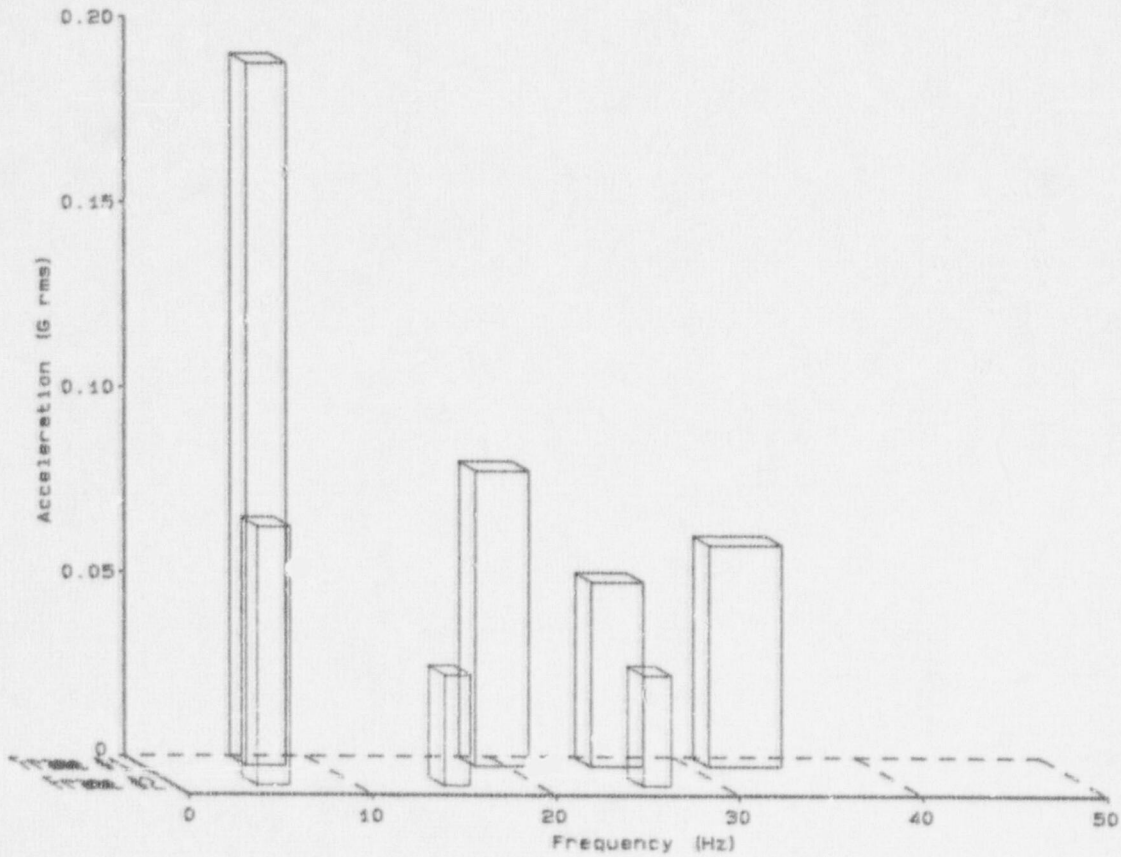

Figure E-70. Band Integrated Acceleration: X direction, top HDU, Test T40.30.

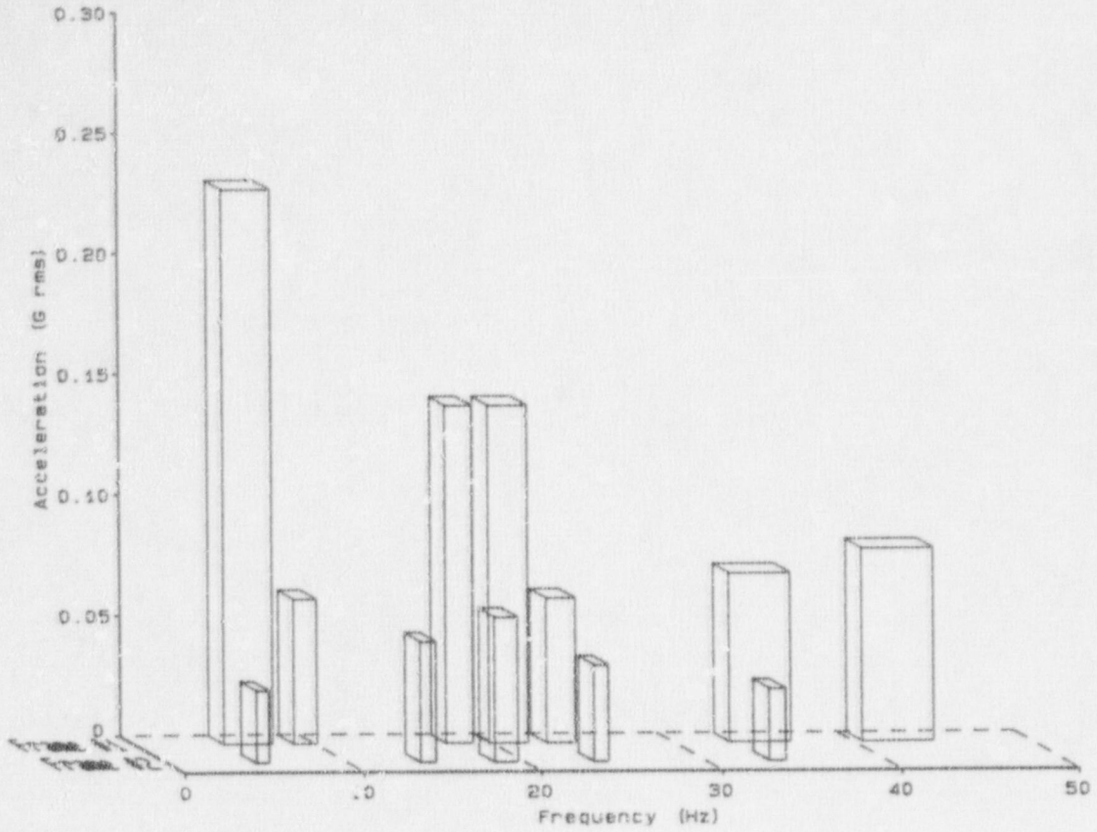

Figure E-71. Band Integrated Acceleration: Y direction, valve operator, Test T40.16.

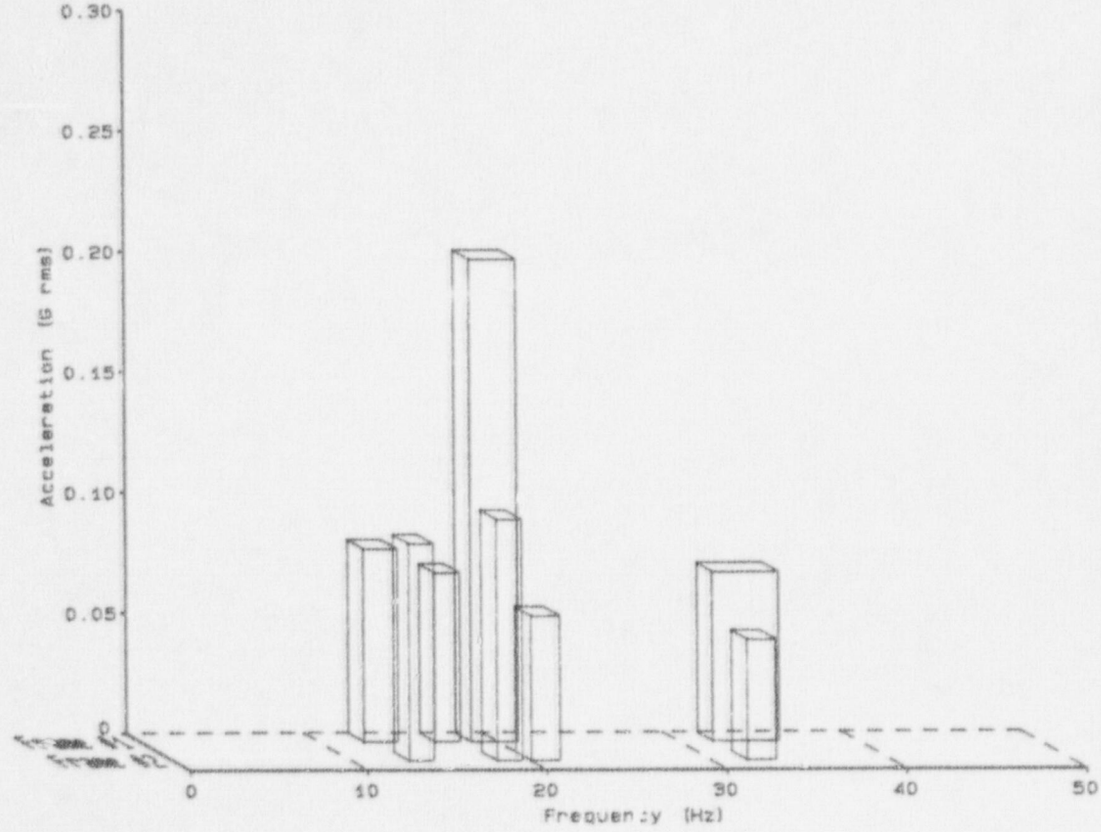

Figure E-72. Band Integrated Acceleration: Y direction, valve operator, Test T40.30.

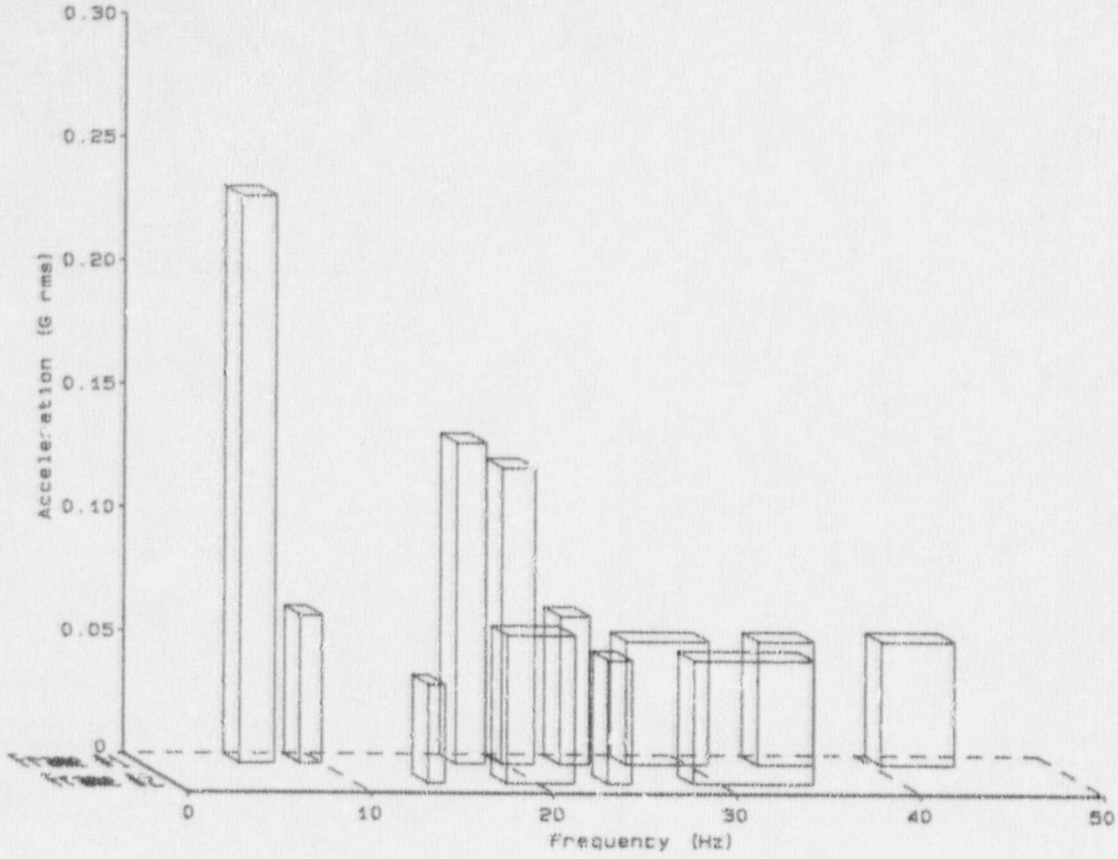

Figure E-73. Band Integrated Acceleration: Y direction, valve body, Test T40.10.

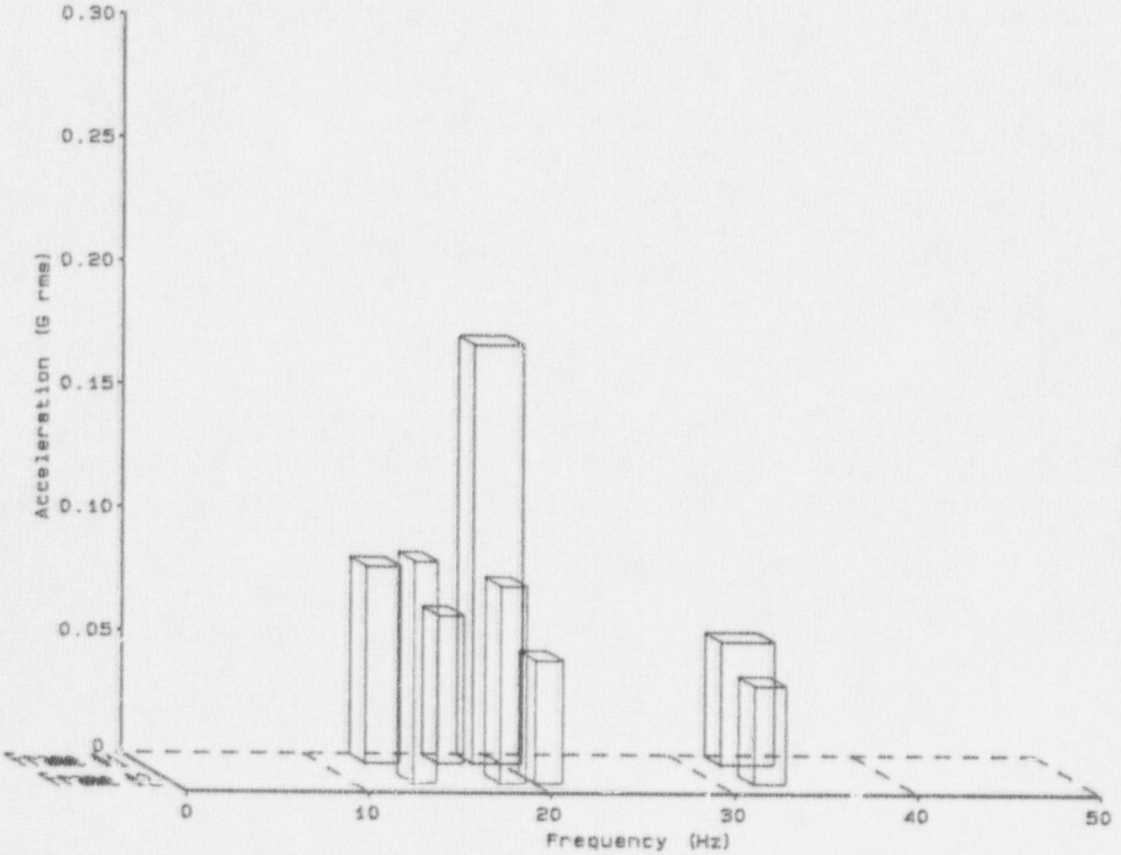

Figure E-74. Band Integrated Acceleration: Y direction, valve body, Test T40.30.

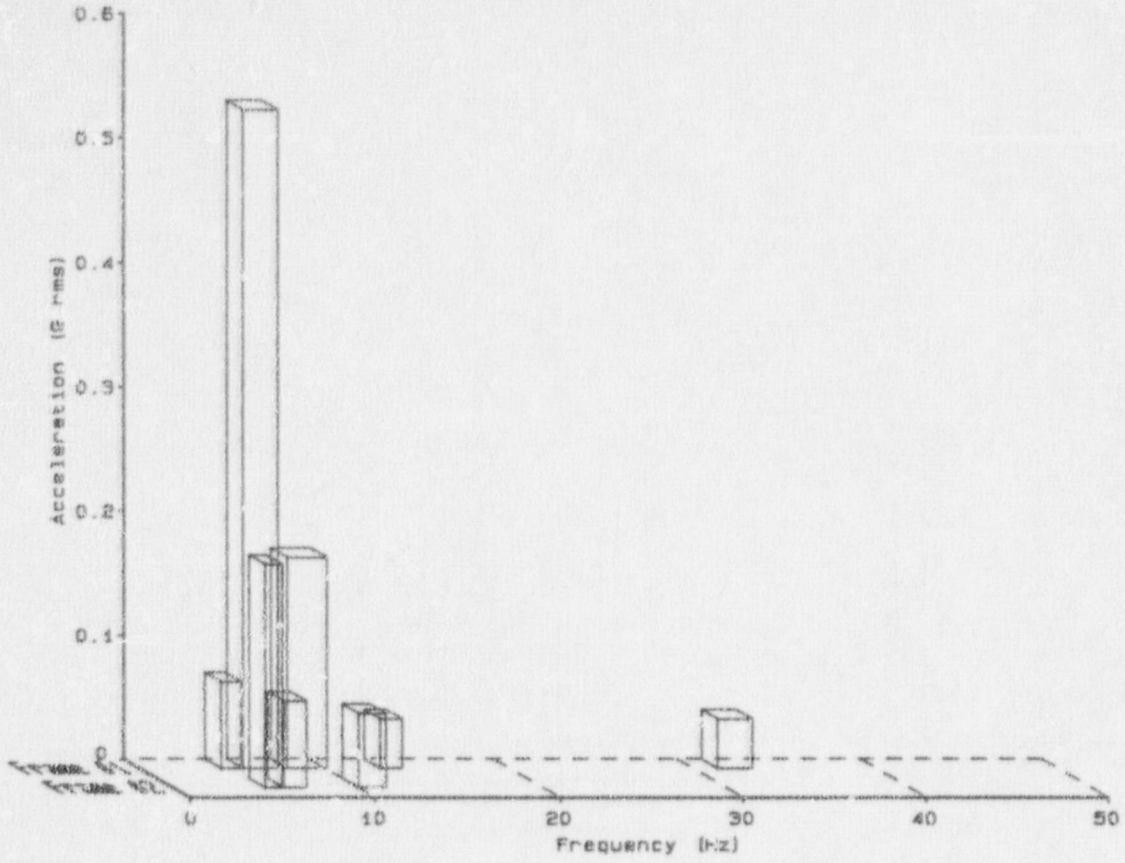

Figure E-75. Band Integrated Acceleration: Y direction, spherical "T", Test T40.10.

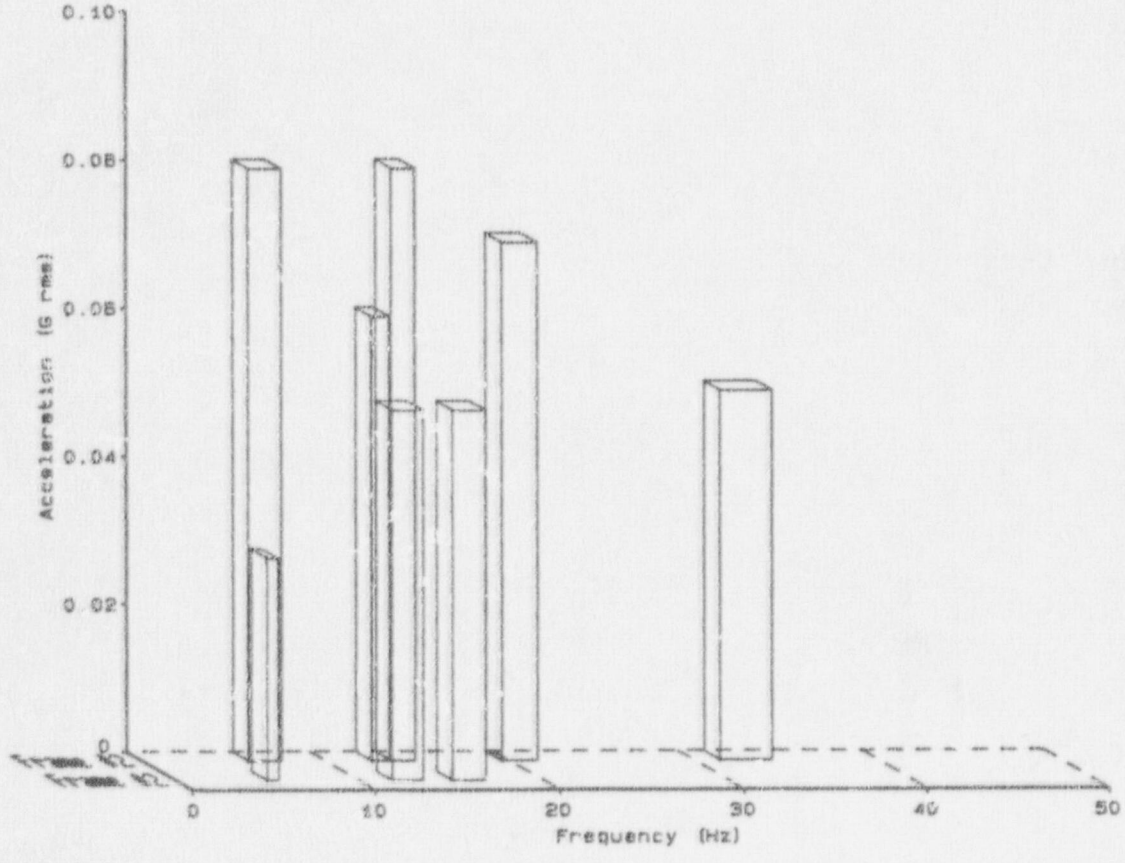

Figure E-76. Band Integrated Acceleration: Y direction, spherical "T", Test T40.30.

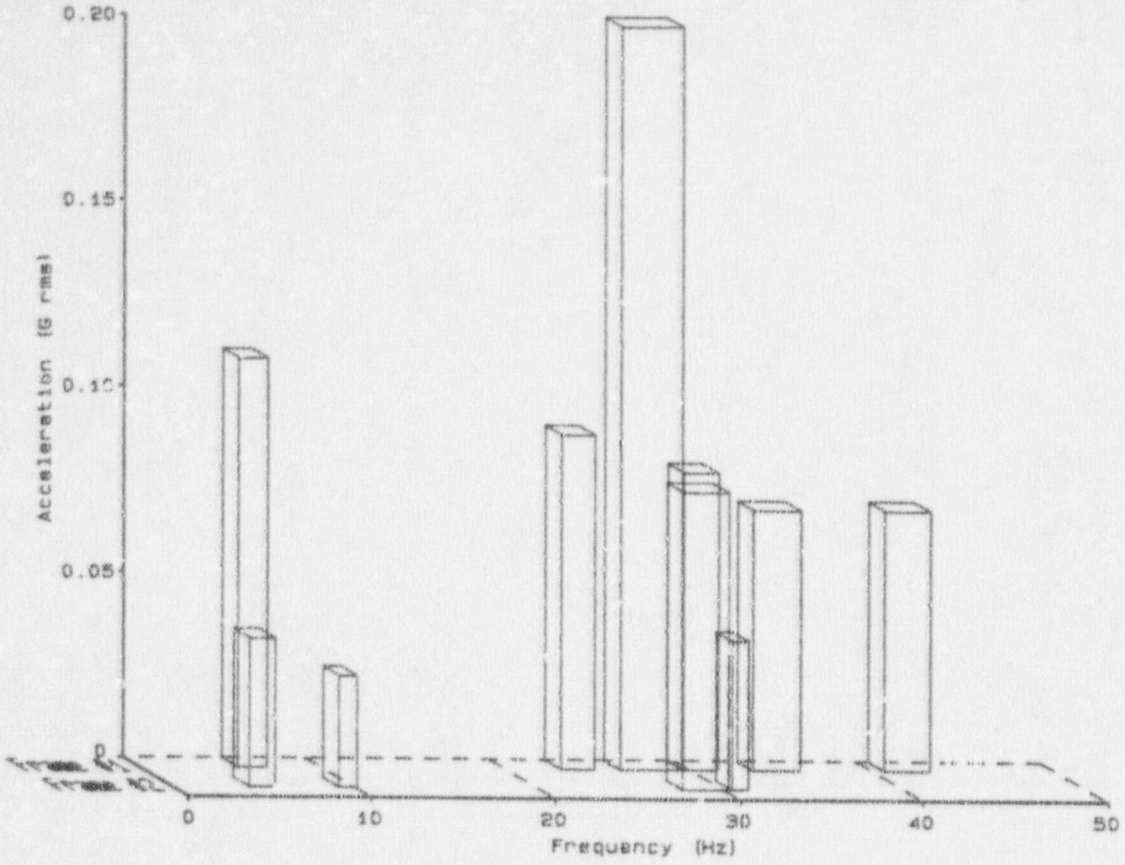

Figure E-77. Band Integrated Acceleration: Y direction, standard "T", Test T40.10.

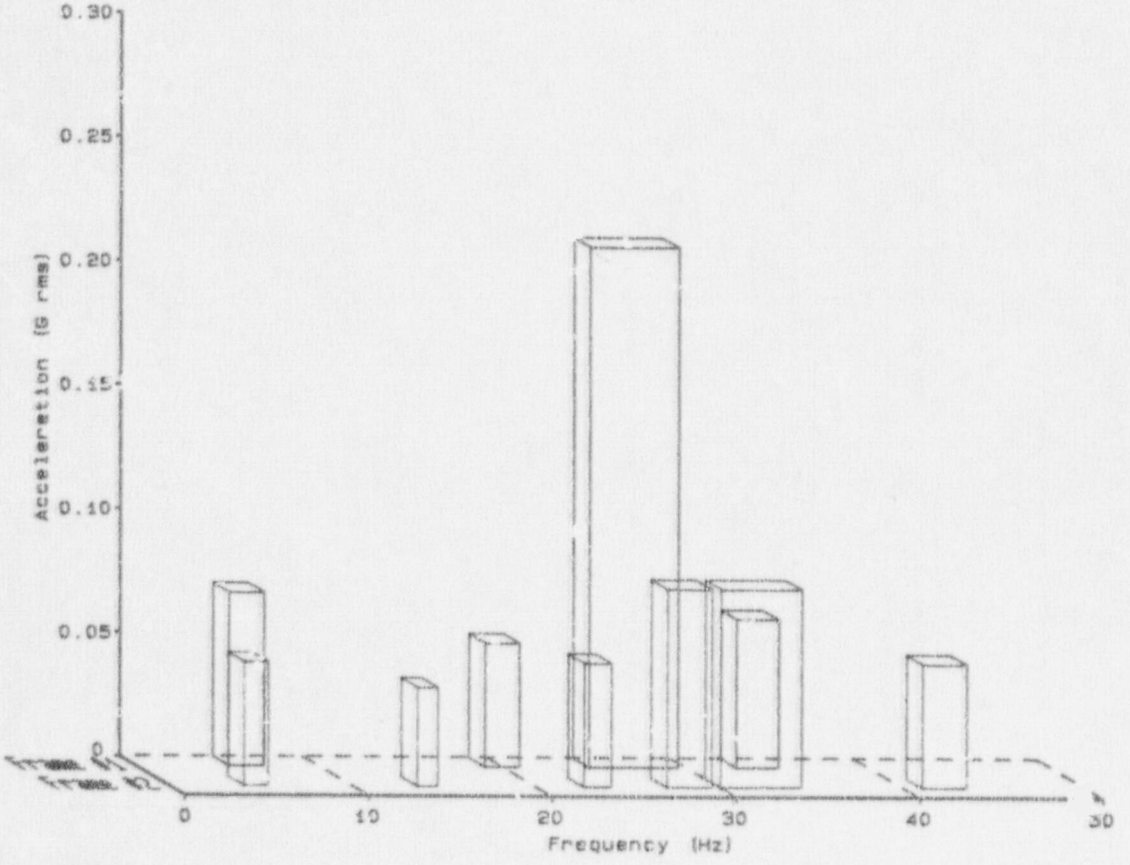

Figure E-78. Band Integrated Acceleration: Y direction, standard "T", Test T40.30.

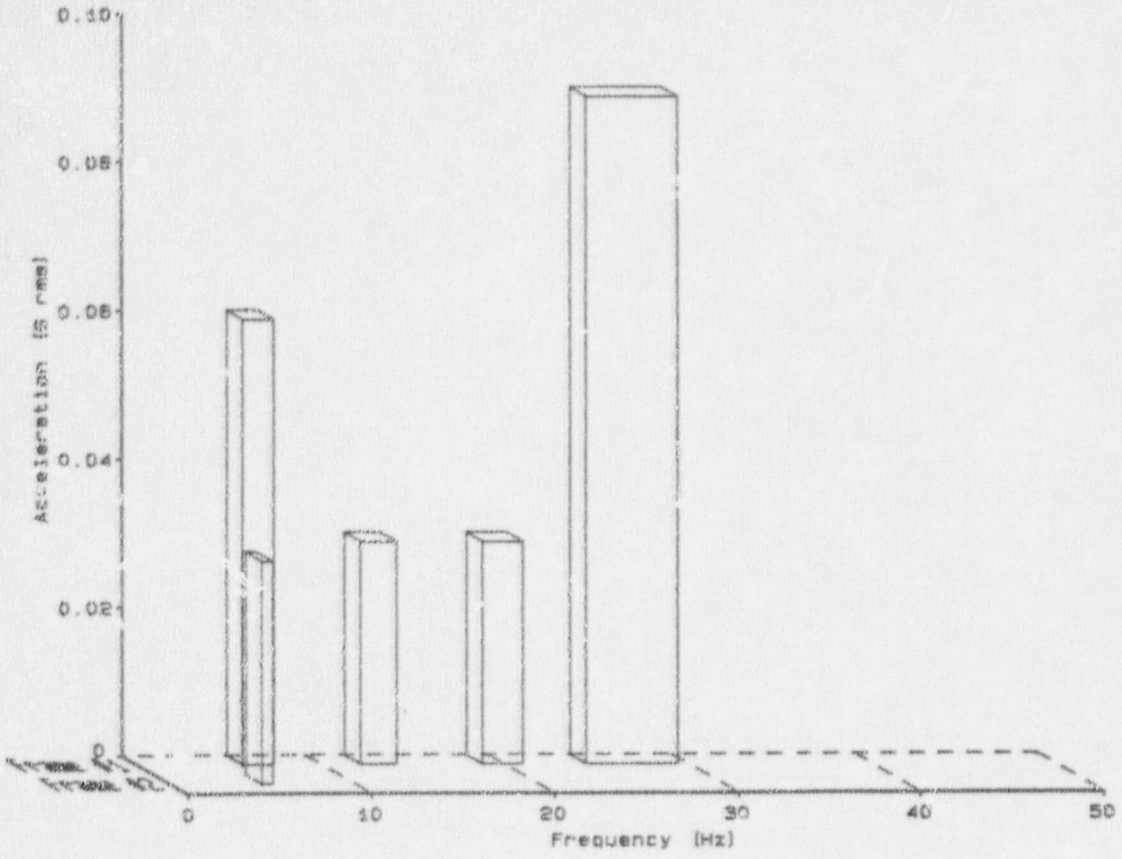

Figure E-79. Band Integrated Acceleration: Y direction, top HDU, Test T40.10.

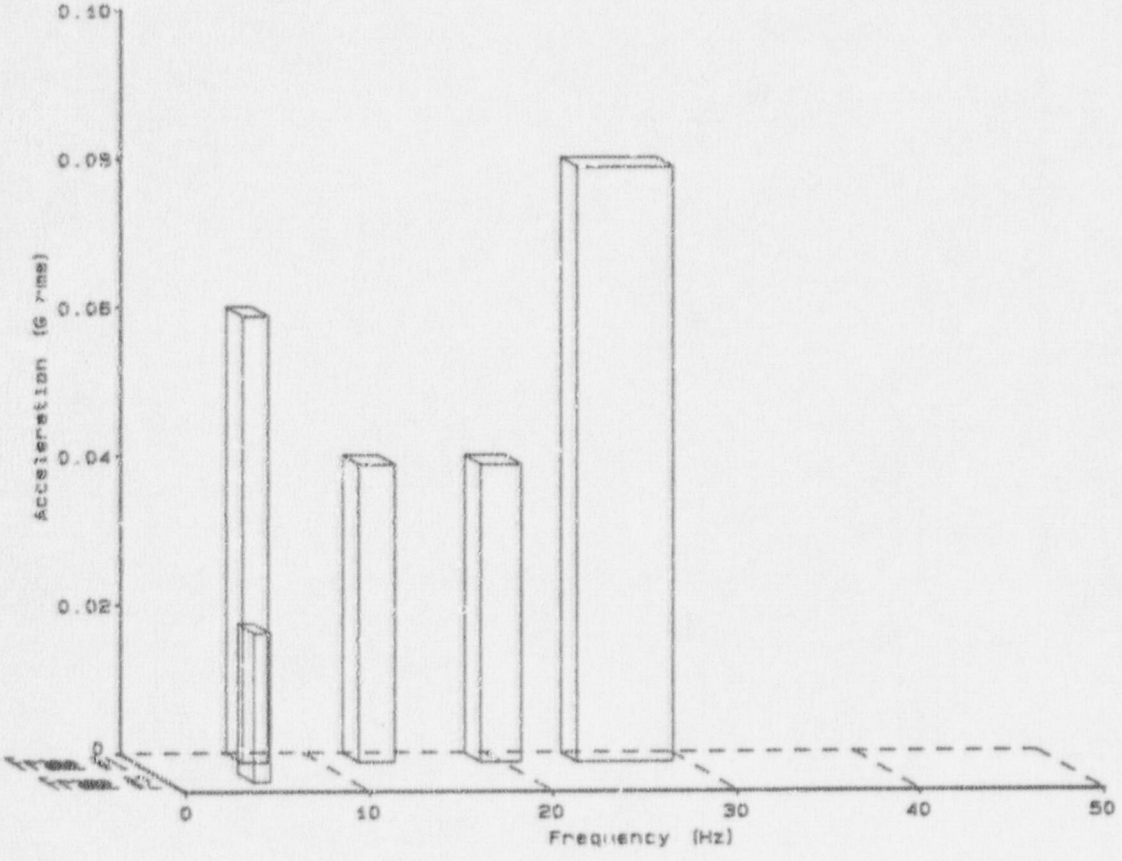

Figure E-80. Band Integrated Acceleration: Y direction, top HDU, Test T40.30.

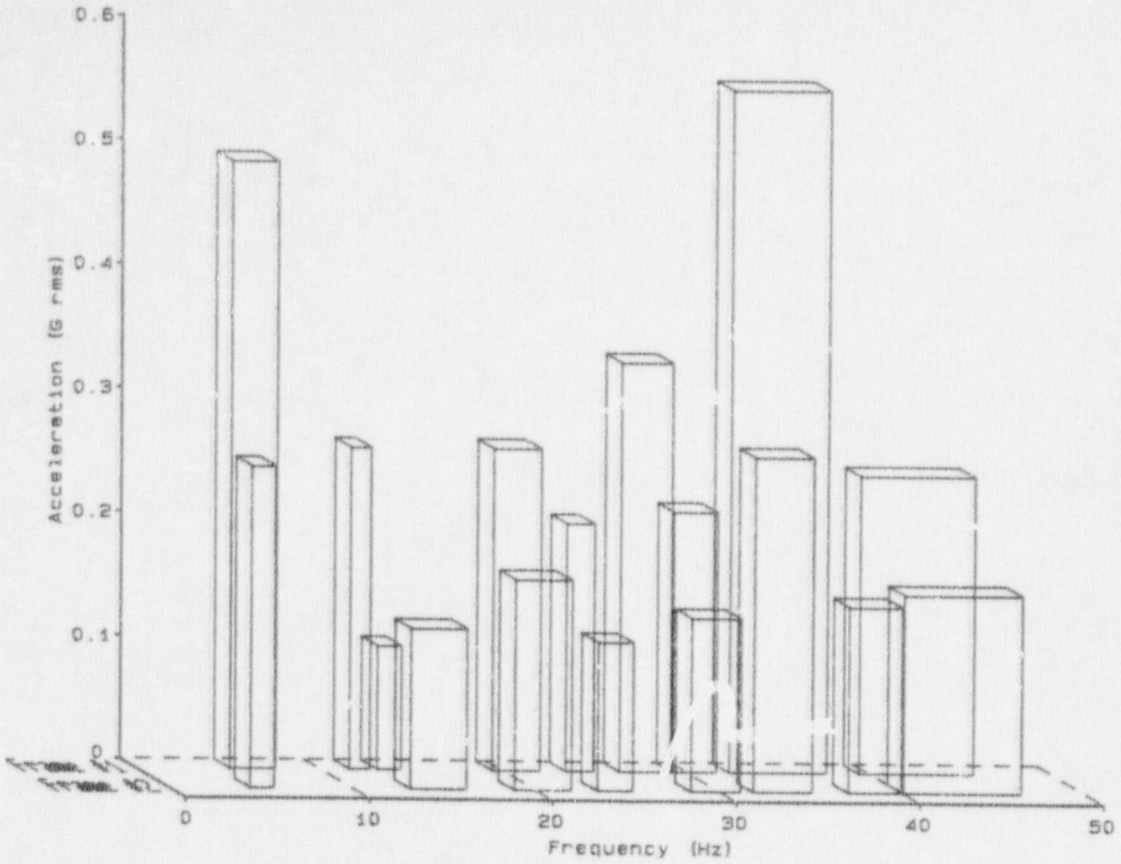

Figure E-81. Band Integrated Acceleration: Z direction, valve operator, Test T40.10.

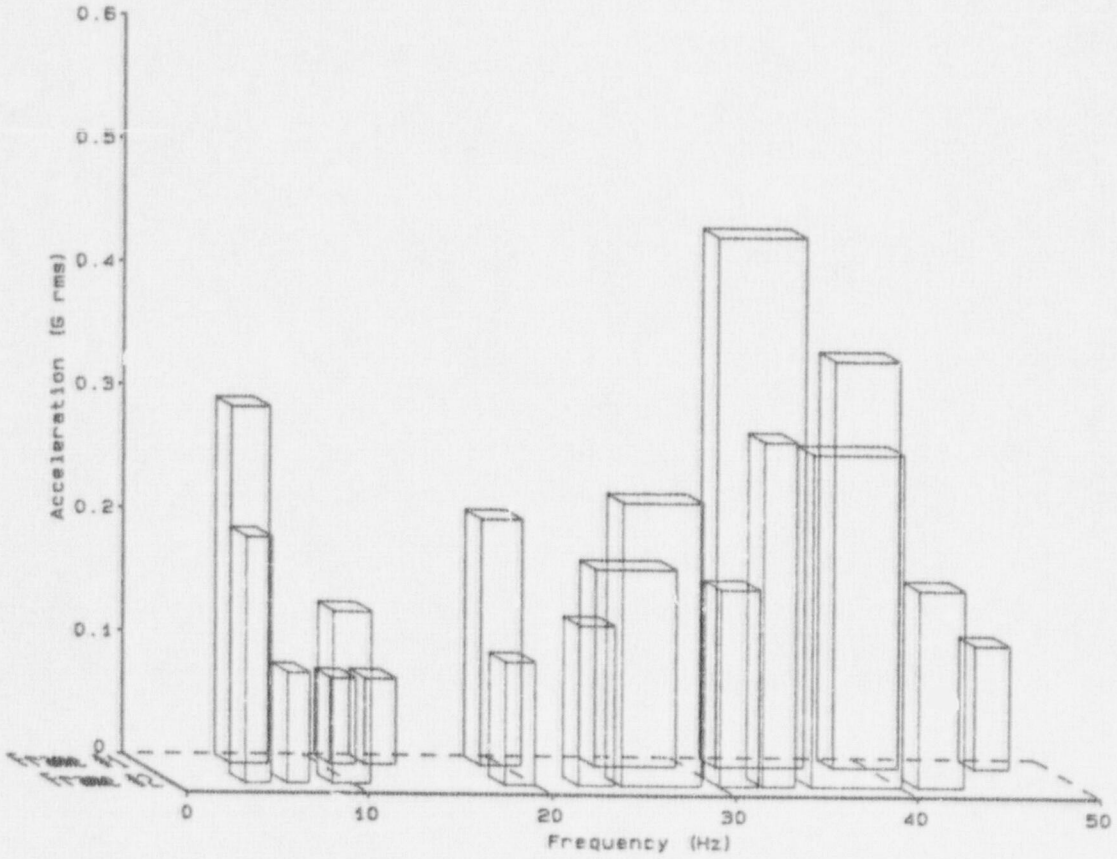

Figure E-82. Band Integrated Acceleration: Z direction, valve operator, Test T40.30.

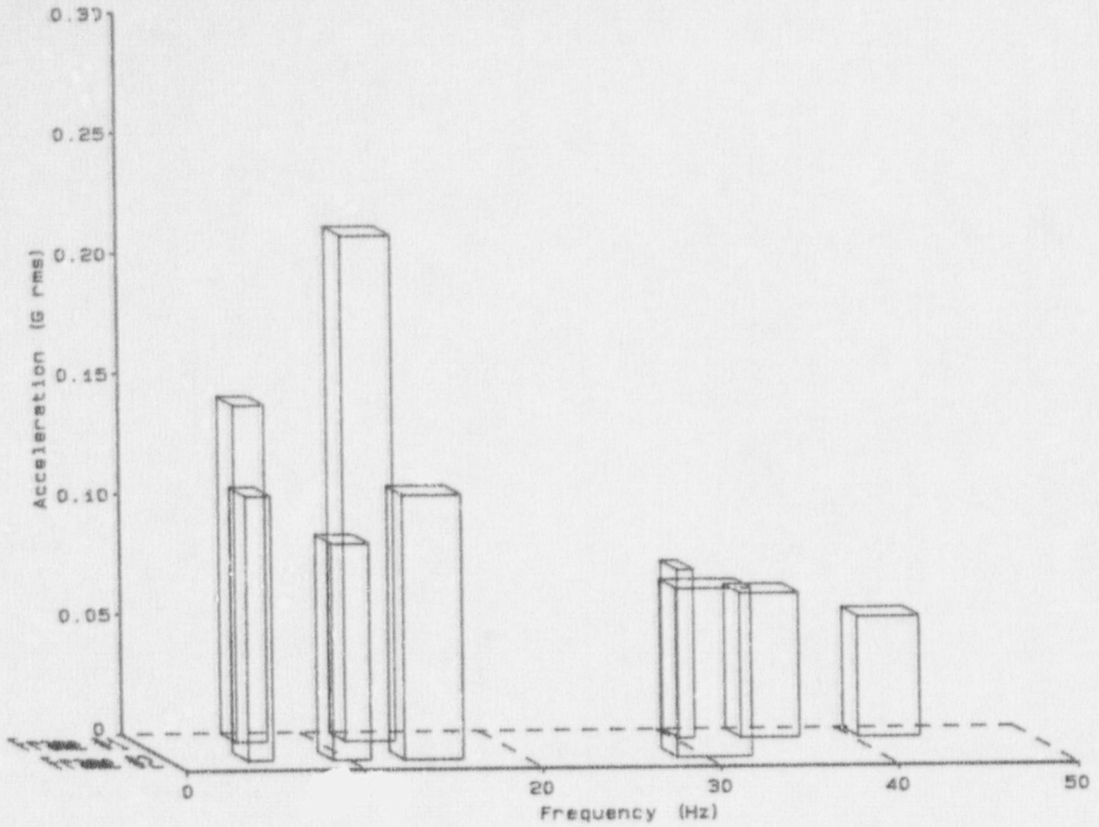

Figure E-83. Band Integrated Acceleration: Z direction, valve body, Test T40.10.

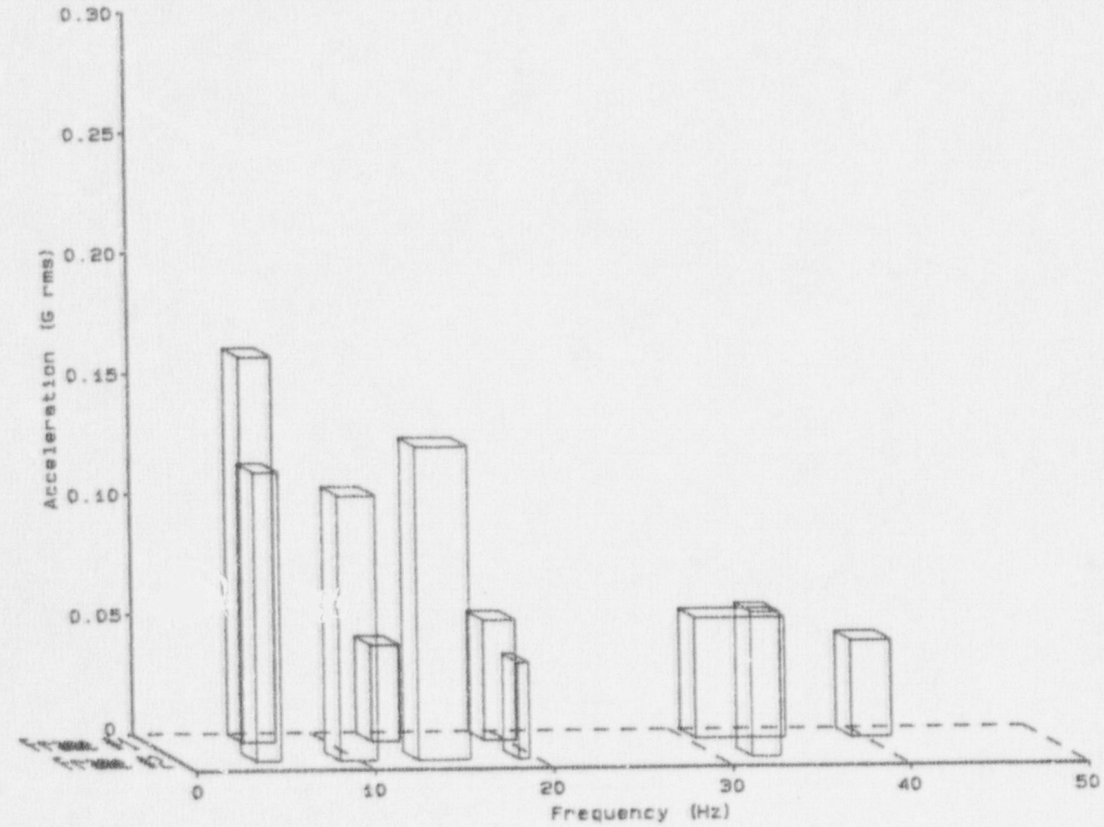

Figure E-84. Band Integrated Acceleration: Z direction, valve body, Test T40.30.

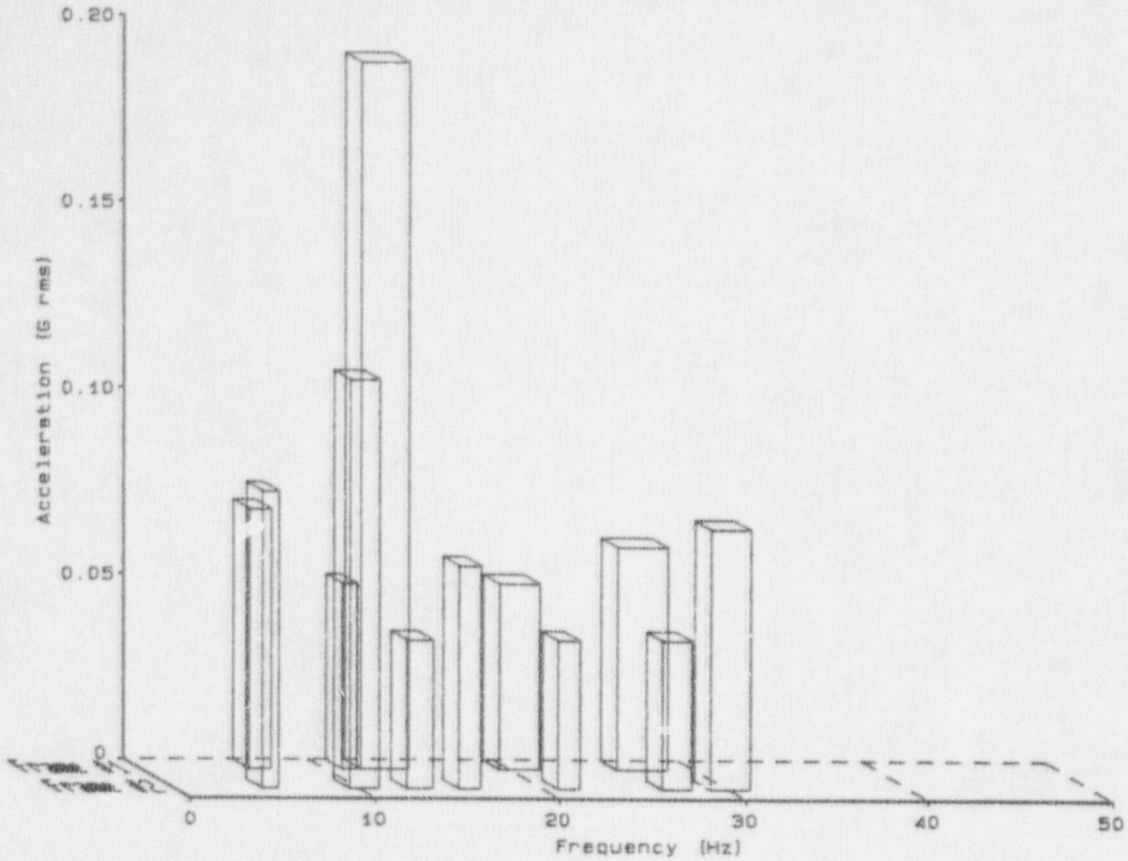

Figure E-85. Band Integrated Acceleration: Z direction, spherical "T", Test T40.10.

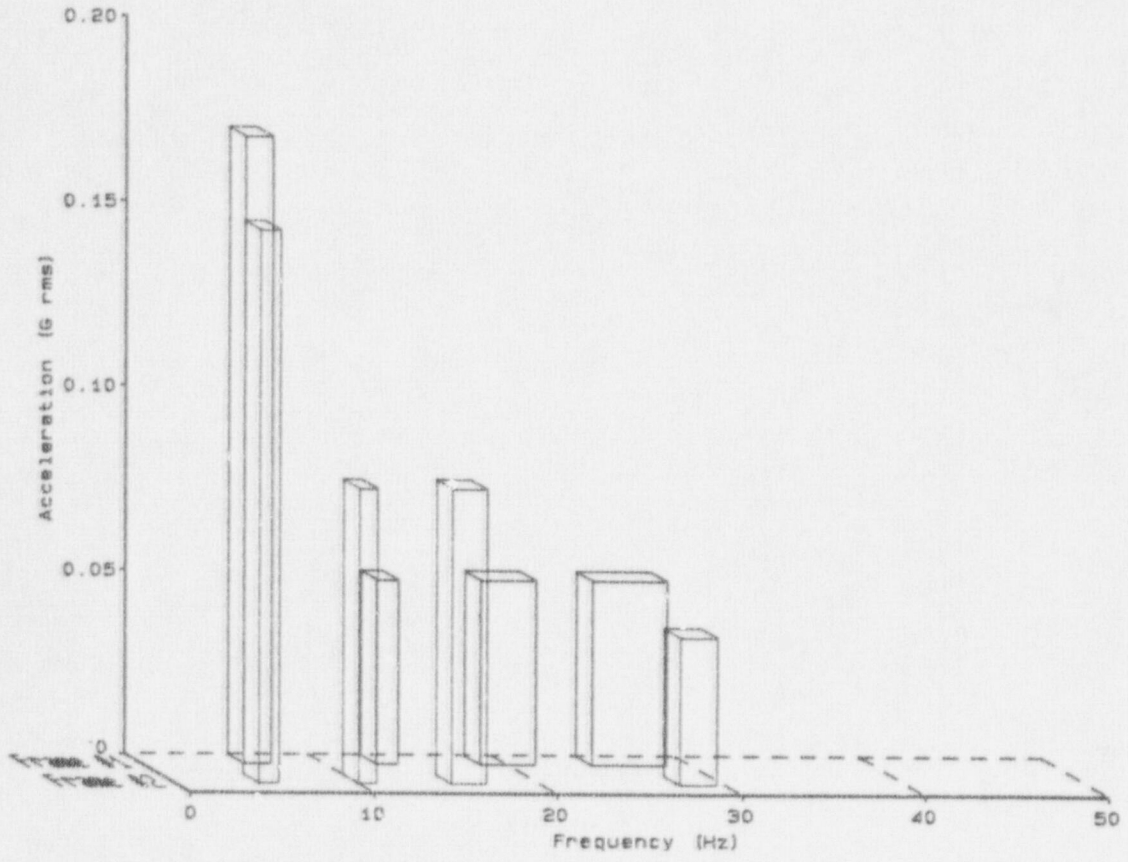

Figure E-86. Band Integrated Acceleration: Z direction, spherical "T", Test T40.30.

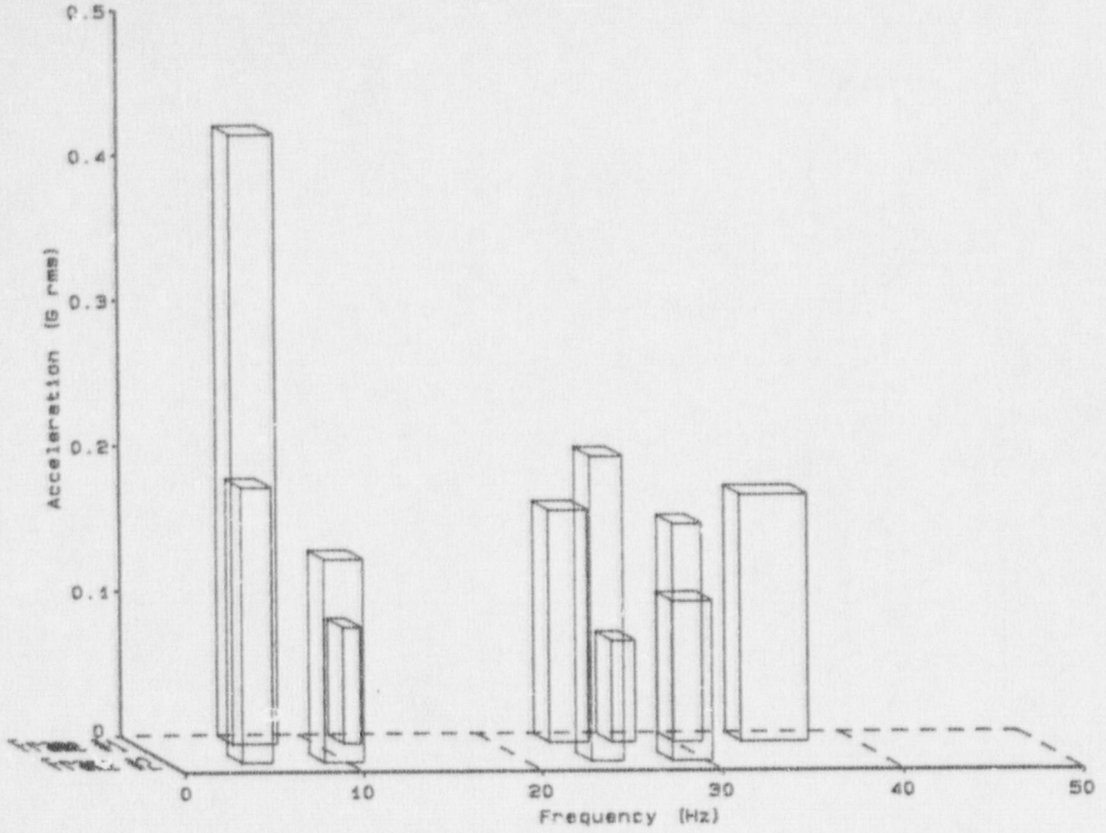

Figure E-87. Band Integrated Acceleration: Z direction, standard "T", Test T40.10.

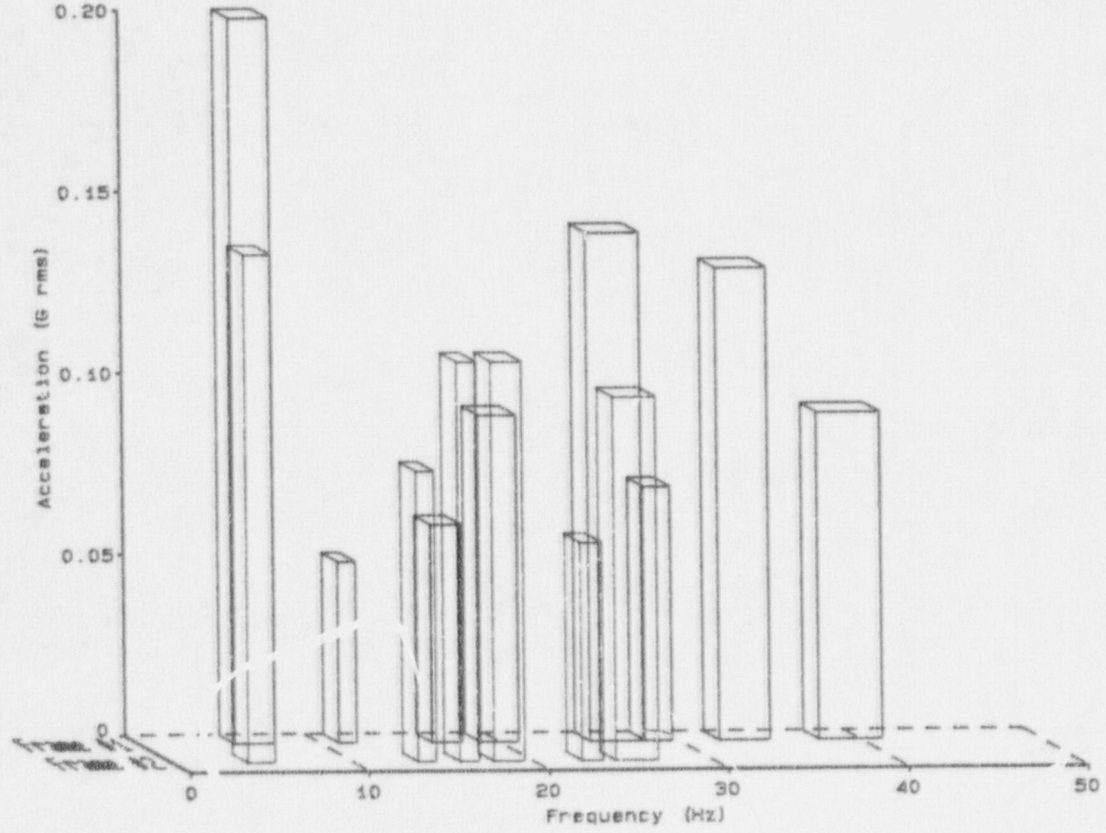

Figure E-88. Band Integrated Acceleration: Z direction, standard "T", Test T40.30.

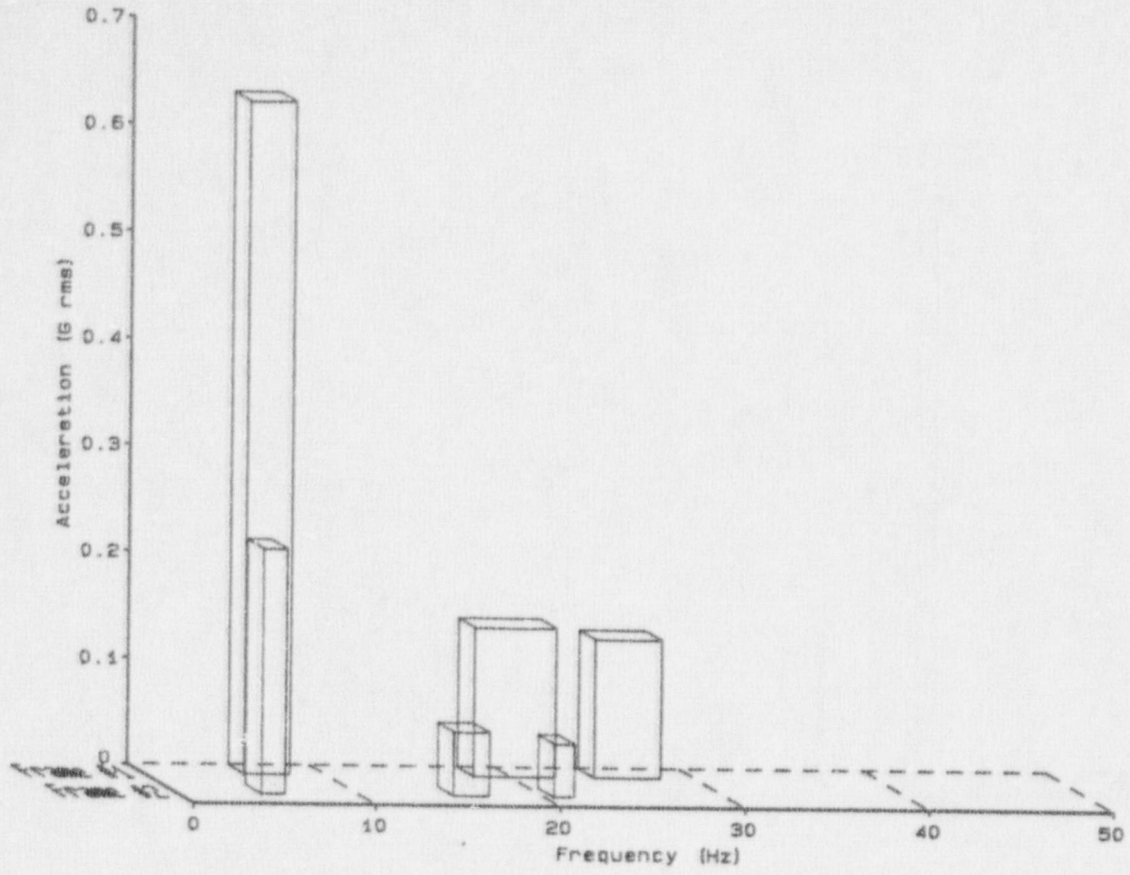

Figure E-89. Band Integrated Acceleration: Z direction, top HDU, Test T40.10.

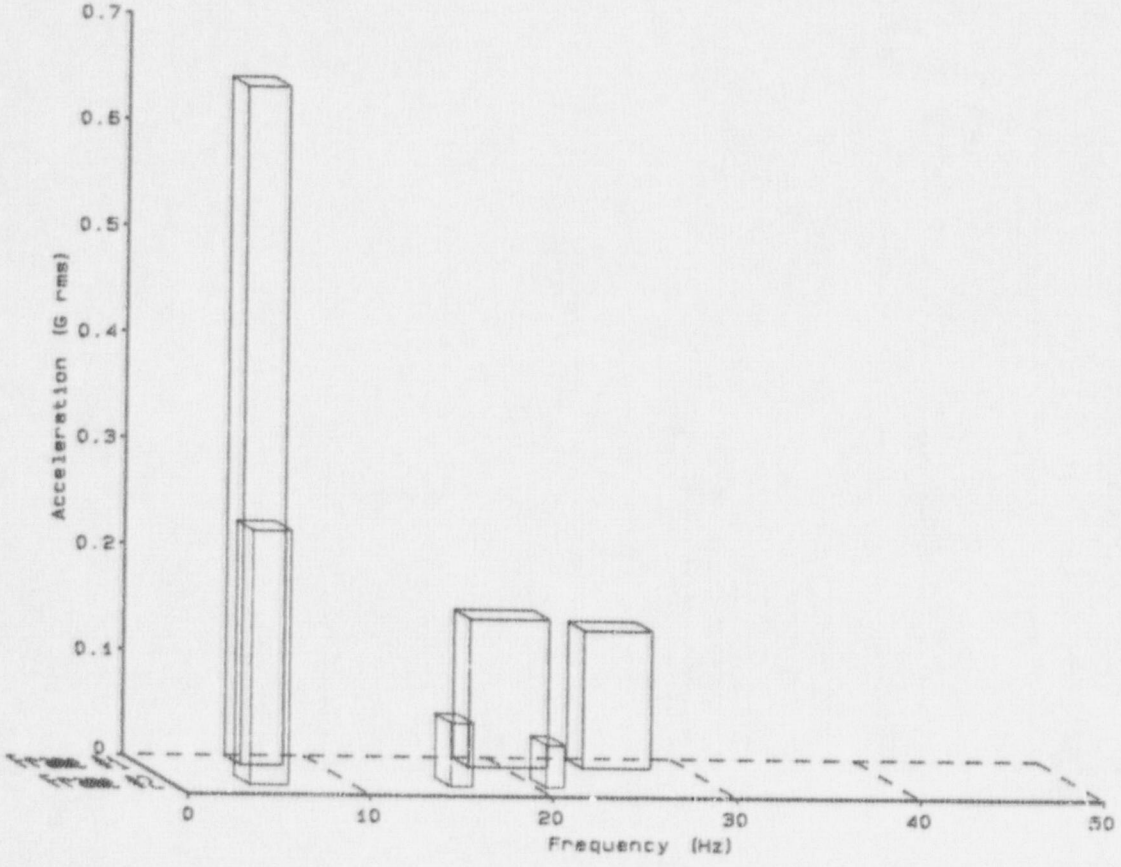

Figure E-90. Band Integrated Acceleration: Z direction, top HDU, Test T40.30.

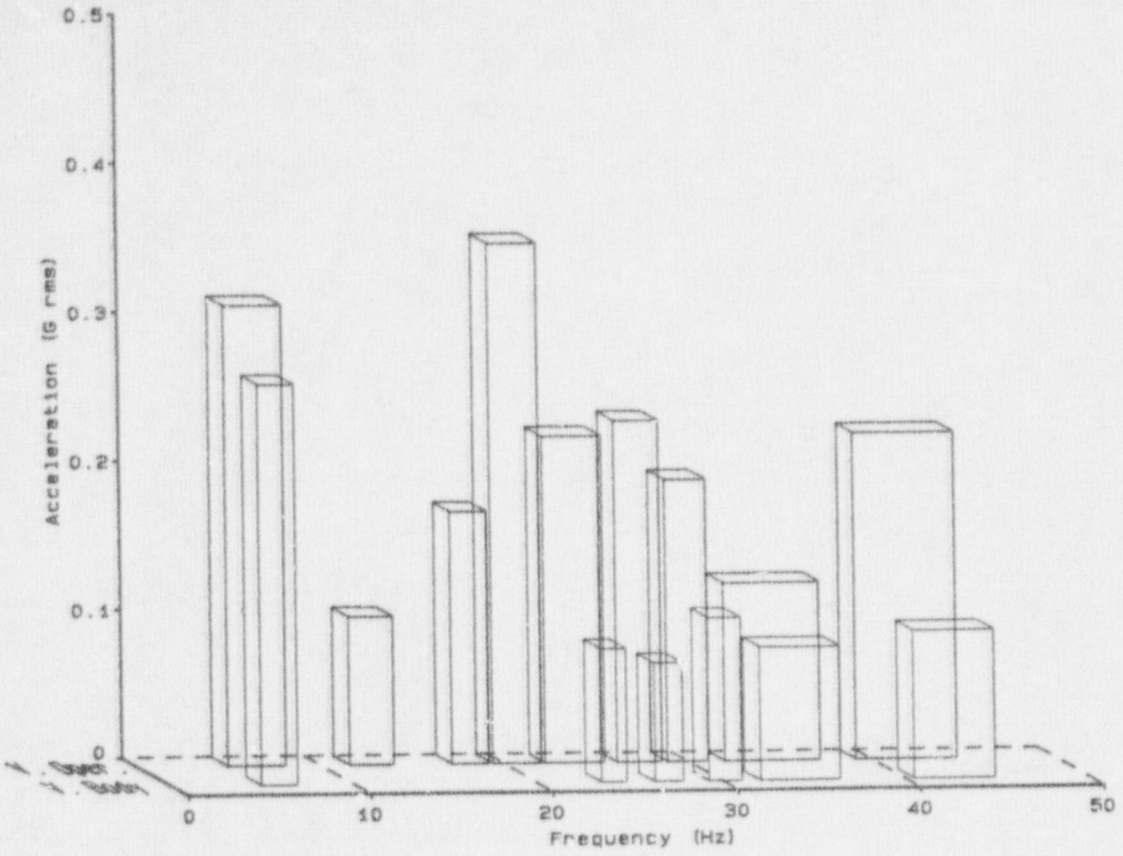

Figure E-91. Band Integrated Acceleration Amplification: Frame #1, X direction, Test T40.10.

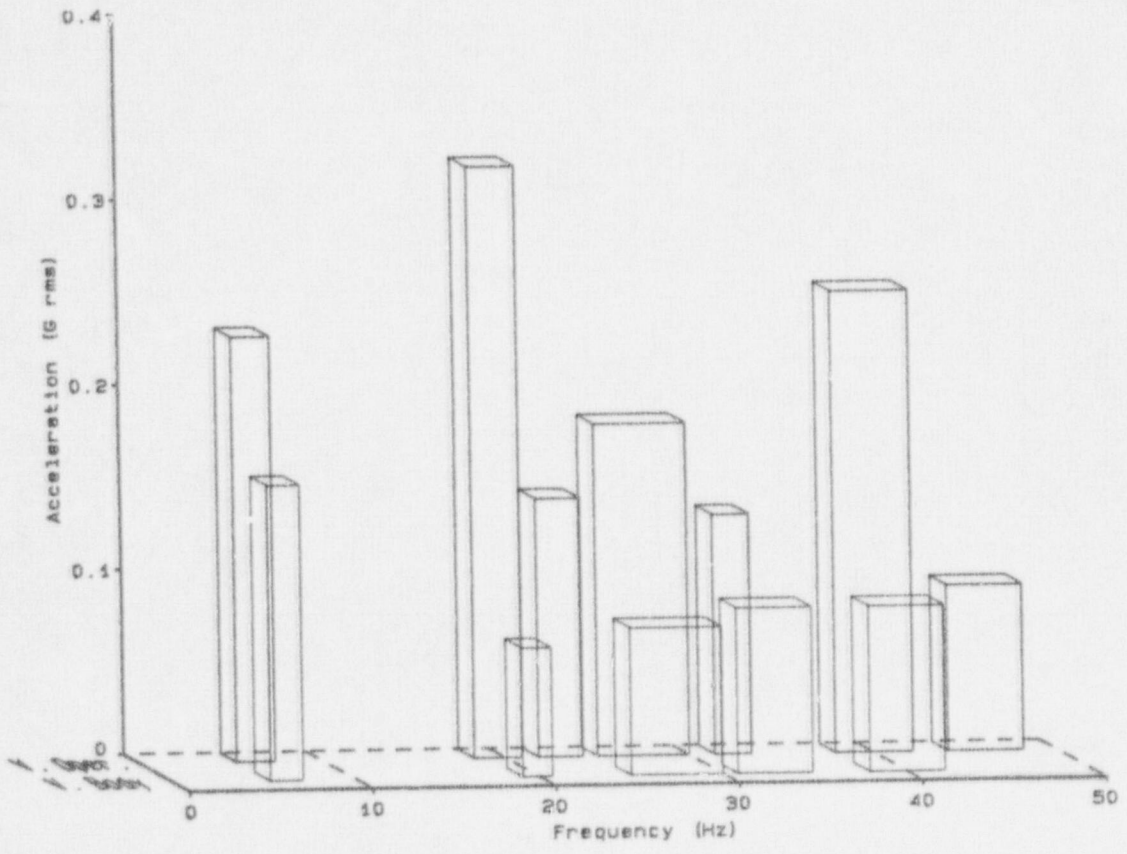

Figure E-92. Band Integrated Acceleration Amplification: Frame #1, X direction, Test T40.30.

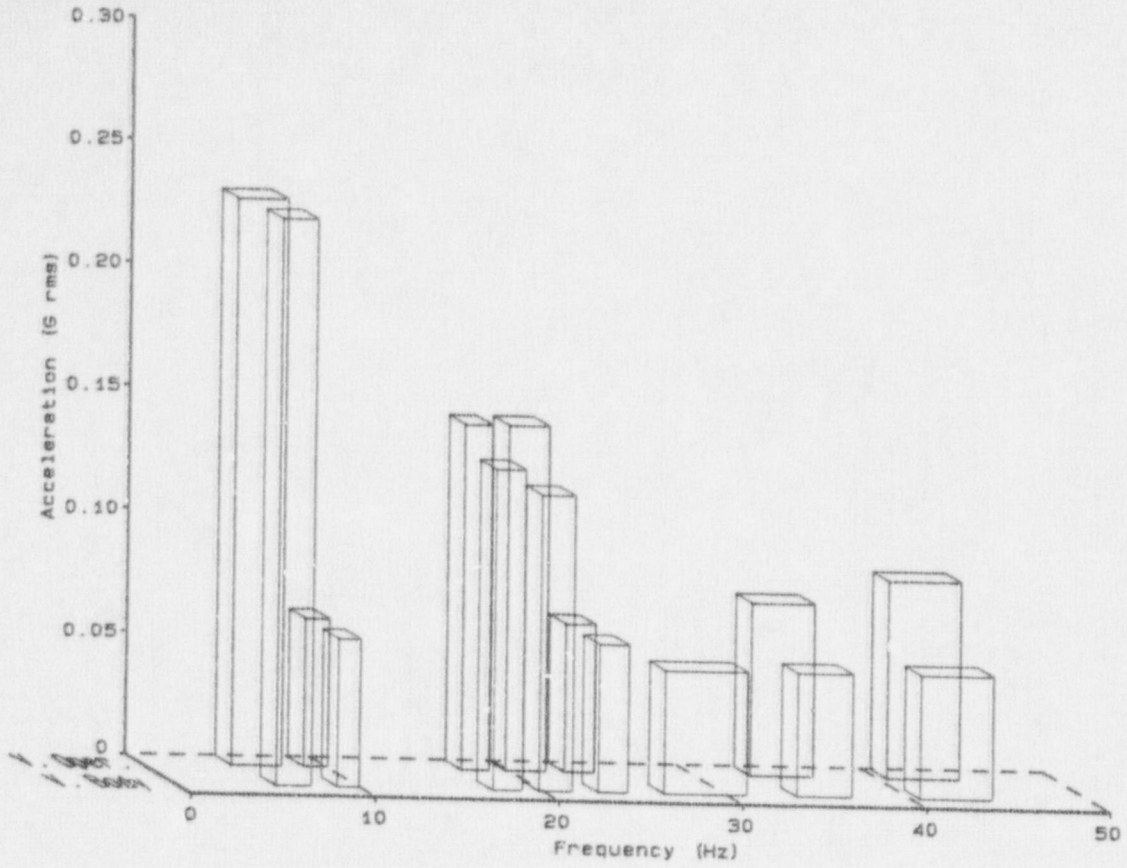

Figure E-93. Band Integrated Acceleration Amplification: Frame #1, Y direction, Test T40.10.

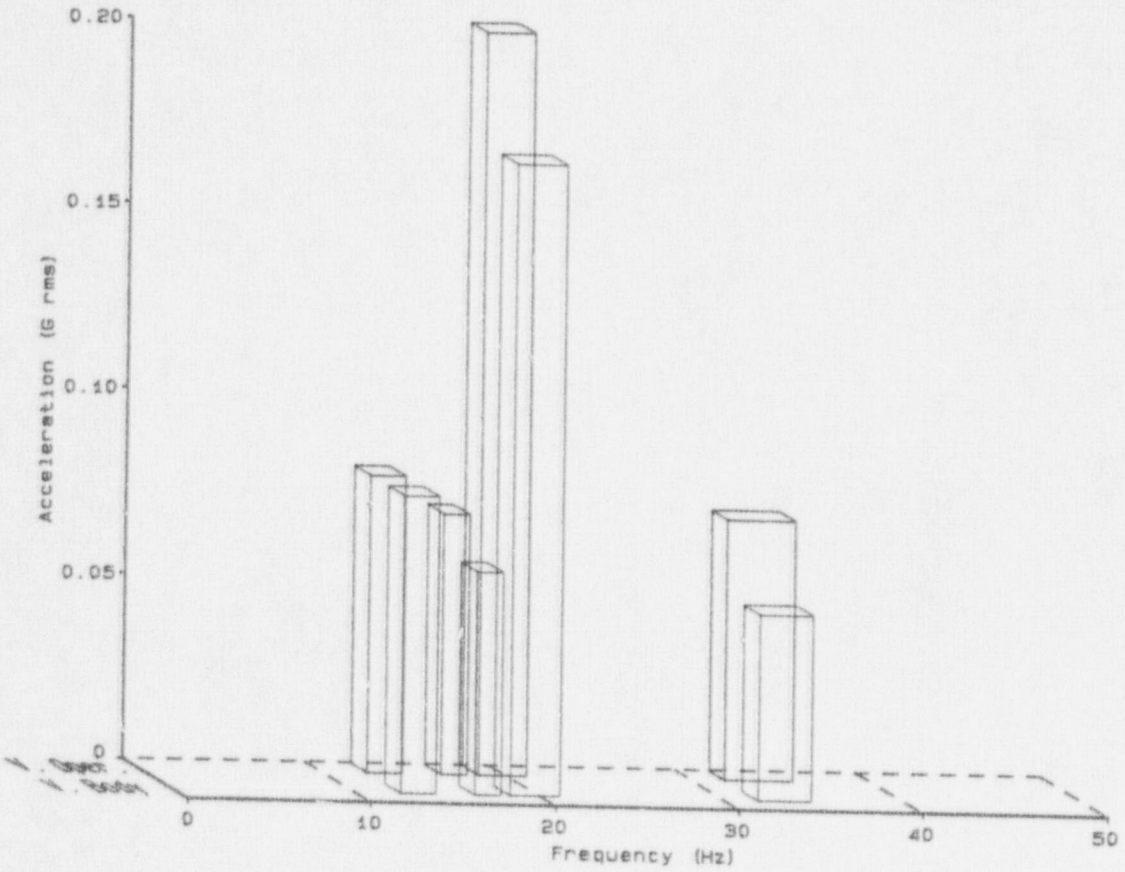

Figure E-94. Band Integrated Acceleration Amplification: Frame #1, Y direction, Test T40.30.

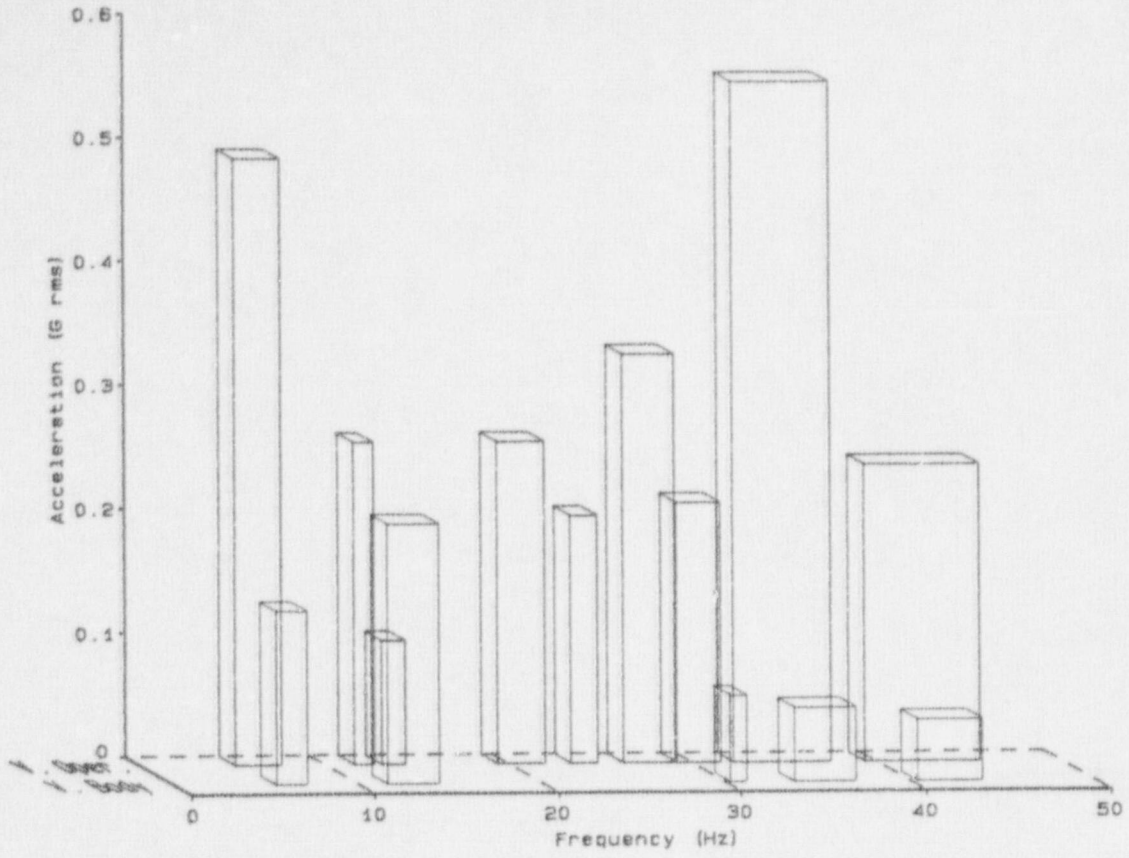

Figure E-95. Band Integrated Acceleration Amplification: Frame #1, Z direction, Test T40.10.

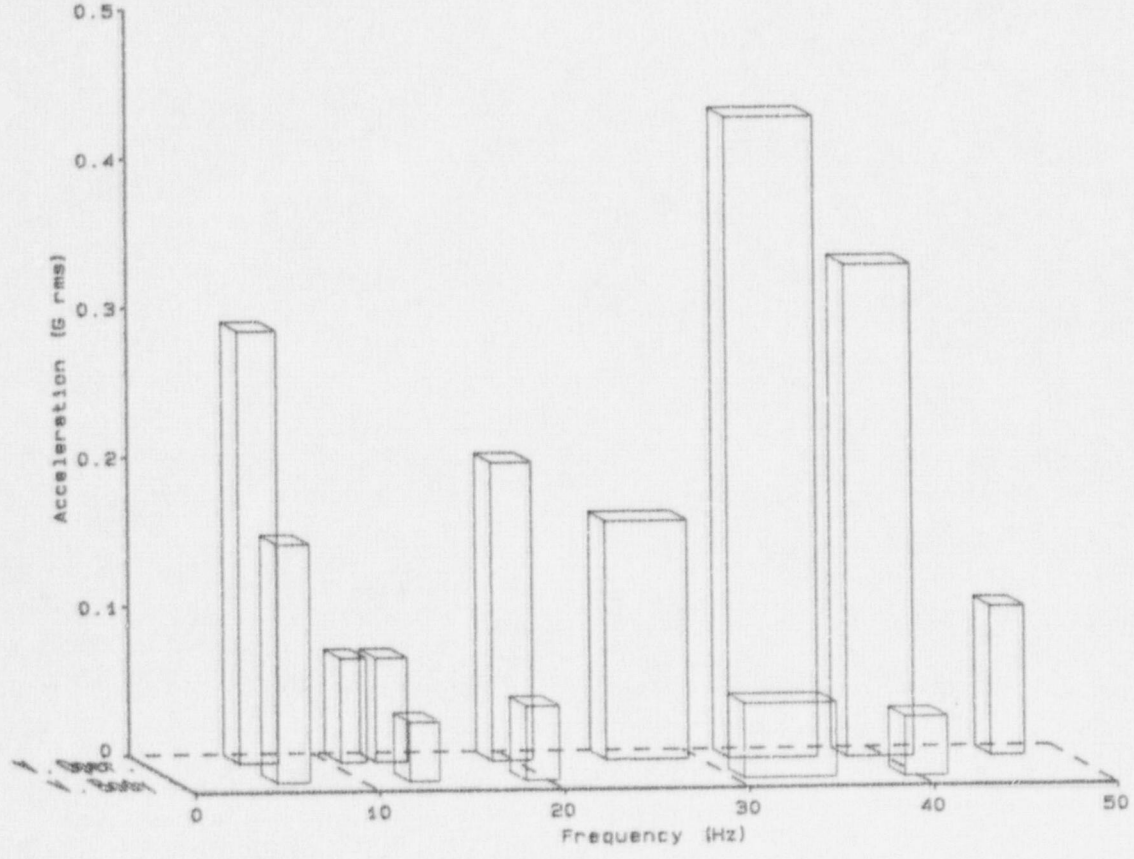

Figure E-96. Band Integrated Acceleration Amplification: Frame #1, Z direction, Test T40.30.

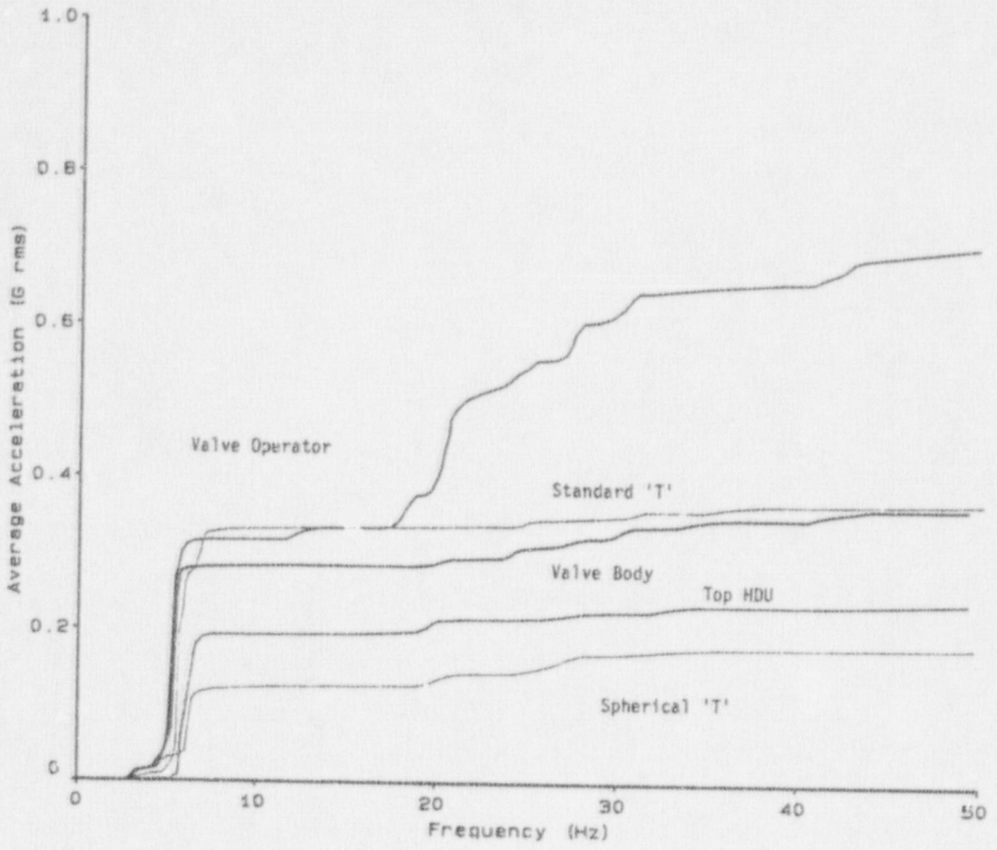

Figure E-97. Average Integrated Acceleration: Frame #1, X direction, Test T40.10.

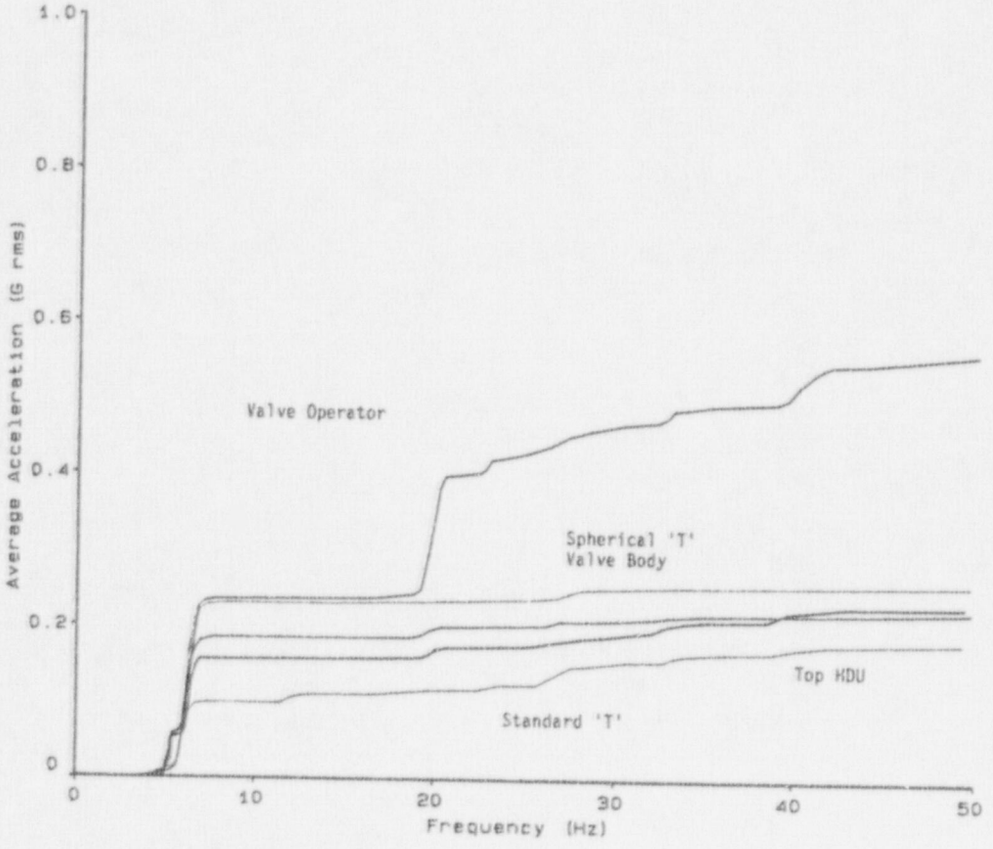

Figure E-98. Average Integrated Acceleration: Frame #1, X direction, Test T40.30.

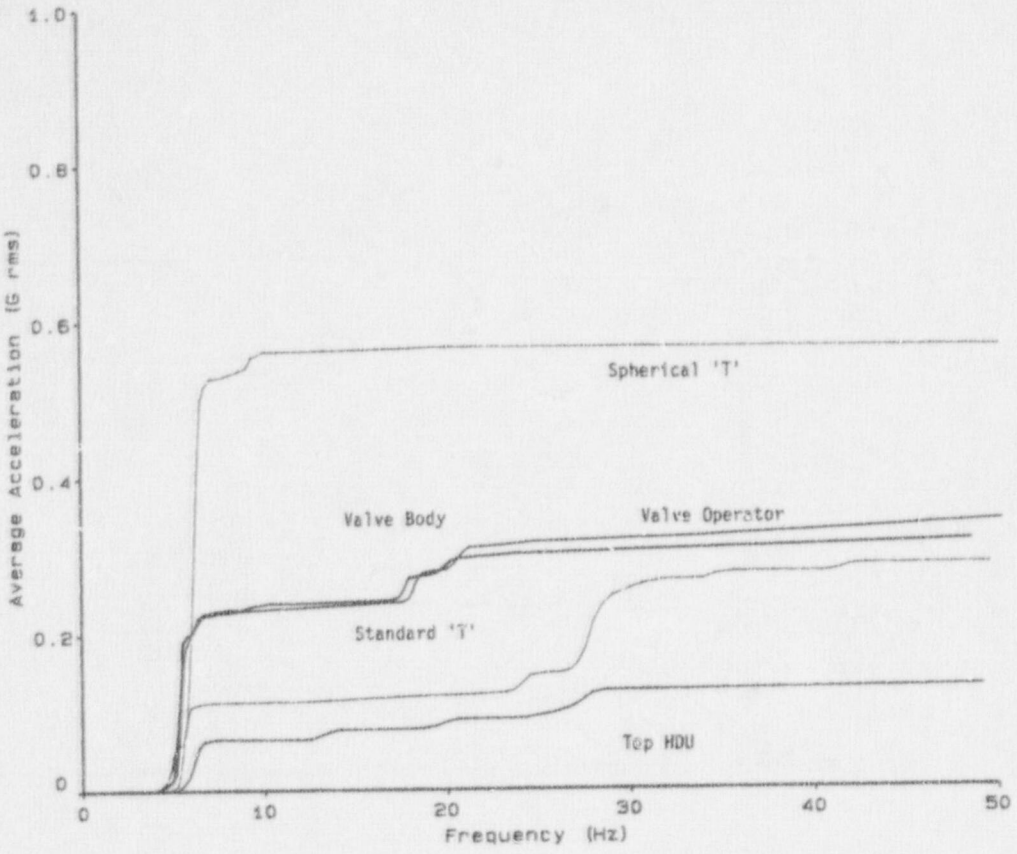

Figure E-99. Average Integrated Acceleration: Frame #1, Y direction, Test T40.10.

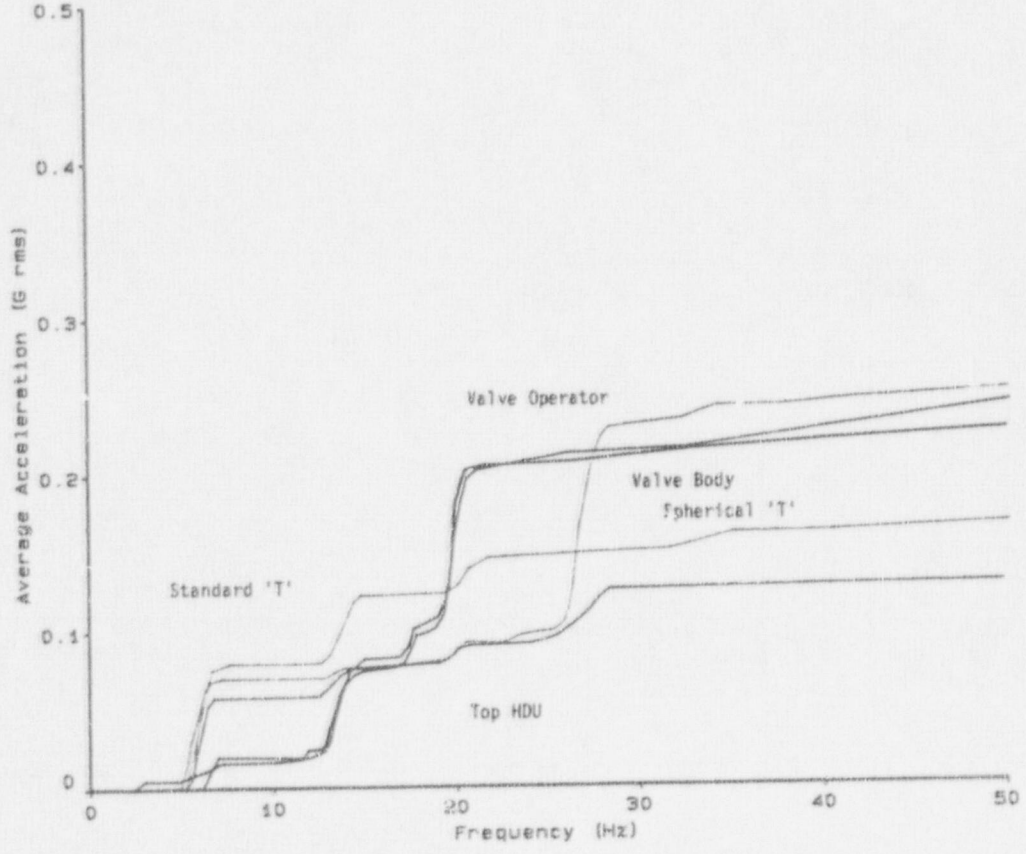

Figure E-100. Average Integrated Acceleration: Frame #1, Y direction, Test T40.30.

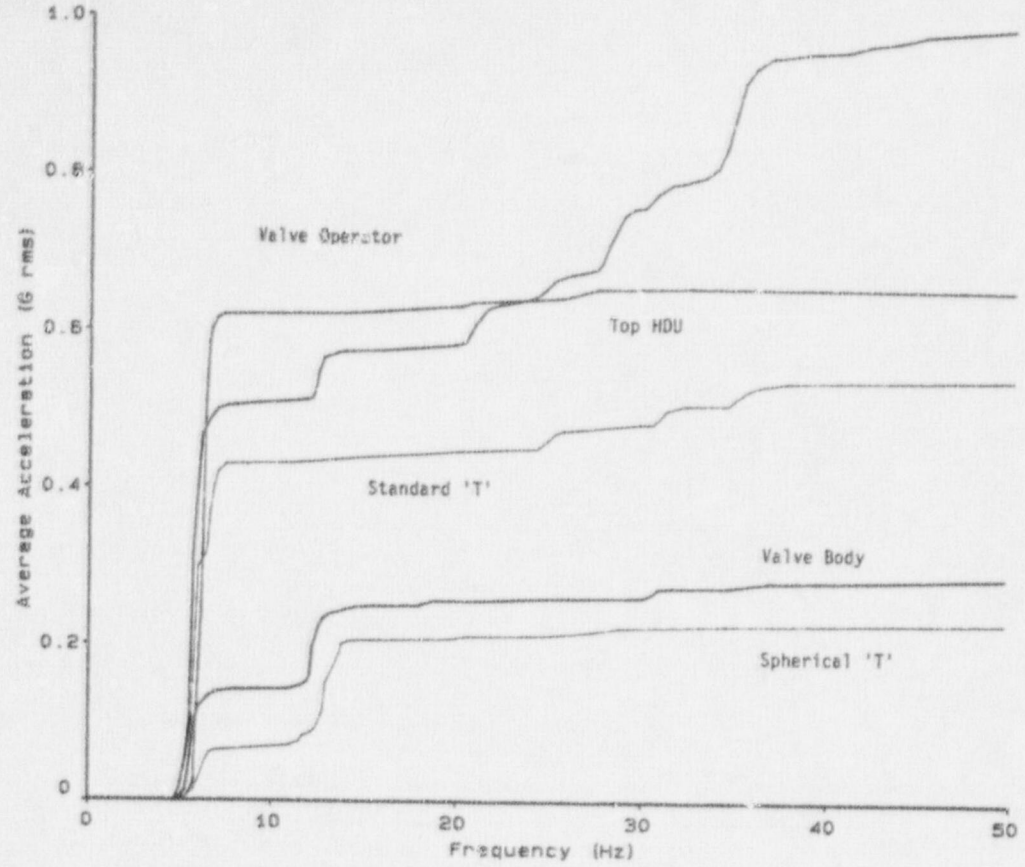

Figure E-101. Average Integrated Acceleration: Frame #1, Z direction, Test T40.10.

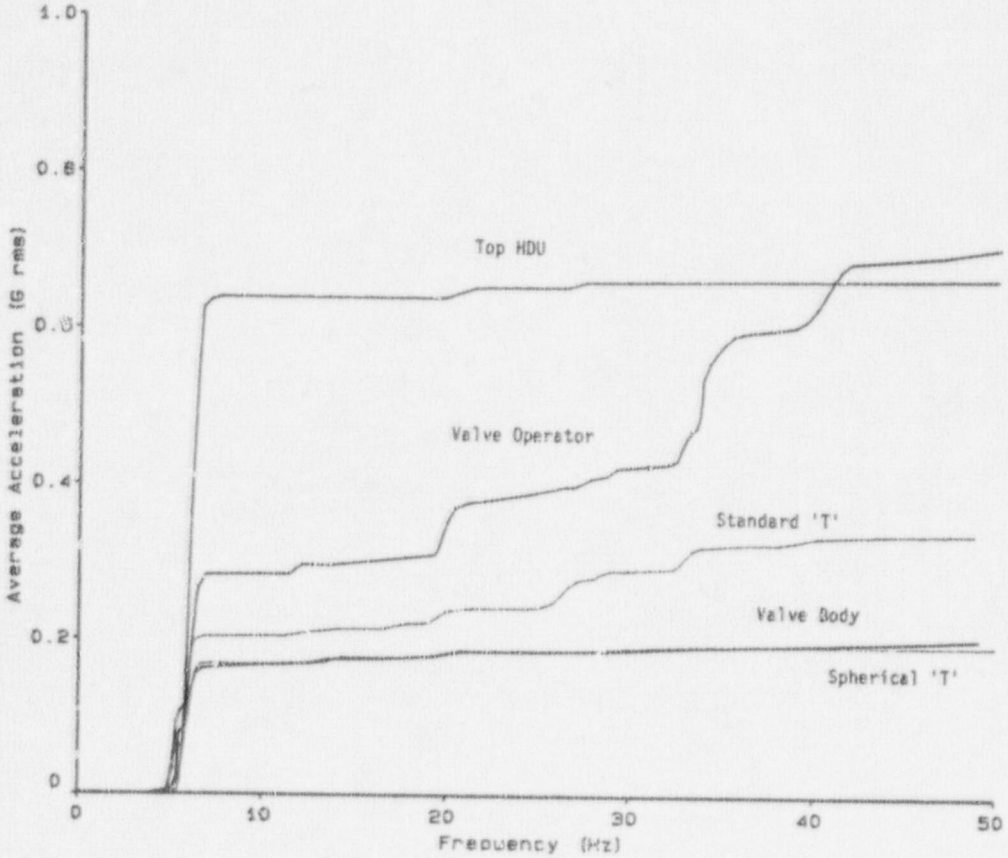

Figure E-102. Average Integrated Acceleration: Frame #1, Z direction, Test T40.30.

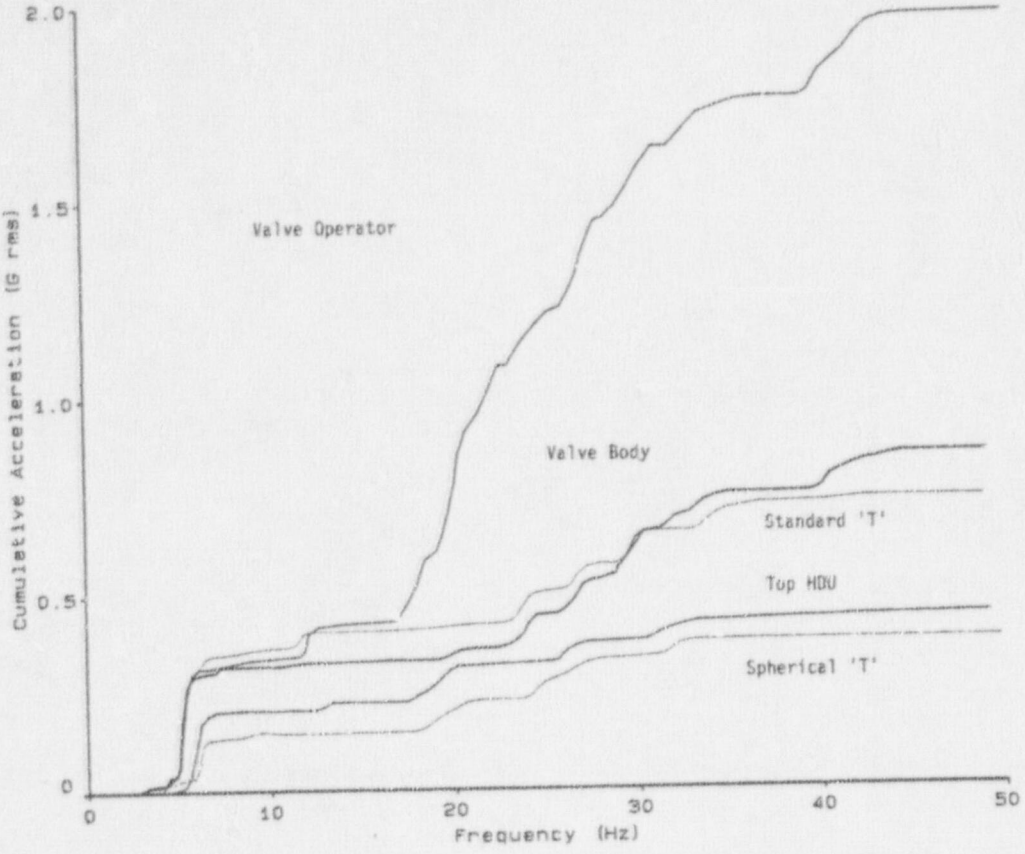

Figure E-103. Cumulative Integrated Acceleration: Frame #1, X direction, Test T40.10.

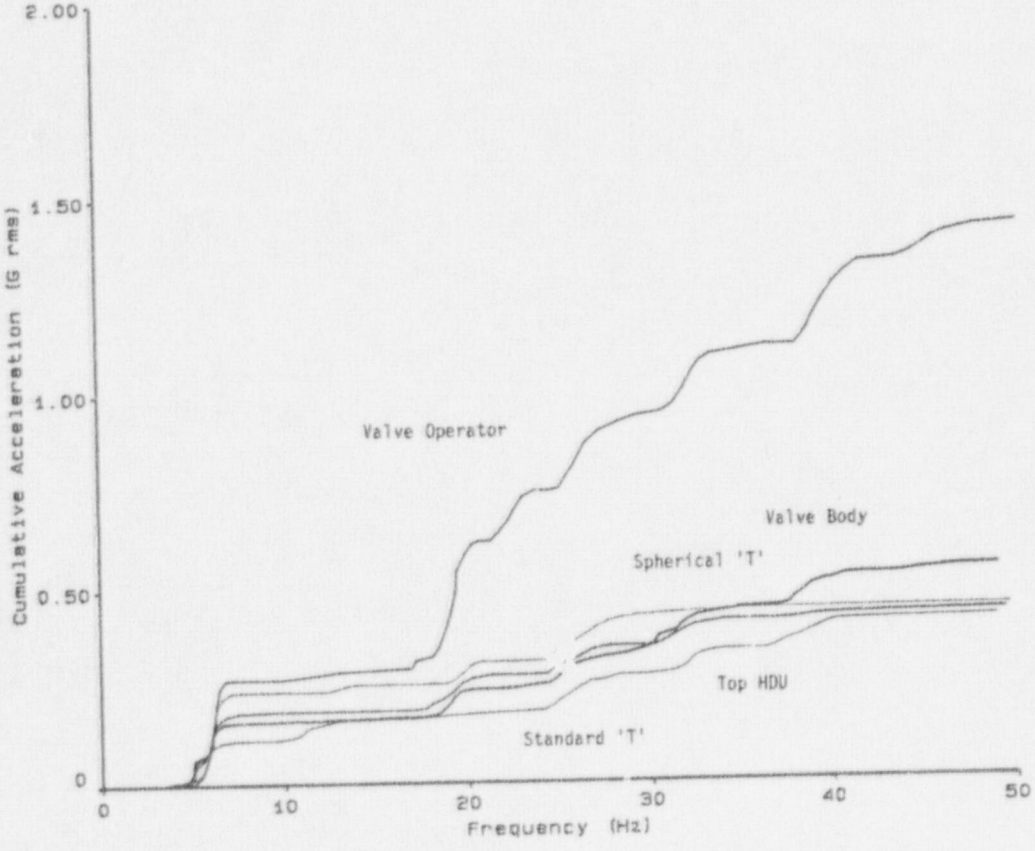

Figure E-104. Cumulative Integrated Acceleration: Frame #1, X direction, Test T40.30.

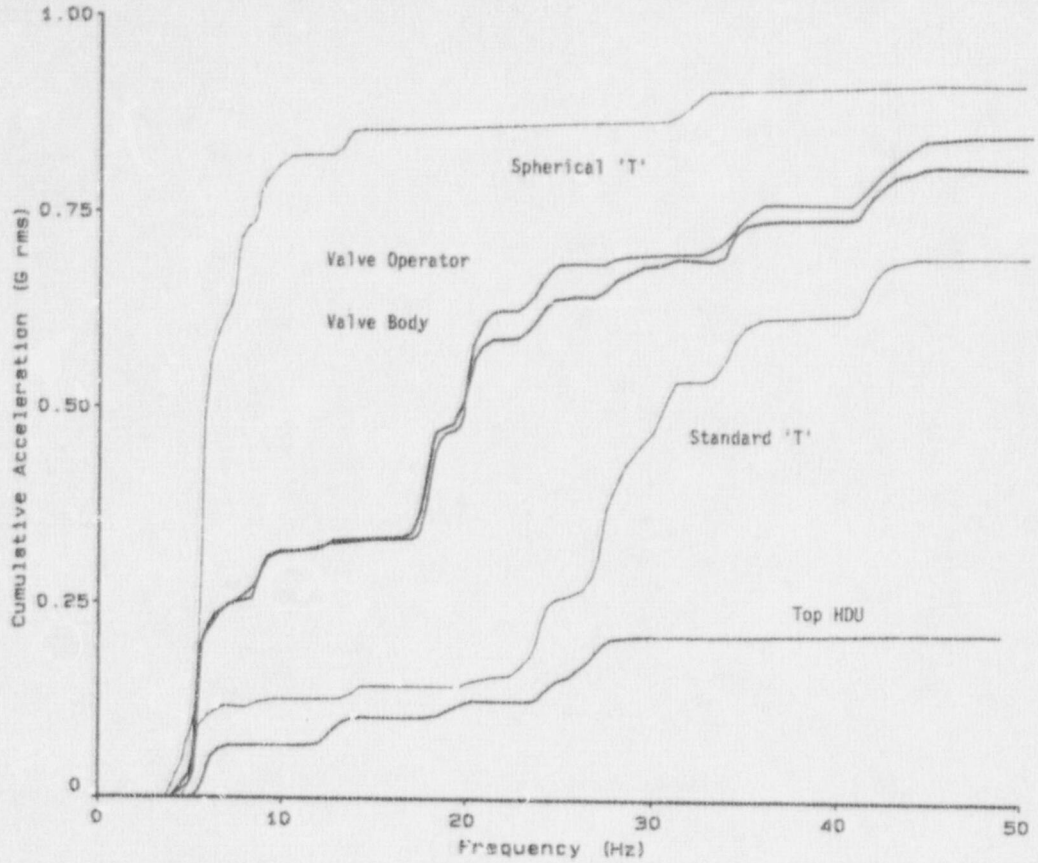

Figure E-105. Cumulative Integrated Acceleration: Frame #1, Y direction, Test T40.10.

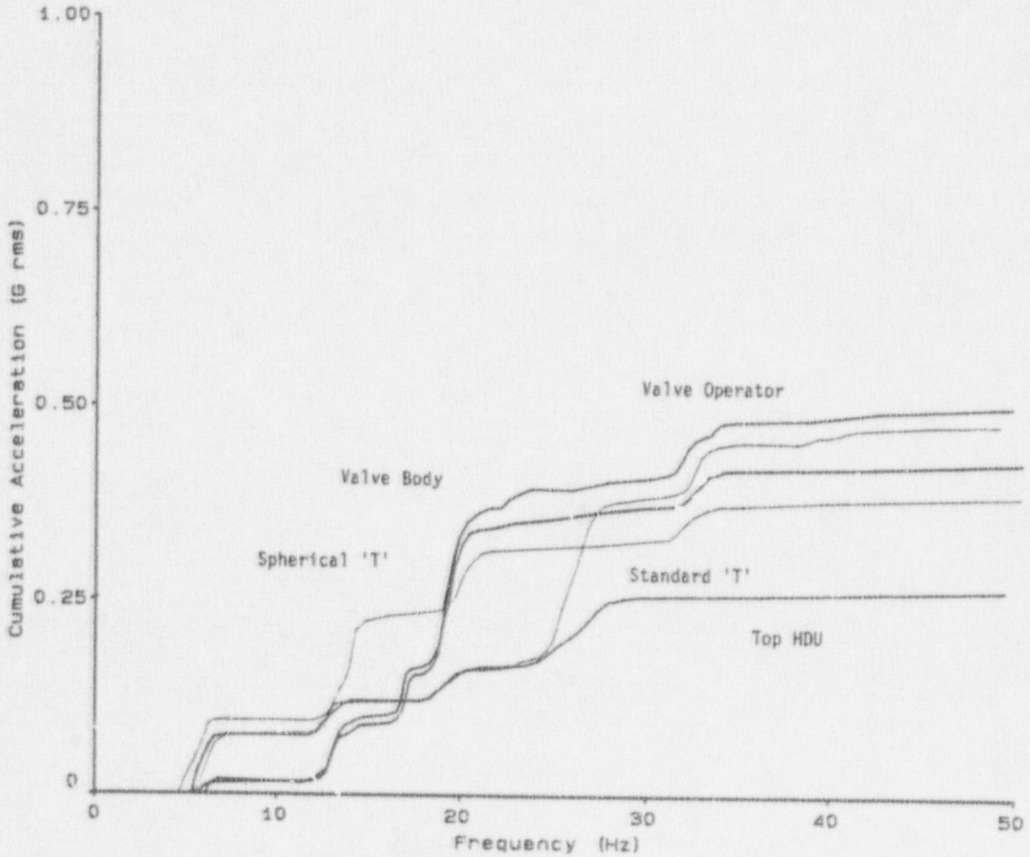

Figure E-106. Cumulative Integrated Acceleration: Frame #1, Y direction, Test T40.30.

Figure E-107. Cumulative Integrated Acceleration: Frame #1, Z direction, Test T40.10.

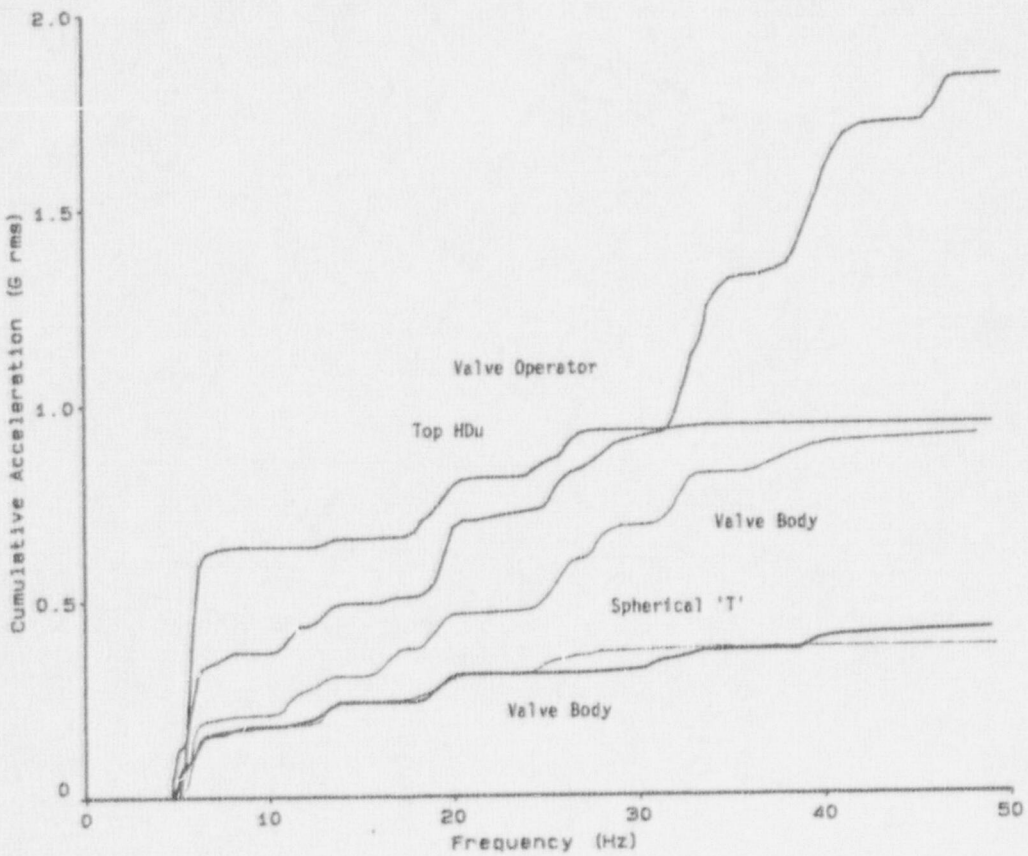

Figure E-108. Cumulative Integrated Acceleration: Frame #1, Z direction, Test T40.30.

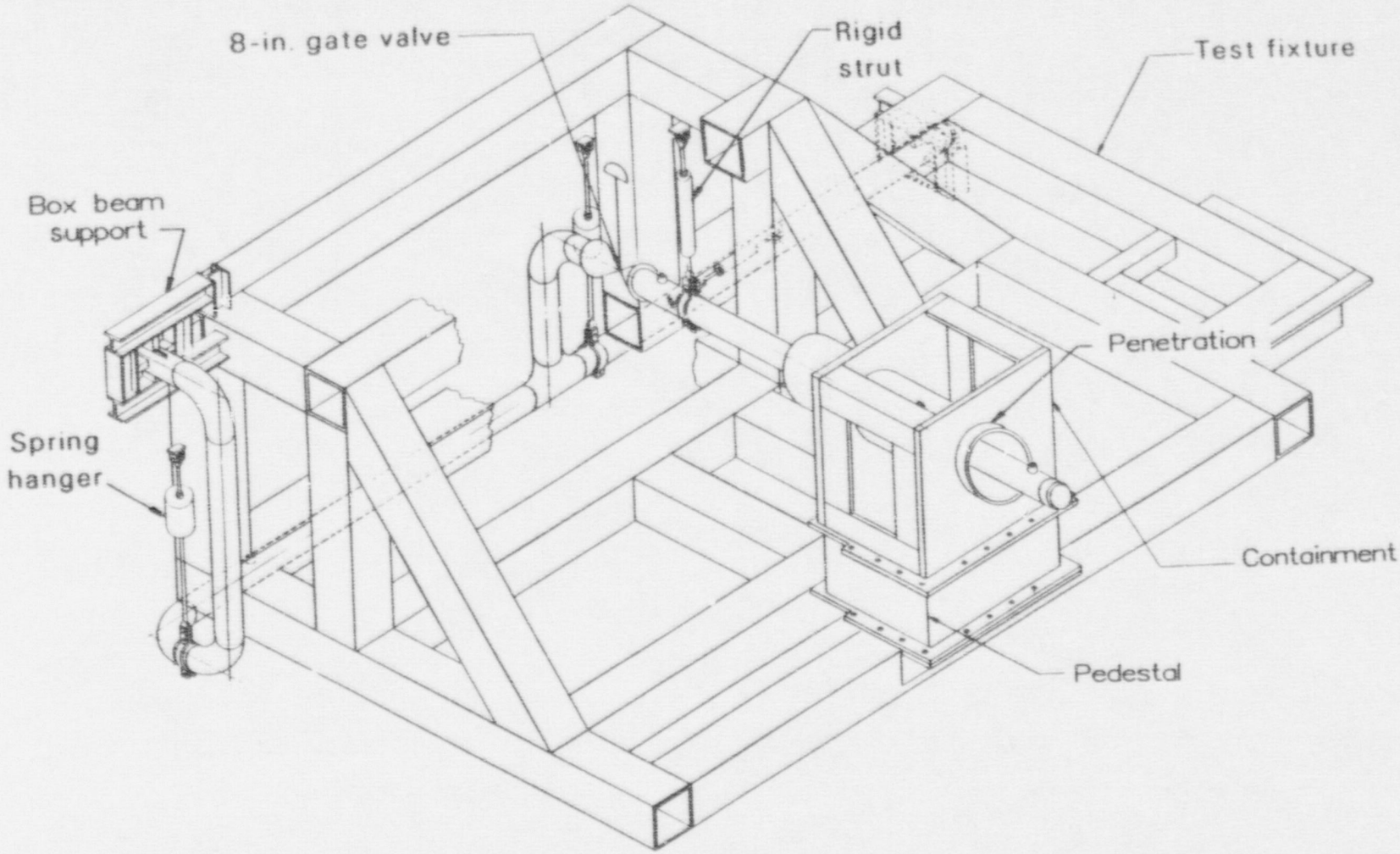

Figure E-109. Sketch showing the location of the 8-in. piping system with gate valve installed in the test fixture.

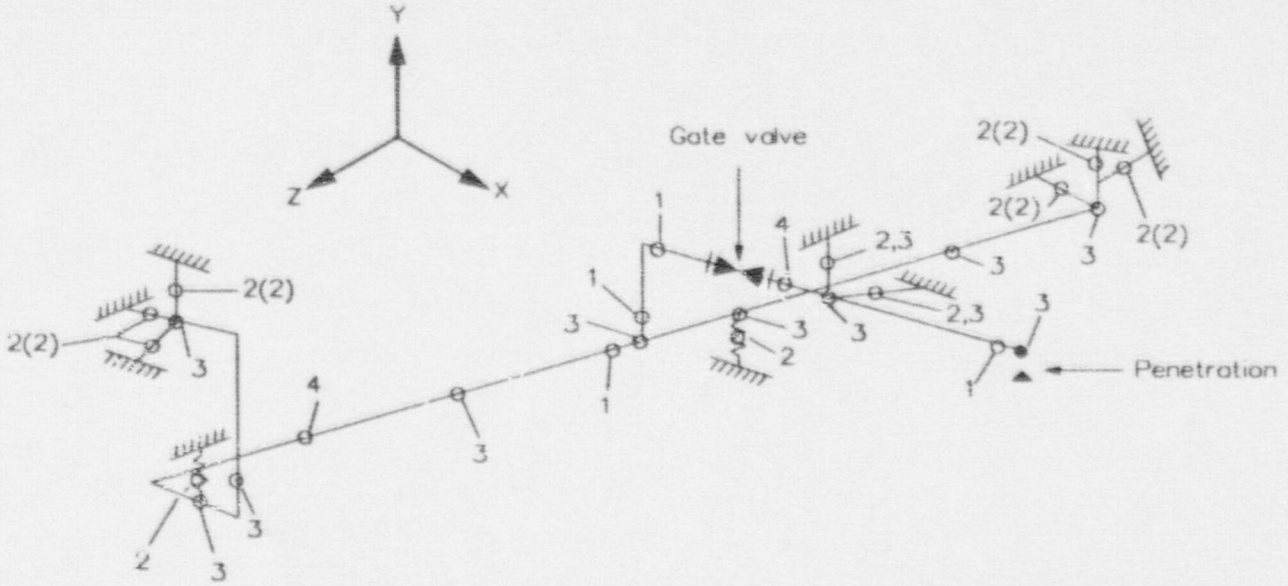

Key	
1- Strain gages on pipe	(6 channels)
2- Strain gages on support	(1 channel)
3- Accelerometers	(3 channels)
4- Static pressure	(1 channels)

For Each Valve-22 Channels	
3 Accelerometers	(9 channels)
1 Stem position	(1 channel)
6 Uniaxial strain	(6 channels)
2 Strain rosette	(6 channels)

MGHG1545

Figure E-110. Piping system configuration and location of instrumentation used for testing the 8-in. piping system with gate valve.

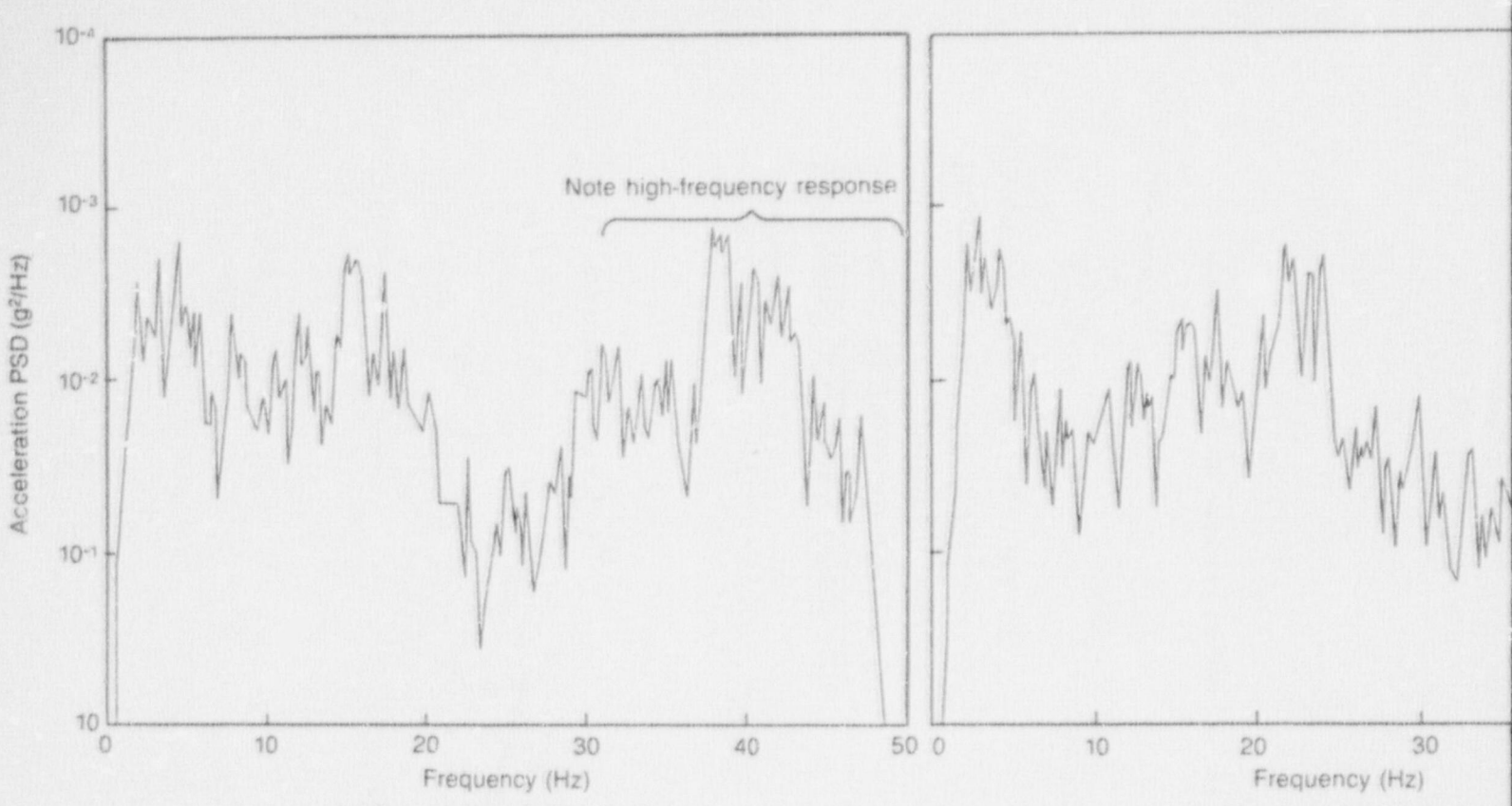

(a) Gate valve operator, X axis

(b) Gate valve actuator, Y axi

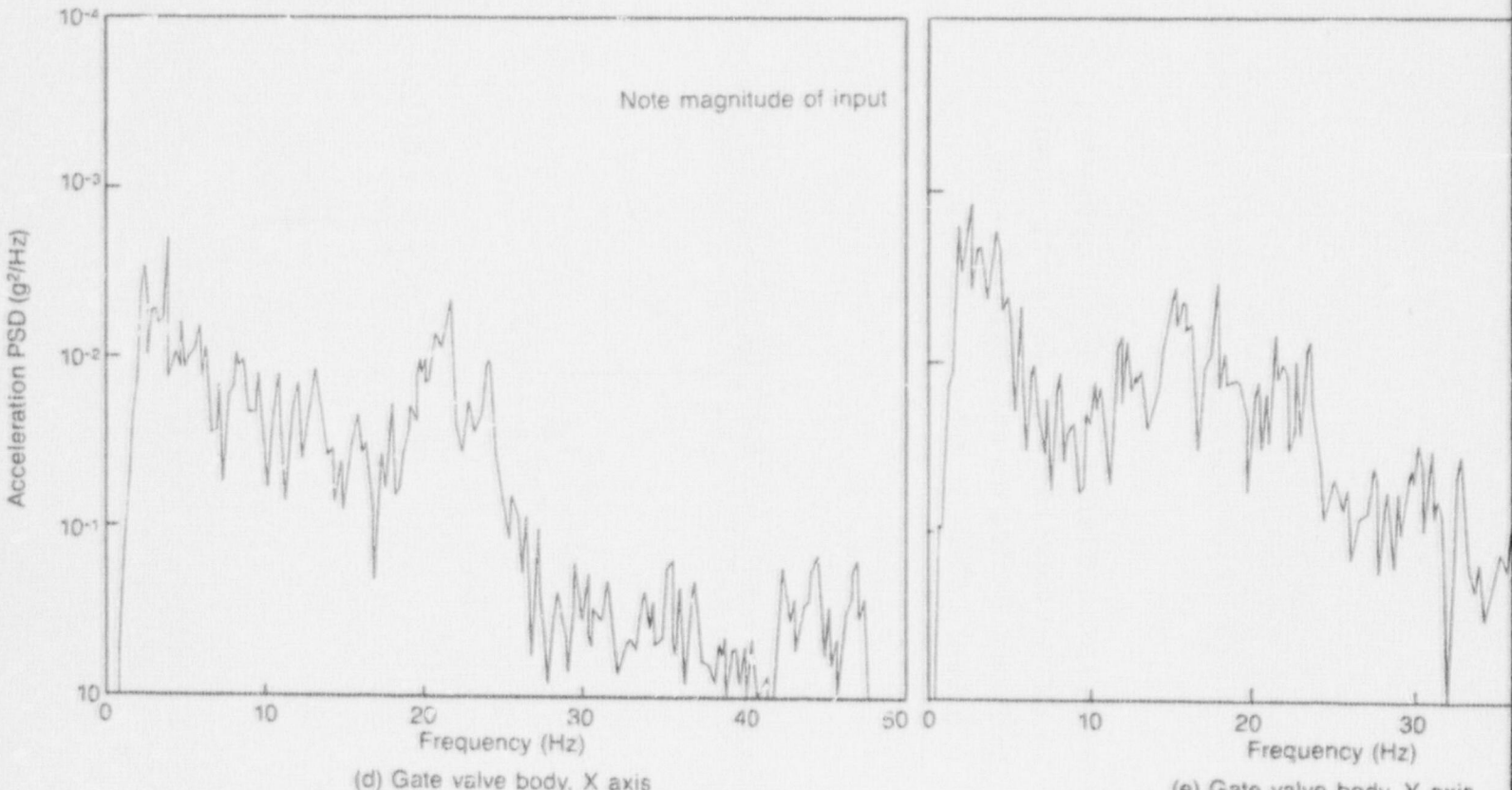

(d) Gate valve body, X axis

(e) Gate valve body, Y axis

Figure E-111. Frequency domain (PSD) comparison of the gate valve body and

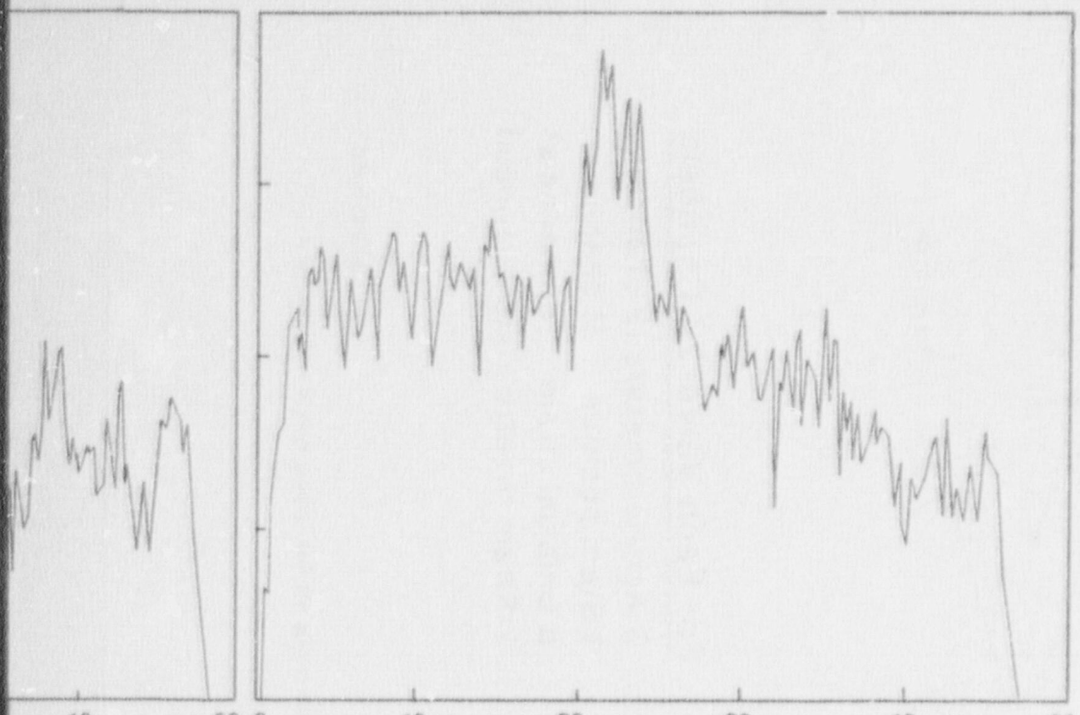

(c) Gate valve actuator, Z axis

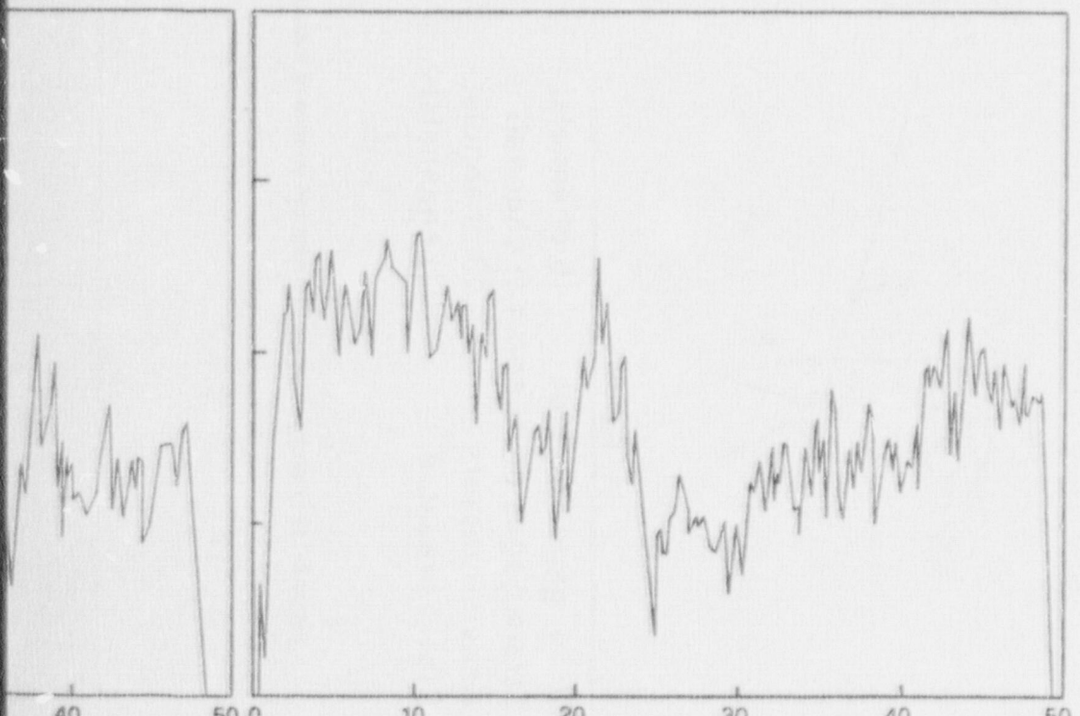

(f) Gate valve body, Z axis

actuator responses in the three global axes.

7-8826

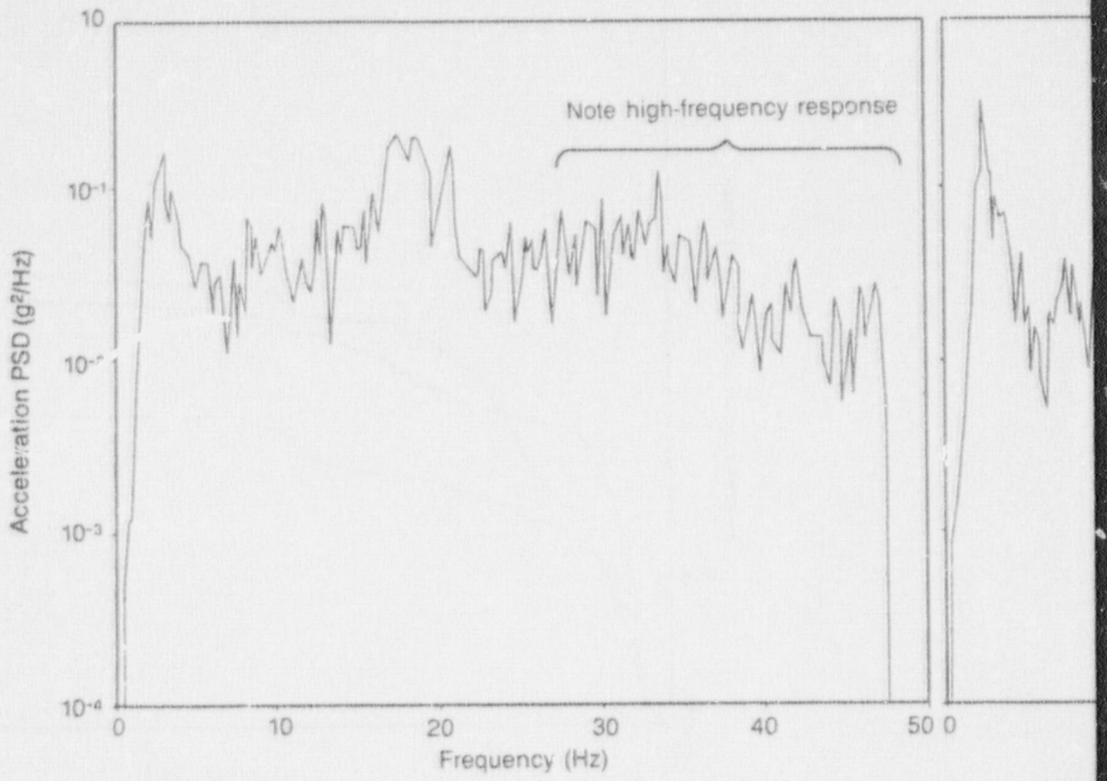

(a) Butterfly valve actuator, X axis

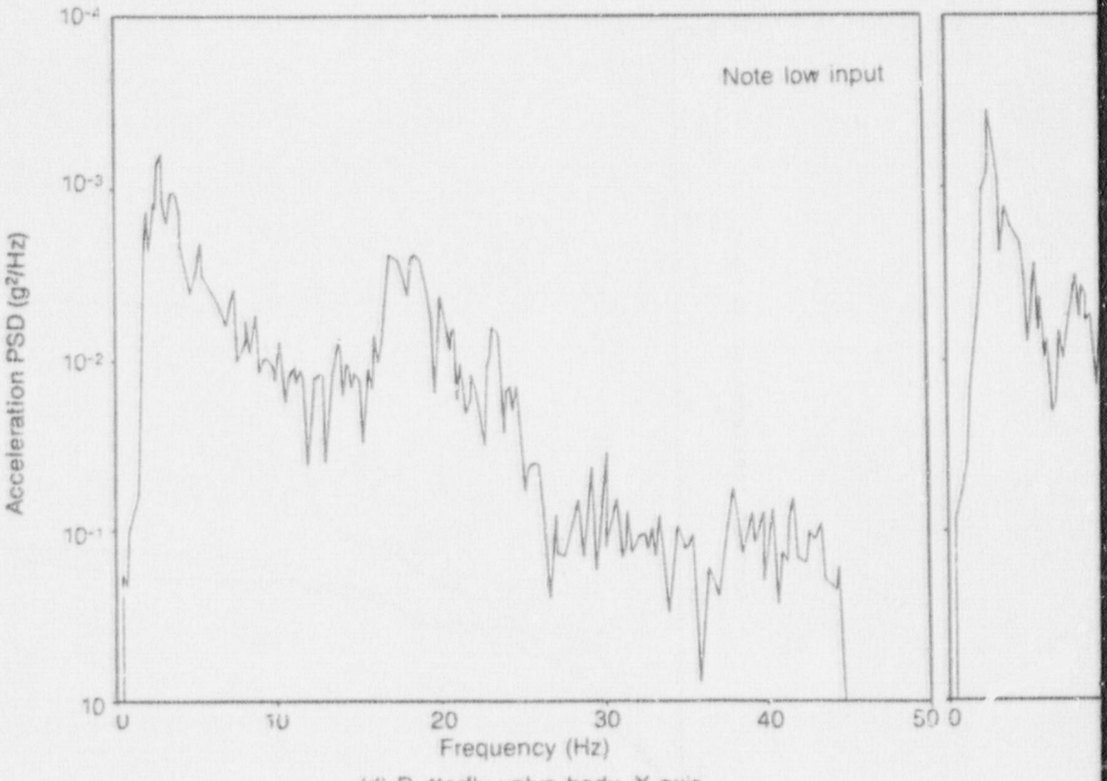

(d) Butterfly valve body, X axis

Figure E-112. Frequency domain (PS

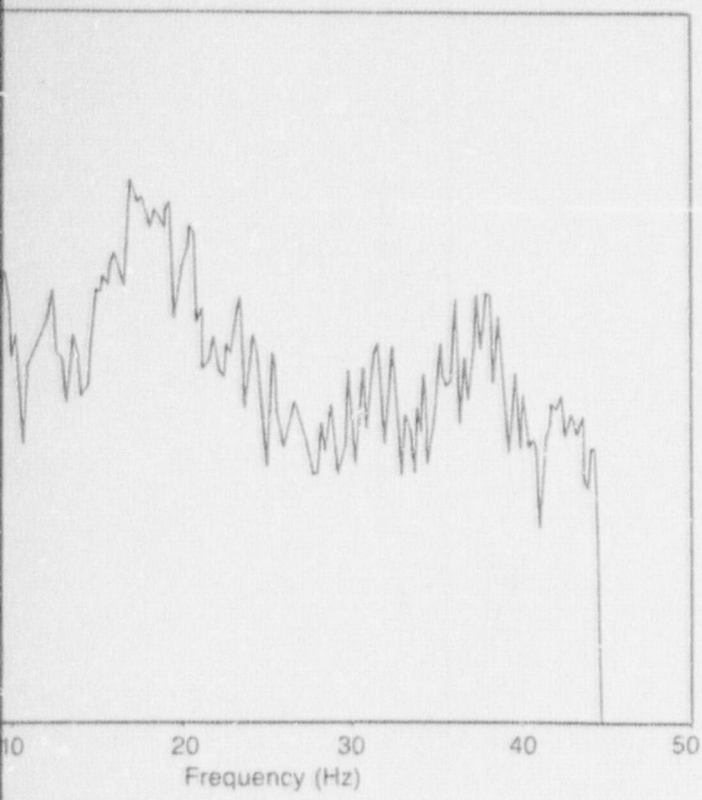

(b) Butterfly valve actuator, Y axis

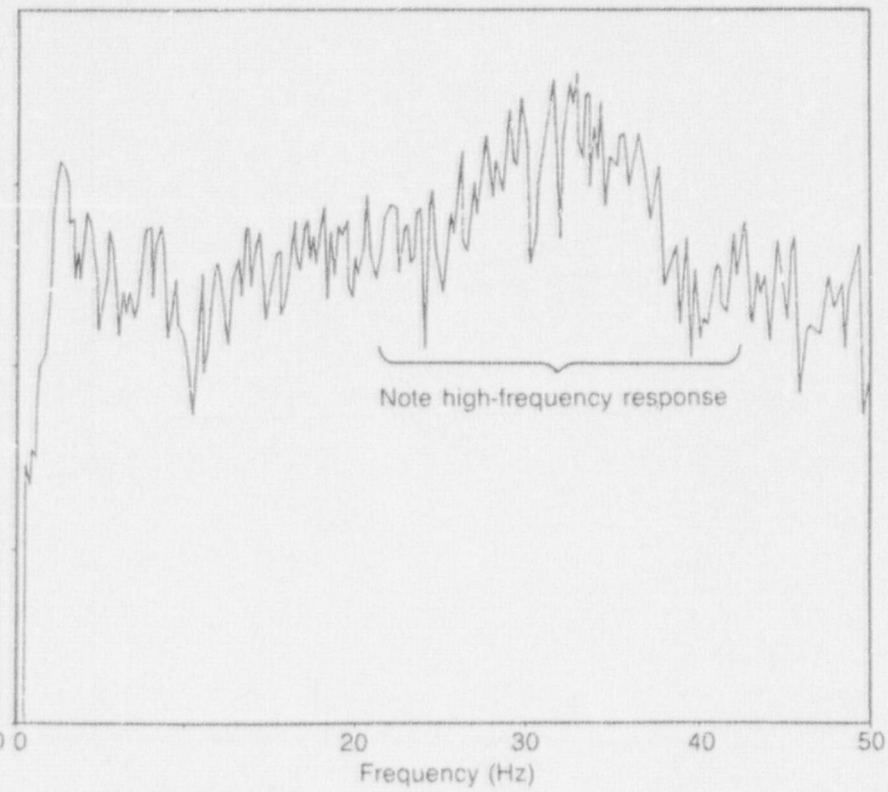

(c) Butterfly valve actuator, Z axis

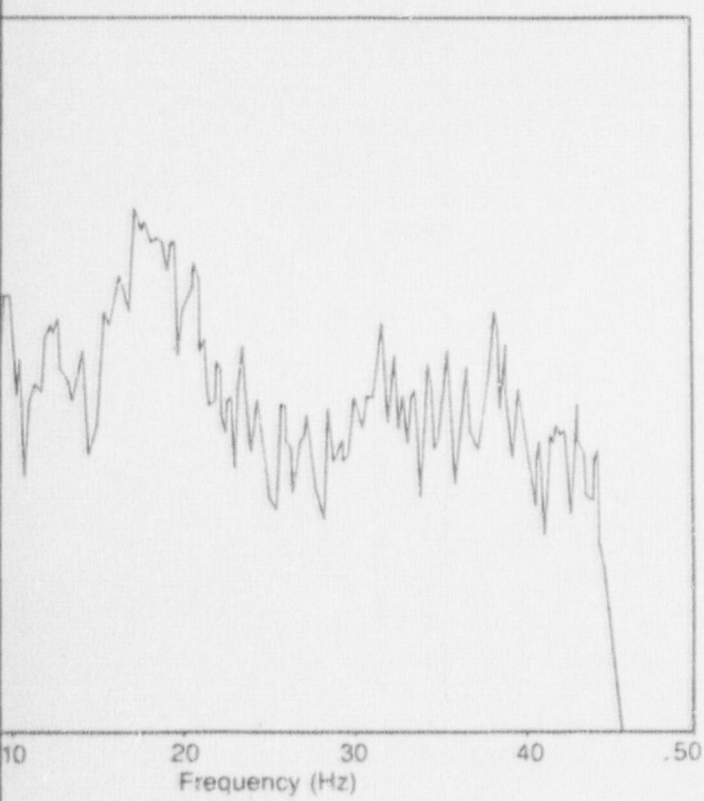

(e) Butterfly valve body, Y axis

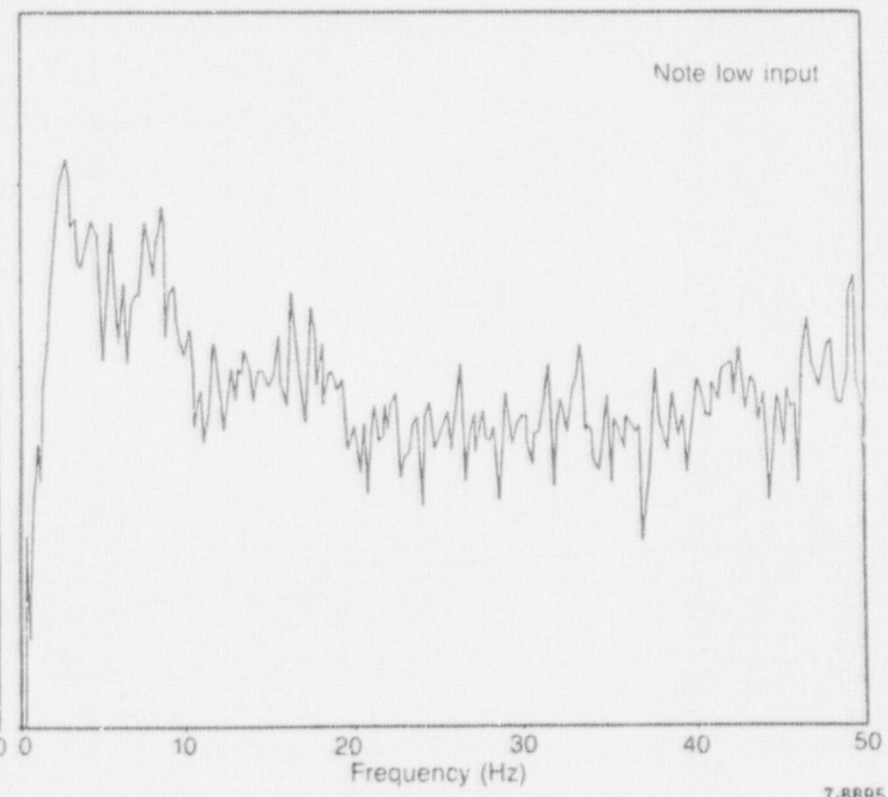

(f) Butterfly valve body, Z axis

7-8895

D) comparison of the butterfly valve body and actuator responses in the three global axes.

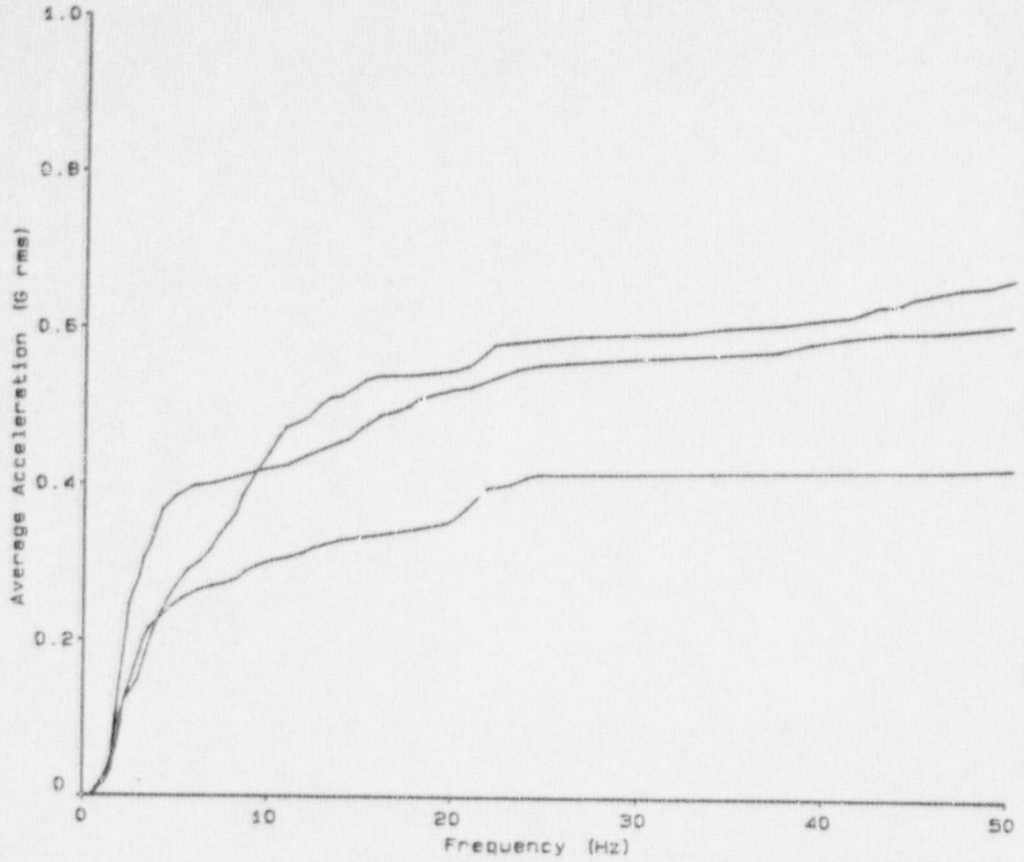

Figure E-113. CPS average acceleration, gate valve body.

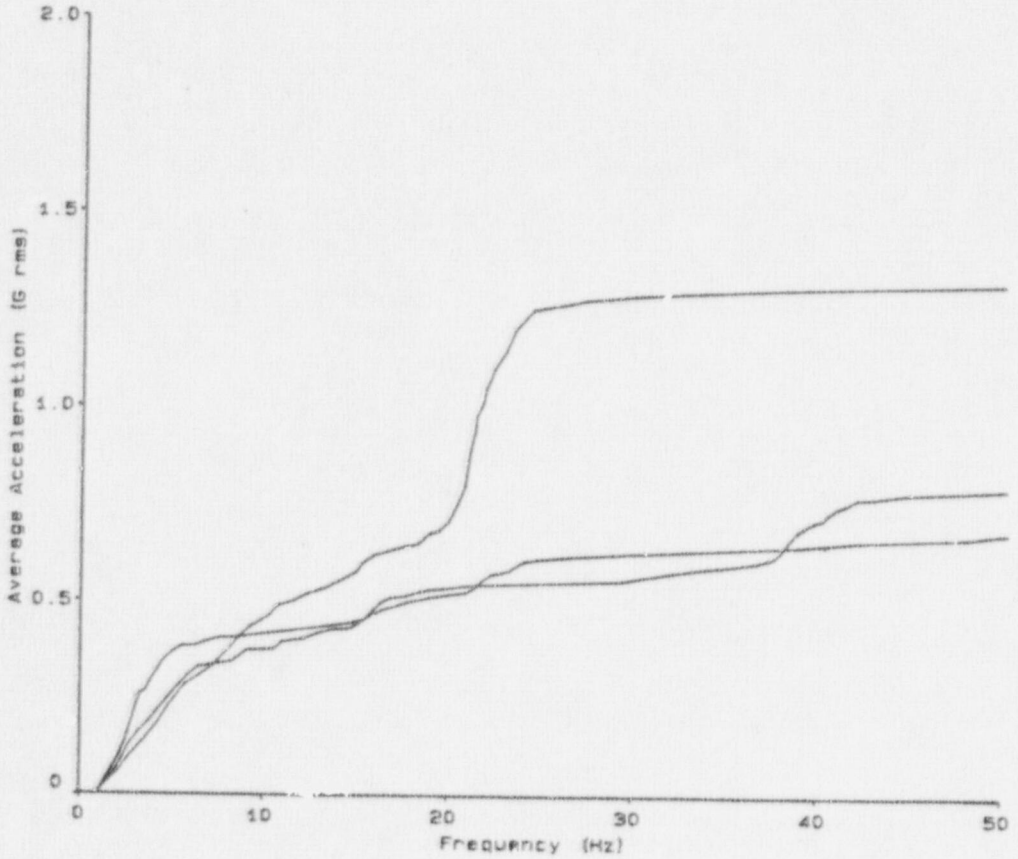

Figure E-114. CPS average acceleration, gate valve actuator.

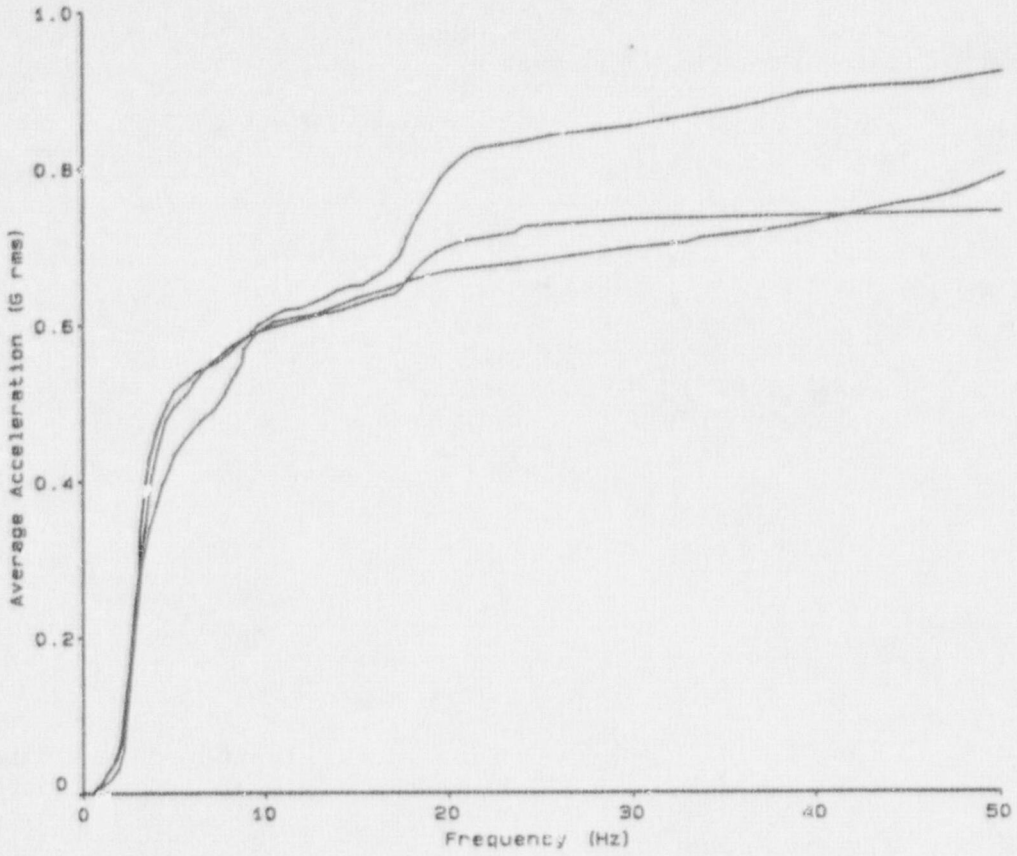

Figure E-115. CPS average acceleration, butterfly valve body.

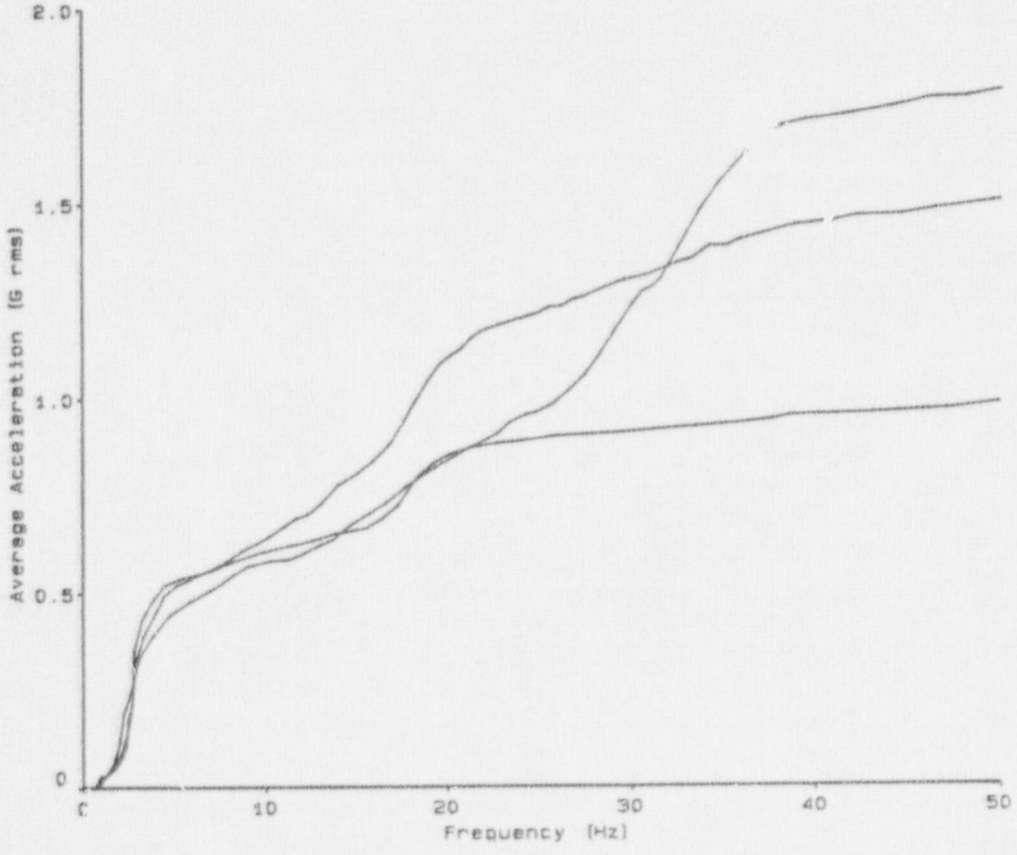

Figure E-116. CPS average acceleration, butterfly valve actuator.

Table E-1. Band-integrated X acceleration

Location	Acceleration (G rms) [Bandwidth (Hz)]			
	Test T40.10		Test T40.30	
	Frame #1	Frame #2	Frame #1	Frame #2
V. Oper.	0.31 [4.9-8.1]	0.48 [4.0-6.1]	0.23 [5.3-7.4]	0.40 [4.1-5.9]
	0.10 [11.6-14.0]	0.09 [7.6-11.0]		0.16 [6.4-7.9]
	0.17 [17.2-19.2]	0.12 [14.0-16.7]		0.16 [13.8-16.6]
	0.35 [19.4-22.1]	0.21 [18.0-22.6]	0.32 [18.3-20.9]	0.29 [17.4-21.0]
	0.22 [22.3-25.5]		0.14 [21.8-24.2]	0.18 [22.3-24.4]
	0.23 [26.2-28.6]	0.28 [22.6-34.2]	0.18 [25.0-30.0]	
	0.19 [28.9-31.1]			0.22 [27.3-32.2]
	0.12 [32.0-37.2]		0.13 [31.4-33.4]	
	0.22 [39.2-44.7]	0.12 [37.2-43.7]	0.25 [38.0-42.2]	0.10 [41.0-44.4]
			0.09 [44.1-48.2]	
	1.91	1.30	1.34	1.51
V. Body	0.27 [4.9-6.9]	0.38 [3.8-6.1]	0.16 [5.3-7.1]	0.37 [4.0-5.9]
				0.12 [6.3-7.9]
	0.07 [23.5-24.9]		0.07 [19.1-20.7]	0.06 [22.5-24.1]
	0.06 [26.4-27.9]	0.07 [25.4-27.5]	0.08 [25.0-30.0]	0.05 [24.6-26.1]
	0.11 [29.3-31.1]	0.12 [28.1-32.8]		0.10 [27.3-30.9]
	0.09 [32.1-36.5]		0.09 [30.8-34.9]	0.08 [31.4-34.0]
	0.10 [40.5-44.9]	0.08 [39.3-43.5]	0.09 [38.0-42.1]	0.07 [41.0-43.8]
	0.74	0.64	0.49	0.85
Sph. Tee	0.11 [6.4-7.7]	0.27 [4.6-5.9]	0.23 [5.6-7.5]	0.42 [4.6-6.1]
		0.07 [9.8-11.1]		
		0.06 [15.3-16.7]		0.06 [15.5-17.0]
	0.07 [18.5-21.6]	0.05 [20.7-22.0]	0.05 [19.6-21.0]	
	0.09 [24.4-28.5]	0.07 [25.4-28.0]	0.09 [24.6-28.2]	0.04 [27.3-28.0]
	0.04 [31.8-33.4]	0.06 [29.0-31.2]		
	0.31	0.58	0.37	0.52
Std. Tee	0.33 [4.9-8.1]	0.30 [4.1-5.9]	0.11 [5.3-7.1]	0.35 [4.0-6.0]
	0.04 [11.5-12.5]	0.07 [9.0-10.4]	0.04 [11.0-12.0]	0.07 [6.2-7.9]
		0.07 [15.2-16.6]		0.11 [14.9-17.0]
				0.09 [17.4-19.5]
	0.08 [23.7-25.0]	0.13 [23.6-25.4]		
	0.06 [26.6-28.1]		0.07 [24.9-27.2]	0.08 [24.7-28.0]
	0.07 [30.0-31.0]			
	0.07 [34.4-37.4]		0.05 [32.2-35.1]	
			0.06 [37.6-41.6]	
	0.65	0.57	0.33	0.70
Top HDU	0.20 [5.6-8.0]	0.06 [4.6-5.6]	0.19 [5.8-8.0]	0.07 [4.6-6.4]
				0.03 [14.8-16.2]
	0.08 [18.4-21.2]		0.08 [18.3-21.2]	
	0.05 [26.0-27.5]		0.05 [24.6-27.4]	0.03 [25.6-27.1]
	0.06 [31.2-34.2]		0.06 [31.0-35.0]	
	0.39	0.06	0.38	0.13

Table E-2. Band-integrated Y acceleration

	Acceleration (G rms) [Bandwidth (Hz)]			
	Test T40.10		Test T40.30	
Location	Frame #1	Frame #2	Frame #1	Frame #2
V. Oper.	0.23 [4.9-7.6]	0.03 [4.9-5.6]		
	0.06 [8.8-10.1]			
		0.05 [14.1-15.0]	0.08 [12.5-14.4]	0.09 [13.2-14.6]
	0.14 [17.4-18.9]	0.06 [18.3-19.6]	0.07 [16.5-17.9]	0.10 [18.1-19.5]
	0.14 [19.8-22.0]		0.20 [18.5-21.1]	0.06 [20.0-21.6]
	0.06 [23.0-24.6]	0.04 [23.8-24.6]		
	0.07 [33.1-36.5]	0.03 [33.5-34.4]	0.07 [31.9-35.6]	0.05 [32.0-33.6]
	0.08 [40.5-44.5]			
	0.78	0.21	0.42	0.30
V. Body	0.23 [5.5-7.4]			
	0.06 [8.8-10.0]			
		0.04 [14.0-14.9]	0.08 [12.5-14.4]	0.09 [13.3-14.6]
	0.13 [17.3-18.9]		0.06 [16.5-17.9]	0.08 [18.1-19.5]
	0.12 [19.8-21.6]	0.06 [18.3-22.0]	0.17 [18.4-21.1]	0.05 [20.0-21.5]
	0.06 [23.0-24.6]	0.05 [23.8-25.1]		
	0.05 [26.6-31.1]			
	0.05 [33.8-36.8]	0.05 [28.5-35.0]	0.05 [31.9-34.8]	0.04 [31.9-33.6]
	0.05 [40.5-44.5]			
	0.75	0.20	0.26	0.26
Sph. Tee	0.07 [4.4-5.5]	0.18 [5.0-5.9]		0.03 [5.0-5.6]
	0.53 [5.6-7.5]	0.07 [6.0-7.2]	0.08 [5.8-7.6]	
	0.17 [8.0-10.1]	0.06 [10.0-11.5]		
	0.04 [13.0-14.2]		0.06 [12.5-13.5]	0.05 [12.8-13.5]
			0.08 [13.6-14.9]	0.05 [15.1-16.9]
			0.07 [19.6-21.5]	
	0.04 [31.3-33.2]		0.05 [31.4-34.2]	
	0.85	0.31	0.34	0.13
Std. Tee	0.11 [5.4-7.0]	0.04 [4.2-5.6]	0.07 [5.1-7.0]	0.05 [4.1-5.4]
		0.03 [9.1-10.1]		
				0.04 [13.5-14.6]
			0.05 [19.0-20.9]	
	0.09 [23.0-24.8]			0.05 [22.6-24.1]
	0.20 [26.2-29.5]	0.08 [27.7-30.2]	0.21 [24.7-29.5]	0.08 [27.1-29.5]
	0.08 [29.6-31.5]	0.04 [30.4-31.3]		0.08 [30.0-34.3]
	0.07 [33.4-36.0]		0.06 [32.7-35.0]	
	0.07 [40.6-43.1]			0.05 [41.0-43.4]
	0.62	0.19	0.39	0.35
Top HDU	0.06 [5.7-7.4]	0.03 [4.9-5.]	0.06 [5.8-7.2]	0.02 [4.6-5.5]
	0.03 [12.1-14.1]		0.04 [12.1-14.1]	
	0.03 [18.8-21.0]		0.04 [18.8-21.0]	
	0.09 [24.4-29.4]		0.08 [24.0-29.2]	
	0.21	0.03	0.22	0.02

Table E-3. Band-integrated Z acceleration

Location	Acceleration (G rms) [Bandwidth (Hz)]			
	Test T40.10		Test T40.30	
	Frame #1	Frame #2	Frame #1	Frame #2
V. Oper.	0.49 [5.1-7.6]	0.26 [4.4-5.7]	0.29 [5.1-7.2]	0.20 [4.1-5.5]
				0.09 [6.4-7.6]
	0.26 [11.6-12.7]		0.07 [10.6-12.0]	0.14 [8.9-11.0]
	0.10 [13.1-14.4]	0.13 [13.1-16.2]	0.07 [12.5-14.2]	
	0.26 [19.4-22.0]	0.17 [18.8-21.9]	0.20 [18.8-21.0]	0.10 [18.3-19.9]
	0.20 [23.4-24.9]	0.12 [23.3-25.2]		0.13 [22.3-24.2]
	0.33 [26.3-29.1]		0.16 [25.0-29.4]	0.23 [24.6-29.0]
	0.21 [29.2-31.6]	0.14 [28.4-31.1]		0.16 [30.0-32.1]
	0.55 [32.3-37.6]	0.27 [31.8-35.0]	0.43 [31.6-36.4]	0.28 [32.3-34.1]
		0.15 [37.0-39.9]	0.33 [38.0-41.6]	0.27 [35.0-40.0]
	0.24 [39.4-45.6]	0.16 [40.0-46.4]		0.16 [40.9-43.4]
			0.10 [45.8-47.7]	
	2.64	1.40	1.65	1.76
V. Body	0.14 [5.5-7.2]	0.11 [4.3-5.7]	0.16 [5.3-7.1]	0.12 [4.2-5.6]
		0.09 [9.1-11.2]		0.11 [8.9-11.0]
	0.21 [11.6-14.4]	0.11 [13.1-16.4]	0.04 [12.5-14.1]	0.13 [13.3-16.2]
			0.05 [18.8-20.6]	0.04 [18.9-19.5]
	0.07 [30.3-31.2]	0.07 [28.4-32.6]		
	0.06 [33.8-37.1]		0.05 [30.6-35.6]	0.06 [31.9-33.5]
	0.05 [40.4-43.9]		0.04 [39.3-41.6]	
	0.53	0.38	0.34	0.46
Sph. Tee	0.07 [5.9-7.3]	0.08 [4.8-5.7]	0.17 [5.6-7.1]	0.15 [4.6-5.7]
	0.05 [10.9-11.7]	0.11 [7.5-11.1]		0.08 [10.0-11.6]
	0.19 [11.9-14.5]	0.04 [12.6-14.0]	0.05 [12.8-14.0]	
		0.06 [15.4-16.6]		0.08 [15.1-17.0]
	0.05 [19.4-21.6]	0.04 [20.8-22.0]	0.05 [18.5-21.5]	
	0.06 [25.8-28.5]	0.04 [26.4-28.0]	0.05 [24.6-28.6]	
		0.07 [29.0-31.1]		0.04 [27.5-29.5]
	0.42	0.44	0.32	0.35
Std. Tee	0.42 [5.4-7.9]	0.19 [4.1-5.8]	0.20 [5.2-7.4]	0.14 [4.1-5.6]
		0.14 [8.7-10.9]		
	0.08 [11.6-12.6]		0.05 [11.0-12.0]	0.08 [13.6-14.6]
			0.06 [16.2-17.9]	0.11 [15.9-17.0]
			0.09 [18.9-21.0]	0.11 [17.8-19.5]
	0.16 [23.1-25.3]	0.21 [23.6-25.4]		0.06 [22.7-23.9]
	0.07 [26.6-27.9]		0.14 [25.0-28.0]	0.10 [24.6-27.0]
	0.15 [30.0-31.6]	0.11 [28.1-30.3]	0.07 [28.1-29.6]	
	0.17 [33.7-37.4]		0.13 [32.2-35.0]	
			0.09 [37.7-41.2]	
	1.05	0.65	0.83	0.60

Table E-3. (continued)

	Acceleration (G rms) [Bandwidth (Hz)]			
	Test T40.10		Test T40.30	
Location	Frame #1	Frame #2	Frame #1	Frame #2
Top HDU	0.63 [5.5-8.0]	0.23 [4.6-5.9]	0.64 [5.6-7.9]	0.24 [4.3-6.4]
		0.06 [15.1-17.0]		0.06 [15.3-16.5]
	0.14 [18.0-22.4]	0.05 [20.5-21.6]	0.14 [18.1-22.4]	0.04 [20.5-21.5]
	0.13 [24.5-28.1]		0.13 [24.3-28.0]	
	0.90	0.34	0.91	0.34

Table E-4. CPS gate valve acceleration

	Acceleration (G rms)								
	X Direction			Y Direction			Z Direction		
Band (Hz)	Body	Oper.	Amp.	Body	Oper.	Amp.	Body	Oper.	Amp.
0-5	0.250	0.305	1.22	0.383	0.382	1.00	0.260	0.276	1.06
5.10	0.196	0.257	1.31	0.184	0.182	0.99	0.368	0.385	1.05
10-15	0.140	0.252	1.80	0.208	0.198	0.95	0.312	0.398	1.28
15-20	0.142	0.338	2.38	0.259	0.267	1.03	0.169	0.398	2.36
20-25	0.195	0.118	0.61	0.188	0.356	1.89	0.206	1.040	5.05
25-30	0.053	0.116	2.19	0.091	0.134	1.47	0.071	0.276	3.89
30-35	0.040	0.216	5.40	0.083	0.109	1.31	0.102	0.211	2.07
35-40	0.036	0.384	10.67	0.135	0.146	1.08	0.116	0.165	1.42
40-45	0.039	0.315	8.08	0.105	0.115	1.10	0.196	0.105	0.54
45-50	0.040	0.126	3.15	0.125	0.149	1.19	0.179	0.088	0.49
Sum	1.131	2.427	2.15	1.761	2.038	1.16	1.979	3.342	1.69

Table E-5. CPS butterfly valve acceleration

Band (Hz)	Acceleration (G rms)								
	X Direction			Y Direction			Z Direction		
	Body	Oper.	Amp.	Body	Oper.	Amp.	Body	Oper.	Amp.
0-5	0.510	0.530	1.04	0.530	0.548	1.03	0.448	0.456	1.02
5.10	0.321	0.429	1.34	0.307	0.329	1.07	0.408	0.402	0.99
10-15	0.203	0.469	2.31	0.245	0.266	1.09	0.211	0.363	1.72
15-20	0.326	0.769	2.36	0.464	0.516	1.11	0.229	0.471	2.06
20-25	0.223	0.537	2.41	0.265	0.323	1.22	0.149	0.527	3.54
25-30	0.090	0.467	5.19	0.145	0.156	1.08	0.155	0.759	4.90
30-35	0.071	0.533	7.51	0.208	0.188	0.90	0.171	1.002	5.86
35-40	0.064	0.417	6.52	0.213	0.238	1.12	0.151	0.678	4.49
40-45	0.064	0.304	4.75	0.142	0.145	1.02	0.192	0.397	2.07
45-50	0.057	0.252	4.42	0.159	0.162	1.02	0.221	0.370	1.67
Sum	1.929	4.707	2.44	2.678	2.871	1.07	2.335	5.425	2.32

NRC FORM 335 (2-89) NRCM 1102, 3201, 3202

U.S. NUCLEAR REGULATORY COMMISSION

BIBLIOGRAPHIC DATA SHEET

(See instructions on the reverse)

1. REPORT NUMBER (Assigned by NRC. Add Vol., Supp., Rev., and Addendum Numbers, if any.)
NUREG/CR-4977
EGG-2505
Vol. 2

2. TITLE AND SUBTITLE
SHAG Test Series
Seismic Research on an Aged United States Gate Valve and on a Piping System in the Decommissioned Heissdampfreaktor (HDR): Appendices

3. DATE REPORT PUBLISHED
MONTH: August
YEAR: 1989

4. FIN OR GRANT NUMBER
A6322

5. AUTHOR(S)
R. Steele, Jr., J.G.Arendts

6. TYPE OF REPORT
Technical

7. PERIOD COVERED (Inclusive Dates)

8. PERFORMING ORGANIZATION – NAME AND ADDRESS (If NRC, provide Division, Office or Region, U.S. Nuclear Regulatory Commission, and mailing address; if contractor, provide name and mailing address.)
Idaho National Engineering Laboratory
EG&G Idaho, Inc.
Idaho Falls, ID 83415

9. SPONSORING ORGANIZATION – NAME AND ADDRESS (If NRC, type "Same as above"; if contractor, provide NRC Division, Office or Region, U.S. Nuclear Regulatory Commission, and mailing address.)
Division of Engineering
Office of Nuclear Regulatory Research
U.S. Nuclear Regulatory Commission
Washington, D.C. 20555

10. SUPPLEMENTARY NOTES

11. ABSTRACT

The Idaho National Engineering Laboratory (INEL) participated in an internationally sponsored seismic research program conducted at a decommissioned experimental reactor facility, the Heissdampfreaktor (HDR), located in the Federal Republic of Germany (FRG). The research program included the study of the effects of excitation, produced during a simulated seismic event, on (a) the operability and integrity of a naturally aged 8-in. motor-operated gate valve installed in the Versuchskreislauf (VKL), an existing piping system in the HDR, (b) the dynamic response of the VKL and the operability of snubbers, and (c) the dynamic responses of various piping support systems installed on the VKL. The INEL work, sponsored by the U.S. Nuclear Regulatory Commission (USNRC), contributes to earthquake investigations being conducted by the Kernforschungszentrum Karlsruhe (KfK) and is part of the general HDR Safety Program performed in behalf of the FRG, Federal Ministry for Research and Technology. This report presents the results of the KfK-designated SHAG (Shakergebäude) test series; these are the first in situ experiments involving an actual nuclear power plant and a full scale piping system under simulated seismic loading. Volume I presents a summary of the tests and results, and Volume II contains appendices that present details and specifics of the tests and results of Volume I.

12. KEY WORDS/DESCRIPTORS (List words or phrases that will assist researchers in locating the report.)
SHAG test series
seismic research program
aged gate valve
piping system
Heissdampfreaktor (HDR)
simulated seismic loading

13. AVAILABILITY STATEMENT
unlimited

14. SECURITY CLASSIFICATION
(This Page)
unclassified
(This Report)
unclassified

15. NUMBER OF PAGES

16. PRICE

NRC FORM 335 (2-89)

*U.S. GOVERNMENT PRINTING OFFICE:1989-241-590:00206

UNITED STATES
NUCLEAR REGULATORY COMMISSION
WASHINGTON, D.C. 20555

OFFICIAL BUSINESS
PENALTY FOR PRIVATE USE, $300

SPECIAL FOURTH-CLASS RATE
POSTAGE & FEES PAID
USNRC
PERMIT No. G-67

120555139531 1 1AN1R1
US NRC-OADM
DIV FOIA & PUBLICATIONS SVCS
TPS PDR-NUREG
P-209
WASHINGTON DC 20555